ÉVFOLYAM
Volume

XIX 2016

GEOMATIKAI KÖZLEMÉNYEK

Publications in Geomatics

HU ISSN 1419-6492

CSFK

MTA CSFK GEODÉZIAI ÉS GEOFIZIKAI INTÉZET
SOPRON

Geomatikai Közlemények

Publications in Geomatics

kiadja az

MTA CSFK GEODÉZIAI ÉS GEOFIZIKAI INTÉZETE

9400 Sopron, Csatkai E. u. 6-8. Pf. 5.
tel.: 99 / 508-340 fax.: 99 / 508-355
e-mail: geomatika@ggki.hu
web: www.geomatika.ggki.hu
web programozó: Lovranits Tamás

felelős kiadó:

Szarka László Csaba
főigazgató

főszerkesztő:

Papp Gábor

angol nyelvi szerkesztő:

Papp Gábor

technikai szerkesztő:

Rács Ágnes

készült a
LŐVÉR PRINT Kft. nyomdájában
9400 Sopron, Ady Endre u. 5.
tel.: 99 / 329-977

megjelent 100 példányban
Sopron, 2016

HU ISSN 1419-6492

GEOMATIKAI

KÖZLEMÉNYEK

XIX.

"Minden nemzet a maga
nyelvén lett tudós,
de idegenen sohasem."

(Bessenyei György)

ÁLTALÁNOS INFORMÁCIÓK ÉS ÚTMUTATÓ

A Geomatikai Közlemények 1998 óta rendszeresen, általában évenként egy alkalommal megjelenő folyóirat. A kiadvány célja, hogy elsősorban magyar és esetenként angol nyelvű fórumot biztosítson a hazai ill. külföldi kutatóknak és szakembereknek, akik a geodézia, fotogrammetria, térinformatika, fizikai geodézia, geofizika, földmágnesség, geodinamika, a Föld belső szerkezete és a Föld körüli térség fizikája, tágabb értelemben véve a geomatika szakterületén elért tudományos eredményeiket szeretnék közzétenni. A kiadványban megjelenő cikkek és tanulmányok a mai normáknak megfelelő lektorálási folyamaton mennek keresztül, azaz mielőtt publikálásra kerülnek legalább kettő független bíráló véleményt alkot a közlésre benyújtott kéziratról. A bírálók nevét alaphelyzetben csak a szerkesztőbizottság ismeri, de a bírálók kérhetik anonimitásuk felfüggesztését. A bírálatok alapján a szerkesztőbizottság eldönti, hogy az adott kézirat megfelel-e a Geomatikai Közlemények formai és tartalmi követelmény-rendszerének, illetve, hogy az esetlegesen felmerülő hibák és hiányosságok kijavíthatók- és pótolhatók-e a kézirat kisebb-nagyobb átdolgozásával.

A Geomatikai Közlemények szerkesztését – amelyet 2011-től már egy, az Interneten keresztül elérhető és működtethető web felület is támogat (www.geomatika.ggki.hu/kozlemenyek ©Lovranits Tamás és Papp Gábor) – társadalmi munkában végző szerkesztőség nagy hangsúlyt fektet a lehető leggyorsabb minőségi munkára. Ez mind a szerzőktől, mind a bírálóktól erőfeszítéseket és fegyelmet kíván, amit a szerkesztőség előre is tisztelettel megköszön. Ennek biztosításához javasoljuk áttanulmányozni a következő anyagokat:

Geomatikai_Közlemények_instrukciók_szerzőknek.docx,
Geomatikai_Közlemények_instrukciók_bírálóknak.pdf,

amelyek a már fent megadott címre belépve letölthetők. A regisztrált felhasználók ugyanezen a címen keresztül végezhetik el a rendszer által koordinált aktuális feladataikat, akár szerzői, akár bírálói szerepkörben. Az új felhasználók ugyanitt regisztrálhatnak, felhasználói név és e-mail cím megadásával.

A feltöltött kéziratokat a szerkesztőség előbírálja, elsősorban az instrukciókban megfogalmazott formai szempontok szerint. Ha a kézirat formailag kielégítőnek bizonyul, akkor elindul a bírálati folyamat, amely általában több ciklust is képez, és egészen addig tart, ameddig a bírálók ill. a szerkesztőség ezt tartalmi-formai indokok miatt szükségesnek tartják. A bírálati fázisokról és az aktuális teendőkről mind a szerzők mind a bírálók automatikus üzenetekben értesülnek.

A Geomatikai Közleményeket az MTA CSFK Geodéziai és Geofizikai Intézete adja ki. A kiadás anyagi hátterét egyrészt a kétévente Sopronban megrendezésre kerülő Geomatika Szeminárium, másrészt különböző pályázatok és tudományos szervezetek (pl. Soproni Tudós Társaság) támogatásai biztosítják. A XIX. kötet megjelenését az MTA CSFK publikációs kerete tette lehetővé.

PREFACE

This special issue of Publications in Geomatics contains only one monograph a main part of which was published as the PhD dissertation of Judit Benedek in 2009 at the West Hungarian University Sopron in Hungarian language. In the meantime the author revised its content based on partly the comments and recommendations of the referees (Dr. László Szarka and Dr. Gyula Tóth) of her thesis work and partly her own experience in the application of the algorithms she wrote for synthetic gravitational modeling. Consequently the monograph is an improved version of the original dissertation containing some new achievements and details in its topic.

The publication of this volume was financed by the Research Centre for Astronomy and Earth Sciences of the Hungarian Academy of Sciences. The manuscript was revised by Dr. Martin Vermeer (Aalto University, Helsinki, Finland) and Dr. Ernő Prácser (MTA CSFK GGI, Sopron, Hungary).

Gábor Papp
editor in chief

*

CONTENTS
TARTALOMJEGYZÉK

SYNTHETIC MODELLING OF THE GRAVITATIONAL FIELD

*Benedek Judit**

This work makes an attempt to summarise and complete the analytical formulas of gravitational potential of the homogeneous polyhedral body and its first and second order derivatives. The Newtonian integral over the volume of a polyhedral body can be expressed as a summation of closed analytical functions evaluated at facet vertices using transformations to surface and line integrals. The ultimate results can be expressed as a sum of arcus tangent and logarithm terms at both ends of every edges of every face. The analytical formulas for the gravitational field of a homogeneous polyhedral body (gravitational potential and its first derivatives) given by Pohànka was implemented in a Fortran program developed by the author and completed with formulas of second derivatives of potential. The numerical stability of polyhedron-based models was studied in points close to and far from the effective source giving the limits where the analytical formulas became senseless or the numerical error dominates in the computed value.

The time needed for calculating the gravitational potential and its first and second order derivatives with the algorithm developed is ~2 times more using polyhedrons than the one optimised by D Nagy for rectangular prisms, applying double precision arithmetic.

In the second part of the work an outlook on the possible future applications of gravity field modelling using polyhedron volume elements is presented.

Keywords: polyhedron, gravity modelling, gravitational potential

A dolgozat célja a homogén poliéder térfogatelem tömegvonzási erőterét leíró potenciált illetve a potenciál első és másodrendű deriváltjait leíró analitikus függvények összefoglalása és a köztük levő kapcsolatok bemutatása a szakirodalomban megtalálható képletek alapján. Azokban az esetekben, amikor csak az elsőrendű deriváltak kerültek publikálásra, a dolgozatban levezetésre kerültek a másodrendű formulák is. A poliéder tömegvonzási erőterét leíró Newton térfogat integrál a poliéder lapokon illetve éleken történő zárt analitikus képletek összegezése, mely a prizmaformulákhoz hasonlóan arcus tangens és logaritmus tagokat tartalmaz. Az analitikus képletek mindegyike felhasználja a nevezetes integrálátalakító tételeket, melyek segítségével áttérhetünk térfogat integrálról felületi integrálra, illetve felületi integrálról vonal integrálra. Modellszámításokhoz a poliéder térfogatelem tömegvonzási potenciáljának és elsőrendű deriváltjainak a Pohànka által közölt képletei illetve a szerző által levezetett potenciál másodrendű derivált képletei kerültek programozásra Fortran nyelven. A tanulmány vizsgálja a poliéder térfogatelem potenciálja, első és másodrendű derivált függvényeinek stabilitását a poliéder közeli illetve távoli tartományaiban, megadva az egyes analitikus függvények értelmezési tartományát és a képletek numerikus stabilitását.

A poliéder térfogatelemek átlag generált erőtér paramétereinek duplapontossággal történő számítás ideje ~2-szerese a prizma térfogatelemhez viszonyítva.

A dolgozat második része egy rövid kitekintés a poliéder térfogatelemmel történő erőtér modellezés lehetséges alkalmazási területeire a geotudományokban.

Kulcsszavak: poliéder, gravitációs modellezés, tömegvonzási potenciál

**MTA CSFK GGI, 9400 Sopron, Csatkai u. 6-8.*
E-mail: geomatika@ggki.hu

CONTENTS

NOTATION

$a \in A$	a is an element of A
$a \notin A$	a is not an element of A
$A \subset B$	A is a subset of B
$\cap$	intersection of two sets
$\cup$	union of two sets
$A \setminus B$	the difference of set A from B
$A \times B$	Cartesian product of A and B, $A \times B = \{(a,b) \mid a \in A, b \in B\}$
R^n	real coordinate space of n dimension, consist of all ordered n-couples $(x_1, x_2, \ldots, x_n)$, where the x_i are real numbers
$\overline{\Omega}$	closure of $\Omega \subseteq R^n$ is a set which contains all its limit points, i.e. $\overline{\Omega} = \Omega \cup \Omega'$, where Ω' is the set of limit points of Ω
$\partial\Omega$	boundary of $\Omega \subseteq R^n$, $\partial\Omega = \overline{\Omega} \setminus \Omega$
$\overline{1,n}$	natural numbers from 1 to n which is the $\{1,2,\ldots,n\}$ set
$\lvert \boldsymbol{x} \rvert$	Euclidian norm of $\boldsymbol{x} \in R^n$, $\lvert \boldsymbol{x} \rvert = \sqrt{x_1^2 + x_2^2 + \ldots + x_n^2}$, where $\boldsymbol{x} = (x_1, x_2, \ldots, x_n)$
$\mathscr{B}(M,\varepsilon)$	is an open 3-ball of radius ε and centre M in R^3 Euclidian space, $\mathscr{B}(M,\varepsilon) = \{M' \in R^3 \mid \lvert MM' \rvert < \varepsilon\}$
$\mathscr{O}(M,\varepsilon)$	is an open 2-ball of radius ε and centre M in R^2 Euclidian space, $\mathscr{O}(M,\varepsilon) = \{M' \in R^2 \mid \lvert MM' \rvert < \varepsilon\}$
$C^p(\Omega)$	Let $\beta = (\beta_1, \beta_2, \ldots, \beta_n) \in N^n$ be a multi-index and let $\lvert \beta \rvert = \beta_1 + \beta_2 + \ldots + \beta_n$ be the order of multi-index, then $D^\beta f = \dfrac{\partial^\beta f(x_1, x_2, \ldots, x_n)}{\partial x_1^{\beta_1} \ldots \partial x_1^{\beta_n}}$. $C^p(\Omega)$ denote the set of all f functions defined on $\Omega \subseteq R^n$ that are continuous in Ω together with all partial derivatives $D^\beta f$, where $\lvert \beta \rvert \le p$.
$\cdot$	denotes the scalar or dot or inner product of two vectors. If $\boldsymbol{a} = (a_1, a_2, a_3)$, $\boldsymbol{b} = (b_1, b_2, b_3)$ then $\boldsymbol{a} \cdot \boldsymbol{b} = (a_1 b_1 + a_2 b_2 + a_3 b_3) = ab\cos\varphi$, where φ is the angle between $\boldsymbol{a}$ and $\boldsymbol{b}$, a and b denotes the magnitude of the vectors $\boldsymbol{a}$ and $\boldsymbol{b}$: $\boldsymbol{a} = \sqrt{a_1^2 + a_2^2 + a_3^2}$, $\boldsymbol{b} = \sqrt{b_1^2 + b_2^2 + b_3^2}$
$\times$	denotes the vector or cross product of two vectors. $\boldsymbol{a} \times \boldsymbol{b}$ is defined as a vector $\boldsymbol{c}$ that is perpendicular to both $\boldsymbol{a}$ and $\boldsymbol{b}$, with a direction given by the right-hand rule and the magnitude equal to the area of the parallelogram that the vectors span, $\lvert \boldsymbol{c} \rvert = ab\sin\varphi$, where φ is the angle between $\boldsymbol{a}$ and $\boldsymbol{b}$, a and b are the vectors magnitude
$\circ$	denotes the dyadic product of $\boldsymbol{a} = (a_1, a_2, a_3)$ and $\boldsymbol{b} = (b_1, b_2, b_3)$ is $\boldsymbol{a} \circ \boldsymbol{b} = \lfloor a_i b_j \rfloor_{i,j=\overline{1,3}}$
∇	denotes the Hamilton or nabla operator: $\nabla = \dfrac{\partial}{\partial x}\boldsymbol{i} + \dfrac{\partial}{\partial y}\boldsymbol{j} + \dfrac{\partial}{\partial z}\boldsymbol{k}$, where $\boldsymbol{i}, \boldsymbol{j}, \boldsymbol{k}$ are the unit vectors of the coordinate system
∇u	if u: $R^3 \to R$ is a scalar field, M is a point in R^3 with x, y, z coordinates, $\boldsymbol{r}_M = (x, y, z)$ is the position vector belonging to the M point, $\operatorname{grad} u = \nabla u = \nabla_{r_M} u(M) = \dfrac{\partial u}{\partial x}\boldsymbol{i} + \dfrac{\partial u}{\partial y}\boldsymbol{j} + \dfrac{\partial u}{\partial z}\boldsymbol{k}$

$\nabla \boldsymbol{u}$ if $\boldsymbol{u}$: $R^3 \rightarrow R^3$ is a vector field, M is a point in R^3 with x, y, z coordinates, $\boldsymbol{u}(M) = u_1(x,y,z)\boldsymbol{i} + u_2(x,y,z)\boldsymbol{j} + u_3(x,y,z)\boldsymbol{k}$ is a vector and

$$\nabla \boldsymbol{u} = \frac{\partial u_1}{\partial x} + \frac{\partial u_2}{\partial y} + \frac{\partial u_3}{\partial z} = \operatorname{div} \boldsymbol{u}$$

dist(M, Ω) is the distance from the point $M \in R^n$ to the $\Omega \subseteq R^n$ domain defined as: $\operatorname{dist}(M, \Omega) = \min_{P \in \Omega} MP$

$\operatorname{proj}_\Omega(M)$ projection of $M \in R^n$ on $\Omega \subseteq R^n$ is a point M' defined as: $\operatorname{proj}_\Omega M = M'$ and $\operatorname{dist}(M, \Omega) = MM'$

Introduction – Precedents and objectives of the research

The research, the results of which are presented in this thesis, is the continuation of the F014284[1] (finished in 1997) and T025318[2] (finished in 2001) National Scientific Research Fund programs (OTKA). The first version of the 3D density model of the lithosphere of the Pannonian basin (Papp 1996a) was created in the framework of F014284 National Scientific Research Fund research program. That model used the rectangular prism as a volume element. Different versions of the geoid were computed by its application for the territory of Hungary. Such a 3D model makes possible – with specific conditions – to determine different parameters of the gravity field (gravitational acceleration, geoid undulation, gravitational potential, gravity anomaly) analytically. Furthermore, because of the rigorous functional relations between the parameters of the field created from the density model by forward modelling, it is possible to test numerical methods (for example a specific solution of the Stokes integral) which transform from one system of parameters to another one. In the T025318 OTKA research program the lithosphere model was extended to describe the Carpathian-Pannonian Region. One of the aims of this program was to determine the gravitational field lines going through the topographic masses using forward modelling techniques. Based on the model calculations it was possible to study the order of difference between the horizontal coordinates of a specific surface point obtained from GPS measurements (Helmert projection) and its projection point corresponding to its elevation coordinate determined by levelling (Pizetti projection). Furthermore, it became possible to compute the free-air gradient (second order partial derivative in the vertical direction of the gravity potential) using analytical methods and it was also possible to determine the terrestrial distribution of deviations from its normal value within the Pannonian Basin (Csapó and Papp 2000). Based on the model used for the investigations detailed above I tested the effect of the point density of gravity data on the accuracy of geoid undulations determined by the Stokes-FFT method (Benedek 2000, 2001). For the test all geodetic boundary values (gravity anomalies) and also the boundary surface to be determined (geoid undulation) were derived analytically from the model.

The OTKA studies mentioned above indicated that the refinement of the model is beneficial in some applications. One possibility is to apply a more realistic volume element which improves the geometrical description of the structural surfaces. Such a simple geometric element is the polyhedron, because it allows creating bodies bounded with oblique surfaces. Its application can provide a more realistic geometrical description of boundary surfaces, without height jump which is an unavoidable artifact of the description made by rectangular prisms. In this way, the artificial gravitational effect due to the step-like structure can be eliminated. The stepped structure mainly influences the second and the third order derivatives of the potential in near surface points. Furthermore, the effect of the Earth's curvature can be taken into consideration during computations, because the polyhedral geometry allows the description of this model in a global coordinate system (e.g. WGS84). Compared to the rectangular prisms the analytical formulas of the polyhedron's gravitational potential and its higher order derivatives are more complicated so their calculation is more time consuming.

One aim of my thesis was to compare the contributions to geoid undulation and gravity anomaly synthetically computed from polyhedron and rectangular prism models describing the crustal structure of the Carpathian-Pannonian region. Furthermore, I wished to compare the second order vertical derivatives determined from these two models in near-surface points by forward modelling. In this comparison I wanted to involve in situ measurements (Csapó and Papp 2000) so I chose the Sóskút testing area of Tech. Univ. Budapest (TUB) as a target area for model computations. The third aim was to give an estimate of the gravitational contribution of the different geological units such as topography, upper mantle and Neogene-Quaternary sedimentary complex to the second derivatives

[1] National Scientific Research Fund Nr. F014284: "High precision modelling of the gravity field and geoid computation in Carpathian-Pannonian Region", 1994-1997, Principal Investigator: Papp Gábor

[2] National Scientific Research Fund Nr. T025318: "The effect of local characteristics of the Earth's gravity field on geodetic coordinates". Simulation studies in the Pannonian basin, 1998-2001, Principal Investigator: Papp Gábor

of disturbing potential, i.e., to the elements of the Eötvös tensor by using the extended, regional scale (Alpine–Pannonian–Carpathian region) lithosphere model. I wanted to study whether the on board gradiometric observations of the GOCE (Gravity and Steady-State Ocean Circulation Experiment) satellite could be applicable to deduce some regional information about the horizontal density variation of the crust as well. I aimed also to derive formulas for the transformation of the computed second derivatives of the potential in local (using the rectangular prism as volume element) and in global (using the polyhedron as volume element) coordinate systems. Based on this I also wanted to determine the effect of the Earth's curvature on field parameters.

I wished to study the analytical behaviour of the formula given for the gravitational potential of the polyhedron volume element and the numerical characteristics of its higher order derivatives in points close to and far from the effective source, and also the accuracy of model computation and the time-consumption of the analytical formulas.

Research methods and results

I applied the theorems of the potential theory to define the domains of formulas describing first and second derivatives of the gravitational potential and the potential itself generated by the polyhedrons.

Using vector analysis I derived analytical formulas for the gravitational potential and its first and second derivatives of the polyhedrons.

I developed a program system in the HP Fortran language for computing the gravitational potential of the polyhedron and the first and second derivatives of the potential.

For the forward modelling of the gravity field related quantities I used different models of the topography of the Alpine–Pannonian–Carpathian (ALPACA) region built up with triangular prisms and polyhedrons as volume elements.

Computational and modelling results were compared to measurements in certain cases and I managed to show the advantages of using the polyhedron models.

I used different coordinate systems (planar and global) which are transformable into one-another. I applied various models (elementary and optimised) of rectangular prisms generated by different methods representing the local (planar) mapping system and polyhedron elements defined in the global Cartesian coordinate system. These models are also transformable into one-another (there is a one-to-one geometrical correspondence between the corner points of prisms and polyhedrons). Using these models I was able to estimate the effect of the Earth's curvature.

In my thesis I summarised and completed the analytical formulas of the gravitational potential and its first and second order derivatives of the polyhedron volume element. Using vector analysis I gave a uniform derivation for the formulas. I demonstrated that passing from surface integrals to contour integrals using either the Gauss-Ostrogradsky or the Stokes theorem leads to finding the same vector function, and to define it one has to solve a quasi-linear differential equation. I proved that the domains of the analytical formulas could be extended to the domains dedused from potential theory, thus the singularities of the formulas can be eliminated.

I studied the numerical stability of the polyhedron-based model in points close to and far from the effective source giving each point location those limits where 1) the analytical formulas become senseless or 2) the numerical error is dominating in computed value. As far as first derivative of the potential is concerned I completed the relation given by Holstein and Ketteridge (1996) and Holstein et al. (1999) with new relations about the potential and its second order derivatives. I showed by double precision computations that using the polyhedral model of the ALPACA region the error of the forward computation of the second order derivatives of the potential is less than 1% within the studied area.

I compared the runtimes of the potential and its derivatives applying the polyhedron algorithm and the code for the rectangular prism optimised by Nagy (1988).

Based on a 5 km × 5 km DTM of the Carpathian Basin and a 500 m × 500 m DTM of Hungary I created polyhedron and different type (elementary and optimised) rectangular prism models for both territories. Both in the elementary rectangular prism and the polyhedron models the horizontal dimensions of the volume elements are equal to the resolution of the relevant DTM, while the vertical

dimensions of the volume elements are equal to the values given by the DTM point. Another rectangular prism model (optimised) was created based on the minimum number of volume elements principle (Kalmár et al. 1995). Using various models developed from a 5 km × 5 km DTM, the order of the average and the standard deviation of the computed gravitational disturbance at the geoid level is about -0.1 mGal and ±0.5 mGal throughout the 800 km × 600 km computational area which includes also the territory of Hungary. In the second application I used models derived from 500 m × 500 m DTM, and the computation was made on a 165 km × 150 km territory of the Northern Mid Mountains Range. The computations which were performed at the geoid level show that the differences between the results computed from optimised prism and polyhedron models appear more remarkable on the low plains than on higher territories.

A big advantage of the polyhedron volume element is that it can describe the surface without jumps in height, so the second order derivatives of potential in *z* are much smoother and more realistic in near surface parts. It can be deduced from the study carried out on the Sóskút test area of TUB that in accordance with the theory the second order derivatives computed from the polyhedron model at 1 m height above the topographic surface are correlating fairly well with topography. To model the second order derivatives of the potential in near-surface points the polyhedron volume element is needed. Even if the rectangular prism model is derived from a 10 m × 10 m DTM the variation of the derivatives between adjacent points (for example points of the 25 m × 25 m grid) can be too (unreal) high. Therefore the correlation between the values itself and the surface is low. In the six point of the Sóskút geodetic network dedicated for studying deformation, vertical gradient (VG) values computed from the polyhedron model of the area fit well with the measurements (Csapó and Papp 2000) apart from a shift, but the values obtained from the rectangular prism model are in contradiction with the measured values.

From results of the synthetic gravitational modelling for the planned orbit altitude (~250 km) of GOCE satellite it was found that the individual contribution of the topography and the upper mantle to the second derivatives of the disturbing potential reaches 1 Eötvös. In case of the Neogene-Quaternary sediments this contribution is several hundredths of an Eötvös unit only, but this is still higher than the projected measurement sensitivity. As the topography and the density distribution of the sediments are known much better than the density contrast at Moho–the boundary between the lower crust and the upper mantle – we can use their synthetically modeled contributions as correction in relation with the measurements at orbit altitude. Residuals (i.e. GOCE measurements – corrections) can be converted into density values with inversion, so the density contrast at the Moho surface can be estimated more precisely.

For forward computation of the contribution of the topography the polyhedron model is recommended (i.e. using a global coordinate system) because of the effect of the Earth's curvature for this component is greater than the sensitivity of the satellite gradiometer. When computing the contribution of the effect of the sediments it is enough to use a local coordinate system, i.e. rectangular prisms because the effect of the curvature is estimated to be in the order of the noise range. If 10% accuracy is enough, then the local system is sufficient for the inversion.

1 The Newton (volume) potential

1.1 Review of the applied mathematical formulas

In this paragraph generally known theorems from potential theory and vector calculus based on the Vlagyimirov (1979) and Tyhonov and Samarsky (1964) works are presented without proof. During this work we will refer to these theorems.

1.1.1 The integral theorems

1. *The divergence theorem (Theorem of Gauss and Ostrogradsky)*

Suppose Σ is a subset of R^n which is compact ($\Sigma \subset R^n$ is compact if and only if it is closed and bounded) and has a piecewise smooth boundary[1] $\partial\Sigma=S$. If $\boldsymbol{n}$ is the outward pointing unit normal field of the boundary $\partial\Sigma=S$, and $\boldsymbol{w}(w_1, w_2, \dots, w_n): \overline{\Sigma} \to R^n$, $w_k = w_k(x_1, x_2, \dots, x_n)$, $k = \overline{1,n}$ is a continuously differentiable vector field on Σ and continuous on the boundary of Σ, $\boldsymbol{w} \in C(\overline{\Sigma}) \cap C^2(\Sigma)$, then we have:

$$\iiint_{\Sigma} \nabla \cdot \boldsymbol{w} dv = \iint_{S} \boldsymbol{w} d\boldsymbol{\sigma} = \iint_{S} \boldsymbol{w} \cdot \boldsymbol{n} d\sigma , \tag{1}$$

where $d\boldsymbol{\sigma}$ is the oriented surface element. This vector is belonging to the surface element $d\sigma$ of S (Fig. 1), has the same direction as the $\boldsymbol{n}$ vector, the length of this vector is equivalent with the area of $d\sigma$ surface element, i.e. $d\boldsymbol{\sigma} = \boldsymbol{n} d\sigma$, and $\nabla \cdot \boldsymbol{w} = div\boldsymbol{w} = \sum_{i=1}^{n} \frac{\partial w_i}{\partial x}$.

Observation

1. In R^3 the theorem stands for a S surface which has a continuously varying tangent plane excepting a finite number of corners and edges.
2. A special case of the Gauss-Ostrogradsky theorem when $\boldsymbol{w} = u$ is a scalar function in R^3, then:

$$\iiint_{\Sigma} \frac{\partial u(x,y,z)}{\partial x} d\,v = \iint_{S} u(x,y,z) \cdot \cos(\boldsymbol{n}, \boldsymbol{i}) d\sigma , \tag{2}$$

   where $\boldsymbol{i}$ is the unit vector in the x direction, and $(\boldsymbol{n},\boldsymbol{i})$ denotes the angle between the normal of the surface and the x axis.
3. In virtue of observation 2:

$$\iiint_{\Sigma} \nabla u dv = \iint_{S} u d\boldsymbol{\sigma} \text{ (gradient theorem)}, \tag{3}$$

where $\nabla u = \text{grad} u = \left(\frac{\partial u}{\partial x_i}\right)_{i=\overline{1,n}}$.

4. The Gauss-Ostrogradsky theorem in a 3D Cartesian coordinate system:

$$\iint_{S} w_1 dydz + w_2 dzdx + w_3 dxdy = \iiint_{\Sigma} \left(\frac{\partial w_1}{\partial x} + \frac{\partial w_2}{\partial y} + \frac{\partial w_3}{\partial z} \right) dxdydz .$$

[1] The surface S belongs to the C^p, $p \geq 1$ classes, which is set of all differentiable functions whose derivative is in C^{p-1}, if for all $x_0 \in S \; \exists \mathscr{U}_{x0}$ vicinity of the point x_0 wherein the surface can be described analytically: $\omega_{x0}(x) = 0$, $x \in \mathscr{U}_{x0}$, where $\text{grad}\omega_{x0}(x) \neq 0$ in $\mathscr{U}_{x0}$, in addition the ω_{x0} function has all partial derivatives of order up to p continuous on $\mathscr{U}_{x0}$. The picewise smooth surface S consists of finite C^1 surfaces.

2. *Stokes theorem*

Let $\boldsymbol{w}$ be a C^1 vector field defined on an open set $\Sigma \subset R^3$. Let S be a bounded and piecewise smooth and oriented surface contained entirely within Σ with boundary $\partial S = \Gamma$ which carries the orientation induced by S which is compatible with the right-hand rule (if we walk along Γ in the direction of the orientation induced by S with and our head points in the direction of the unit normal for S, then S will be on our left-hand side) (Fig 1). Then:

$$\iint_S (\nabla \times \boldsymbol{w}) \cdot d\boldsymbol{\sigma} = \iint_S (\nabla \times \boldsymbol{w}) \cdot \boldsymbol{n} d\sigma = \int_\Gamma \boldsymbol{w} \cdot d\boldsymbol{l}\,, \tag{4}$$

where $\nabla \times \boldsymbol{w} = \text{rot}\, \boldsymbol{w} = \left(\frac{\partial w_3}{\partial y} - \frac{\partial w_2}{\partial z}, \frac{\partial w_1}{\partial z} - \frac{\partial w_3}{\partial x}, \frac{\partial w_2}{\partial x} - \frac{\partial w_1}{\partial y} \right)$ and $d\boldsymbol{l}$ is the oriented line element of the Γ curve.

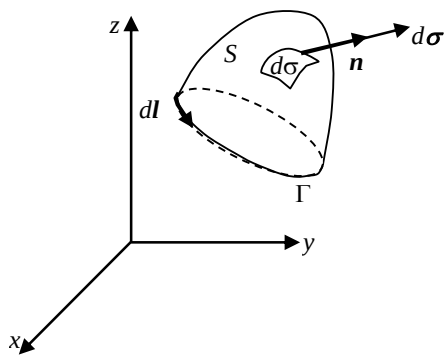

Fig. 1 The illustration of the quantities used in the Stokes theorem

3. *Green theorem*

Let Γ be a positively oriented[1], piecewise smooth, simple closed[2] curve in R^2. Let $S \subset R^2$ be the region bounded by Γ. If $\boldsymbol{w}(w_1, w_2): S \cup \Gamma \to R^2$ and $\boldsymbol{w} \in C^1(S) \cap C(\Gamma \cup S)$, then:

$$\iint_S \left(\frac{\partial w_2}{\partial x} - \frac{\partial w_1}{\partial y} \right) dxdy = \int_\Gamma \boldsymbol{w} \cdot d\boldsymbol{l}\,. \tag{5}$$

Observations

1. The theorem holds for Γ having continuous tangent except at a number of finite points, or more generally, a set of zero measure.
2. The Green theorem is a special case of the Stokes theorem taking the $\boldsymbol{w}(w_1, w_2), w_k = w_k(x, y), k = \overline{1,2}$, planar vector field. This relation can easily be derived using the following relation:

$$\text{rot}\, \boldsymbol{w}(w_1, w_2) = \text{rot}\, \boldsymbol{w}(w_1, w_2, 0) = \left(0, 0, \frac{\partial w_2}{\partial x} - \frac{\partial w_1}{\partial y} \right).$$

3. The Green theorem is a special case of Gauss-Ostogradsky theorem for n=2. In this case $\Sigma \equiv S$, $\partial\Sigma \equiv \Gamma$, $\boldsymbol{w}(w_1, w_2), w_i = w_i(x, y)$ is a plane vector field, $\boldsymbol{n} = (n_1, n_2)$ is the normal vector of Γ. Let α and β be the angle of a Γ curve with the coordinate axes.

[1] If we walk in the direction of the positive orientation for Γ then the interior of Γ is always on our left-hand side
[2] Is a closed curve which does not intersect itself

We have:

$$\iint_S \frac{\partial w_2}{\partial x} dxdy = \int_\Gamma w_2 n_1 dl = \int_\Gamma w_2 \cos\alpha dl \text{ and } -\iint_S \frac{\partial w_1}{\partial y} dxdy = -\int_\Gamma w_1 n_2 dl = \int_\Gamma w_1 \cos\beta dl$$

and this yields the relation (5).

4. The relation (5) in case of $\boldsymbol{w} = u$ scalar function is:

$$\iint_S \frac{\partial u(x,y)}{\partial x} d\sigma = \int_\Gamma u(x,y) \cdot \cos(\boldsymbol{n},\boldsymbol{i}) dl \,. \tag{6}$$

4. *Green formulas*

Let $\Sigma \subset R^n$ be a bounded solid region, with a piecewise C^1 (smooth) boundary surface $\partial\Sigma=S$. Let $\boldsymbol{n}$ be the unit outward normal vector on S. Let u and v be scalar fields (vector-scalar function), $u,v \in C^1(\overline{\Sigma}) \cap C^2(\Sigma)$, one gets:

$$\int_\Sigma \nabla u \cdot \nabla v dv = \int_S u \frac{\partial v}{\partial \boldsymbol{n}} d\sigma - \int_\Sigma u \Delta v dv \text{ (Green first identity)}, \tag{7}$$

$$\int_\Sigma (u\Delta v - v\Delta u) dv = \int_S \left(u \frac{\partial v}{\partial \boldsymbol{n}} - v \frac{\partial u}{\partial \boldsymbol{n}} \right) d\sigma \text{ (Green second identity)}, \tag{8}$$

where $\nabla u = \operatorname{grad} u = \left(\frac{\partial u}{\partial x_1}, \frac{\partial u}{\partial x_2}, \ldots, \frac{\partial u}{\partial x_n} \right)$, $\Delta u = \frac{\partial^2 u}{\partial x_1^2} + \frac{\partial^2 u}{\partial x_2^2} + \ldots + \frac{\partial^2 u}{\partial x_n^2}$ is the Laplace operator, $\frac{\partial u}{\partial \boldsymbol{n}} = \sum_{i=1}^{n} \frac{\partial u}{\partial x_i} \cdot$ is the directional derivative of u in the direction of the outward pointing normal $\boldsymbol{n}$ to the surface element $d\sigma$.

Observation

1. Green first relation can be extend for unbounded regions if $\exists\, r_0$ so that for $r \geq r_0$ then $|u| < \frac{A}{r}$ and $\left| \frac{\partial u}{\partial x_i} \right| < \frac{A}{r^2}$ comes true, where A is a constant.

5. *Consequences of Green identities*

Let $\Sigma \subset R^n$ be a bounded set, with a piecewise C^1 (smooth) boundary surface $\partial\Sigma=S$. Let $\boldsymbol{r}_M$ and $\boldsymbol{r}_P$ be the position vectors of the M and $P \in \overline{\Sigma}$ points, $\boldsymbol{r}_{MP} = \boldsymbol{r}_P - \boldsymbol{r}_M$ and $r_{MP} = |\boldsymbol{r}_{MP}|$ is the length of $\overrightarrow{MP}$ vector, σ_n is surface of the n dimensional unit sphere. If $u \in C^2(\overline{\Sigma})$, then:

$$u(M) = \frac{1}{(n-2)\sigma_n} \int_S \left[\frac{1}{r_{MP}^{n-2}} \frac{\partial u(P)}{\partial \boldsymbol{n}} - u(P) \frac{\partial}{\partial \boldsymbol{n}_P} \left(\frac{1}{r_{MP}^{n-2}} \right) \right] d\sigma_P - \frac{1}{(n-2)\sigma_n} \int_\Sigma \Delta u(P) \frac{1}{r_{MP}^{n-2}} dv_P \quad ,\forall M \in \Sigma \subset R^n,$$

$n \geq 3$ (9)

$$u(M) = \frac{1}{2\pi} \int_S \left[\ln \frac{1}{r_{MP}} \frac{\partial u(P)}{\partial \boldsymbol{n}} - u(P) \frac{\partial}{\partial \boldsymbol{n}_P} \left(\ln \frac{1}{r_{MP}} \right) \right] d\sigma_P - \frac{1}{2\pi} \int_\Sigma \Delta u(P) \ln \frac{1}{r_{MP}} dv_P \,, \forall M \in \Sigma \subset R^2 \,. \tag{10}$$

If $u \in C^1(\overline{\Sigma})$ is harmonic on Σ (i.e. $\Delta u(P) = 0, \forall P \in \Sigma \subset R^n$), then:

$$u(M)=\frac{1}{4\pi}\int_S\left[\frac{1}{r_{MP}^{n-2}}\frac{\partial u(P)}{\partial \boldsymbol{n}}-u(P)\frac{\partial}{\partial \boldsymbol{n}_P}\left(\frac{1}{r_{MP}^{n-2}}\right)\right]d\sigma_P\,,\ \forall M\in\Sigma\subset R^n,\ n\geq 3, \tag{11}$$

$$u(M)=\frac{1}{4\pi}\int_S\left[\ln\frac{1}{r_{MP}}\frac{\partial u(P)}{\partial \boldsymbol{n}}-u(P)\frac{\partial}{\partial \boldsymbol{n}_P}\left(\ln\frac{1}{r_{MP}}\right)\right]d\sigma_P\,,\ \forall M\in\Sigma\subset R^2. \tag{12}$$

Observation

1. Relation (9) stands for $u\in C^2(\Sigma)\cap C^1(\overline{\Sigma})$ too.

6. *Green's theorem in complex form*

Let $f=f(z,\bar{z})$ be a complex valued function of a complex variable, $z=x+iy, \bar{z}=x-iy$, $f\in C^1(S\cup\Gamma)$ where C denotes the set of complex numbers, Γ is the boundary of the S region, then (Kwok 1989):

$$\int_\Gamma f(z,\bar{z})dz=2i\iint_S\frac{\partial f}{\partial \bar{z}}dxdy\,. \tag{13}$$

1.1.2 Theorems regarding to potential theory

7. *Theorem*

Let $\Sigma\subset R^n$ be a bounded region, let $\boldsymbol{r}_M$ and $\boldsymbol{r}_P$ be the position vectors of the M, $P\in\Sigma$ points, $\boldsymbol{r}_{MP}=\boldsymbol{r}_P-\boldsymbol{r}_M$, and $r_{MP}=|\boldsymbol{r}_{MP}|$ is the length of the $\overrightarrow{MP}$ vector and let C be a constant value.
If $\alpha<n$, then the

$$I(M)=\int_\Sigma\frac{C}{r_{MP}^{\alpha}}dv_P\,,\ \forall M\in\Sigma \tag{14}$$

improper integral exists (is convergent). If $\alpha\geq n$, the improper integral (14) is not convergent.

Observation

1. In case of $\alpha<n$ for $\forall M\in\Sigma$ points the $I(M)$ is uniformly convergent.
2. It can be show that in points $M\in\Sigma$, where $I(M)$ is uniformly convergent, the I is continuous. In this way $I(M)=\int_\Sigma\frac{C}{r_{MP}^{\alpha}}dv_P$ exists and is continuous for every $\alpha<n$.
3. For $n=3$ $I(M)=\iiint_\Sigma\frac{C}{r_{MP}}dv_P$ and $I(M)=\iiint_\Sigma\frac{C}{r_{MP}^2}dv_P$ integrals exist and are continuous for $\forall M\in R^3$.

8. *Theorem*

Let $\Sigma\subset R^n$ be a bounded set, let $\boldsymbol{r}_M$ and $\boldsymbol{r}_P$ be the position vectors of the M, $P\in\Sigma$ points, $\boldsymbol{r}_{MP}=\boldsymbol{r}_P-\boldsymbol{r}_M$ and $r_{MP}=|\boldsymbol{r}_{MP}|$ is the length of the $\overrightarrow{MP}$ vector.
If ρ is an integrable function on Σ and $\rho=0$ on the exterior of Σ, then:

$$I(M)=\int_\Sigma\frac{\rho(P)}{r_{MP}^{\alpha}}dv_P\,,\ M\in\Sigma,\ 0<\alpha<n \tag{15}$$

the volume potential is an improper integral, having singularity in $P=M$ and fulfils the following properties:

1. For $\forall M \in \Sigma$ the $I(M)$ exists (is convergent).
2. In the exterior of Σ the function I is infinitely differentiable ($I \in C^{\infty}\left(R^n \setminus \overline{\Sigma}\right)$) in addition the differential of I can be obtained simply by applying the differential operator behind the integral:

$$D^{\beta} I(M) = \int_{\Sigma} \rho(P) \frac{\partial^{|\beta|}}{\partial x_1^{\beta_1} \partial x_2^{\beta_2} \ldots \partial x_n^{\beta_n}} \left(\frac{1}{r_{MP}^{\alpha}} \right) dv_P, \quad \forall M \in R^3 \setminus \overline{\Sigma}, \tag{16}$$

where $\beta = (\beta_1, \beta_2, \ldots, \beta_n)$, $|\beta| = \beta_1 + \beta_2 + \ldots + \beta_n$.

3. The behaviour of derivatives in the infinite can be characterized by:

$$D^{\beta} I(M) = O\left(r_M^{-\alpha - |\beta|}\right) \text{ if } r_M \to \infty. \tag{17}$$

4. If ρ is bounded on Σ, then $I \in C^{p}(R^n)$, where p is the largest integer with the property that $\alpha + p < n$. In this case the computation of derivatives can perform by applying the differential operator behind the integral.

Observation

The properties of the I integral can given in the following form:

$$I_1(M) = \int_S \frac{\rho(P)}{r_{MP}^{\alpha}} d\sigma_P, \; M \in S, \; 0 < \alpha < n\text{-}1, \tag{18}$$

$$I_2(M) = \int_L \frac{\rho(P)}{r_{MP}^{\alpha}} dl_P, \; M \in L, \; 0 < \alpha < n\text{-}2, \tag{19}$$

where $S \subset R^n$ is a bounded region and a piecewise smooth (C^1) surface, L is a segment in R^n, $\boldsymbol{r}_M$ and $\boldsymbol{r}_P$ are the position vectors of the M, P points, $\boldsymbol{r}_{MP} = \boldsymbol{r}_P - \boldsymbol{r}_M$, and $r_{MP} = |\boldsymbol{r}_{MP}|$ is the length of the $\overrightarrow{MP}$ vector.

If ρ is a bounded function on S and L, then the I_1 and I_2 improper integrals have the following properties:

1. For $\forall M \in S$ $I_1(M)$ exists (is convergent).
2. For $\forall M \in L$ $I_2(M)$ exists (is convergent).
3. In the exterior of S the function I_1 is infinitely differentiable ($I_2 \in C^{\infty}\left(R^n \setminus S\right)$) in addition the differential of I_1 can be obtained simply by applying the differential operator behind the integral.
4. In the exterior of L the function I_2 is infinitely differentiable ($I_2 \in C^{\infty}\left(R^n \setminus L\right)$), in addition the differential of I_2 can be obtained simply by applying the differential operator behind the integral.
5. The $I_2 \in C^{\infty}\left(R^n \setminus L\right)$, where p is the largest integer with the property that $\alpha + p + 1 < n$.

9. *Theorem – Properties of harmonic functions*

1. Let S be a closed, piecewise C^1 (smooth) surface in G region, $S \subset \Sigma$ and let $\boldsymbol{n}$ be the normal vector of this surface. If $u \in C^2(\Sigma)$ is harmonic on G ($\Delta u(M) = 0, \forall M \in \Sigma$) then:

$$\int_S \frac{\partial u}{\partial \boldsymbol{n}} d\sigma = 0. \tag{20}$$

2. If Σ is a bounded region and $u \in C^2(\Sigma) \cap C^1(\overline{\Sigma})$ is not a constant function, u is harmonic on Σ ($\Delta u(M) = 0, \forall M \in \Sigma$), then the extreme values of u in $\overline{\Sigma}$ region are not realized in Σ, in other words:

$$\min_{P \in \partial\Sigma} u(P) < u(M) < \max_{P \in \partial\Sigma} u(P), \ \forall M \in \Sigma. \tag{21}$$

3. If Σ is a bounded region, $\min_{P \in \partial\Sigma} u(P) < u(M) < \max_{P \in \partial\Sigma} u(P)$ is not a constant function, u is harmonic on $R^n \setminus \overline{\Sigma}$ and $u(\infty) = \lim_{|\boldsymbol{r}_M| \to \infty} u(M) = 0$, then holds the maximum principle:

$$|u(M)| \le \max_{P \in \partial\Sigma} u(P), \ \forall M \in R^n \setminus \Sigma. \tag{22}$$

10. *Theorem - Volume potential*

Let $\Sigma \subset R^3$ be a bounded region, with a piecewise smooth boundary $\partial\Sigma$ (consisting of a finite number of C^1 surface elements). Let $\boldsymbol{r}_M$ and $\boldsymbol{r}_P$ be position vectors of the $M(x,y,z) \in R^3$ and $P(\xi,\eta,\zeta) \in \Sigma$ points, $\boldsymbol{r}_{MP} = \boldsymbol{r}_P - \boldsymbol{r}_M = (\xi - x, \eta - y, \varsigma - z)$, $r_{MP} = |\boldsymbol{r}_{MP}|$ is the length of the $\overrightarrow{MP}$ vector.

If ρ is integrable and bounded on Σ, and in the exterior of Σ it holds that $\rho = 0$, then the

$$V(M) = \iiint_{\Sigma} \frac{\rho(P)}{r_{MP}} dv_P \tag{23}$$

volume potential is defined in all space, $M \in R^3$ and one gets:

1. The first derivatives of V are uniformly convergent then in consequence are continuous functions in the whole space ($V \in C^1(R^3)$). In addition the different partial derivatives of V can be obtained simply by applying the adequate partial differential operator behind the integral:

$$\frac{\partial V}{\partial x}(M) = \iiint_{\Sigma} \rho(P) \frac{\partial}{\partial x}\left(\frac{1}{r_{MP}}\right) dv_P = \iiint_{\Sigma} \rho(P) \frac{\xi - x}{r_{MP}^3} dv_P, \ \forall M \in R^3.$$

$$\frac{\partial V}{\partial y}(M) = \rho(P) \iiint_{\Sigma} \frac{\partial}{\partial y}\left(\frac{1}{r_{MP}}\right) dv_P = \iiint_{\Sigma} \rho(P) \frac{\eta - y}{r_{MP}^3} dv_P, \ \forall M \in R^3. \tag{24}$$

$$\frac{\partial V}{\partial z}(M) = \iiint_{\Sigma} \rho(P) \frac{\partial}{\partial z}\left(\frac{1}{r_{MP}}\right) dv_P = \iiint_{\Sigma} \rho(P) \frac{\varsigma - z}{r_{MP}^3} dv_P, \ \forall M \in R^3.$$

Rewriting (24) in vectorial form we have:

$$\nabla_{r_M} V(M) = \left(\frac{\partial V}{\partial x}, \frac{\partial V}{\partial y}, \frac{\partial V}{\partial z}\right)_{(M)} = \iiint_{\Sigma} \rho(P) \frac{\boldsymbol{r}_{MP}}{r_{MP}^3} dv_P, \ \forall M \in R^3.$$

2. Outside the area Σ the function V is infinitely differentiable, i.e, $V \in C^{\infty}(R^3 \setminus \overline{\Sigma})$. In addition the differential of V can be obtained simply by applying the differential operator behind the integral:

$$D^{\beta} V(M) = \iiint_{\Sigma} \rho(P) \frac{\partial^{|\beta|}}{\partial x^{\beta_1} \partial y^{\beta_2} \partial z^{\beta_3}} \left(\frac{1}{r_{MP}}\right) dv_P, \ \ \forall M \in R^3 \setminus \overline{\Sigma}, \tag{25}$$

where $\beta = (\beta_1, \beta_2, \ldots, \beta_n)$, $|\beta| = \beta_1 + \beta_2 + \ldots + \beta_n$.

3. The behaviour of derivatives in the infinite can be characterized by:

$$D^{\beta} V(M) = O\left(r_M^{-1-|\beta|}\right) \text{ if } r_M \to \infty. \tag{26}$$

4. For β = (2,2,2) based on 2 we can conclude, that V is harmonic in the exterior of region Σ. On $R^3 \setminus \overline{\Sigma}$ the *Laplace equation* holds:

$$\Delta V(M) = \iiint_{\Sigma} \rho(P) \left(\frac{-r_{MP}^2 + 3(\xi - x)^2}{r_{MP}^5} + \frac{-r_{MP}^2 + 3(\eta - y)^2}{r_{MP}^5} + \frac{-r_{MP}^2 + 3(\varsigma - z)^2}{r_{MP}^5} \right) dv_P = 0, \forall M \in R^3 \setminus \overline{\Sigma} \tag{27}$$

5. If $\rho \in C(\overline{\Sigma}) \cap C^1(\Sigma)$ then exists the second partial derivatives of V on Σ ($V \in C^2(\Sigma)$) and the following holds:

$$\Delta V(M) = -4\pi\rho(M), \forall M \in \Sigma \text{ (Poisson equation).} \tag{28}$$

6. Let S be a closed and piecewise smooth surface outside the Σ region ($S \subset R^3 \setminus \overline{\Sigma}$) and let $\boldsymbol{n}$ be normal vector of the S surface, then:

$$\iint_S \frac{\partial V}{\partial \boldsymbol{n}} d\sigma = 0 . \tag{29}$$

7. Based on the maximum principle of harmonic functions we have:

$$|u(M)| \le \max_{P \in \partial\Sigma} u(P), \ \forall M \in R^n \setminus \Sigma . \tag{30}$$

8. Let S be a closed and piecewise smooth surface outside the Σ region ($S \subset R^3 \setminus \overline{\Sigma}$), let $\boldsymbol{n}$ be normal vector of the S surface and let ω be the region enclosed by the S surface, then for every M points of ω we have:

$$V(M) = -\frac{1}{4\pi} \iint_S \left[\frac{1}{r_{MP}} \frac{\partial V}{\partial \boldsymbol{n}} \bigg|_P - V(P) \frac{\partial}{\partial \boldsymbol{n}_P} \left(\frac{1}{r_{MP}} \right) \right] d\sigma_P, \forall M \in \omega, \tag{31}$$

i.e. the volume integral can be expressed as sum of a simple-layer and a double-layer potential.
If S is a potential surface ($V(P) = V_0 = const, \forall P \in S$) and ω is the region enclosed by the S surface, $\boldsymbol{n}$ is the normal vector of the S surface, then

$$V(M) = -\frac{1}{4\pi} \iint_S \frac{1}{r_{MP}} \frac{\partial V}{\partial \boldsymbol{n}} \bigg|_P d\sigma_P, \ \forall M \in \omega,, \tag{32}$$

i.e. the volume integral can be expressed as sum of a simple-layer potential with respect to the potential surface.

Observations

1. Let ρ be bounded and continuous almost everywhere (it is only discontinuous on a set of zero measure, this means that if we choose a random point on the function, the probability that it is continuous is exactly 1, in addition these conditions are sufficient for Riemann integrability of ρ), then the volume potential and its first order partial derivatives exist and are continuous in all space. As consequence of this statement is that the potential and its derivatives are continuous even in those points where for example ρ has a jump. In addition despite the boundary of Σ consisting of points where the function ρ has a discontinuity ($\rho = 0$ in the exterior of Σ, $\rho \neq 0$ in Σ). The volume potential and its first order partial derivatives exist and are continuous on the boundary of Σ.
2. The second order partial derivatives of volume potential are not defined in those points where ρ has a discontinuity, e.g., on the boundary of Σ.
3. $V(\infty) = \lim_{r_M \to \infty} V(M) = 0$.

4. The potential of a sphere with centre in origin, radius R_0 and constant density $\rho \equiv \rho_0$:

$$V(M)=\begin{cases} \dfrac{4\pi\rho_0 R_0^3}{3r_M} & \text{if } r_M \geq R_0 \\ 2\pi\rho_0 R_0^2 - \dfrac{2\pi\rho_0}{3} r_M^2 & \text{if } r_M \leq R_0 \end{cases}.$$

5. In case of two dimensions :

$$V(M)=\iint_S \rho(P)\ln\frac{1}{r_{MP}}d\sigma_P .$$

If $\rho \in C(\bar{S})$, then $V(M)\in C^1(R^2)$ is harmonic on $R^2 \setminus \bar{S}$.
If $\rho \in C^1(\bar{S})$, then $V(M)\in C^2(R^2)$.

11. *Theorem – Simple-layer potential*

Let $\Sigma \subset R^3$ be a region and let $\partial\Sigma$ be a bounded and piecewise smooth two side surface. Let be $M(x, y, z)\in R^3$ and $P(\xi,\eta,\zeta)\in\Sigma$. $\boldsymbol{r}_{MP} = \boldsymbol{r}_P - \boldsymbol{r}_M = (\xi - x, \eta - y, \varsigma - z)$ and $r_{MP} = |\boldsymbol{r}_{MP}|$ is the length of the $\overrightarrow{MP}$ vector.
If μ is continuous on the boundary of G ($\mu\in C(\partial\Sigma)$), then the simple layer potential:

$$V^{(0)}(M)=\iint_{\partial\Sigma}\frac{\mu(P)}{r_{MP}}d\sigma_P \tag{33}$$

is defined in all space $M\in R^3$ and has the following properties:
1. $V^{(0)}\in C(R^3)$.
2. $V^{(0)}(\infty)=0$.
3. $V^{(0)}\in C^\infty(R^3\setminus\partial\Sigma)$ is harmonic in all space excepting the boundary of Σ, i.e.,
$\Delta V^{(0)}(M)=0, \forall M\in R^3\setminus\partial\Sigma$.
4. If $\partial\Sigma$, the boundary of the Σ region, is a bounded, closed, and a C^2 surface, then the directional derivatives of the simple-layer potential along the exterior normal to the $\partial\Sigma$ surface are defined on $\partial\Sigma$ surface. Accordingly we can define the following function:

$$\frac{\partial V^{(0)}}{\partial \boldsymbol{n}}:\partial\Sigma\to R$$

$$\frac{\partial V^{(0)}}{\partial \boldsymbol{n}}(M)=\iint_{\partial\Sigma}\mu(P)\cdot\frac{\partial}{\partial \boldsymbol{n}_M}\left(\frac{1}{r_{MP}}\right)d\sigma_P=\iint_{\partial\Sigma}\mu(P)\cdot\frac{\cos\psi_{MP}}{r_{MP}^2}d\sigma\ ,\ \forall M\in\partial\Sigma, \tag{34}$$

where ψ_{MP} is the angle between the exterior normal to the $\partial\Sigma$ surface at point P and vector $\overrightarrow{MP}$, i.e., $\psi_{MP}=(\boldsymbol{r}_{MP},\boldsymbol{n}_P)$. The function defined in (34) is continous on $\partial\Sigma$ and the following relations hold:

$$\left(\frac{\partial V^{(0)}}{\partial \boldsymbol{n}}\right)_+(M_0)=\lim_{\substack{M\to M_0\\ M\in\Sigma}}\frac{\partial V^{(0)}}{\partial \boldsymbol{n}_{M_0}}(M)=2\pi\mu(M_0)+\frac{\partial V^{(0)}}{\partial \boldsymbol{n}_{M_0}}(M_0), \forall M_0\in\partial\Sigma .$$

$$\left(\frac{\partial V^{(0)}}{\partial \boldsymbol{n}}\right)_-(M_0)=\lim_{\substack{M\to M_0\\ M\in R^3\setminus\bar{\Sigma}}}\frac{\partial V^{(0)}}{\partial \boldsymbol{n}_{M_0}}(M)=-2\pi\mu(M_0)+\frac{\partial V^{(0)}}{\partial \boldsymbol{n}_{M_0}}(M_0), \forall M_0\in\partial\Sigma . \tag{35}$$

5. The formula of the simple-layer potential for two variables:

$$V^{(0)}(M)=\int_{\Gamma}\mu(P)\ln\frac{1}{r_{MP}}dl_P\,, \tag{36}$$

in this case Γ is a planar curve.

6. According to (35) we have:

$$\left(\frac{\partial V^{(0)}}{\partial \boldsymbol{n}}\right)_{+}(M_0)-\left(\frac{\partial V^{(0)}}{\partial \boldsymbol{n}}\right)_{-}(M_0)=4\pi\mu(M_0),\ \forall M_0\in\partial\Sigma\,.$$

Observation

1.The potential of the surface S_{R_0} of the homogeneous sphere (simple-layer potential) with centre in the origin of the coordinate system, with constant density $\mu(M)=\nu_0$ and radius R_0 is:

$$V^{(0)}(M)=\begin{cases}\dfrac{4\pi R_0^2\nu_0}{r_M}=\dfrac{M}{r_M} & \text{if } r_M\geq R_0\\[2ex] 4\pi R_0\nu_0=\dfrac{M}{R_0} & \text{if } r_M\leq R_0\end{cases}$$

, where $M = 4\pi R_0\nu_0$ is the mass distributed on the surface of the sphere.

2. If $\mu\in C(\Gamma)$, then the simple-layer potential for two variables, i.e., in R^2, belongs to the class of function $C(R^2)$ and is harmonic except in Γ.

12. Theorem - Double-layer potential

Let $\Sigma\subset R^3$ be a region, let $\partial\Sigma$ be a bounded and piecewise smooth two side surface. Let be $M(x,y,z)\in R^3$ and $P(\xi,\eta,\zeta)\in\Sigma$. $\boldsymbol{r}_{MP}=|\boldsymbol{r}_{MP}|$ is the length of the $\overrightarrow{MP}$ vector and let $\boldsymbol{n}_P$ be the directional derivatives of simple-layer potential along the exterior normal to the $\partial\Sigma$ surface at point P. If ν is continuous function on the boundary of G ($\nu\in C(\partial\Sigma)$), then the double-layer potential

$$V^{(1)}(M)=\iint_{\partial\Sigma}\nu(P)\frac{\partial}{\partial \boldsymbol{n}_P}\left(\frac{1}{r_{MP}}\right)d\sigma_P=\iint_{\partial\Sigma}\nu(P)\frac{\cos(\boldsymbol{r}_{PM},\boldsymbol{n}_P)}{r_{MP}^2}d\sigma_P \tag{37}$$

exists in all space ($M\in R^3$) and has the following properties:

1. $V^{(1)}(\infty)=0$.

2. $V^{(1)}$ is infinitely derivable and is harmonic in all space without the boundary of Σ

$$V^{(1)}\in C^{\infty}(R^3\backslash\partial\Sigma),\ \Delta V^{(1)}(M)=0,\ \forall\, M\in R^3\backslash\partial\Sigma\,.$$

3. If $\partial\Sigma$ the boundary of Σ is bounded, closed and a C^2 surface, then $V^{(1)}\in C(\partial\Sigma)$ and $V^{(1)}\in C(R^3\backslash\partial\Sigma)$. Approaching $\partial\Sigma$ points from the exterior or interior of the region Σ, we get the limits $V_+^{(1)}$ and $V_-^{(1)}$ for $V^{(1)}$ which are fulfilling the following relations:

$$V_+^{(1)}(M_0)=\lim_{\substack{M\to M_0\\ M\in\Sigma}}V^{(1)}(M)=2\pi\nu(M_0)+V^{(1)}(M_0),\forall M_0\in\partial\Sigma\,.$$

$$V_-^{(1)}(M_0)=\lim_{\substack{M\to M_0\\ M\in R^3\backslash\Sigma}}V^{(1)}(M)=-2\pi\nu(M_0)+V^{(1)}(M_0),\forall M_0\in\partial\Sigma\,. \tag{38}$$

4. The double-layer potential for two variables, i.e., in R^2, is expressed as:

$$V^{(1)}(M)=\int_{\Gamma}\nu(P)\frac{\partial}{\partial \boldsymbol{n}_P}\left(\ln\frac{1}{r_{MP}}\right)dl_P=\int_{\Gamma}\nu(P)\frac{\cos(\boldsymbol{r}_{PM},\boldsymbol{n}_P)}{r_{MP}}dl_P\,, \tag{39}$$

here Γ is a plane curve.

Observation

1. From (38) we can get:

$$V_{+}^{(1)}(M_0)-V_{-}^{(1)}(M_0)=4\pi\mu(M_0),\ \forall M_0\in\partial\Sigma\,.$$

2. In case of a constant $\nu\equiv\nu_0$ density the value of double-layer potential in point *M* is equal with the solid[1] angle $\omega_{\partial G}$ (from which the ∂Σ surface can be visible from the point *M*):

$$V^{(1)}(M)=\nu_0\iint_{\partial\Sigma}\frac{\cos(\boldsymbol{r}_{PM},\boldsymbol{n}_P)}{r_{MP}^2}d\sigma_P=\nu_0\cdot\omega_{\partial\Sigma}(M),\ \forall M\in R^3\setminus\partial\Sigma\,. \tag{40}$$

3. Let $\nu\equiv\nu_0$ be the constant density and let ∂Σ be a bounded, closed and two side C^2 surface, then:

$$V^{(1)}(M)=\begin{cases}-4\pi\nu_0 & \text{if } M\in\mathrm{Int}(\Sigma)\\ -2\pi\nu_0 & \text{if } M\in\partial\Sigma\\ 0 & \text{if } M\in\mathrm{Ext}(\Sigma)\end{cases}. \tag{41}$$

This means that the constant density induce a constant potential function on the three disjoint regions: ∂Σ, Ext(Σ), Int(Σ). Let these values be $V_{\partial\Sigma}^{(1)}$, $V_{\mathrm{Ext}(\Sigma)}^{(1)}$, $V_{\mathrm{Int}(\Sigma)}^{(1)}$ respectively. Using (41) we can get:

$$\begin{aligned}V_{\mathrm{Ext}(\Sigma)}^{(1)}&=V_{\partial\Sigma}^{(1)}+2\pi\nu_0\\ V_{\mathrm{Int}(\Sigma)}^{(1)}&=V_{\partial\Sigma}^{(1)}-2\pi\nu_0\end{aligned}. \tag{42}$$

The expressions of (41) and (42) in R^2 are:

$$V^{(1)}(M)=\begin{cases}-2\pi\nu_0 & \text{if } M\in\mathrm{Int}(\Sigma)\\ -\pi\nu_0 & \text{if } M\in\partial\Sigma\\ 0 & \text{if } M\in\mathrm{Ext}(\Sigma)\end{cases}, \tag{43}$$

$$\begin{aligned}V_{\mathrm{Ext}(\Sigma)}^{(1)}&=V_{\partial\Sigma}^{(1)}+\pi\nu_0\\ V_{\mathrm{Int}(\Sigma)}^{(1)}&=V_{\partial\Sigma}^{(1)}-\pi\nu_0\end{aligned}. \tag{44}$$

4. In R^2 holds a relation similar to (38) with π instead of 2π.

5. In R^2 space in case of a constant $\nu\equiv\nu_0$ density the value of the double-layer potential in a point *M* is equal with the angle described by the *MP* segment while the point *P* runs over the Γ curve:

$$V^{(1)}(M)=\int_{\Gamma}\nu(P)\frac{\cos(\boldsymbol{r}_{PM},\boldsymbol{n}_P)}{r_{MP}}dl_P=P_1MP_2\,,$$

where P_1 and P_2 are the start and end points of the Γ arc.

[1] The solid angle ω subtended by a surface ∂Σ is defined as the surface area of a unit sphere centered at the observation point *M* covered by the surface projection onto the sphere along the line connecting ∂Σ with M

1.2 The analytical formulas of gravitational potential and its derivatives of the homogeneous polyhedron volume element

The notation in this section follows the notation presented by Pohànka (1988), Holstein and Ketteridge (1996), Holstein et al. (1999) and Holstein (2002a, 2002b). The vector analysis tools were used in the deduction of formulas instead of other methods like the coordinate geometry in order to avoid the coordinate transformations.

The computations were performed on an Hp Unix 11.i system, A-Class 1440 MHz PA 8500 CPU processor and the programs were written in the HP Fortran programming language.

In the Section 1.2.1 is presented a review of literature regarding to the gravitational potential of a polyhedron and its derivatives. The object of Section 1.2.2 is to give the domain of definition of these functions based on theorems of potential theory. The notation used in deduction of analytical formulas of the gravitational potential and its derivatives is presented in Section 1.2.3.

The analytical formulas are deduced converting the volume integral to surface integrals (divergence theorem) and those to line integrals (Stokes or Gauss-Ostrogradsky theorem). The formally different analytical formulas found in the literature arise from the different strategies for the reduction of the initial 3D integral to 1D integrals. The Section 1.2.4 consists of the general solution of the differential equation needed for the Gauss-Ostrogradsky theorem. The different kind of particular solutions of the differential equation can provide different solutions presented e.g., by Pohànka (1988), Götze and Lahmeyer (1988), Petrovič (1996). Holstein (2002a) introduced the (C_{ij}, Ω_{ij}) constant system which will be presented in this section. Guptasarma and Singh (1999) and Singh and Guptasarma (2001) derived analytical formulas up to first derivatives of gravitational potential, which were completed in this work with the analytical formulas of second order derivatives. Werner and Scheeres (1997) discussed in detail the geometrical interpretation of the constant Ω_i. Holstein (2002a, 2002b) introduces the vector invariant quantities which allows to describe the gravitational potential and its first and second derivatives in terms of these quantities. In Section 1.2.6 the simplification of analytical formulas of gravitational potential and its first and second derivatives are given taken into account the reductions due to common edges based on the the work of Werner and Scheeres (1997). In the Section 1.2.7 a different way of deduction of the analytical formulas of first derivatives of potential is presented. Holstein (2002b) deduces two different analytical expressions of first derivatives of gravitational potential using the vector invariants. In this section the formulas of first derivatives of gravitational potential were deduced in some other way such as by using a proper local coordinate system, or based on geometrical interpretation, or using dyads. In the Section 1.2.8 the analytical expression of second order derivatives of potential is presented. Section 1.2.9 deals with the different analytical formulas of constants (C_{ij}, Ω_{ij}) found in the literature, with the domain of definition of these constants and the domain of stability of analytical expression of particular constants. In Section 1.2.10 the numerical instability of constants far from the source is investigated that increases with the distance from the target, while the anomaly decreases. Similarly the numerical instability near to the target is presented too. A limited range of target distances beyond which the calculations are dominated by rounding error are determined for the mentioned two extreme positions of the computation point regarding the gravitational source. Holstein and Ketteridge (1996) and Holstein et al. (1999) describe the magnitude of numerical errors of analytical formulas of first derivatives of gravitational potential by an exponential function of two parameters, one the distance of the gravitational source from observation point and the second the source dimension. This relation was proved by the authors theoretically and confirmed by model computation. The model computation given by Holstein et al. (1999) was reproduced with a self-written program in Fortran-Programming languages. We repeat the model computation considering the exponent of above mentioned function as a parameter. In this way we can estimate the exponent parameter belonging to the potential and belonging to the second derivatives of potential. These exponential relations with the estimated exponent can provide the limit of the distance of the observation point and the arbitrary gravitational source for which the computational error (computational error = theoretical value – computed value) is beyond an a priori chosen p percent. In addition we have proved that the numerical error committed in the gravity field related quantities with the realistic ALCAPA density model (Benedek and Papp

2009) is below 1%. Pohànka (1988) investigated the error induced by small ε quantities introduced to avoid the singularities of analytical expression for the first derivatives of potential. A similar investigation to estimate the error due to the ε quantity in the analytical formulas of potential and its second derivatives of its are presented in Section 1.2.11. We investigated numerically the value of ε for which the committed numerical error will be the same order of magnitude as the ε. We compare the computational time of different analytical expressions of C_{ij} and Ω_{ij}. In Section 1.2.12 we describe the algorithm for computation of the potential and its first and second derivatives in case of the special polyhedron with five faces. Furthermore in Section 1.2.12 we present our algorithm for determination of face positive orientation in case of general polyhedron (convex or concave polyhedron with an arbitrary number of faces) and the face normal vector consistent with this orientation.

1.2.1 Overview of the literature

Prisms are mainly used for local modelling if flat earth approximation based on planar geodetic coordinates is allowed. Nagy et al. (2000) gave an extended reference of the earliest applications of prisms in gravity field modelling. The paper of Zach (1811) can be mentioned as the earliest publication in this area. Beyond rectangular prisms the polyhedrons or tesseroids can also be used to discretize the density distribution of 3D models to describe adequately the geological structures. The polyhedron is a relatively new volume element (Okabe 1979, Cady 1980). Its application improves the geometrical description of the bounding surfaces (density interfaces) compared to flat topped rectangular prisms because it is able to provide continuity where it is reasonable. The spatial resolution of the model can be arbitrarily synchronized to the resolution of the available geometrical data (points of the interfaces) and physical parameters (e.g. mass density distribution). Furthermore, the effect of the Earth's curvature can easily be taken into account in the computations (Benedek and Papp 2009), because the polyhedral geometry allows the description of any density model not only in a local (planar) but in a global geodetic coordinate system (e.g. WGS84) too. Analytical expressions for the gravitational field of a polyhedral body with either linearly or non-linearly varying density are also available (Garcia-Abdealem, 1992, 2005, Pohànka 1998, Hansen 1999, Holstein 2003, Zhou 2009). This improvement enables the modelling of the continuous density variation inside the volume element if geology justifies its existence.

The modelling of the gravitational field of the asteroid 4769 Castalia is an example of the application of the polyhedron volume element in space geodesy. The surface of asteroid was described by a polyhedral surface with 3300 faces (Werner and Scheeres 1997). Hikida and Wieczorek (2007) describe the crust-mantle boundary by polyhedron faces and the crust-mantle boundary is determined by inversion.

Although very complex modeller systems equipped by graphical user interface, like IGMAS (Götze and Lahmeyer 1988) also exist and are available for the research community, basic research usually needs high flexibility in program coding to defer to the continuously varying requirements and aims (http://www.gravity.uni-kiel.de/igmas/). Mahatsente et al. (1999), Kuder (2002), Ebbing and Götze (2001) present applications of this program.

In the direct (forward) modelling in general the gravitational potential and its derivatives generated by certain homogeneous volume elements (prism, polyhedron, tesseroid etc) are computed analytically or numerically (expanding the gravitational potential into a harmonic series). The latter one can be realised by spherical harmonics expansion of the gravitational potential generated by the volume element (MacMillan 1958) which is an approximation of exact analytical formula due to the fact that only a finite number of terms are taken into account in the expansion. The error of approximation increases and its convergence is slow near the boundary of the convergence region (the exterior of the sphere which includes the volume element). The series is divergent outside the convergence region and numerically unstable, i.e. any mass rearrangement can induce the divergence of the series. Another way to approximate the gravitational potential generated by irregular volume elements is the substitution of a continous mass distribution with discrete point masses. The advantage of the point masses approximation is the convergence of gravitational potential with increasing the number of point masses, the drawback is the very slow convergence with increasing the computation

point distance from the source. Furthermore in the vicinity of the source the point mass approximation of the gravitational field suffers from spectral distortion (Papp and Wang 1996).

Similar to the prism the gravitational potential and its derivatives generated by a polyhedron can be described analytically. From Theorem 9 of potential theory discussed in Section 1.1.1 we can deduce that the potential and its first derivatives are continuous in all space (in R^3). Therefore the analytical formulas of these functions can be extended continuously to the whole space (Nagy et al. 2000). In case of the second derivatives of potential the domain of discontinuity is the polyhedron surface. In these points the second derivatives have a discontinuity of the second kind.

In the literature we can find several formally different analytical expressions published in papers by Paul (1974), Barnett (1976), Okabe (1979), Götze and Lahmeyer (1988), Pohànka (1988), Kwok (1991a, 1991b), Ivan (1996), Holstein and Ketteridge (1996), Petrovič (1996), Tsoulis and Petrovič (2001), Werner and Scheeres (1997), Holstein et al. (1999), Holstein (2002a, 2002b), Guptasarma and Singh (1999), Singh and Guptasarma (2001), Furness (2000). The equivalence of the different analytical expressions of gravitational potential and its derivatives given in these publications will be discussed in the following sections. All the analytical formulas are obtained transforming the volume integral to line integrals. This can be realised in two steps, first the volume integral is transformed to a surface integral using the Gauss-Ostrogradsky theorem (Theorem 1 in Section 1.1.1) excepting Furness (1994), where this transformation is realised applying the Green theorem (Theorem 3). Then the surface integral is calculated directly (Paul 1974, Barnett 1976) or is transformed to line integrals applying the Stokes (Theorem 2) or the Gauss-Ostrogradsky formula (Theorem 1 for $n = 2$). Werner and Scheeres (1997) present the deduction of analytical formulas of second order of derivatives of gravitational potential, Holstein (2002a, 2002b) gave these formulas using the concept of vector invariant by means of which the analytical formulas become a linear combination of them. This kind of expression is very advantageous from a programming point of view. Formally the different analytical formulas for gravitational potential and its derivatives given in the literature in fact are the primitive function of a volume integral, because these analytical expressions are identical aside from a constant on their common domain of definition. These identities will be demonstrated during this work. In the mentioned publications the analytical expressions of gravitational potential and its derivatives are deduced for a general polyhedron volume element. Paul (1974) and Barnett (1976) gave solutions valid for a special polyhedron with triangular faces.

From a programing point of view the simplification of analytical formulas means implementation of vector analysis instead of the application of coordinate geometry. Furthermore the analytical formulas written in vectorial form are more simple (Götze and Lahmayer 1988, Pohànka 1988, Petrovič 1996, Tsoulis and Petrovič 2001, Werner and Scheeres 1997, Holstein et al. 1999, Holstein 2002a,b, Guptasarma and Singh 1999, Singh and Guptasarma 2001, Furness 2000). Kwok (1991a, 1991b) use the complex analysis tools to deduce the formulas. The authors not always give the maximal domain of definition concerning to the analytical expression of gravity related quantities. Paul (1974) and Götze and Lahmeyer (1988) gave the exterior domain of polyhedron as domain of definition of first derivatives of potential. Barnett (1976) applied a larger domain of definition as the union of exterior and interior domain of polyhedron. Okabe (1979) gave the maximal feasible domain of definition for the first and second derivatives of gravitational potential generated by a polyhedron. In case of first derivatives the maximal domain is the whole space, while in case of second derivatives as the maximal feasible domain the union of interior and exterior of polyhedron is given.

The error analysis of analytical formulas of gravitational potential and its first derivatives are investigated too (Holstein and Ketteridge 1996, Holstein et al. 1999). The relation between the rate of numerical error and the geometrical parameters defining the position of computation point relative to the polyhedron volume element is deduced.

The calculation of the closed formulae given for the gravitational potential and its higher order derivatives, however, needs more runtime than that of the rectangular prism computations. But the new computational feasibility (parallel programing, largest memory capacity) allows the applicability in 3D gravitational modelling in regional and even in global scale of polyhedron

1.2.2 The analytical properties of gravitational potential and its derivatives based on theorems of potential theory

In general in the gravitational modelling the computation of gravity field parameters is limited to the exterior of mass sources (e.g. the exterior or the surface of Earth) which means the limitation of analytical expressions of gravitational potential or its derivatives on the exterior domain of volume elements. But certain investigations (for example the plumbline modelling) make it necessary to extend the computational domain to the interior of the masses. Therefore is important to give the maximal feasible domain of definition derived from the potential theory where the gravitational potential and its derivatives are defined. In case of existence of analytical formulas describing the gravity field related quantities generated by a source model (e.g. prism, polyhedron) we have to distinguish the *domain of definition of the analytical expression* which is a subset of the *domain of definition deduced from potential theory* of the gravitational functions(Nagy et al. 2000). Is important to compare these two sets and investigate the limits of the analytical expressions in points which are not belonging to the domain of definition of analytical expression but they are point of domain derived from potential theory. In the following we will discuss in detail the domain of definition of gravitational potential and its derivatives generated by a polyhedron based on potential theory.

The gravitational potential generated by a homogeneous polyhedron volume element ($\rho \equiv \rho_0, \forall P \in \Sigma \subset R^3$) is described by the volume integral given in Theorem 10:

$$U(M) = G \iiint_{\Sigma} \frac{\rho_0}{r_{MP}} dv_P = G\rho_0 \iiint_{\Sigma} \frac{1}{r_{MP}} dv_P , \tag{45}$$

where $U(M)$ is the gravitational potential in the observation point M, G is the gravitational constant, Σ ($\Sigma \subset R^3$) denotes the body of the polyhedron, $\boldsymbol{r}_{MP} = \boldsymbol{r}_P - \boldsymbol{r}_M$, $r_{MP} = |\boldsymbol{r}_{MP}|$ is the vector and its norm determined by the an arbitrary point of polyhedron P and the observation point M.

Since the $\rho \equiv \rho_0$ constant density function fulfils the $\rho \in C(\overline{\Sigma}) \cap C^1(\Sigma)$ condition, by right of Theorem 10 the following statements are valid:

1. U and its partial derivatives are continuous functions in all space, namely:

$$U \in C^1(R^3).$$

From this arise the next important issue: The gravitational force between the homogeneous polyhedron mass and the unit mass in M is given by the formula:

$$\boldsymbol{F}(\boldsymbol{r}_M) = \nabla_{\boldsymbol{r}_M} U(M) = G\rho_0 \iiint_{\Sigma} \nabla_{\boldsymbol{r}_M} \left(\frac{1}{r_{MP}} \right) d\, v_P = -G\rho \iiint_{\Sigma} \frac{\boldsymbol{r}_{MP}}{r_{MP}^3} d\, v_P , \; M \in R^3 \tag{46}$$

and is defined and continuous in the whole space.

2. U is infinitely differentiable on exterior of Σ:

$$U \in C^{\infty}(R^3 \setminus \overline{\Sigma}). \tag{47}$$

3. U is harmonic function on exterior of Σ:

$$\Delta U(M) = 0 \text{ (Laplace equation).} \tag{48}$$

4. The second order partial derivatives of U are continuous in interior of Σ and it holds:

$$\Delta U(M) = -4\pi\rho_0 G , \; \forall M \in \Sigma \text{ (Poisson equation).} \tag{49}$$

5. $U(\infty) = \lim_{r_M \to \infty} U(M) = 0$. (50)

6. $\left|U(M)\right| \le \max_{P\in\partial\Sigma} U(P),\ \forall M \in R^3 \setminus \Sigma$. (51)

1.2.3 The scalar and vectorial quantities assigned to the polyhedron

According to the polyhedron definition its surface can be given as the union of polygonal planes. Since any non-convex polyhedron can be split into a finite number of convex polyhedrons without limiting generality all the following statements are demonstrated only for the convex case. In the case of convex polyhedron denoted by Σ the polygonal faces are also convex sets, so:

$$\partial\Sigma = \bigcup_{i=\overline{1,n}} S_i ,$$

where S_i is the ith convex polygonal face, n is the number of polyhedron faces. Let $l(i)$ be the number of edges and let L_{ij} be one of the edges of S_i, i.e:

$$\partial S_i = \bigcup_{j=\overline{1,l(i)}} L_{ij} .$$

Let j be the index of an edge of the ith face (Fig. 2), let M_i be the projection of M point onto the S_i face ($M_i = \text{proj}_{S_i} M$) and let M_{ij} be the projection of M_i onto the L_{ij} edge ($M_{ij} = \text{proj}_{L_{ij}} M$) (Fig. 3). Let $P \in \Sigma$ be an arbitrary point of polyhedron. In the following we list the vector and scalar quantities used in this work and its geometrical interpretation:

$\boldsymbol{r}_{MP}$, r_{MP}	is the vector and its norm determined by the an arbitrary point of polyhedron P and the observation point M
$\boldsymbol{a}_{ij}$	is the position of vector that represents the position of the jth vertex of ith polygonal face in relation to the origin of coordinate system
$\boldsymbol{n}_i$	is the normal vector of S_i polygonal face
$\boldsymbol{l}_{ij}$, $\boldsymbol{\mu}_{ij}$	is the directed line segment L_{ij} and the unit vector of this. Directions of $\boldsymbol{l}_{ij}$ and $\boldsymbol{\mu}_{ij}$ vectors are defined by the positive direction of the boundary of polygonal face ∂S_i. If you walk in the positive direction around ∂S_i with your head pointing in the direction of $\boldsymbol{n}_i$, the surface will always be on your left
($\boldsymbol{\mu}_{ij}$, $\boldsymbol{n}_i$, $\boldsymbol{v}_{ij}$)	is the right-handed orthonormal basis assigned to the $L_{i,j}$ segment, so that $\boldsymbol{v}_{ij} = \boldsymbol{\mu}_{ij} \times \boldsymbol{n}_i$
$\boldsymbol{r}_{1ij}$, $\boldsymbol{r}_{2ij}$	are the vectors determined by the vertices of segment L_{ij} and the observation point M
$\boldsymbol{r}_{0ij}$, r_{0ij}	is the vector determined by the M_{ij} and the M points and its vector norm
$\boldsymbol{s}_{MP}$, s_{MP}	is the vector determined by an arbitrary point of polyhedron $P \in S_i$ and the $M_i = \text{proj}_{S_i} M$ point and its vector norm
h_i	is the signed distance of M point from the S_i face, i.e $h_i = \text{proj}_{\boldsymbol{n}_i} r_{MP}$ where $P \in S_i$ is an arbitrary point. The h_i is negative, if M is situated in the half-space defined by S_i plane and determined by the pointing direction of S_i surface normal $\boldsymbol{n}_i$
h_{ij}	is the signed distance of M_i pointed to the L_{ij} segment, i.e $h_{ij} = \text{proj}_{\boldsymbol{v}_{ij}} r_{MP}$ where $P \in S_i$ is an arbitrary point. The h_{ij} is positive if M_i is situated in the half-pane defined by the L_{ij} segment which includes the S_i polygonal face, otherwise h_{ij} is negative. h_{ij} is independent from the $P \in L_{ij}$ point
l_{ij}	is the length of the L_{ij} segment

l	is the signed distance of $P \in L_{ij}$ point from the M_{ij} point
l_{1ij}, l_{2ij}	are the projection (signed distance) of $\boldsymbol{r}_{1ij}$ and $\boldsymbol{r}_{2ij}$ vectors to the $\boldsymbol{l}_{ij}$ vector, i.e $l_{1ij} = vet_{\boldsymbol{r}_{1ij}} \boldsymbol{l}_{ij}$ and $l_{2ij} = vet_{\boldsymbol{r}_{2ij}} \boldsymbol{l}_{ij}$
Δ_{klij}	the triangular faces enclosed by the projection of $\boldsymbol{r}_{kij}$, $\boldsymbol{r}_{lij}$ vectors to the S_i plane, where $k,l = \overline{0,2}, k \neq l$

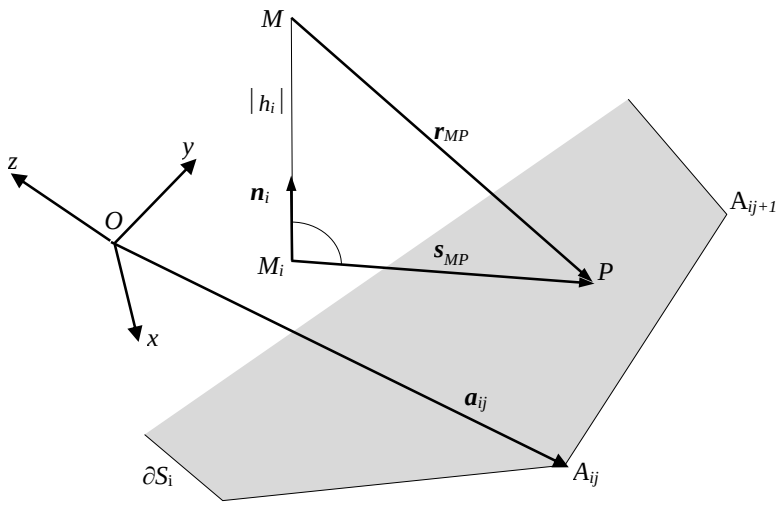

Fig. 2 The scheme of S_i polygonal face and ∂S_i boundary polygonal line. M is an arbitrary point in the space, M_i is its projection on the S_i plane, P is an arbitrary point belonging to the polygonal face

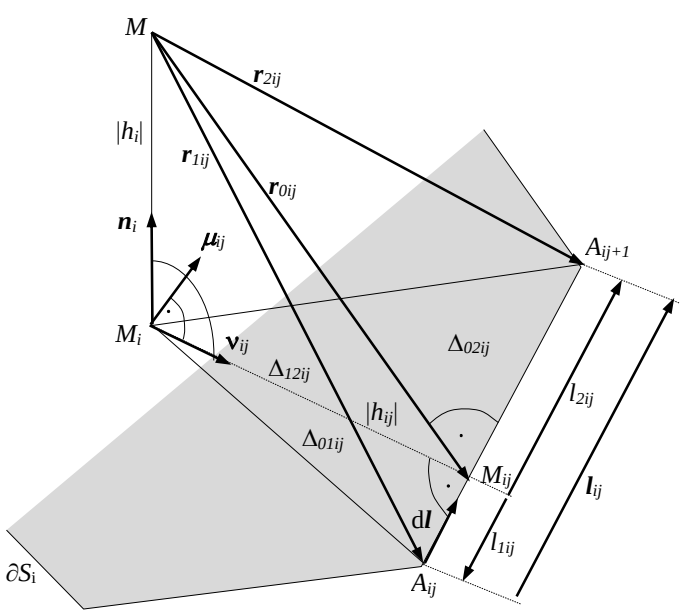

Fig. 3 Represents the scalar and vectorial quantities belonging to the L_{ij} segment. ($\boldsymbol{\mu}_{ij}$, $\boldsymbol{n}_i$, $\boldsymbol{\nu}_{ij}$) is a right-handed orthonormal system. $\mathbf{r}_{1ij}$ and $\mathbf{r}_{2ij}$ are vectors determined by the ij vertices and the M point. Δ_{01ij}, Δ_{02ij}, Δ_{12ij} denotes successively the $M_iM_{ij}A_{ij+1}$, $M_iM_{ij}A_{ij+1}$ and $M_iA_{ij}A_{ij+1}$ triangular faces

In the algorithm developed by myself computing the polyhedron gravitational field parameters the polyhedron is defined by the coordinates of vertices. For each face is given the list of vertices which define the orientation of the polygonal line. In the following the face i is considered fixed. In case of convex polyhedron all faces are convex polygons so the normal vector of vectorial product of any two consecutive vertex vectors (e.g. $\boldsymbol{l}_{i1}^0 = \boldsymbol{a}_{i2}^0 - \boldsymbol{a}_{i1}^0, \boldsymbol{l}_{i2}^0 = \boldsymbol{a}_{i3}^0 - \boldsymbol{a}_{i2}^0$, where the 0 upper index indicates the initial orientation of the closed polygonal line) gives a vector perpendicular to the S_i plane additionally these three vectors form an right-handed system. In the following we need the external normal vector of face i, so it is necessary to check the previously determined direction and change it if necessary. As a first step we choose arbitrarily an inner point of the polyhedron, let the geometric centre (centroid) be this point. Using the convexity condition of polyhedron, the decision of correctness of direction of vectorial product defined by the initial orientation of polygonal line can be reduced to verifying if this direction points in the opposite half-space limited by S_i and the centroid. If the direction points in the half-space limited by S_i the vectorial product gives the inner normal vector, in this case we have to change the initial orientation of ∂S_i polygonal line and otherwise the initial orientation will remain unchanged. We repeat for every face the same procedure, which in mathematical formulation means:

$f\left(\boldsymbol{a}_{i1} + \boldsymbol{l}_{i1} \times \boldsymbol{l}_{i2}\right) \cdot f\left(x_G, y_G, z_G\right) < 0$, where $f(x,y,z) = \begin{vmatrix} x & y & z & 1 \\ x_{i1} & y_{i1} & z_{i1} & 1 \\ x_{i2} & y_{i2} & z_{i2} & 1 \\ x_{i3} & y_{i3} & z_{i3} & 1 \end{vmatrix}$, x_{ij}, y_{ij}, z_{ij} are the components of the $\boldsymbol{a}_{ij}$ vector, j=1,2,3 or any other three arbitrary points of the ith face, $\left(x_G, y_G, z_G\right) = \sum_{i=1}^{n} \frac{\sum_{j}^{l(i)+1} \boldsymbol{a}_{ij}}{l(i)+1} \Big/ n$,

where n is the number of faces, $l(i)$ is the number of edges of ith face, i, j denotes consecutively the face and the vertex indices belonging to a certain face. If the inequality is fulfilled the initial orientation of S_i is retained, so the final vertices ordering (positive direction) and the external normal of S_i are: $\boldsymbol{a}_{ij} = \boldsymbol{a}_{ij}^0$, $\boldsymbol{l}_{ij} = \boldsymbol{l}_{ij}^0$, $j = \overline{1, l(i)}$ and $\boldsymbol{n}_i = \frac{\boldsymbol{l}_{i1} \times \boldsymbol{l}_{i2}}{\left|\boldsymbol{l}_{i1} \times \boldsymbol{l}_{i2}\right|}$. Otherwise $\boldsymbol{a}_{ij} = \boldsymbol{a}_{i\,l(i)+2-j}^0$, $j = \overline{2, l(i)}$, $\boldsymbol{l}_{ij} = -\boldsymbol{l}_{ij}^0$ and $\boldsymbol{n}_i = -\frac{\boldsymbol{l}_{i1}^0 \times \boldsymbol{l}_{i2}^0}{\left|\boldsymbol{l}_{i1}^0 \times \boldsymbol{l}_{i2}^0\right|} = \frac{\boldsymbol{l}_{i1} \times \boldsymbol{l}_{i2}}{\left|\boldsymbol{l}_{i1} \times \boldsymbol{l}_{i2}\right|}$ (Fig. 4). In case of concave polygonal faces the vectorial product can be determined using Pohànka (1988) formula: $\boldsymbol{n}_i = \sum_{j=2}^{l(i)-1} \left(\boldsymbol{a}_{ij} - \boldsymbol{a}_{i1}\right) \times \left(\boldsymbol{a}_{ij+1} - \boldsymbol{a}_{i1}\right) \Big/ \left| \sum_{j=2}^{l(i)-1} \left(\boldsymbol{a}_{ij} - \boldsymbol{a}_{i1}\right) \times \left(\boldsymbol{a}_{ij+1} - \boldsymbol{a}_{i1}\right) \right|$.

Supposing a bounded model, the concave polyhedron can be inscribed in the $[x_{\min}, x_{\max}] \times [y_{\min}, y_{\max}] \times [z_{\min}, z_{\max}]$ prism, where $x_{\max} = \max \left\{ x_P \mid P\left(x_P, y_P, z_P\right) \in \Omega \right\}$ and $x_{\min} = \min \left\{ x_P \mid P\left(x_P, y_P, z_P\right) \in \Omega \right\}$ denotes the maximum and the minimum of x coordinates of polyhedron vertices. Similarly we define the $y_{\max}$, $y_{\min}$, $z_{\max}$, $z_{\min}$ values. Accordingly $T(x_{\max}, y_{\max}, z_{\max})$ will belong to the exterior domain of the polyhedron. Straight lines are taken extending from this point indefinitely in directions determined by each face inner point e.g. by its centroid in case of convex face. The next steps are to marking of normal vector belonging to polyhedron faces:

1. One arbitrary face and its arbitrary inner point P (e.g. the face geometric centre in case of convex face) is fixed.
2. We determine the number of intersection T_i of the half-line belonging to the fixed face with the other faces of the polyhedron (Fig.4).
3. Once the distance is determined for all these points from the T point, then the T_i points are ordered on the basis of their respective distances with the T point, the point having the smallest distance is ranked first. Using the fact that the T_{i-1} T_i segments alternate from outside to inside in successive

set $|TT_1|$ is situated in the exterior domain of polyhedron, $|T_1T_2|$ is situated in the inner domain of polyhedron, $|T_2T_3|$ is situated in the exterior domain of polyhedron and so on (Fig.4).

4. After the ranking step the rank order of point P is checked. In case of even order the direction of the normal vector of fixed face points in opposite direction with semi-space determined by the fixed face and the T point, otherwise the normal vector points in this semi-space. In other words we determine the normal vector pointing in the exterior domain of polyhedron and the positive orientation for each of the faces.

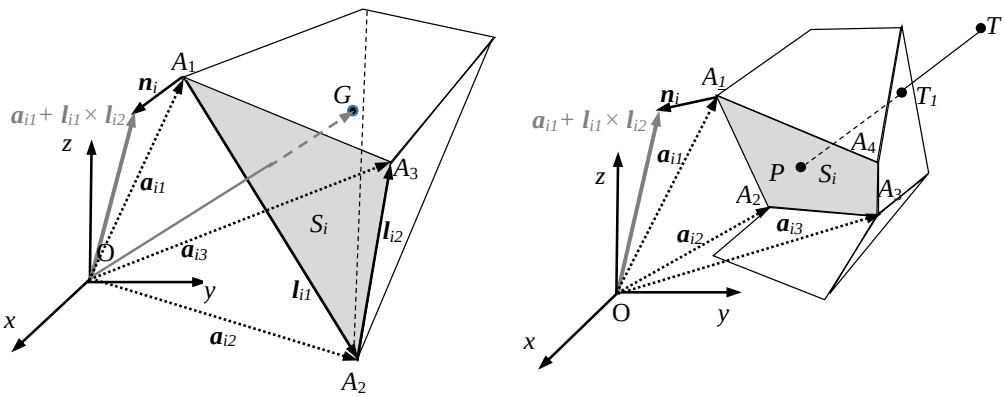

a) b)

Fig. 4 Determination of the normal vector of S_i face pointing into the exterior domain of polyhedron in case of a) convex and b) concave body

The expression of vector quantities belonging to the Fig. 2 and Fig. 3 are listed below:

$$r_{MP} = \boldsymbol{r}_P - \boldsymbol{r}_M,\ r_{MP} = \left|\boldsymbol{r}_P - \boldsymbol{r}_M\right|,$$

$$\boldsymbol{l}_{ij} = \boldsymbol{a}_{ij+1} - \boldsymbol{a}_{ij},\ l_{ij} = \left|\boldsymbol{a}_{ij+1} - \boldsymbol{a}_{ij}\right|,$$

$$\boldsymbol{n}_i = \frac{\boldsymbol{l}_{i1} \times \boldsymbol{l}_{i2}}{\left|\boldsymbol{l}_{i1} \times \boldsymbol{l}_{i2}\right|},\ \boldsymbol{\mu}_{ij} = \frac{\boldsymbol{a}_{ij+1} - \boldsymbol{a}_{ij}}{\left|\boldsymbol{a}_{ij+1} - \boldsymbol{a}_{ij}\right|},\ \boldsymbol{v}_{ij} = \boldsymbol{\mu}_{ij} \times \boldsymbol{n}_i,$$

$$\boldsymbol{r}_{1ij} = \boldsymbol{a}_{ij} - \boldsymbol{r}_M,\ \boldsymbol{r}_{2ij} = \boldsymbol{a}_{ij+1} - \boldsymbol{r}_M,$$

$$r_{0ij} = \left|\boldsymbol{r}_{1ij} \times \boldsymbol{\mu}_{ij}\right|,\ h_i = \boldsymbol{r}_{MP} \cdot \boldsymbol{n}_i = \boldsymbol{r}_{1ij} \cdot \boldsymbol{n}_i = \boldsymbol{r}_{2ij} \cdot \boldsymbol{n},\ h_{ij} = \boldsymbol{r}_{1ij} \cdot \boldsymbol{v}_{ij},\ P \in S_i,$$

$$l_{1ij} = \boldsymbol{r}_{1ij} \cdot \boldsymbol{\mu}_{ij},\ l_{2ij} = \boldsymbol{r}_{2ij} \cdot \boldsymbol{\mu}_{ij} = l_{1ij} + l_{ij},$$

where r_{MP}, r_{0ij}, l_{ij} are positive scalar quantities, the sign of h_i, h_{ij}, l_{1ij}, l_{2ij} quantities depends on the position of computation point M, on the S_i plane and on the L_{ij} edge.

1.2.4 Review of different demonstration techniques of the analytical formulas of gravitational potential generated by a polyhedron volume element

The gravitational potential in the observation point M generated by a polyhedron volume element Σ is described by a volume integral. The analytical expression of volume integral can be obtained transforming the volume integral to line integrals. This can be realised in two steps, first the volume integral is transformed into a surface integral. We start with the formula:

$$U(M) = G\rho_0 \iiint_{\Sigma} \frac{1}{r_{MP}} dv_P = \frac{G\rho_0}{2} \iiint_{\Sigma} \nabla_{r_P} \cdot \frac{\boldsymbol{r}_{MP}}{r_{MP}} dv_P. \tag{52}$$

Following we used the relations:

$$\frac{\partial r_{MP}}{\partial \xi}=\frac{\xi-x}{r_{MP}}\,,\ \frac{\partial r_{MP}}{\partial \eta}=\frac{\eta-y}{r_{MP}}\,,\ \frac{\partial r_{MP}}{\partial \zeta}=\frac{\zeta-z}{r_{MP}}\ \text{and}$$

$$\nabla_{r_P}\cdot\frac{\boldsymbol{r}_{MP}}{r_{MP}}=\frac{\partial}{\partial \xi}\left(\frac{\xi-x}{r_{MP}}\right)+\frac{\partial}{\partial \eta}\left(\frac{\eta-y}{r_{MP}}\right)+\frac{\partial}{\partial \zeta}\left(\frac{\zeta-z}{r_{MP}}\right)=\frac{2}{r_{MP}}\,,$$

where $M(x,y,z)$ is the observation point, $P(\zeta,\eta,\varsigma)\in\Sigma$ is an arbitrary point of polyhedron volume element.

If $M\in Ext\Sigma$ is situated in the exterior domain of polyhedron body Σ, then $\frac{\boldsymbol{r}_{MP}}{r_{MP}}$ is defined on Σ and fulfils the condition of the Gauss-Ostrogradsky theorem (Theorem 1), so we have:

$$\iiint_{\Sigma}\nabla_{r_P}\cdot\frac{\boldsymbol{r}_{MP}}{r_{MP}}dv_P=\iint_{\partial\Sigma}\frac{\boldsymbol{r}_{MP}}{r_{MP}}d\boldsymbol{\sigma}_P\,. \tag{53}$$

If $M\in \mathrm{Int}\Sigma$ is situated in the interior domain of Σ, then $\frac{\boldsymbol{r}_{MP}}{r_{MP}}$ is not defined in the point $P=M$, thus it does not fulfill the condition of Gauss-Ostrogradsky theorem in Σ domain. The theorem can be applied on a proper subset $\Sigma_\varepsilon=\Sigma\setminus\mathscr{B}(M,\varepsilon)$, where $\mathscr{B}(M,\varepsilon)$ is an 3-dimensional open ball of radius ε and center M:

$$\iiint_{\Sigma_\varepsilon}\nabla_{r_P}\cdot\frac{\boldsymbol{r}_{MP}}{r_{MP}}dv_P=\iint_{\partial\Sigma_\varepsilon}\frac{\boldsymbol{r}_{MP}}{r_{MP}}d\boldsymbol{\sigma}_P\,.$$

If the radius of ball gets close to zero, the following relations are valid:

$$U(M)=\lim_{\varepsilon\to 0}\iint_{\Sigma_\varepsilon}\nabla_{r_P}\cdot\frac{\boldsymbol{r}_{MP}}{r_{MP}}dv_P=\lim_{\varepsilon\to 0}\iint_{\partial\Sigma_\varepsilon}\frac{\boldsymbol{r}_{MP}}{r_{MP}}\cdot d\boldsymbol{\sigma}_P=\lim_{\varepsilon\to 0}\left(\iint_{\partial\Sigma}\frac{\boldsymbol{r}_{MP}}{r_{MP}}\cdot d\boldsymbol{\sigma}_P-\iint_{\partial\mathscr{B}(M,\varepsilon)}\frac{\boldsymbol{r}_{MP}}{r_{MP}}\cdot d\boldsymbol{\sigma}_P\right)=\iint_{\partial\Sigma}\frac{\boldsymbol{r}_{MP}}{r_{MP}}\cdot d\boldsymbol{\sigma}_P\,,$$

The limit of second term is zero. This can be seen as follow:

$$\iint_{\partial\mathscr{B}(M,\varepsilon)}\frac{\boldsymbol{r}_{MP}}{r_{MP}}\cdot d\boldsymbol{\sigma}_P=\iint_{\partial\mathscr{B}(M,\varepsilon)}\frac{\boldsymbol{r}_{MP}}{r_{MP}}\cdot\boldsymbol{n}d\sigma_P=\iint_{\partial\mathscr{B}(M,\varepsilon)}\frac{\boldsymbol{r}_{MP}}{r_{MP}}\cdot\frac{\boldsymbol{r}_{MP}}{r_{MP}}d\sigma_P=\iint_{\partial\mathscr{B}(M,\varepsilon)}d\sigma_P=4\pi\varepsilon^2\to 0\ \text{ if } \varepsilon\to 0.$$

Using this result we have:

$$\iiint_{\Sigma}\nabla_{r_P}\cdot\frac{\boldsymbol{r}_{MP}}{r_{MP}}dv_P=\iint_{\partial\Sigma}\frac{\boldsymbol{r}_{MP}}{r_{MP}}\cdot d\boldsymbol{\sigma}_P$$

for every $M\in R^3$ point. Thus we can write:

$$U(M)=\frac{G\rho_0}{2}\iiint_{\Sigma}\nabla_{r_P}\cdot\frac{\boldsymbol{r}_{MP}}{r_{MP}}dv_P=\frac{G\rho_0}{2}\iint_{\partial\Sigma}\frac{\boldsymbol{r}_{MP}}{r_{MP}}\cdot d\boldsymbol{\sigma}_P=\frac{G\rho_0}{2}\iint_{\partial\Sigma}\frac{\boldsymbol{r}_{MP}}{r_{MP}}\cdot\boldsymbol{n}d\sigma_P=\frac{G\rho_0}{2}\sum_{i=1}^{n}\iint_{S_i}\frac{\boldsymbol{r}_{MP}}{r_{MP}}\cdot\boldsymbol{n}d\sigma_P=$$

$$=\frac{G\rho_0}{2}\sum_{i=1}^{n}h_i\iint_{S_i}\frac{1}{r_{MP}}d\sigma_P\,,\ \forall M\in R^3. \tag{54}$$

Paul (1974) calculates the surface integrals on triangular faces analitically using a proper coordinate transformation for every triangular face. For every $A_{i1}A_{i2}A_{i3}$ triangle we define the (x_i',y_i',z_i') right-handed coordinate system with origin in A_{i1} and the axis defined as $x_i'=\overrightarrow{A_{i1}A_{i2}}$, $y_i'\perp A_{i1}A_{i2}$ and $y_i'\subset(A_{i1}A_{i2}A_{i3})$, $z_i'\perp x_i'$ and $z_i'\perp y_i'$. The formulas (Paul, 1974) in these local coordinate systems described in are disadvantageous from programming point of view. Furthermore in case of a general polyhedron with arbitrary polygonal faces the calculation of multiple integrals on a general polygonal face is awkwardish, therefore it is more convenient to convert the double integrals to line integrals

using Gauss-Ostrogradsky or Stokes formula. The requirement for applying the Stokes theorem is to find for every S_i face a $\boldsymbol{f}_i(\boldsymbol{r}_P)$ vector-vector function achieving:

$$\nabla_{\boldsymbol{r}_P} \times \boldsymbol{f}_i(\boldsymbol{r}_P) \cdot \boldsymbol{n}_i = \mathrm{rot}\, \boldsymbol{f}_i(\boldsymbol{r}_P) \cdot \boldsymbol{n}_i = \frac{1}{r_{MP}}, \ \forall P \in S_i. \tag{55}$$

Condition for applying the Gauss-Ostrogradsky theorem is the existence of an $\boldsymbol{f}_i(\boldsymbol{r}_P)$ vector-vector function:

$$\nabla_{\boldsymbol{r}_P} \cdot \boldsymbol{f}_i(\boldsymbol{r}_P) = \frac{1}{r_{MP}}, \ \forall P \in S_i. \tag{56}$$

The $\boldsymbol{f}_i(\boldsymbol{r}_P)$ function is not uniquely defined by (55) and (56) respectively which explains the different analytical formulas of gravitational potential and its derivatives found in the literature. Kwok (1991 a) gives a special solution to resolve conversion of double integral to line integrals using a the Green's theorem in complex form. The obtained formulas are identical with formulas presented in the papers by Götze and Lahmeyer (1988) and Petrovič (1996). Barnett (1976) and Okabe (1979) but instead of vector analysis he used the analytical geometry tools. The obtained analytical formulas are identical with those given by Pohànka (1988), Holstein and Ketteridge (1996) and Werner and Scheeres (1997). The aim is to choose such function $\boldsymbol{f}$ which is defined in all points of the S_i face and satisfying the (55) and (56) requirements too (Pohànka 1988, Holstein 2002a, Holstein and Ketteridge 1996, Werner and Scheeres 1997). Götze and Lahmeyer (1988), Petrovič (1996) use function $\boldsymbol{f}$ which is singular at points inside S_i. Table 1 summarises all $\boldsymbol{f}$ functions used in the literature and their properties. Hereinafter the verification of (55) and (56) conditions for all particular $\boldsymbol{f}_i$ given in Table 1 is discussed.

$$\text{I. } \nabla_{\boldsymbol{r}_P} \cdot \left(\frac{\boldsymbol{s}_{MP}}{s_{MP}^2} r_{MP} \right) = r_{MP} \left(\nabla_{\boldsymbol{r}_P} \cdot \frac{\boldsymbol{s}_{MP}}{s_{MP}^2} \right) + \frac{\boldsymbol{s}_{MP}}{s_{MP}^2} \cdot \left(\nabla_{\boldsymbol{r}_P} r_{MP} \right) = r_{MP} \left(\frac{1}{s_{MP}^2} \left(\nabla_{\boldsymbol{r}_P} \cdot \boldsymbol{s}_{MP} \right) + \boldsymbol{s}_{MP} \cdot \nabla_{\boldsymbol{r}_P} \frac{1}{s_{MP}^2} \right) + \frac{\boldsymbol{s}_{MP}}{s_{MP}^2} \cdot \frac{\boldsymbol{s}_{MP}}{r_{MP}}$$

$$= r_{MP} \left(\frac{2}{s_{MP}^2} - 2\boldsymbol{s}_{MP} \cdot \frac{\boldsymbol{s}_{MP}}{s_{MP}^4} \right) + \frac{\boldsymbol{s}_{MP}}{s_{MP}^2} \cdot \frac{\boldsymbol{s}_{MP}}{r_{MP}^2} = \frac{1}{r_{MP}}.$$

$$\text{II. } \nabla_{\boldsymbol{r}_P} \cdot \frac{\boldsymbol{s}_{MP}}{r_{MP} + |h_i|} = \nabla_{\boldsymbol{r}_P} \cdot \left(\frac{\boldsymbol{s}_{MP}}{s_{MP}^2} \left(r_{MP} - |h_i| \right) \right) = \left(r_{MP} - |h_i| \right) \left(\nabla_{\boldsymbol{r}_P} \cdot \frac{\boldsymbol{s}_{MP}}{s_{MP}^2} \right) + \frac{\boldsymbol{s}_{MP}}{s_{MP}^2} \cdot \nabla_{\boldsymbol{r}_P} \left(r_{MP} - |h_i| \right) = \frac{\boldsymbol{s}_{MP}}{s_{MP}^2} \cdot \nabla_{\boldsymbol{r}_P} \left(r_{MP} \right) = \frac{1}{r_{MP}}.$$

III.

$$\nabla_{\boldsymbol{r}_P} \times \left(\boldsymbol{n}_i \times \left(\frac{\boldsymbol{s}_{MP}}{s_{MP}} \right) \frac{r_{MP} - |h_i|}{s_{MP}} \right) \cdot \boldsymbol{n}_i = \left(\frac{r_{MP} - |h_i|}{s_{MP}^2} \nabla_{\boldsymbol{r}_P} \times \left(\boldsymbol{n}_i \times \boldsymbol{s}_{MP} \right) + \nabla_{\boldsymbol{r}_P} \left(\frac{r_{MP} - |h_i|}{s_{MP}^2} \right) \times \left(\boldsymbol{n}_i \times \boldsymbol{s}_{MP} \right) \right) \cdot \boldsymbol{n}_i =$$

$$= \left(2 \frac{r_{MP} - |h_i|}{s_{MP}^2} \boldsymbol{n}_i + \frac{s_{MP}^2 - 2\left(r_{MP}^2 - r_{MP} |h_i| \right)}{r_{MP} s_{MP}^4} \boldsymbol{s}_{MP} \times \left(\boldsymbol{n}_i \times \boldsymbol{s}_{MP} \right) \right) \cdot \boldsymbol{n}_i =$$

$$= 2 \frac{r_{MP} - |h_i|}{s_{MP}^2} + \frac{s_{MP}^2 - 2 r_{MP} \left(r_{MP} - |h_i| \right)}{r_{MP} s_{MP}^4} s_{MP}^2 = \frac{1}{r_{MP}}.$$

The following relations were used:

$$\nabla(u\boldsymbol{w}) = u \nabla \cdot \boldsymbol{w} + (\nabla u) \cdot \boldsymbol{w} \ \text{ and} \tag{57}$$

$$\nabla \times (u\boldsymbol{w}) = u(\nabla \times \boldsymbol{w}) + \nabla u \times \boldsymbol{w}. \tag{58}$$

Table 1. Domain of definition of the proper ***f*** function and its properties

Author	***f***	Domain of definition	Properties
1. Götze and Lahmeyer (1988) 2. Petrovič (1996)	$\boldsymbol{f}_i(\boldsymbol{r}_P)=\frac{\boldsymbol{s}_{MP}}{s_{MP}^2}r_{MP}=$ $=\frac{\boldsymbol{s}_{MP}}{r_{MP}}+\frac{h_i^2}{r_{MP}}\frac{\boldsymbol{s}_{MP}}{s_{MP}^2}$	If $M_i \in \overline{S}_i$, then $\boldsymbol{f}_i$ is not defined in the point $P = M_i$	$\nabla_{\boldsymbol{r}_P}\cdot\boldsymbol{f}_i(\boldsymbol{r}_P)=\frac{1}{r_{MP}}$
Pohànka (1988)	$\boldsymbol{f}_i(\boldsymbol{r}_P)=\frac{\boldsymbol{s}_{MP}}{r_{MP}+\lvert h_i\rvert}=$ $=\frac{\boldsymbol{s}_{MP}}{s_{MP}^2}\left(r_{MP}-\lvert h_i\rvert\right)$	S_i	$\nabla_{\boldsymbol{r}_P}\cdot\boldsymbol{f}_i(\boldsymbol{r}_P)=\frac{1}{r_{MP}}$
Holstein and Ketteridge (1996)	$\boldsymbol{f}_i(\boldsymbol{r}_P)=\boldsymbol{n}_i\times\left(\frac{\boldsymbol{s}_{MP}}{s_{MP}}\right)\frac{r_{MP}-\lvert h_i\rvert}{s_{MP}}=$ $=\boldsymbol{n}_i\times\frac{\boldsymbol{s}_{MP}}{\left(r_{MP}+\lvert h_i\rvert\right)}$	S_i	$\left(\nabla_{\boldsymbol{r}_P}\times\boldsymbol{f}_i(\boldsymbol{r}_P)\right)\cdot\boldsymbol{n}_i=\frac{1}{r_{MP}}$

We will give the general solution of equation (56) on the set of functions $\left\{\boldsymbol{f}_i(\boldsymbol{r}_P)\in S_i \mid \boldsymbol{f}_i(\boldsymbol{r}_P)=c(x',y')\boldsymbol{s}_{MP}\right\}$, where (x', y') is a local coordinate system in S_i with origin in M_i, $\boldsymbol{s}_{MP}$ is the position vector of point P, $\boldsymbol{s}_{MP}=(x',y')$ and $r_{MP}=\sqrt{x'^2+y'^2+h_i^2}$. We resolve the $\nabla_{\boldsymbol{r}_P}\cdot\boldsymbol{f}_i(\boldsymbol{r}_P)=\frac{1}{r_{MP}}$ equation in the (x',y') local coordinate system. Equation $\nabla_{\boldsymbol{r}_P}\cdot\boldsymbol{f}_i(\boldsymbol{r}_P)=\nabla_{\boldsymbol{r}_P}\cdot\left(c(x',y')(x',y')\right)=\frac{1}{r_{MP}}$ leads to the following two first order quasilinear equations (Polyanin et al. 2002):

$$x'\frac{\partial c(x',y')}{\partial x'}+y'\frac{\partial c(x',y')}{\partial y'}=-2c(x',y')+\frac{1}{\sqrt{x'^2+y'^2+h_i^2}},$$

whose general form of solutions is :

$$c(x',y')=x'^{-2}\phi\left(\frac{y'}{x'}\right)+\frac{\sqrt{x'^2+y'^2+h_i^2}}{x'^2+y'^2}=\frac{\phi^*\left(\frac{y'}{x'}\right)+r_{MP}}{s_{MP}^2},$$

where $\phi^*\left(\frac{y'}{x'}\right)=\left[1+\left(\frac{y'}{x'}\right)^2\right]\phi\left(\frac{y'}{x'}\right)$, $r_{MP}=\sqrt{x'^2+y'^2+h_i^2}$, $s_{MP}=\sqrt{x'^2+y'^2}$.

The general solution of (56) is: $\boldsymbol{f}_i(\boldsymbol{r}_P)=\frac{\phi^*\left(\frac{y'}{x'}\right)+r_{MP}}{s_{MP}^2}\boldsymbol{s}_{MP}$,

where ϕ^* is an arbitrary function. In case of $\phi^*=0$ we get the function $\boldsymbol{f}_i$ which derives solution given by Götze and Lahmeyer (1988) and Petrovič (1996), in case of $\phi^*=-\lvert h_i\rvert$ the $\boldsymbol{f}_i$ which leads to Pohànka (1988) solution. $\phi^*=-\lvert h_i\rvert$ is the only one function for which $\boldsymbol{f}_i$ is defined on the whole S_i face and fulfils the Gauss-Ostrogradsky theorem in this domain (see demonstration II.).

The sets of the vector functions fulfilling (55) or (56) conditions are the same, namely A=B, where

$$A=\left\{\boldsymbol{f}\,\middle|\,\left(\nabla_{\boldsymbol{r}_P}\times\boldsymbol{f}_i(\boldsymbol{r}_P)\right)\cdot\boldsymbol{n}_i=\frac{1}{r_{MP}}\right\}\text{ and }B=\left\{\boldsymbol{f}\,\middle|\,\nabla_{\boldsymbol{r}_P}\cdot\boldsymbol{f}_i(\boldsymbol{r}_P)=\frac{1}{r_{MP}}\right\}.$$

If the range of vector functions of A and B sets are set of vectors in S_i, then it can be readily derived that:

$$\boldsymbol{f}^{Stokes}=\boldsymbol{n}_i\times\boldsymbol{f}^{Gauss-Ostrogradsky},$$

where $\boldsymbol{n}_i$ is the normal vector of S_i face, $\boldsymbol{f}^{Stokes}$ is element of $A=\left\{\boldsymbol{f}\,\middle|\,\left(\nabla_{\boldsymbol{r}_P}\times\boldsymbol{f}_i(\boldsymbol{r}_P)\right)\cdot\boldsymbol{n}_i=\frac{1}{r_{MP}}\right\}$ set, whereas $\boldsymbol{f}^{Gauss-Ostrogradsky}$ is element of $B=\left\{\boldsymbol{f}\,\middle|\,\nabla_{\boldsymbol{r}_P}\cdot\boldsymbol{f}_i(\boldsymbol{r}_P)=\frac{1}{r_{MP}}\right\}$ set. If we use the function given in the paper by Holstein and Ketteridge (1996) from the set of functions fulfilling condition (55) and applying the Stokes theorem we will get the following line integral:

$$U(M)=\frac{G\rho_0}{2}\sum_{i=1}^{n}h_i\iint_{S_i}\frac{1}{r_{MP}}d\sigma_P=\frac{G\rho_0}{2}\sum_{i=1}^{n}h_i\iint_{S_i}\nabla_{\boldsymbol{r}_P}\times\boldsymbol{f}_i(\boldsymbol{r}_P)\cdot\boldsymbol{n}_i d\sigma_P=\frac{G\rho_0}{2}\sum_{i=1}^{n}h_i\int_{\partial S_i}\boldsymbol{f}(\boldsymbol{r}_P)d\boldsymbol{l}_P=$$

$$=\frac{G\rho_0}{2}\sum_{i=1}^{n}h_i\sum_{j=1}^{l(i)}\int_{L_{ij}}\boldsymbol{f}(\boldsymbol{r}_P)\boldsymbol{\mu}_{ij}dl_P=\frac{G\rho_0}{2}\sum_{i=1}^{n}h_i\sum_{j=1}^{l(i)}\int_{L_{ij}}\boldsymbol{n}_i\times\frac{\boldsymbol{s}_{MP}}{\left(r_{MP}+|h_i|\right)}\cdot\boldsymbol{\mu}_{ij}dl_P=\frac{G\rho_0}{2}\sum_{i=1}^{n}h_i\sum_{j=1}^{l(i)}h_{ij}\int_{L_{ij}}\frac{1}{r_{MP}+|h_i|}dl_P. \tag{59}$$

Using the function given by Pohànka (1988) which fulfills condition (56) and applying the Gauss-Ostogradsky theorem we will get the same line integral like in (59):

$$U(M)=\frac{G\rho_0}{2}\sum_{i=1}^{n}h_i\int_{S_i}\frac{1}{r_{MP}}d\sigma_P=\frac{G\rho_0}{2}\sum_{i=1}^{n}h_i\int_{S_i}\nabla_{\boldsymbol{r}_P}\cdot\boldsymbol{f}_i(\boldsymbol{r}_P)d\sigma_P=\frac{G\rho_0}{2}\sum_{i=1}^{n}h_i\int_{\partial S_i}\boldsymbol{f}(\boldsymbol{r}_P)\cdot\boldsymbol{v}dl_P=$$

$$=\frac{G\rho_0}{2}\sum_{i=1}^{n}h_i\sum_{j=1}^{l(i)}\int_{L_{ij}}\boldsymbol{f}(\boldsymbol{r}_P)\cdot\boldsymbol{v}_{ij}dl_P=\frac{G\rho_0}{2}\sum_{i=1}^{n}h_i\sum_{j=1}^{l(i)}\int_{L_{ij}}\frac{\boldsymbol{s}_{MP}}{r_{MP}+|h_i|}\cdot\boldsymbol{v}_{ij}dl_P=\frac{G\rho_0}{2}\sum_{i=1}^{n}h_i\sum_{j=1}^{l(i)}h_{ij}\int_{L_{ij}}\frac{1}{r_{MP}+|h_i|}dl_P. \tag{60}$$

Here we used the following relation

$$\left(\boldsymbol{n}_i\times\boldsymbol{s}_{MP}\right)\cdot\boldsymbol{\mu}_{ij}=\left(\boldsymbol{n}_i\times\boldsymbol{\mu}_{ij}\right)\cdot\boldsymbol{s}_{MP}=\boldsymbol{v}_{ij}\cdot\boldsymbol{s}_{MP}=\boldsymbol{v}_{ij}\cdot\boldsymbol{r}_{MP}=h_{ij}, \tag{61}$$

where $\boldsymbol{v}_{ij}$ and $\boldsymbol{\mu}_{ij}$ are the normal vector and the unit vector of the jth segment of the ∂S_i polygonal line.

Furthermore, choosing $\boldsymbol{f}_i$ which leads to solutions given is Götze and Lahmeyer (1988) and Petrovič (1996) (Table 1) the transformation of the surface integral to line integral by Gauss-Ostogradsky theorem is possible only on $S_{i\varepsilon}=S_i\setminus\mathscr{O}(M_i,\varepsilon)$ domain due to $\boldsymbol{f}_i$ singularity in M_i. $\mathscr{O}(M_i,\varepsilon)$ indicates the inner domain of the circle with centre in M_i and radius ε. In virtue of Gauss-Ostogradsky theorem in case of $\boldsymbol{f}_i$ with singularity it holds:

$$U(M)=\lim_{\varepsilon\to0}\frac{G\rho_0}{2}\sum_{i=1}^{n}h_i\iint_{S_{i\varepsilon}}\frac{1}{r_{MP}}d\sigma_P=\lim_{\varepsilon\to0}\frac{G\rho_0}{2}\sum_{i=1}^{n}h_i\iint_{S_{i\varepsilon}}\nabla_{\boldsymbol{r}_P}\cdot\boldsymbol{f}_i(\boldsymbol{r}_P)d\sigma_P=\lim_{\varepsilon\to0}\frac{G\rho_0}{2}\sum_{i=1}^{n}h_i\iint_{\partial S_{i\varepsilon}}\boldsymbol{f}(\boldsymbol{r}_P)\cdot\boldsymbol{v}dl_P=$$

$$=\lim_{\varepsilon\to0}\frac{G\rho_0}{2}\sum_{i=1}^{n}h_i\left(\iint_{\partial S_i}\boldsymbol{f}(\boldsymbol{r}_P)\cdot\boldsymbol{v}dl_P+\iint_{S_i\cap\mathscr{O}(M_i,\varepsilon)}\boldsymbol{f}(\boldsymbol{r}_P)\cdot\boldsymbol{v}dl_P\right)=$$

$$=\frac{G\rho_0}{2}\sum_{i=1}^{n}h_i\left(\sum_{j=1}^{l(i)}\int_{L_{ij}}\boldsymbol{f}(\boldsymbol{r}_P)\cdot\boldsymbol{v}_{ij}dl_P-\lim_{\varepsilon\to0}\iint_{S_i\cap\mathscr{O}(M_i,\varepsilon)}\boldsymbol{f}(\boldsymbol{r}_P)\frac{\boldsymbol{s}_{MP}}{s_{MP}}dl\right)=$$

$$=\frac{G\rho_0}{2}\sum_{i=1}^{n}h_i\left(\sum_{j=1}^{l(i)}h_{ij}\int_{L_{ij}}\left(\frac{1}{r_{MP}}+\frac{h_i^2}{r_{MP}s_{MP}^2}\right)dl_P-\lim_{\varepsilon\to 0}\iint_{S_i\cap\mathscr{C}(M_i,\varepsilon)}\left(\frac{s_{MP}}{r_{MP}}+\frac{h_i^2}{r_{MP}s_{MP}}\right)dl_P\right)=$$

$$=\frac{G\rho_0}{2}\sum_{i=1}^{n}h_i\left(\sum_{j=1}^{l(i)}h_{ij}\int_{L_{ij}}\left(\frac{1}{r_{MP}}+\frac{h_i^2}{r_{MP}s_{MP}^2}\right)dl_P-\lim_{R_{MP}\to 0}\iint_{S_i\cap\mathscr{C}(M_i,\varepsilon)}\left(\frac{s_{MP}}{r_{MP}}+\frac{h_i^2}{r_{MP}s_{MP}}\right)dl_P\right)=$$

$$=\frac{G\rho_0}{2}\sum_{i=1}^{n}h_i\left(\sum_{j=1}^{l(i)}h_{ij}\int_{L_{ij}}\frac{1}{r_{MP}}dl_P+h_i^2\sum_{j=1}^{l(i)}h_{ij}\int_{L_{ij}}\frac{1}{r_{MP}s_{MP}^2}dl_P-|h_i|\theta_i\right). \tag{62}$$

Here was used the following relation:

$$\lim_{R_{MP}\to 0}\iint_{S_i\cap\mathscr{C}(M_i,\varepsilon)}\left(\frac{s_{MP}}{r_{MP}}+\frac{h_i^2}{r_{MP}s_{MP}}\right)dl_P=\lim_{R_{MP}\to 0}\left(\frac{s_{MP}}{r_{MP}}+\frac{h_i^2}{r_{MP}s_{MP}}\right)\iint_{S_i\cap\mathscr{C}(M_i,R_{MP})}dl_P=$$

$$=\lim_{R_{MP}\to 0}\left(\frac{s_{MP}}{\sqrt{s_{MP}+h_i^2}}+\frac{h_i^2}{s_{MP}\sqrt{s_{MP}+h_i^2}}\right)\theta_i s_{MP}=|h_i|\theta_i. \tag{63}$$

θ_i is the angle belonging to the $S_i\cap\mathscr{C}(M_i,\varepsilon)$ arc,

$$\theta_i=\begin{cases}2\pi & \text{if} \quad M_i\in\operatorname{Int}S_i\\ \pi & \text{if } M_i\in\partial S_i\setminus\{A_{i1},A_{i2},\ldots,A_{il(i)}\}\\ A_{ij-1}A_{ij}A_{ij+1}=\pi-\arccos(\boldsymbol{\mu}_{ij}\cdot\boldsymbol{\mu}_{ij-1}) & \text{if } M_i=A_{ij}\in\{A_{i1},A_{i2},\ldots,A_{il(i)}\}\\ 0 & \text{if} \quad M_i\in\operatorname{Ext}S_i\end{cases}. \tag{64}$$

The last step in deduction of the analytical formula of gravitation potential is the evaluation of line integrals. By right of the (59), (60) and (62) relations this is carried out by evaluation of the following primitive functions:

$$\int\frac{1}{r_{MP}+|h_i|}dl\,,\ \int\frac{1}{r_{MP}}dl\,,\ \int\frac{1}{r_{MP}s_{MP}^2}dl\,. \tag{65}$$

According to Pohànka (1988) we introduce the $c(h_i,h_{ij},l)=\int\frac{h_{ij}}{r_{MP}+|h_i|}dl$ and $c_{ij}=\int_{L_{ij}}\frac{h_{ij}}{r_{MP}+|h_i|}dl$ notations. Here we will get a solution of first indefinite integrals in (65):

$$c(h_i,h_{ij},l)=\int\frac{h_{ij}}{r_{MP}+|h_i|}dl=\int\frac{h_{ij}}{\sqrt{l^2+h_{ij}^2+h_i^2}+|h_i|}dl=-\int\frac{h_{ij}}{t}dt+2h_{ij}|h_i|\int\frac{1}{(t+|h_i|)^2+h_{ij}^2}dt$$

$$=-h_{ij}\ln\left(\sqrt{l^2+h_{ij}^2+h_i^2}-l\right)+2|h_i|\operatorname{atan}\frac{\sqrt{l^2+h_{ij}^2+h_i^2}-l+|h_i|}{h_{ij}}=-h_{ij}\ln(r_{MP}-l)+2|h_i|\operatorname{atan}\frac{r_{MP}-l+|h_i|}{h_{ij}}. \tag{66}$$

In the course of deduction the $\sqrt{l^2+h_{ij}^2+h_i^2}=l+t$ substitution was used. Applying another $\sqrt{l^2+h_{ij}^2+h_i^2}=t-l$ substitution we get:

$$c(h_i,h_{ij},l)=\int\frac{h_{ij}}{r_{MP}+|h_i|}dl=\int\frac{h_{ij}}{t}dt-2h_{ij}|h_i|\int\frac{1}{(t+|h_i|)^2+h_{ij}^2}dt=h_{ij}\ln(r_{MP}+l)-2|h_i|\operatorname{atan}\frac{r_{MP}+l+|h_i|}{h_{ij}}\ . \tag{67}$$

$$c_{ij}=\int_{L_{ij}}\frac{h_{ij}}{r_{MP}+|h_i|}dl=\left[-h_{ij}\ln\left(r_{MP}-l\right)+2|h_i|\operatorname{atan}\frac{r_{MP}-l+|h_i|}{h_{ij}}\right]_{l_{1ij}}^{l_{2ij}}=$$

$$=\left[h_{ij}\ln\left(r_{MP}+l\right)-2|h_i|\operatorname{atan}\frac{r_{MP}-l+|h_i|}{h_{ij}}\right]_{l_{1ij}}^{l_{2ij}} \tag{68}$$

Pohànka (1988) gave an advantageous form of c_{ij} from programming point of view presented below:

$$c_{ij}=\int_{L_{ij}}\frac{h_{ij}}{r+|h_i|}dl=h_{ij}\left(\operatorname{sign}\left(l_{2ij}\right)\ln\frac{r_{2ij}+|l_{2ij}|}{r_{0ij}}-\operatorname{sign}\left(l_{2ij}\right)\ln\frac{r_{1ij}+|l_{1ij}|}{r_{0ij}}\right)-$$

$$-2|h_i|\operatorname{atan}\frac{2h_{ij}\left(l_{2ij}-l_{1ij}\right)}{\left(r_{2ij}+r_{1ij}\right)^2-\left(l_{2ij}-l_{1ij}\right)^2+2\left(r_{2ij}+r_{1ij}\right)|h_i|}\,. \tag{69}$$

Based on Holstein (2002) we define the C_{ij} and the Ω_{ij} quantities:

$$c_{ij}=h_{ij}C_{ij}-h_i\Omega_{ij} \tag{70}$$

The integral form of the quantities C_{ij}, Ω_{ij}, Ω_i are:

$$C_{ij}=\int_{L_{ij}}\frac{1}{r_{MP}}dl\,,\ \Omega_{ij}=\int_{\Delta_{12ij}}\frac{h_i}{r_{MP}^3}d\sigma_P\,,\ \Omega_i=\int_{S_i}\frac{h_i}{r_{MP}^3}d\sigma_P\qquad. \tag{71}$$

Using (66)-(69) C_{ij} and Ω_{ij} can be written as follows (Table 4):

$$C_{ij}^{Pohanka^1}=-\left[\ln\left(r_{MP}-l\right)\right]_{l_{1ij}}^{l_{2ij}}\,,\ C_{ij}^{Pohanka^2}=\left[\ln\left(r_{MP}+l\right)\right]_{l_{1ij}}^{l_{2ij}}\,,$$

$$C_{ij}^{Pohanka^3}=\operatorname{sign}\left(l_{2ij}\right)\ln\frac{r_{2ij}+|l_{2ij}|}{r_{0ij}}-\operatorname{sign}\left(l_{2ij}\right)\ln\frac{r_{1ij}+|l_{1ij}|}{r_{0ij}}\,. \tag{72}$$

$$\Omega_{ij}^{Pohanka^1}=\left[2\operatorname{sign}\left(h_i\right)\cdot\operatorname{atan}\frac{r_{MP}-l+|h_i|}{h_{ij}}\right]_{l_{1ij}}^{l_{2ij}}\,,\ \Omega_{ij}^{Pohanka^2}=-\left[2\operatorname{sign}\left(h_i\right)\cdot\operatorname{atan}\frac{r_{MP}+l+|h_i|}{h_{ij}}\right]_{l_{1ij}}^{l_{2ij}}\,,$$

$$\Omega_{ij}^{Pohanka^3}=2\operatorname{sign}\left(h_i\right)\cdot\operatorname{atan}\frac{2h_{ij}\left(l_{2ij}-l_{1ij}\right)}{\left(r_{2ij}+r_{1ij}\right)^2-\left(l_{2ij}-l_{1ij}\right)^2+2\left(r_{2ij}+r_{1ij}\right)|h_i|}\,, \tag{73}$$

where the upper indices denotes the author name. Holstein and Ketteridge (1996) used different expressions for $c(h_i,h_{ij},l)$ and for c_{ij}, which explains the formally different analytical formulas of first derivatives of gravitational potential found in the literature (Pohànka 1988, Holstein and Ketteridge 1996). According to Holstein and Ketteridge (1996) is holding:

$$c(h_i,h_{ij},l)=\int\frac{h_{ij}}{r_{MP}+|h_i|}dl=\int\frac{r_{MP}-|h_i|}{l^2+h_{ij}^2}dl=\int\frac{r_{MP}}{l^2+h_{ij}^2}dl-\int\frac{|h_i|}{l^2+h_{ij}^2}dl=\int\frac{r_{MP}^2}{r_{MP}\left(l^2+h_{ij}^2\right)}dl-\int\frac{|h_i|}{l^2+h_{ij}^2}dl=$$

$$=\int\frac{l^2+h_{ij}^2+h_i^2}{r_{MP}\left(l^2+h_{ij}^2\right)}dl-\int\frac{|h_i|}{l^2+h_{ij}^2}dl=\int\frac{r_{MP}^2}{r_{MP}\left(l^2+h_{ij}^2\right)}dl-\int\frac{|h_i|}{l^2+h_{ij}^2}dl=$$

$$=\int\frac{l^2+h_{ij}^2+h_i^2}{r_{MP}\left(l^2+h_{ij}^2\right)}dl-\int\frac{|h_i|}{l^2+h_{ij}^2}dl=\int\frac{1}{r_{MP}}dl+h_i^2\int\frac{1}{r_{MP}\left(l^2+h_{ij}^2\right)}dl-|h_i|\int\frac{1}{l^2+h_{ij}^2}dl\,. \tag{74}$$

The analytical expressions of the indefinite integrals in (74) are:

$$1.\ \int \frac{1}{r_{MP}}\,dl = \int \frac{1}{\sqrt{l^2+h_{ij}^2+h_i^2}}\,dl = \ln\left(l+\sqrt{l^2+h_{ij}^2+h_i^2}\right) = \ln\left(l+r\right), \tag{75}$$

$$2.\ \int \frac{1}{r_{MP}\left(l^2+h_{ij}^2\right)}\,dl = \int \frac{1}{r_{MP}R_{MP}^2}\,dl = \int \frac{1}{l^3\sqrt{1+\frac{h_{ij}^2+h_i^2}{l^2}}\left(1+\frac{h_{ij}^2}{l^2}\right)}\,dl = -\int \frac{1}{h_{ij}^2t^2+h_i^2}\,dt =$$

$$= -\frac{1}{h_{ij}h_i}\operatorname{atan}\left(\frac{th_{ij}}{h_i}\right) = -\frac{1}{h_{ij}h_i}\operatorname{atan}\left(\frac{rh_{ij}}{lh_i}\right) = \frac{1}{h_{ij}h_i}\operatorname{atan}\left(\frac{lh_i}{rh_{ij}}\right). \tag{76}$$

The second indefinite integral can be evaluated simply by using the $\sqrt{1+\frac{h_{ij}^2+h_i^2}{l^2}} = \frac{r}{l} = t$ $\sqrt{1+\frac{h_{ij}^2+h_i^2}{l^2}} = \frac{r}{l} = t$ substitution. The last identity in (76) is based on the following common relation:

$$\operatorname{atan} x + \operatorname{atan}\frac{1}{x} = \begin{cases} \pi/2 & \text{if } x>0 \\ -\pi/2 & \text{if } x<0 \end{cases}.$$

$$3.\ \int \frac{1}{l^2+h_{ij}^2}\,dl = \frac{1}{h_{ij}}\operatorname{atan}\frac{l}{h_{ij}}. \tag{77}$$

From (74)-(77) we get the analytical expression for the indefinite integral $c(h_i,h_{ij},l)$ and for c_{ij} which is its definite integral along the L_{ij} line (Holstein and Ketteridge 1996):

$$c(h_i,h_{ij},l) = h_{ij}\ln\left(r_{MP}+l\right) + h_i\operatorname{atan}\left(\frac{h_i l}{rh_{ij}}\right) - \left|h_i\right|\operatorname{atan}\left(\frac{l}{h_{ij}}\right), \tag{78}$$

$$c_{ij} = \int_{L_{ij}} \frac{h_{ij}}{r_{MP}+\left|h_i\right|}\,dl = \left[h_{ij}\ln\left(\frac{r_{MP}+l}{r_{0ij}}\right) + h_i\operatorname{atan}\left(\frac{h_i l}{r_{MP}h_{ij}}\right) - \left|h_i\right|\operatorname{atan}\left(\frac{l}{h_{ij}}\right)\right]_{l_{1ij}}^{l_{2ij}} =$$

$$= \left[h_{ij}\ln\left(\frac{r_{MP}+l}{r_{0ij}}\right) - \left|h_i\right|\operatorname{atan}\left(\frac{h_{ij}l}{r_{0ij}^2+r_{MP}\left|h_i\right|}\right)\right]_{l_{1ij}}^{l_{2ij}}. \tag{79}$$

Using (79) the expression of C_{ij} and Ω_{ij} constants introduced in (70) are:

$$C_{ij} = \int_{L_{ij}} \frac{1}{r_{MP}}\,dl = \left[\ln\left(\frac{r_{MP}+l}{r_{0ij}}\right)\right]_{l_{1ij}}^{l_{2ij}}, \tag{80}$$

$$\Omega_{ij} = \operatorname{sign}\left(h_i\right)\cdot\left[\operatorname{atan}\left(\frac{l}{h_{ij}}\right)\right]_{l_{1ij}}^{l_{2ij}} - \left[\operatorname{atan}\left(\frac{h_i l}{r_{MP}h_{ij}}\right)\right]_{l_{1ij}}^{l_{2ij}} = \operatorname{sign}\left(h_i\right)\cdot\left[\operatorname{atan}\left(\frac{h_{ij}l}{r_{0ij}^2+r_{MP}\left|h_i\right|}\right)\right]_{l_{1ij}}^{l_{2ij}}. \tag{81}$$

The analytical expressions of C_{ij} given in (80) are used as well by Petrovič (1996) and Götze and Lahmeyer (1988), therefor we will use for this constant as upper index *HPGL* based on the initials of the authors (Table 4). Analogously the two expressions of Ω_{ij} given in (81) are marked with *Holstein*[1] and *Holstein*[2] upper indices (Table 4):

$$C_{ij}^{HPGL} = \left[\ln\left(\frac{r_{MP} + l}{r_{0ij}} \right) \right]_{l_{1ij}}^{l_{2ij}},$$

$$\Omega_{ij}^{Holstein^1} = \operatorname{sign}(h_i) \cdot \left[\operatorname{atan}\left(\frac{l}{h_{ij}} \right) \right]_{l_{1ij}}^{l_{2ij}} - \left[\operatorname{atan}\left(\frac{h_i l}{r_{MP} h_{ij}} \right) \right]_{l_{1ij}}^{l_{2ij}},$$

$$\Omega_{ij}^{Holstein^2} = \operatorname{sign}(h_i) \cdot \left[\operatorname{atan}\left(\frac{h_{ij} l}{r_{0ij}^2 + r_{MP} |h_i|} \right) \right]_{l_{1ij}}^{l_{2ij}}.$$

Holstein and Ketteridge (1996) and Holstein et al. (1999) gave analytical forms of C_{ij} and Ω_{ij} which are advantageous from programming aspects:

$$C_{ij}^{HWS} = \ln\left(\frac{r_{2ij} + r_{1ij} + l_{ij}}{r_{2ij} + r_{1ij} - l_{ij}} \right) = 2 \operatorname{atanh}\left(\frac{1 + \dfrac{r_{2ij} + r_{1ij}}{l_{ij}}}{1 - \dfrac{r_{2ij} + r_{1ij}}{l_{ij}}} \right), \tag{82}$$

$$C_{ij}^{Holstein} = \begin{cases} \operatorname{sign}(l_{2ij}) \ln\left(\dfrac{r_{2ij} + |l_{2ij}|}{r_{1ij} + |l_{1ij}|} \right) & \text{if } \operatorname{sign}(l_{2ij}) = \operatorname{sign}(l_{1ij}) \\ \operatorname{sign}(l_{2ij}) \ln\left(\dfrac{(r_{2ij} + |l_{2ij}|)(r_{1ij} + |l_{1ij}|)}{r_{0ij}^2} \right) & \text{if } \operatorname{sign}(l_{2ij}) \neq \operatorname{sign}(l_{1ij}) \end{cases}, \tag{83}$$

$$\Omega_{ij}^{Holstein^3} = \begin{cases} 2\operatorname{sign}(h_i) \cdot \operatorname{atan} \dfrac{2 h_{ij} (l_{2ij} - l_{1ij})}{(r_{2ij} + r_{1ij} + d_{ij})(r_{2ij} + r_{1ij} - d_{ij}) + 2(r_{2ij} + r_{1ij}) |h_i|} & \text{if } \operatorname{sign}(l_{2ij}) = \operatorname{sign}(l_{1ij}) \\ 2\operatorname{sign}(h_i) \cdot \operatorname{atan} \dfrac{2 h_{ij} (l_{2ij} - l_{1ij})}{(r_{2ij} + r_{1ij} + d_{ij})^2 / a_{ij} + 2(r_{2ij} + r_{1ij}) |h_i|} & \text{if } \operatorname{sign}(l_{2ij}) \neq \operatorname{sign}(l_{1ij}) \end{cases}, \tag{84}$$

where $a_{ij} = (r_{2ij} + l_{2ij})(r_{1ij} - l_{1ij}) / r_0^2$, $d_{ij} = l_{2ij} - l_{1ij}$.

Werner and Scheeres (1996) used the same analytical form of C_{ij} as given in (82), therefore the *HWS* upper index was chosen for notation of adherent C_{ij}. The equivalency between (82) and (80) is demonstrated below. We start with the identity:

$r_{ij0}^2 = (r_{2ij} - l_{2ij})(r_{2ij} + l_{2ij}) = (r_{1ij} - l_{1ij})(r_{1ij} + l_{1ij})$. On this basis we can write:

$\dfrac{r_{2ij} - l_{2ij}}{r_{1ij} + l_{1ij}} = \dfrac{r_{1ij} - l_{1ij}}{r_{2ij} + l_{2ij}}$. Additionally:

$$\frac{r_{2ij} - l_{2ij} + r_{1ij} + l_{1ij}}{r_{1ij} + l_{1ij}} = \frac{r_{1ij} - l_{1ij} + r_{2ij} + l_{2ij}}{r_{2ij} + l_{2ij}} \Leftrightarrow \frac{r_{2ij} + r_{1ij} - l_{ij}}{r_{1ij} + l_{1ij}} = \frac{r_{1ij} + r_{2ij} + l_{ij}}{r_{2ij} + l_{2ij}} \Leftrightarrow \frac{r_{2ij} + r_{1ij} - l_{ij}}{r_{1ij} + r_{2ij} + l_{ij}} = \frac{r_{1ij} + l_{1ij}}{r_{2ij} + l_{2ij}}.$$

This demonstrates the equivalency of the (82) and (80) formulas on the common domain of definition. Götze and Lahmeyer (1988) and Petrovič (1996) deduced the equation (62) too. In order to get the analytical formulas of gravitational potential from this equation the analytical expressions of the last two indefinite integrals in (65) are necessary, namely:

$$\int \frac{1}{r_{MP}} dl = \ln\left(r_{MP} + l\right) \text{ and } \int \frac{1}{r_{MP} s_{MP}^2} dl = \frac{1}{h_i h_{ij}} \operatorname{atan}\left(\frac{l^2 + h_{ij}^2 + l r_{MP}}{h_i h_{ij}}\right). \tag{85}$$

The analytical expressions (85) and (76) are primitive function of $\frac{1}{r_{MP} s_{MP}^2}$. They are formally different, but it can be easily verified that the these two expressions differ in the $\frac{1}{h_i h_{ij}} \operatorname{atan}\left(\frac{h_{ij}}{h_i}\right)$ constant. The expression of C_{ij} and Ω_{ij} constants based on Götze and Lahmeyer (1988) and Petrovič (1996) are:

$$\sum_{j=1}^{l(i)} c_{ij}^{Petrovic} = \sum_{j=1}^{l(i)} \left(h_{ij} \int_{L_{ij}} \frac{1}{r_{MP}} dl_P + h_i^2 h_{ij} \int_{L_{ij}} \frac{1}{r_{MP} s_{MP}^2} dl_P \right) - |h_i| \theta_i = \sum_{j=1}^{l(i)} \left[h_{ij} \ln\left(r_{MP} + l\right) + h_i \operatorname{atan}\left(\frac{h_i l}{r_{MP} h_{ij}}\right) \right]_{l_{1ij}}^{l_{2ij}}$$

$$- |h_i| \theta_i = \sum_{j=1}^{l(i)} h_{ij} C_{ij} - h_i \Omega_i \,, \tag{86}$$

where

$$C_{ij}^{HPGL} = \int_{L_{ij}} \frac{1}{r_{MP}} dl = \left[\ln\left(\frac{r_{MP} + l}{r_{0ij}}\right) \right]_{l_{1ij}}^{l_{2ij}}, \tag{87}$$

$$\Omega_i^{Petrovic} = -\sum_{j=1}^{l(i)} \left[\operatorname{atan}\left(\frac{h_i l}{r_{MP} h_{ij}}\right) \right]_{l_{1ij}}^{l_{2ij}} + \operatorname{sign}\left(h_i\right) \theta_i \,. \tag{88}$$

$$\sum_{j=1}^{l(i)} c_{ij}^{G-L} = \sum_{j=1}^{l(i)} \left[h_{ij} \ln\left(r_{MP} + l\right) + h_i \operatorname{atan}\left(\frac{l^2 + h_i^2 + l r_{MP}}{h_i h_{ij}}\right) \right]_{l_{1ij}}^{l_{2ij}} - |h_i| \theta_i = \sum_{j=1}^{l(i)} h_{ij} C_{ij} - h_i \Omega_i \,, \tag{89}$$

where:

$$C_{ij}^{HPGL} = \left[\ln\left(\frac{r_{MP} + l}{r_{0ij}}\right) \right]_{l_{1ij}}^{l_{2ij}}, \tag{90}$$

$$\Omega_i^{G-L} = -\sum_{j=1}^{l(i)} \left[\operatorname{atan}\left(\frac{l^2 + h_i^2 + l r_{MP}}{h_i h_{ij}}\right) \right]_{l_{1ij}}^{l_{2ij}} + \operatorname{sign}\left(h_i\right) \theta_i \,. \tag{91}$$

Making use of c_{ij}, C_{ij} and Ω_{ij} constants, the expression of gravitational potential takes the form:

$$U(M) = \frac{G\rho_0}{2} \sum_{i=1}^{n} h_i \int_{S_i} \frac{1}{r_{MP}} d\sigma = \frac{G\rho_0}{2} \sum_{i=1}^{n} h_i \sum_{j=1}^{l(i)} c_{ij} = \frac{G\rho_0}{2} \sum_{i=1}^{n} h_i \left(\sum_{j=1}^{l(i)} h_{ij} C_{ij} - h_i \Omega_i \right), \tag{92}$$

which is a linear combination of C_{ij} and Ω_i constants. Different analytical forms of these constants show different properties from programming point of view with regard to their stability domain. Guptasarma and Singh (1999) and Singh and Guptasarma (2001) use another system of constants, namely (P_{ij}, Q_{ij}, R_{ij}) to describe the analytical formulas for the first derivatives of potential. The gravitational potential can be described with these constants too, as follows:

$$h_{ij} C_{ij} = \int_{L_{ij}} \frac{\boldsymbol{r} \cdot \boldsymbol{v}_{ij} dl}{r_{MP}} = \int_{L_{ij}} \frac{\boldsymbol{r} \cdot \left(\boldsymbol{\mu}_{ij} \times \boldsymbol{n}_i\right) dl}{r_{MP}} = \int_{L_{ij}} \frac{\boldsymbol{r}_{1ij} \cdot \left(d\boldsymbol{l} \times \boldsymbol{n}_i\right)}{r_{MP}} = \int_{L_{ij}} \frac{\boldsymbol{r}_{1ij} \cdot \left(d\boldsymbol{l} \times \boldsymbol{n}_i\right)}{r_{MP}} =$$

$$=\left(x_{1ij}-x\right)\left(n_{i,3}\int_{L_{ij}}\frac{d\eta}{r_{MP}}-n_{i,2}\int_{L_{ij}}\frac{d\varsigma}{r_{MP}}\right)+\left(y_{1ij}-y\right)\left(n_{i,1}\int_{L_{ij}}\frac{d\varsigma}{r_{MP}}-n_{i,3}\int_{L_{ij}}\frac{d\xi}{r_{MP}}\right)+\left(z_{1ij}-z\right)\left(n_{i,2}\int_{L_{ij}}\frac{d\xi}{r_{MP}}-n_{i,1}\int_{L_{ij}}\frac{d\eta}{r_{MP}}\right)=$$

$$=\left(x_{1ij}-x\right)\left(n_{i,3}Q_{ij}-n_{i,2}R_{ij}\right)+\left(y_{1ij}-y\right)\left(n_{i,1}R_{ij}-n_{i,3}P_{ij}\right)+\left(z_{1ij}-z\right)\left(n_{i,2}P_{ij}-n_{i,1}Q_{ij}\right)=$$

$$=I_{ij}\boldsymbol{r}_{1ij}\cdot\left(\boldsymbol{l}_{ij}\times\boldsymbol{n}_i\right), \tag{93}$$

where $d\boldsymbol{l}=(d\xi, d\eta, d\zeta)$, $\boldsymbol{r}_M=(x,y,z)$, $\boldsymbol{r}_P=(\xi,\eta,\zeta)$, $\boldsymbol{n}_i=(n_{i,1},n_{i,2},n_{i,3})$,
$\boldsymbol{l}_{ij}=\boldsymbol{r}_{2ij}-\boldsymbol{r}_{1ij}=(x_{2ij}-x_{1ij},y_{2ij}-y_{1ij},z_{2ij}-z_{1ij})$.

P_{ij}, Q_{ij}, R_{ij} are successively the value of $\int_{L_{ij}}\frac{d\xi}{r_{MP}}$, $\int_{L_{ij}}\frac{d\eta}{r_{MP}}$, $\int_{L_{ij}}\frac{d\varsigma}{r_{MP}}$ line integrals.

Since $P(\xi, \eta, \varsigma)\in L_{ij}$, it holds: $\frac{\xi-x_{1ij}}{x_{2ij}-x_{1ij}}=\frac{\eta-y_{1ij}}{y_{2ij}-y_{1ij}}=\frac{\varsigma-z_{1ij}}{z_{2ij}-z_{1ij}}$.

Applying the $\frac{\xi-x_{1ij}}{x_{2ij}-x_{1ij}}=t$ substitution, we get:

$r_{MP}=\sqrt{(\xi-x)^2+(\eta-y)^2+(\varsigma-z)^2}=\sqrt{l_{ij}^2t^2+2\boldsymbol{r}_{1ij}\boldsymbol{l}_{ij}t+\boldsymbol{r}_{1ij}^2}$, where $l_{ij}=|\boldsymbol{l}_{ij}|$. Making use of these relations, P_{ij}, Q_{ij}, R_{ij} takes the form:

$$P_{ij}=\int_{L_{ij}}\frac{d\xi}{r_{MP}}=\left(x_{2ij}-x_{1ij}\right)\int_0^1\frac{dt}{\sqrt{\boldsymbol{l}_{ij}^2t^2+2\boldsymbol{r}_{1ij}\boldsymbol{l}_{ij}t+\boldsymbol{r}_{1ij}^2}}=\left(x_{2ij}-x_{1ij}\right)I_{ij}, \tag{94}$$

and similarly

$$Q_{ij}=\left(y_{2ij}-y_{1ij}\right)I_{ij},\quad R_{ij}=\left(z_{2ij}-z_{1ij}\right)I_{ij}, \tag{95}$$

where

$$I_{ij}=\begin{cases}\frac{1}{l_{ij}}\ln\frac{\sqrt{\boldsymbol{l}_{ij}^2+2\boldsymbol{r}_{1ij}\boldsymbol{l}_{ij}+\boldsymbol{r}_{1ij}^2}+l_{ij}+\boldsymbol{r}_{1ij}\boldsymbol{\mu}_{ij}}{r_{1ij}+\boldsymbol{r}_{1ij}\boldsymbol{\mu}_{ij}} & \text{if } r_{1ij}+\boldsymbol{r}_{1ij}\boldsymbol{\mu}_{ij}\neq 0\\ \frac{1}{l_{ij}}\ln\frac{\left|l_{ij}-r_{1ij}\right|}{r_{1ij}} & \text{if } r_{1ij}+\boldsymbol{r}_{1ij}\boldsymbol{\mu}_{ij}=0\end{cases}. \tag{96}$$

The expression of the gravitational potential in terms of P_{ij}, Q_{ij}, R_{ij}, I_{ij} constants are:

$$U(M)=\frac{G\rho_0}{2}\sum_{i=1}^{n}h_i\left(\sum_{j=1}^{l(i)}h_{ij}C_{ij}-h_i\Omega_i\right)=$$

$$=\frac{G\rho_0}{2}\sum_{i=1}^{n}h_i\sum_{j=1}^{l(i)}\left(x_{1ij}-x\right)\left(n_{i,3}Q_{ij}-n_{i,2}R_{ij}\right)+\left(y_{1ij}-y\right)\left(n_{i,1}R_{ij}-n_{i,3}P_{ij}\right)+\left(z_{1ij}-z\right)\left(n_{i,2}P_{ij}-n_{i,1}Q_{ij}\right)-$$

$$-\frac{G\rho_0}{2}\sum_{i=1}^{n}h_i^2\Omega_i=\frac{G\rho_0}{2}\left(\sum_{i=1}^{n}h_i\sum_{j=1}^{l(i)}I_{ij}\boldsymbol{r}_{1ij}\left(\boldsymbol{l}_{ij}\times\boldsymbol{n}_i\right)-\sum_{i=1}^{n}h_i^2\Omega_i\right). \tag{97}$$

1.2.5 Geometrical interpretation of C_{ij} and Ω_{ij} constants. Definition and interpretation of particular vector invariants defined by means of these constants

The geometrical interpretation of the Ω_i constant will be introduced in detail in the following part based on results presented by Werner and Scheeres (1997).

$$\sum_{j=1}^{l(i)} c_{ij} = \iint_{S_i} \frac{1}{r_{MP}} d\sigma_P = \iint_{S_i} \frac{r_{MP}^2 + h_i^2}{r_{MP}^3} d\sigma_P - \iint_{S_i} \frac{h_i^2}{r_{MP}^3} d\sigma_P = \iint_{S_i} \nabla_{\boldsymbol{r}_P} \cdot \frac{\boldsymbol{s}_{MP}}{r_{MP}} d\sigma_P - \iint_{S_i} \frac{(\boldsymbol{r}_{MP} \cdot \boldsymbol{n}_i)^2}{r_{MP}^3} d\sigma_P =$$

$$= \int_{\partial S_i} \frac{\boldsymbol{s}_{MP}}{r_{MP}} \cdot \boldsymbol{v} dl - (\boldsymbol{n}_i \cdot \boldsymbol{r}_{MP}) \iint_{S_i} \frac{1}{r_{MP}^2} \frac{\boldsymbol{r}_{MP} \cdot \boldsymbol{n}_i}{r_{MP}} d\sigma_P = \sum_{j=1}^{l(i)} h_{ij} \int_{L_{ij}} \frac{1}{r_{MP}} dl - h_i \iint_{S_i} \frac{\cos(\boldsymbol{r}_{MP}, \boldsymbol{n}_i)}{r_{MP}^2} d\sigma_P = \sum_{j=1}^{l(i)} h_{ij} C_{ij} - h_i \Omega , \tag{98}$$

where

$$C_{ij} = \int_{L_{ij}} \frac{1}{r_{MP}} dl , \ \Omega_i = \iint_{S_i} \frac{h_i}{r_{MP}^3} d\sigma_P = \iint_{S_i} \frac{\cos(\boldsymbol{r}_{MP}, \boldsymbol{n}_i)}{r_{MP}^2} d\sigma_P . \tag{99}$$

We can concluded from the 2th remark of Theorem 12 that Ω_i is equal to the magnitude of that solid angle related to the area S_i subtended at point M. The solid angle for an arbitrary oriented surface S subtended at a point P is equal to the solid angle of projection of surface S to the unit sphere with centre P, which can be calculated as a surface integral. Additionally,

$$\Omega_i = \sum_{j=1}^{l(i)} \Omega_{ij} \text{ , where } \Omega_{ij} = \iint_{\Delta_{12ij}} \frac{1}{r_{MP}^2} \frac{\boldsymbol{r}_{MP} \cdot \boldsymbol{n}_i}{r_{MP}} d\sigma_P = h_i \iint_{\Delta_{12ij}} \frac{1}{r_{MP}^3} d\sigma_P . \tag{100}$$

The following differential equation:

$$\nabla_{\boldsymbol{r}_P} \cdot \boldsymbol{f}_i(\boldsymbol{r}_P) = \frac{1}{r_{MP}^3} \tag{101}$$

is solved similarly to (56) on the set of functions $\{ \boldsymbol{f}_i(\boldsymbol{r}_P) \in S_i \mid \boldsymbol{f}_i(\boldsymbol{r}_P) = c(x', y') \boldsymbol{s}_{MP} \}$, where (x', y') is a coordinate system situated in the S_i plane with the origin in M_i. In this system $\boldsymbol{s}_{MP} = (x', y')$ is the position vector of P situated in S_i , $r_{MP} = \sqrt{x'^2 + y'^2 + h_i^2}$ is the MP vector norm (Fig. 2). The equation $\nabla_{\boldsymbol{r}_P} \cdot \boldsymbol{f}_i(\boldsymbol{r}_P) = \frac{1}{r_{MP}^3}$ leads to a quasilinear differential equation, whose general solution can be written as:

$$\boldsymbol{f}_i(\boldsymbol{r}_P) = \left(\frac{r_{MP} \phi^* \left(\frac{y'}{x'} \right) - 1}{s_{MP}^2 r_{MP}} \right) \boldsymbol{s}_{MP} . \tag{102}$$

Choosing $\phi^* = \frac{1}{|h_i|}$ the $\boldsymbol{f}_i$ will be defined in Δ_{12ij} (Fig. 3) and fulfils the condition of Gauss-Ostrogradsky theorem in this domain:

$$\Omega_{ij} = h_i \int_{\partial \Delta_{12ij}} \boldsymbol{f}_i \cdot \boldsymbol{v} dl = h_i \int_{\partial \Delta_{12ij}} \left(\frac{r_{MP} \left| h_i^{-1} \right| - 1}{s_{MP}^2 r_{MP}} \right) \boldsymbol{s}_{MP} \cdot \boldsymbol{v} dl = h_i \int_{L_{ij}} \left(\frac{r_{MP} \left| h_i^{-1} \right| - 1}{s_{MP}^2 r_{MP}} \right) \boldsymbol{s}_{MP} \cdot \boldsymbol{v}_{ij} dl =$$

$$=h_i h_{ij}\int_{L_{ij}}\left(\frac{1}{|h_i|s_{MP}^2}-\frac{1}{s_{MP}^2 r_{MP}}\right)dl=\left[\operatorname{sign}(h_i)\cdot\operatorname{atan}\left(\frac{l}{h_{ij}}\right)-\operatorname{atan}\left(\frac{h_i l}{r_{MP}h_{ij}}\right)\right]_{l_{1ij}}^{l_{2ij}}. \tag{103}$$

We consider the following relation:

$\left[\operatorname{atan}\left(\frac{l}{h_{ij}}\right)\right]_{l_{1ij}}^{l_{2ij}}=\operatorname{sign}(h_{ij})\left[\operatorname{atan}\left(\frac{l}{|h_{ij}|}\right)\right]_{l_{1ij}}^{l_{2ij}}=\operatorname{sign}(h_{ij})A_{ij}M_iA_{ij+1}$, where the term $\left[\operatorname{atan}\left(\frac{l}{h_{ij}}\right)\right]_{l_{1ij}}^{l_{2ij}}$ in fact is the signed angle $A_{ij}M_iA_{ij+1}$. h_{ij} is positive if M is leaving from left when we moving along the ∂S_i and negative when M is leaving from right. Summing these angles along the ∂S_i, we get the angle θ_i at which the ∂S_i closed curve is visible from the M_i point:

$$\sum_j^{l(i)}\left[\operatorname{atan}\left(\frac{l}{h_{ij}}\right)\right]_{l_{1ij}}^{l_{2ij}}=\theta_i\ . \tag{104}$$

Ω_{ij} constants (103) are substituted in the formula (91):

$$U(M)=\frac{G\rho_0}{2}\sum_{i=1}^{n}h_i\sum_{j=1}^{l(i)}c_{ij}=\frac{G\rho_0}{2}\sum_{i=1}^{n}h_i\left(\sum_{j=1}^{l(i)}h_{ij}C_{ij}-h_i\Omega_i\right)=\frac{G\rho_0}{2}\sum_{i=1}^{n}h_i\left(\sum_{j=1}^{l(i)}\left(h_{ij}C_{ij}-h_i\Omega_{ij}\right)\right). \tag{105}$$

Holstein 2002a, 2002b introduced the $\boldsymbol{b}_{ij}$ vector invariants as a function of C_{ij} and Ω_{ij} constants:

$$\boldsymbol{b}_{ij}=\boldsymbol{v}_{ij}C_{ij}-\boldsymbol{n}_i\Omega_{ij}\,. \tag{106}$$

Using the following relations: $h_{ij}=\boldsymbol{v}_{ij}\cdot\boldsymbol{r}_{MP}$ if $P\in L_{ij}$ and $h_i=\boldsymbol{n}_i\cdot\boldsymbol{r}_{MP}$ if $P\in S_i$ we can derive:

$$c_{ij}=\boldsymbol{b}_{ij}\cdot\boldsymbol{r}_{MP}\ \text{ if } P\in L_{ij}.$$

If $P = A_{ij}$ the above relation becomes:

$$c_{ij}=\boldsymbol{b}_{ij}\cdot\boldsymbol{r}_{1ij}\,. \tag{107}$$

The potential formula with vector quantities:

$$U(M)=\frac{G\rho_0}{2}\sum_{i=1}^{n}\boldsymbol{n}_i\cdot\boldsymbol{r}_i\sum_{j=1}^{l(i)}\boldsymbol{b}_{ij}\cdot\boldsymbol{r}_{1ij}\,, \tag{108}$$

where $\boldsymbol{r}_i=\boldsymbol{r}_{MP}$ is the position vector of an arbitrary point $P\in S_i$.

Based on the Remark 2 of Theorem 12 in Section 1.1.1 and on relations (99) and (100) the Ω_i and Ω_{ij} in fact denote the solid angles associated to the point M and the areas S_i and respectively Δ_{12ij}. From definition the absolute value of solid angle of a planar polygonal region is equal with the area of spherical polygon image projected on the unit sphere centred in M. (Fig. 5). In case of unit sphere the area of spherical polygon is equal with the spherical excess (Bronstejn and Szemengyajev 1987), so we have:

$$|\Omega_i|=\operatorname{Area}\left(S_i^*=A_{i1}^*A_{i2}^*\ldots A_{ij}^*\ldots A_{il(i)}^*A_{i1}^*\right)=\sum_{j=1}^{l(i)}S_{ij}-(l(i)-2)\pi \tag{109}$$

$$\left|\Omega_{ij}\right|=\operatorname{Area}\left(\Delta_{ij}^*=M_i^*A_{ij}^*A_{ij+1}^*\right)=\alpha+\beta+\gamma-\pi \tag{110}$$

where S_{ij} is the angle belonging to the edge MA_{ij} and equal to the angle defined by the planes $MA_{ij-1}A_{ij}$ and $MA_{ij}A_{ij+1}$. Let α be the angle determined by the MM_iA_{ij} and MM_iA_{ij+1}. This is equal with the

$A_{ij}M_iA_{ij+1}$ angle. Let β and γ be the angles enclosed by the $MA_{ij-1}A_{ij}$ and $MA_{ij}A_{ij+1}$ and respectively by the $MA_{ij-1}A_{ij}$ and $MA_{ij}A_{ij+1}$ planes.

We will demonstrate that the absolute value of the Ω_{ij} constant defined by (103) is identical with the spherical excess given by (110). Allowing for the fact that $\alpha, \beta, \gamma \in (0,\pi)$ we have:

$$\alpha = A_{ij}M_iA_{ij+1} = \left[\operatorname{atan}\left(\frac{l}{|h_{ij}|}\right)\right]_{l_{1ij}}^{l_{2ij}} \tag{111}$$

and $\gamma = A_{ij}QR$, where Q and R fulfil the conditions $A_{ij}Q \perp MA_{ij+1}$, $A_{ij}Q \perp MA_{ij+1}$ (Fig. 5). Thus $A_{ij}R \perp (M_iA_{ij+1}M)$ and from this arise $RQ \perp MA_{ij+1}$. By right of definition the angle between the $MA_{ij-1}A_{ij}$ and $MA_{ij}A_{ij+1}$ planes is an angle smaller than 180° defined by straight lines $A_{ij}Q$ and RQ which are perpendicular to the common edge $A_{ij}M, A_{ij}Q, RQ \perp MA_{ij+1}$.

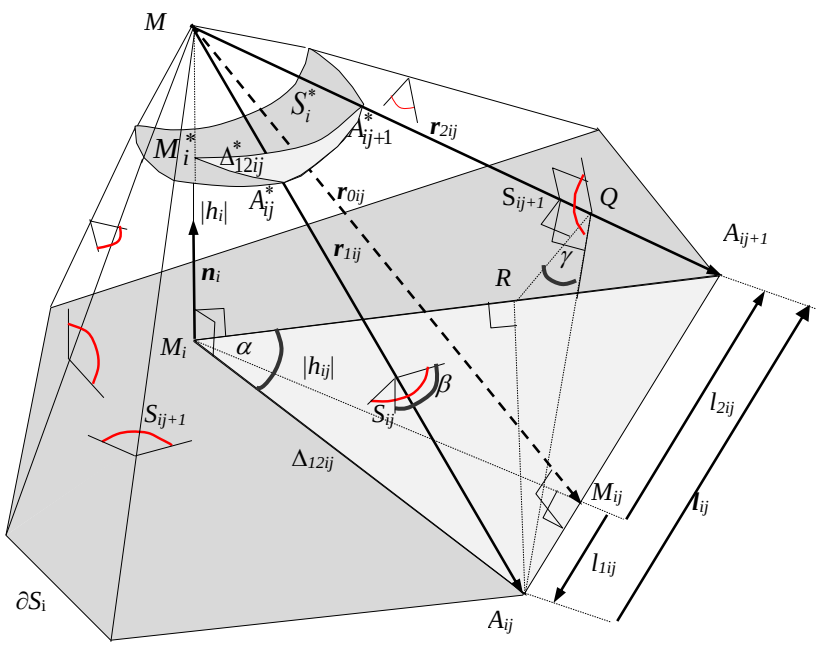

Fig. 5 The S_i planar polygon and the adherent spherical polygon image S_i^* projected on the unit sphere centred in M, the plane and spherical triangle faces Δ_{12ij} and Δ_{12ij}^*. S_{ij} is the angle between the $MA_{ij-1}A_{ij}$ and $MA_{ij}A_{ij+1}$ faces

It is easy to demonstrate that: $\tan\gamma^* = \dfrac{r_{MP}|h_{ij}|}{|h_i||l_1|}$, where $\gamma^* = \begin{cases} \gamma & \text{if } \gamma \in (0,\pi/2) \\ \pi-\gamma & \text{if } \gamma \in (\pi/2,\pi) \end{cases}$, thus

$$\gamma = \begin{cases} \operatorname{atan}\left(\dfrac{r_{MP}|h_{ij}|}{|h_i||l_2|}\right) & \text{if } \gamma \in (0,\pi/2) \\ \pi - \operatorname{atan}\left(\dfrac{r_{MP}|h_{ij}|}{|h_i||l_2|}\right) & \text{if } \gamma \in (\pi/2,\pi) \end{cases}. \tag{112}$$

The same identity holds for β. Starting from (103) we have:

$$\left|\Omega_{ij}\right| = \left|\operatorname{sign}(h_i)\cdot\operatorname{sign}(h_{ij})\left[\operatorname{atan}\left(\frac{l}{h_{ij}}\right)-\operatorname{atan}\left(\frac{h_i l}{r_{MP}h_{ij}}\right)\right]_{l_{1ij}}^{l_{2ij}}\right| = \left[\operatorname{atan}\left(\frac{l}{|h_{ij}|}\right)-\operatorname{atan}\left(\frac{|h_i|l}{r_{MP}|h_{ij}|}\right)\right]_{l_{1ij}}^{l_{2ij}} =$$

$$= \begin{cases} \operatorname{atan}\left(\frac{l_2}{|h_{ij}|}\right)-\operatorname{atan}\left(\frac{l_1}{|h_{ij}|}\right)+\operatorname{atan}\left(\frac{r_{MP}|h_{ij}|}{|h_i|l_2}\right)-\operatorname{atan}\left(\frac{r_{MP}|h_{ij}|}{|h_i|l_1}\right)-\pi & \text{if } l_2>0, l_1<0 \\ \operatorname{atan}\left(\frac{l_2}{|h_{ij}|}\right)-\operatorname{atan}\left(\frac{l_1}{|h_{ij}|}\right)+\operatorname{atan}\left(\frac{r_{MP}|h_{ij}|}{|h_i|l_2}\right)-\operatorname{atan}\left(\frac{r_{MP}|h_{ij}|}{|h_i|l_1}\right) & \text{if } l_1>0, l_2>0 \\ \operatorname{atan}\left(\frac{l_2}{|h_{ij}|}\right)-\operatorname{atan}\left(\frac{l_1}{|h_{ij}|}\right)+\operatorname{atan}\left(\frac{r_{MP}|h_{ij}|}{|h_i|l_2}\right)-\operatorname{atan}\left(\frac{r_{MP}|h_{ij}|}{|h_i|l_1}\right) & \text{if } l_1<0, l_2<0 \end{cases} = \alpha+\beta+\gamma-\pi. \tag{113}$$

Here the following identity was used: $\operatorname{atan} x + \operatorname{atan}\frac{1}{x} = \begin{cases} \pi/2 & \text{if } x>0 \\ -\pi/2 & \text{if } x<0 \end{cases}$.

In addition the (113) relation yields the geometrical interpretation of the atan terms in expression (102) of Ω_{ij} .Starting from the geometrical interpretation of Ω_i and Ω_{ij} (Werner and Scheeres 1997) we can derive a more compact formula for these quantities. In the first step the relation (27) derived by Werner and Scheeres 1997 will be demonstrated below for a special case.

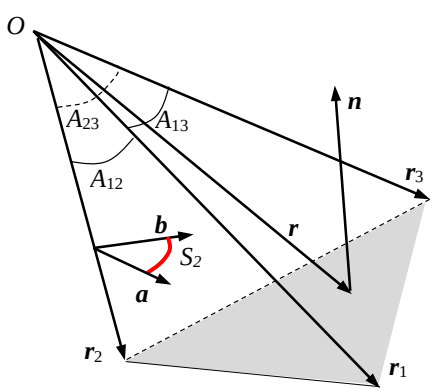

Fig. 6 The solid angle Ω defined by the vectors $\boldsymbol{r}_1$, $\boldsymbol{r}_2$, $\boldsymbol{r}_3$; the angle S_2 determined by the planes ($\boldsymbol{r}_1$, $\boldsymbol{r}_2$) and ($\boldsymbol{r}_2$, $\boldsymbol{r}_3$) and equal with the angle between the $\boldsymbol{a}$ and $\boldsymbol{b}$ vectors. $\boldsymbol{a}$, $\boldsymbol{b}$ are vectors situated in planes ($\boldsymbol{r}_1$, $\boldsymbol{r}_2$) and ($\boldsymbol{r}_2$, $\boldsymbol{r}_3$) and perpendiculars to $\boldsymbol{r}_2$. $\boldsymbol{n}$ is a normal vector of the plane defined by the endpoints of $\boldsymbol{r}_1$, $\boldsymbol{r}_2$, $\boldsymbol{r}_3$ vectors, $\boldsymbol{r}$ denotes the position vectors of vectors with start point *O* and endpoint on this plane

A_{12}, A_{13}, A_{23} denote the angles consecutively of vectors $\boldsymbol{r}_1$ and $\boldsymbol{r}_2$, $\boldsymbol{r}_1$ and $\boldsymbol{r}_3$, $\boldsymbol{r}_2$ and $\boldsymbol{r}_3$. S_2 denotes the angle of ($\boldsymbol{r}_1$, $\boldsymbol{r}_2$) and ($\boldsymbol{r}_2$, $\boldsymbol{r}_3$) planes. We determine that vectors denoted by $\boldsymbol{a}$ and $\boldsymbol{b}$, with the property that $\boldsymbol{a}$ is situated in the plane defined by $\boldsymbol{r}_1$ and $\boldsymbol{r}_2$, $\boldsymbol{a}\in(\boldsymbol{r}_1, \boldsymbol{r}_2)$ and $\boldsymbol{a}\perp\boldsymbol{r}_2$. Similarly the vector $\boldsymbol{b}$ fulfils $\boldsymbol{b}\in(\boldsymbol{r}_2, \boldsymbol{r}_3)$ and $\boldsymbol{b}\perp\boldsymbol{r}_2$ conditions (Fig. 6). From this S_2 is equal with the angle of vectors $\boldsymbol{a}$ and $\boldsymbol{b}$. Let $\hat{\boldsymbol{r}}_1, \hat{\boldsymbol{r}}_2, \hat{\boldsymbol{r}}_3, \hat{\boldsymbol{a}}, \hat{\boldsymbol{b}}$ successively be the unit vectors of $\boldsymbol{r}_1$, $\boldsymbol{r}_2$, $\boldsymbol{r}_3$, $\boldsymbol{a}$, $\boldsymbol{b}$ vectors. Since $S_2\in(0,\pi)$, therefore $\sin S_2>0$.

$$\boldsymbol{a} = (\boldsymbol{r}_2\times\boldsymbol{r}_1)\times\boldsymbol{r}_2 = \boldsymbol{r}_1(\boldsymbol{r}_2\cdot\boldsymbol{r}_2)-\boldsymbol{r}_2(\boldsymbol{r}_2\cdot\boldsymbol{r}_1) = \boldsymbol{r}_1 r_2^2 - \boldsymbol{r}_2 r_1 r_2\cos A_{12} = r_1 r_2^2(\hat{\boldsymbol{r}}_1-\hat{\boldsymbol{r}}_2\cos A_{12}).$$

Similarly:

$$\boldsymbol{b} = \boldsymbol{r}_2\times(\boldsymbol{r}_3\times\boldsymbol{r}_2) = \boldsymbol{r}_3(\boldsymbol{r}_2\cdot\boldsymbol{r}_2)-\boldsymbol{r}_2(\boldsymbol{r}_2\cdot\boldsymbol{r}_3) = \boldsymbol{r}_3 r_2^2 - \boldsymbol{r}_2 r_3 r_2\cos A_{23} = r_3 r_2^2(\hat{\boldsymbol{r}}_3-\hat{\boldsymbol{r}}_2\cos A_{23}).$$

$$\cos S_2 = \frac{\boldsymbol{a}\cdot\boldsymbol{b}}{|\boldsymbol{a}||\boldsymbol{b}|} = \frac{r_1 r_3 r_2^4 \left(\hat{\boldsymbol{r}}_1 - \hat{\boldsymbol{r}}_2 \cos A_{12}\right)\left(\hat{\boldsymbol{r}}_3 - \hat{\boldsymbol{r}}_2 \cos A_{23}\right)}{r_1 r_3 r_2^4 \sqrt{\left(\hat{\boldsymbol{r}}_1 - \hat{\boldsymbol{r}}_2 \cos A_{12}\right)^2}\sqrt{\left(\hat{\boldsymbol{r}}_3 - \hat{\boldsymbol{r}}_2 \cos A_{23}\right)^2}} = \frac{\cos A_{13} - \cos A_{23}\cos A_{12}}{\sqrt{1-\cos^2 A_{12}}\sqrt{1-\cos^2 A_{23}}}, \tag{114}$$

$$\sin S_2 = \left|\hat{\boldsymbol{r}}_2 \cdot \left(\hat{\boldsymbol{a}} \times \hat{\boldsymbol{b}}\right)\right| = \frac{\left|\hat{\boldsymbol{r}}_2 \cdot \left(\hat{\boldsymbol{r}}_1 \times \hat{\boldsymbol{r}}_3\right)\right|}{\sqrt{\left(1-\cos^2 A_{12}\right)}\sqrt{\left(1-\cos^2 A_{23}\right)}}, \tag{115}$$

where:

$$\cos A_{12} = \frac{\boldsymbol{r}_1 \cdot \boldsymbol{r}_2}{|\boldsymbol{r}_1||\boldsymbol{r}_2|} = \hat{\boldsymbol{r}}_1 \cdot \hat{\boldsymbol{r}}_2,\ \cos A_{23} = \frac{\boldsymbol{r}_2 \cdot \boldsymbol{r}_3}{|\boldsymbol{r}_2||\boldsymbol{r}_3|} = \hat{\boldsymbol{r}}_2 \cdot \hat{\boldsymbol{r}}_3,\ \cos A_{13} = \frac{\boldsymbol{r}_1 \cdot \boldsymbol{r}_3}{|\boldsymbol{r}_1||\boldsymbol{r}_3|} = \hat{\boldsymbol{r}}_1 \cdot \hat{\boldsymbol{r}}_3 \tag{116}$$

The area of spherical triangle defined by a trihedral, is equal with the spherical excess of spherical triangle (Werner and Scheeres 1997), therefore:

$$\tan\frac{S_1 + S_2 + S_3 - \pi}{2} = \frac{\left|\hat{\boldsymbol{r}}_1 \cdot \left(\hat{\boldsymbol{r}}_2 \times \hat{\boldsymbol{r}}_3\right)\right|}{1 + \cos A_{12} + \cos A_{12} + \cos A_{12}} = \frac{\left|\boldsymbol{r}_1 \cdot \left(\boldsymbol{r}_2 \times \boldsymbol{r}_3\right)\right|}{r_1 r_2 r_3 + r_1 \boldsymbol{r}_2 \cdot \boldsymbol{r}_3 + r_2 \boldsymbol{r}_1 \cdot \boldsymbol{r}_3 + r_3 \boldsymbol{r}_1 \cdot \boldsymbol{r}_3}.$$

Since $\frac{S_1 + S_2 + S_3 - \pi}{2} \in (0, \pi)$ this angle can be uniquely determined using the atan2[1] $\in(-\pi, \pi)$ trigonometric function:

$$S_1 + S_2 + S_3 - \pi = 2\,\mathrm{atan}\,2\left(\left|\boldsymbol{r}_1 \cdot \left(\boldsymbol{r}_2 \times \boldsymbol{r}_3\right)\right|, r_1 r_2 r_3 + r_1 \boldsymbol{r}_2 \cdot \boldsymbol{r}_3 + r_2 \boldsymbol{r}_1 \cdot \boldsymbol{r}_3 + r_3 \boldsymbol{r}_1 \cdot \boldsymbol{r}_2\right). \tag{117}$$

Based on (117) we can established that the solid angle Ω defined by $\boldsymbol{r}_1$, $\boldsymbol{r}_2$, $\mathbf{r}_3$ vectors is equal with spherical excess assigned by them. The sign of Ω is identic with the sign of scalar product $\boldsymbol{n}\cdot\mathbf{r}$, where $\boldsymbol{n}$ is the normal vector of the plane stretched by the $\boldsymbol{r}_1$, $\boldsymbol{r}_2$, $\boldsymbol{r}_3$ vectors and $\boldsymbol{r}$ denotes the position vectors of the plane points respect to the point O (Fig. 6). If $\boldsymbol{r}_1$, $\boldsymbol{r}_2$, $\boldsymbol{r}_3$ defines a right-hand system, then O and $\boldsymbol{n}$ are situated on different side of the plane stretched by the $\boldsymbol{r}_1$, $\boldsymbol{r}_2$, $\boldsymbol{r}_3$ vectors, thus $\boldsymbol{n}\cdot\boldsymbol{r}$ will positive quantity. Otherwise if O and $\boldsymbol{n}$ are on the same side of plane $\boldsymbol{n}\cdot\boldsymbol{r}$ will be negative. Thus $\mathrm{sign}(\boldsymbol{n}\cdot\boldsymbol{r}) = \mathrm{sign}(\boldsymbol{r}_1\cdot(\boldsymbol{r}_2\times\boldsymbol{r}_3))$ and:

$$\Omega = 2\,\mathrm{atan}\,2\left(\boldsymbol{r}_1 \cdot \left(\boldsymbol{r}_2 \times \boldsymbol{r}_3\right), r_1 r_2 r_3 + r_1 \boldsymbol{r}_2 \cdot \boldsymbol{r}_3 + r_2 \boldsymbol{r}_1 \cdot \boldsymbol{r}_3 + r_3 \boldsymbol{r}_1 \cdot \boldsymbol{r}_2\right). \tag{118}$$

Substituting in (118) instead of $\boldsymbol{r}_1$, $\boldsymbol{r}_2$, $\boldsymbol{r}_3$ successively the vectors $h_i\boldsymbol{n}_i$, $\boldsymbol{r}_{1ij} = \boldsymbol{a}_{ij} - \boldsymbol{r}_M$, $\boldsymbol{r}_{2ij} = \boldsymbol{a}_{ij+1} - \boldsymbol{r}_M$ we get $|\Omega_{ij}|$. Taking into account that ($\boldsymbol{n}_i$, $\boldsymbol{r}_{1ij}$, $\boldsymbol{r}_{2ij}$) vectors form a right-hand system, we can derive:

$$\begin{aligned}\Omega_{ij}^{W-S} &= \mathrm{sign}\left(h_{ij}\right)\cdot\mathrm{sign}\left(h_i\right)\cdot\left|\Omega_{ij}\right| = \\ &= 2\,\mathrm{sign}\left(h_{ij}\right)\cdot\mathrm{atan}\,2\left(\mathrm{sign}\left(h_i\right)\left|h_i \boldsymbol{n}_i\left(\boldsymbol{r}_{1ij} \times \boldsymbol{r}_{2ij}\right)\right|, |h_i| r_{1ij} r_{2ij} + |h_i| \boldsymbol{r}_{1ij}\boldsymbol{r}_{2ij} + h_i r_{1ij} \boldsymbol{n}_i \boldsymbol{r}_3 + h_i r_{2ij} \boldsymbol{r}_1 \boldsymbol{r}_2\right) \\ &= 2\,\mathrm{sign}\left(h_{ij}\right)\cdot\mathrm{atan}\,2\left(\left(h_i \boldsymbol{n}_i\left(\boldsymbol{r}_{1ij} \times \boldsymbol{r}_{2ij}\right)\right), |h_i| r_{1ij} r_{2ij} + |h_i| \boldsymbol{r}_{1ij}\boldsymbol{r}_{2ij} + h_i r_{1ij} \boldsymbol{n}_i \boldsymbol{r}_3 + h_i r_{2ij} \boldsymbol{r}_1 \boldsymbol{r}_2\right).\end{aligned} \tag{119}$$

As we previously mentioned h_{ij} is positive if the orientation of ∂S_i curve corresponds to right-hand rule and is negative otherwise. The expression of Ω_{ij} notated by (81) contains two or four arctg terms, but (119) and (73) formulas contains only one term.

---

[1] atan2(y,x) is the arc tangent value in term of radian of the argument of the complex number x+iy. If $y\neq0$, then $\mathrm{atan}2(y,x)=\begin{cases}\varphi\cdot\mathrm{sign}(y) & \text{if } x>0\\ \frac{\pi}{2}\cdot\mathrm{sign}(y) & \text{if } x=0\\ (\pi-\varphi)\cdot\mathrm{sign}(y) & \text{if } x<0\end{cases}$. If $y = 0$, then $\mathrm{atan}2(0,x)=\begin{cases}0 & \text{if } x>0\\ NaN & \text{if } x=0\\ \pi & \text{if } x<0\end{cases}$, where $\varphi\in[0,\pi/2[$, $\tan\varphi=|y/x|$.

Ω_i can be computed using (100). According to this formula Ω_i is sum of Ω_{ij} terms, as follows its value can be computed using least of $l(i)$ number of atan terms. Accordingly with (109) another possibility to compute Ω_i is using of S_{ij} angles (Fig. 5). To compute Ω_i the computation of $l(i)$ number of atan terms are required. This formula permits the recursive computation of $|\Omega_i|$ (Werner and Scheeres, 1997). In case of convex polyhedron we have $S_{ij} \in (0, \pi)$ for $\forall i \in \overline{1,n}, \forall j \in \overline{1,l(i)}$.

$$|\Omega_i| = \sum_{j=1}^{l(i)} S_{ij} - (l(i)-2)\pi = \sum_{j=1}^{l(i)} (S_{ij} - \pi) + 2\pi = x_{l(i)} + 2\pi \in (0,2\pi), \tag{120}$$

where $x_k = \sum_{j=1}^{k} (S_{ij} - \pi) \in (-2\pi, 0)$. The recursive relation for x_k:

$$\begin{bmatrix} \cos\ x_k \\ \sin\ x_k \end{bmatrix} = \begin{bmatrix} \cos\ x_{k-1} & -\sin\ x_{k-1} \\ \sin\ x_{k-1} & \cos\ x_{k-1} \end{bmatrix} \begin{bmatrix} \cos\ (S_{ik} - \pi) \\ \sin\ (S_{ik} - \pi) \end{bmatrix},\ k = 1, l(i),\ x_0 = 0, \tag{121}$$

Using (114), (115) and (116): $\cos(S_{ik} - \pi) = \frac{r_{ik-1} \cdot r_{ik+1} - (r_{ik} \cdot r_{ik+1})(r_{ik-1} \cdot r_{ik})}{\sqrt{1-(r_{ik-1} \cdot r_{ik})^2}\sqrt{1-(r_{ik} \cdot r_{ik+1})^2}}$ and

$$\sin(S_{ik} - \pi) = \frac{|r_{ik} \cdot (r_{ik-1} \times r_{ik+1})|}{\sqrt{1-((r_{ik-1} \cdot r_{ik})^2)}\sqrt{1-((r_{ik} \cdot r_{ik+1})^2)}},\ k = \overline{1, l(i)}, \tag{122}$$

where $\boldsymbol{r}_{ik}$ and $\hat{\boldsymbol{r}}_{ik}$ denotes position vector corresponding to the kth vertex of ith face with origin in M and the unit vector of this $\left(\hat{\boldsymbol{r}}_{ik} = \frac{\boldsymbol{a}_{ik} - \boldsymbol{r}_M}{|\boldsymbol{a}_{ik} - \boldsymbol{r}_M|}\right)$. Considering the $\hat{\boldsymbol{r}}_{i0} = \hat{\boldsymbol{r}}_{il(i)}$, $\hat{\boldsymbol{r}}_{il(i)+1} = \hat{\boldsymbol{r}}_{i1}$ conditions, after $l(i)$ steps we will get the value of $\cos x_{l(i)}$ and $\sin x_{l(i)}$ which holds $\cos|\Omega_i| = \cos x_{l(i)}$ and $\sin|\Omega_i| = \cos x_{l(i)}$ based on (120). $|\Omega_i|$ can be determined using the atan2 function. Taking into account that the value of the atan2 function is in the $(-\pi, \pi)$ interval because of the angle $|\Omega_i|$ is in the $(0, 2\pi)$ interval, the following relation is valid:

$$|\Omega_i| = \begin{cases} \operatorname{atan2}(\cos x_{l(i)}, \sin x_{l(i)}) & \text{if} \quad \operatorname{atan2}(\cos x_{l(i)}, \sin x_{l(i)}) \geq 0 \\ \pi - \operatorname{atan2}(\cos x_{l(i)}, \sin x_{l(i)}) & \text{if} \quad \operatorname{atan2}(\cos x_{l(i)}, \sin x_{l(i)}) < 0 \end{cases}. \tag{123}$$

The examination of the inequality in (123) can be avoided using half an angle in atan2: $\tan(x_{l(i)}/2) = \frac{1 - \cos x_{l(i)}}{\sin x_{l(i)}} \in (0, \pi)$. Based on this we have the following relation:

$$|\Omega_i| = 2 \cdot \operatorname{atan2}(1 - \cos x_{l(i)}, \sin x_{l(i)}).$$

The Ω_i and the scalar product $\boldsymbol{n} \cdot \boldsymbol{r}_i$ have the same sign where $\boldsymbol{r}_i$ denotes the position vector of S_i points with respect to the origin M. This sign is independent from the $\boldsymbol{r}_i$, thus:

$$\Omega_i = 2\operatorname{sign}(\boldsymbol{n} \cdot \boldsymbol{r}_i) \cdot \operatorname{atan2}(1 - \cos x_{l(i)}, \sin x_{l(i)}) \tag{124}$$

The convex S_i can be divided into (n-2) triangles. Due to (118) the computation of Ω_i can be performed using only ($l(i)$-2) atan terms (Werner and Scheeres 1997):

$$\Omega_i^{WS} = 2\sum_{k=2}^{l(i)-1} \operatorname{atan2}(\boldsymbol{r}_1 \cdot (\boldsymbol{r}_k \times \boldsymbol{r}_{k+1}), r_1 r_k r_{k+1} + r_1 \boldsymbol{r}_k \cdot \boldsymbol{r}_{k+1} + r_k \boldsymbol{r}_1 \cdot \boldsymbol{r}_{k+1} + r_{k+1} \boldsymbol{r}_1 \cdot \boldsymbol{r}_k). \tag{125}$$

1.2.6 The analytical formula of gravitational potential generated by polyhedron allowing for the common edge of faces

Using (104) we have:

$$U(M)=\frac{G\rho_0}{2}\sum_{i=1}^{n}h_i\left(\sum_{j=1}^{l(i)}h_{ij}C_{ij}\right)-\frac{G\rho_0}{2}\sum_{i=1}^{n}h_i\left(h_i\Omega_i\right)=\frac{G\rho_0}{2}\sum_{face}\sum_{edge}\left(\boldsymbol{n}_i\cdot\boldsymbol{r}_i\right)\left(\boldsymbol{v}_{ij}\cdot\boldsymbol{r}_{1ij}\right)C_{ij}-\frac{G\rho_0}{2}\sum_{face}\left(\boldsymbol{n}_i\cdot\boldsymbol{r}_i\right)\left(\boldsymbol{n}_i\cdot\boldsymbol{r}_i\right)\Omega_i=$$

$$=\frac{G\rho_0}{2}\sum_{face}\left(\sum_{edge}\left(\boldsymbol{r}_{1ij}\cdot\boldsymbol{n}_i\right)\left(\boldsymbol{v}_{ij}\cdot\boldsymbol{r}_{1ij}\right)C_{ij}\right)-\frac{G\rho_0}{2}\sum_{face}\left(\boldsymbol{r}_i\cdot\boldsymbol{n}_i\right)\left(\boldsymbol{n}_i\cdot\boldsymbol{r}_i\right)\Omega_i\ . \tag{126}$$

Let E be the number of polyhedron edges. Then the $2E=\sum_{i=1}^{n}l(i)$ sum is equal to the number of terms in the $\sum_{i=1}^{n}\sum_{j=1}^{l(i)}=\sum_{face}\sum_{edge}$ sum. Every edge belongs to two faces, let i and i^* be the order of these and let j, j^* be the order of common edge of the i, i^* faces. Let $\left(\boldsymbol{n}_i,\boldsymbol{v}_{ij},\boldsymbol{\mu}_{ij}\right)$ and $\left(\boldsymbol{n}_{i^*},\boldsymbol{v}_{i^*j^*},\boldsymbol{\mu}_{i^*j^*}\right)$ be the coordinate systems belonging to the common edges $L_{ij}=L_{i^*j^*}$, where $\boldsymbol{n}_i$ and $\boldsymbol{n}_{i^*}$ are the normal vectors of the S_i and S_{i^*} faces. For the point $P\in L_{ij}=L_{i^*j^*}$ situated on the common edge it holds that $\boldsymbol{r}_{1ij}=\boldsymbol{r}_{1i^*j^*}$ (Fig. 7). The direction of the ij^{th} and $i^*j^{*\text{ th}}$ edges are opposite in case of positive direction of faces belonging to these edges, thus

$$C_{edge}=C_{ij}=\left[\ln\left(\frac{r_{MP}+l}{r_{0ij}}\right)\right]_{l_{1ij}}^{l_{2ij}}=-\left[\ln\left(\frac{r_{MP}+l}{r_{0i^*j^*}}\right)\right]_{l_{2i^*j^*}}^{l_{1i^*j^*}}=-C_{i^*j^*}\ . \tag{127}$$

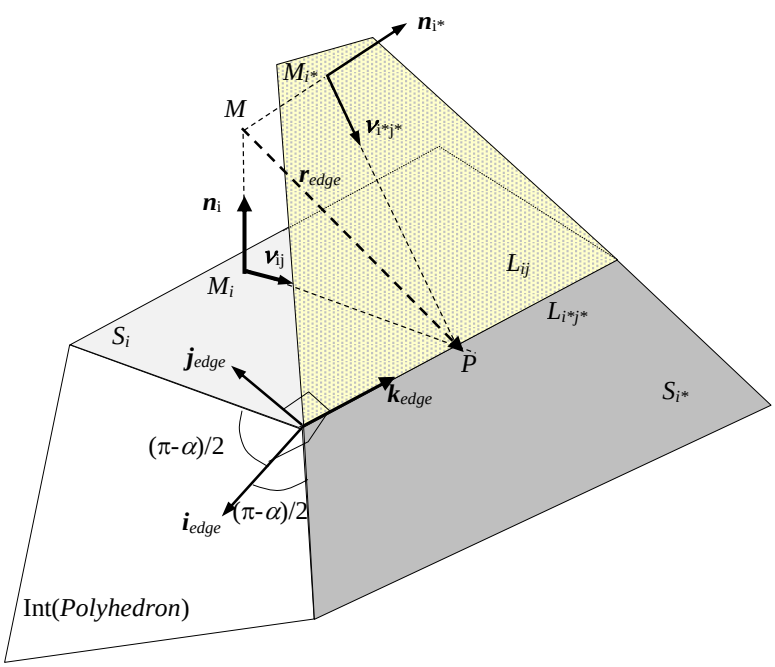

Fig. 7 The S_i, S_{i^*} are the polyhedron faces belonging to the common $L_{ij}=L_{i^*j^*}$ edges. $\left(\boldsymbol{n}_i,\boldsymbol{v}_{ij},\boldsymbol{\mu}_{ij}\right)$ and $\left(\boldsymbol{n}_{i^*},\boldsymbol{v}_{i^*j^*},\boldsymbol{\mu}_{i^*j^*}\right)$ are the associated coordinate systems. The vector system ($\boldsymbol{i}_{edge}$, $\boldsymbol{j}_{edge}$, $\boldsymbol{k}_{edge}$) of the common edge is a right handed coordinate system. The dashed part represents extension of S_{i^*} polyhedron face in Ext(*Polyhedron*) $\subset R^3$

Using the fact that in the sum (127) every edge belongs to two different faces, we can conclude:

$$U(M)=\frac{G\rho_0}{2}\sum_{edge}C_{ij}\left(\boldsymbol{r}_{edge}\cdot\left(\boldsymbol{n}_i\circ\boldsymbol{v}_{ij}-\boldsymbol{n}_{i^*}\circ\boldsymbol{v}_{i^*j^*}\right)\boldsymbol{r}_{edge}\right)-\frac{G\rho_0}{2}\sum_{face}\Omega_i\left(\boldsymbol{r}_i\cdot\left(\boldsymbol{n}_i\circ\boldsymbol{n}_i\right)\cdot\boldsymbol{r}_i\right), \tag{128}$$

where $\circ$ denotes the dyadic product[1]. In (128) the following property of dyadic product was used:

$$(\boldsymbol{c}\cdot\boldsymbol{a})(\boldsymbol{b}\cdot\boldsymbol{c})=\boldsymbol{c}\cdot(\boldsymbol{a}\circ\boldsymbol{b})\cdot\boldsymbol{c}\,.$$

Let be

$$\phi_{edge}=\boldsymbol{n}_i\circ\boldsymbol{v}_{ij}-\boldsymbol{n}_{i^*}\circ\boldsymbol{v}_{i^*j^*}\text{ and }\phi_i=\boldsymbol{n}_i\circ\boldsymbol{n}_i\,. \tag{129}$$

Using the fact that in the sum (127) every edge belongs to the two polyhedron faces, we can conclude:

$$U(M)=\frac{G\rho_0}{2}\sum_{edge}C_{edge}\left(\boldsymbol{r}_{edge}\cdot\phi_{edge}\cdot\boldsymbol{r}_{edge}\right)-\frac{G\rho_0}{2}\sum_{face}\Omega_i\boldsymbol{r}_i\cdot\phi_i\cdot\boldsymbol{r}_i\,. \tag{130}$$

In (130) the number of terms are $E+n$, where E denotes the number of edges, n denotes the number of faces. In (105) the number of terms are $2E+n$.

From the definition of ϕ_i it followes that ϕ_i is a symmetric dyad. Henceforth based on Werner and Scheeres (1997) we will demonstrate that ϕ_{edge} is a symmetric dyad too. Let α be the angle of normal vectors $\boldsymbol{n}_i$ and $\boldsymbol{n}_{i*}$, which is α = arcos($\boldsymbol{n}_i\cdot\boldsymbol{n}_{i*}$). The angle of S_i and S_{i*} faces with the common edge $L_{ij}=L_{i*j*}$ is $\pi-\alpha$. We define a local coordinate system ($\boldsymbol{i}_{edge}$, $\boldsymbol{j}_{edge}$, $\boldsymbol{k}_{edge}$) where $\boldsymbol{i}_{edge}$ is oriented towards the insideof polyhedron and the angles enclosed by this vector with S_i and S_{i*} are the same, namely $(\pi-\alpha)/2$ i.e., it bisects the angle between the faces. Direction of the vector $\boldsymbol{k}_{edge}$ has to coincide with the L_{ij} edge direction, accordingly we have $\boldsymbol{k}_{edge}=\boldsymbol{\mu}_{ij}$ or $\boldsymbol{k}_{edge}=\boldsymbol{\mu}_{i*j*}$. The $\boldsymbol{j}_{edge}$ is chosen so that ($\boldsymbol{i}_{edge}$, $\boldsymbol{j}_{edge}$, $\boldsymbol{k}_{edge}$) is a right-handed system. For $\boldsymbol{n}_i$, $\boldsymbol{n}_{i*}$, $\boldsymbol{\nu}_{ij}$, $\boldsymbol{\nu}_{i*j*}$ vectors and for ϕ_{edge} dyad we have:

$$\boldsymbol{n}_i=\cos(\pi-\alpha/2)\boldsymbol{i}_{edge}+\sin(\pi-\alpha/2)\boldsymbol{j}_{edge}=-\cos(\alpha/2)\boldsymbol{i}_{edge}+\sin(\alpha/2)\boldsymbol{j}_{edge} \tag{131}$$

$$\boldsymbol{n}_{i^*}=\cos(\pi+\alpha/2)\boldsymbol{i}_{edge}+\sin(\pi+\alpha/2)\boldsymbol{j}_{edge}=-\cos(\alpha/2)\boldsymbol{i}_{edge}-\sin(\alpha/2)\boldsymbol{j}_{edge}, \tag{132}$$

$$\boldsymbol{v}_{ij}=\cos(3\pi/2-\alpha/2)\boldsymbol{i}_{edge}+\sin(3\pi/2-\alpha/2)\boldsymbol{j}_{edge}=-\sin(\alpha/2)\boldsymbol{i}_{edge}-\cos(\alpha/2)\boldsymbol{j}_{edge} \tag{133}$$

$$\boldsymbol{v}_{i^*j^*}=\cos(3\pi/2+\alpha/2)\boldsymbol{i}_{edge}+\sin(3\pi/2+\alpha/2)\boldsymbol{j}_{edge}=\sin(\alpha/2)\boldsymbol{i}_{edge}-\cos(\alpha/2)\boldsymbol{j}_{edge} \tag{134}$$

$$\begin{aligned}\boldsymbol{v}_{ij}&=\cos(3\pi/2-\alpha/2)\boldsymbol{i}_{edge}+\sin(3\pi/2-\alpha/2)\boldsymbol{j}_{edge}=-\sin(\alpha/2)\boldsymbol{i}_{edge}-\cos(\alpha/2)\boldsymbol{j}_{edge}=\\&=\sin\alpha\left(\boldsymbol{i}_{edge}\circ\boldsymbol{i}_{edge}-\boldsymbol{j}_{edge}\circ\boldsymbol{j}_{edge}\right)\end{aligned} \tag{135}$$

Since $\boldsymbol{i}_{edge}\circ\boldsymbol{i}_{edge}-\boldsymbol{j}_{edge}\circ\boldsymbol{j}_{edge}$ is a symmetric dyad ϕ_{edge} is a symmetric dyad too.

[1] $\boldsymbol{a}\circ\boldsymbol{b}=\left[a_ib_j\right]_{i,j=\overline{1,3}}$, where $\boldsymbol{a}=(a_1,a_2,a_3)$, $\boldsymbol{b}=(b_1,b_2,b_3)$

1.2.7 The analytical formulas of first derivatives of gravitational potential generated by homogeneous polyhedron volume element

Using the introduced c_{ij}, Ω_i, C_{ij}, Ω_{ij} scalar and the $\boldsymbol{b}_{ij}$ vector quantities the gravitational potential and its first derivatives can expressed as linear combinations of these quantities. We start with applying the gradient operator to gravitational potential

$$\nabla_{\boldsymbol{r}_M} U(M) = G\rho_0 \nabla_{\boldsymbol{r}_M} \int_{\Sigma} \frac{1}{r_{MP}} dv_P = G\rho_0 \int_{\Sigma} \nabla_{\boldsymbol{r}_M} \frac{1}{r_{MP}} dv_P = -G\rho_0 \int_{\Sigma} \nabla_{\boldsymbol{r}_P} \frac{1}{r_{MP}} dv_P = -G\rho_0 \int_{\partial\Sigma} \frac{1}{r_{MP}} d\boldsymbol{\sigma}_P =$$

$$= -G\rho_0 \sum_{i=1}^{n} \int_{S_i} \frac{1}{r_{MP}} \boldsymbol{n}_i d\sigma_P = -G\rho_0 \sum_{i=1}^{n} \boldsymbol{n}_i \int_{S_i} \frac{1}{r_{MP}} d\sigma_P = -G\rho_0 \sum_{i=1}^{n} \boldsymbol{n}_i \sum_{j=1}^{l(i)} c_{ij} \ . \tag{136}$$

To transform the volume integral to surface integral we used Corollary 3 of Gauss-Ostrogradsky theorem. Based on the relation (98) the formula for the first derivatives of gravitational potential in terms of introduced scalar quantities can be written:

$$\nabla_{\boldsymbol{r}_M} U(M) = -G\rho_0 \sum_{i=1}^{n} \boldsymbol{n}_i \sum_{j=1}^{l(i)} c_{ij} = -G\rho_0 \sum_{i=1}^{n} \boldsymbol{n}_i \left(\sum_{j=1}^{l(i)} h_{ij} C_{ij} - h_i \Omega_i \right) = -G\rho_0 \sum_{i=1}^{n} \boldsymbol{n}_i \left(\sum_{j=1}^{l(i)} \left(h_{ij} C_{ij} - h_i \Omega_{ij} \right) \right). \tag{137}$$

Furthermore the formula of the first derivatives of gravitational potential in terms of introduced vector quantities is (Holstein 2002b, equation 2):

$$\nabla_{\boldsymbol{r}_M} U(M) = -G\rho_0 \sum_{i=1}^{n} \boldsymbol{n}_i \sum_{j=1}^{l(i)} \boldsymbol{b}_{ij} \cdot \boldsymbol{r}_{1ij} \ . \tag{138}$$

Using the U_k, $k = \overline{1,3}$ notation for the components of gravity vector, i.e,

$\nabla_{\boldsymbol{r}_M} U = \left(\frac{\partial U}{\partial x}, \frac{\partial U}{\partial y}, \frac{\partial U}{\partial z} \right) = (U_1, U_2, U_3)$, then the following relations hold:

$$U_k(M) = -G\rho_0 \sum_{i=1}^{n} n_i^k \sum_{j=1}^{l(i)} c_{ij} = -G\rho_0 \sum_{i=1}^{n} n_i^k \left(\sum_{j=1}^{l(i)} \left(h_{ij} C_{ij} - h_i \Omega_{ij} \right) \right) \tag{139}$$

$$U_k(M) = -G\rho_0 \sum_{i=1}^{n} \boldsymbol{n}_i \cdot \boldsymbol{e}_k \sum_{j=1}^{l(i)} \boldsymbol{b}_{ij} \cdot \boldsymbol{r}_{1ij} \ , \qquad k = \overline{1,3} \ , \tag{140}$$

where $\boldsymbol{n}_i^k$ denotes the kth component of $\boldsymbol{n}_i$ vector and $\boldsymbol{e}_k, k = \overline{1,3}$ are the unit vectors of the coordinate system.

The number of terms in (137) is $2E+n$, where E is the number of polyhedron edges and n is the number of polyhedron faces. Using dyads the number of terms can be reduced to $E+n$ terms:

$$\nabla_{\boldsymbol{r}_M} U(M) = -G\rho_0 \sum_{i=1}^{n} \boldsymbol{n}_i \left(\sum_{j=1}^{l(i)} \boldsymbol{v}_{ij} \cdot \boldsymbol{r}_{1ij} C_{ij} - \boldsymbol{n}_i \cdot \boldsymbol{r}_i \Omega_i \right) = -G\rho_0 \sum_{i=1}^{n} \left(\sum_{j=1}^{l(i)} C_{ij} \boldsymbol{n}_i \left(\boldsymbol{v}_{ij} \cdot \boldsymbol{r}_{1ij} \right) \right) + G\rho_0 \sum_{i=1}^{n} \Omega_i \boldsymbol{n}_i \left(\boldsymbol{n}_i \cdot \boldsymbol{r}_i \right) =$$

$$= -G\rho_0 \sum_{edge} C_{ij} \left(\boldsymbol{n}_i \left(\boldsymbol{v}_{ij} \cdot \boldsymbol{r}_{edge} \right) - \boldsymbol{n}_{i^*} \left(\boldsymbol{v}_{i^* j^*} \cdot \boldsymbol{r}_{edge} \right) \right) + G\rho_0 \sum_{face} \Omega_i \boldsymbol{n}_i \left(\boldsymbol{n}_i \cdot \boldsymbol{r}_i \right) =$$

$$= -G\rho_0 \sum_{edge} C_{edge} \boldsymbol{\phi}_{edge} \boldsymbol{r}_{edge} + G\rho_0 \sum_{face} \Omega_i \boldsymbol{\phi}_i \boldsymbol{r}_i \ . \tag{141}$$

The last relation in (141) is identical with the Equation 15 found in the paper by Werner and Scheeres (1997). In (141) we used the following properties of dyadic product:

$$\boldsymbol{a}(\boldsymbol{b}\cdot\boldsymbol{c})=(\boldsymbol{a}\circ\boldsymbol{b})\boldsymbol{c}\,, \tag{142}$$

in virtue of this we have:

$\boldsymbol{n}_i(\boldsymbol{v}_{ij}\cdot\boldsymbol{r}_{1ij})-\boldsymbol{n}_{i^*}(\boldsymbol{v}_{i^*j^*}\cdot\boldsymbol{r}_{1i^*j^*})=\boldsymbol{n}_i(\boldsymbol{v}_{ij}\cdot\boldsymbol{r}_{edge})-\boldsymbol{n}_{i^*}(\boldsymbol{v}_{i^*j^*}\cdot\boldsymbol{r}_{edge})=(\boldsymbol{n}_i\circ\boldsymbol{v}_{ij}-\boldsymbol{n}_{i^*}\circ\boldsymbol{v}_{i^*j^*})\boldsymbol{r}_{edge}=\phi_{edge}\ \boldsymbol{r}_{edge}$, and $\boldsymbol{n}_i(\boldsymbol{n}_i\cdot\boldsymbol{r}_i)=(\boldsymbol{n}_i\circ\boldsymbol{n}_i)\boldsymbol{r}_i=\phi_i\boldsymbol{r}_i$.

Henceforth we deduce formulas differing from (137) and (138) which is identical with the Equation 16 presented by Holstein (2002). Deduction of these formulas differs from the demonstration presented in this paper. We start with the following equation:

$$\nabla\left(\frac{\partial}{\partial x_k}\left(\frac{1}{r_{MP}}\right)\boldsymbol{r}_{MP}\right)=\frac{\partial}{\partial x_k}\left(\frac{1}{r_{MP}}\right), \tag{143}$$

where $x_1=x$, $x_2=y$, $x_3=z$.

To prove (143) we use the property (57) of the ∇ operator. For $x_1=x$ we have:

$$\nabla\left(\frac{\partial}{\partial x}\left(\frac{1}{r}\right)\boldsymbol{r}\right)=3\frac{\partial}{\partial x}\left(\frac{1}{r}\right)+\nabla\left(\frac{\partial}{\partial x}\left(\frac{1}{r}\right)\right)\boldsymbol{r}=$$

$$=3\frac{\partial}{\partial x}\left(\frac{1}{r}\right)+\left(\frac{-r^2+3(x-\xi)^2}{r^5},\frac{3(x-\xi)(y-\eta)}{r^5},\frac{3(x-\xi)(z-\zeta)}{r^5}\right)\boldsymbol{r}=\frac{\partial}{\partial x}\left(\frac{1}{r}\right),$$

Here we used the $\nabla\cdot\boldsymbol{r}=3$ identity. In the following we present the deduction of analytical formulas of first derivatives of gravitational potential for $k=1$:

$$U_1(M)=G\rho_0\frac{\partial}{\partial x_1}\iiint_\Omega\frac{1}{r_{MP}}d\Omega_P=G\rho_0\iiint_\Omega\frac{\partial}{\partial x_1}\frac{1}{r_{MP}}d\Omega_P=-G\rho_0\iiint_\Omega\frac{\partial}{\partial\xi_1}\left(\frac{1}{r_{MP}}\right)d\Omega_P=$$

$$=-G\rho_0\iint_{\partial\Omega}\nabla_{\boldsymbol{r}_P}\cdot\left(\frac{\partial}{\partial\xi_1}\left(\frac{1}{r_{MP}}\right)\boldsymbol{r}_{MP}\right)d\boldsymbol{\sigma}_P=-G\rho_0\sum_{i=1}^{n}\iint_{S_i}\frac{\partial}{\partial\xi_1}\left(\frac{1}{r_{MP}}\right)\boldsymbol{r}_{MP}\cdot\boldsymbol{n}_i d\sigma_P=-G\rho_0\sum_{i=1}^{n}h_i\iint_{S_i}\frac{\xi-x}{r_{MP}^3}d\sigma_P. \tag{144}$$

In order to realise the conversion from surface integral to line integral we have to solve the following differential equation:

$$\nabla_{\boldsymbol{r}_P}\cdot\boldsymbol{f}_i(\boldsymbol{r}_P)=\frac{\xi-x}{r_{MP}^3}. \tag{145}$$

We resolve this equation in the (x', y', z') coordinate system, with unit vectors: $\boldsymbol{e}'_2=\boldsymbol{e}_1$, $\boldsymbol{e}'_3=\boldsymbol{n}_i$, $\boldsymbol{e}'_2=\dfrac{\boldsymbol{e}_1\times\boldsymbol{n}_i}{\sin(\boldsymbol{n}_i,\boldsymbol{e}_1)}$. To compute U_2, U_3 we substitute $\boldsymbol{e}_1$ successively with $\boldsymbol{e}_2$ and $\boldsymbol{e}_3$. $\boldsymbol{e}'_2$ is defined so that $(\boldsymbol{e}'_1,\boldsymbol{e}'_2,\boldsymbol{e}'_3)$ is an orthonormal basis set, i.e., $\boldsymbol{e}'_1=\boldsymbol{e}'_2\times\boldsymbol{e}'_3$. The transformation matrix between the $(\boldsymbol{e}_1,\boldsymbol{e}_2,\boldsymbol{e}_3)$ and $(\boldsymbol{e}'_1,\boldsymbol{e}'_2,\boldsymbol{e}'_3)$ systems has the form:

$$A=\begin{bmatrix}-\sqrt{n_{i,2}^2+n_{i,3}^2} & 0 & n_{i,1}\\ n_{i,1}n_{i,2}\Big/\sqrt{n_{i,2}^2+n_{i,3}^2} & -n_{i,3}\Big/\sqrt{n_{i,2}^2+n_{i,3}^2} & n_{i,2}\\ n_{i,1}n_{i,3}\Big/\sqrt{n_{i,2}^2+n_{i,3}^2} & n_{i,2}\Big/\sqrt{n_{i,2}^2+n_{i,3}^2} & n_{i,3}\end{bmatrix},$$

where $n_{i,j}$, $j=\overline{1,3}$ are the components of the $\boldsymbol{n}_i$ vector in the ($\boldsymbol{e}_1$, $\boldsymbol{e}_2$, $\boldsymbol{e}_3$) system, that is $\boldsymbol{n}_i = n_{i,1}\boldsymbol{e}_1 + n_{i,2}\boldsymbol{e}_2 + n_{i,3}\boldsymbol{e}_3$ and $n_{i,j} = \boldsymbol{n}_i \cdot \boldsymbol{e}_j = \cos(\boldsymbol{n}_i, \boldsymbol{e}_j)$, $j=\overline{1,3}$, the upper indices denote the exponent. The equation of linear transformation between the two systems is:

$$(x, y, z)^T = A \cdot (x', y', z')^T , \tag{146}$$

where ^{T} denotes the matrix transpose operator. Written $\dfrac{\xi - x}{r_{MP}^3}$ in ($\boldsymbol{e}'_1$,$\boldsymbol{e}'_2$,$\boldsymbol{e}'_3$) system we have:

$$\frac{\xi - x}{r_{MP}^3} = -\sqrt{n_{i,2}^2 + n_{i,3}^2}\,\frac{\xi' - x'}{r_{MP}^3} + n_{i,1}\frac{\zeta' - z'}{r_{MP}^3} = -\sin(\boldsymbol{n}_i, \boldsymbol{e}_1)\frac{\xi' - x'}{r_{MP}^3} + \cos(\boldsymbol{n}_i, \boldsymbol{e}_1)\frac{h_i}{r_{MP}^3} \quad . \tag{147}$$

The expressions of r_{MP} in these two systems are:

$$r_{MP} = \sqrt{(\xi - x)^2 + (\eta - y)^2 + (\zeta - z)^2} = \sqrt{(\xi' - x')^2 + (\eta' - y')^2 + (\zeta' - z')^2} = \sqrt{(\xi' - x')^2 + (\eta' - y')^2 + h_i^2}$$

It is easy to see that: $\nabla \cdot \left(\dfrac{1}{r_{MP}}, 0\right) = \dfrac{\xi' - x'}{r_{MP}^3}$.

Using the solution (102) of equation $\nabla \cdot \boldsymbol{f}_i(\boldsymbol{r}_P) = \dfrac{h_i}{r_{MP}^3}$ given in Section 1.2.4 and the relation (147) we can convert the surface (144) into line integrals using the Gauss-Ostrogradsky theorem:

$$\iint_{S_i} \frac{\partial}{\partial \xi_1}\left(\frac{1}{r_{MP}}\right) d\sigma_P = \iint_{S_i} \frac{\xi - x}{r_{MP}^3} d\sigma_P = -\sin(\boldsymbol{n}_i, \boldsymbol{e}_1)\iint_{S_i} \frac{\xi' - x'}{r_{MP}^3} d\sigma_P + \cos(\boldsymbol{n}_i, \boldsymbol{e}_1)\iint_{S_i} \frac{h_i}{r_{MP}^3} d\sigma_P =$$

$$= -\sin(\boldsymbol{n}_i, \boldsymbol{e}_1)\iint_{S_i}\left(\frac{1}{r_{MP}}, 0\right) \cdot \boldsymbol{\nu} dl + \cos(\boldsymbol{n}_i, \boldsymbol{e}_1)\iint_{S_i} \boldsymbol{f}(\boldsymbol{r}_P) \cdot \boldsymbol{\nu} dl =$$

$$= -\sin(\boldsymbol{n}_i, \boldsymbol{e}_1)\sum_{j=1}^{l(i)}\int_{L_{ij}}\left(\frac{1}{r_{MP}}, 0\right) \cdot \left(\boldsymbol{\nu}_{ij} \cdot \boldsymbol{e}'_1, \sqrt{1 - (\boldsymbol{\nu}_{ij} \cdot \boldsymbol{e}'_1)^2}\right) dl + \cos(\boldsymbol{n}_i, \boldsymbol{e}_1)\sum_{j=1}^{l(i)}\int_{L_{ij}}\left(\frac{r_{MP}\left|h_i^{-1}\right| - 1}{s_{MP}^2 r_{MP}}\right)\boldsymbol{s}_{MP} \cdot \boldsymbol{\nu}_{ij} dl =$$

$$= \sin(\boldsymbol{n}_i, \boldsymbol{e}_1)\sum_{j=1}^{l(i)}\frac{\cos(\boldsymbol{\nu}_{ij}, \boldsymbol{e}_1)}{\sin(\boldsymbol{n}_i, \boldsymbol{e}_1)}\int_{L_{ij}}\frac{1}{r_{MP}} dl + \cos(\boldsymbol{n}_i, \boldsymbol{e}_1)\sum_{j=1}^{l(i)} h_{ij}\int_{L_{ij}}\left(\frac{1}{|h_i| s_{MP}^2} - \frac{1}{s_{MP}^2 r_{MP}}\right) dl \ . \tag{148}$$

$\boldsymbol{\nu}$ denotes the normal vector of ∂S_i. In (148) to evaluate the $\boldsymbol{\nu}_{ij} \cdot \boldsymbol{e}'_1$ product we use the expression of $\boldsymbol{e}'_1$ in ($\boldsymbol{e}_1$, $\boldsymbol{e}_2$, $\boldsymbol{e}_3$) coordinate system based on the (146) relation and we use the $\boldsymbol{\nu}_{ij}\boldsymbol{n}_i = 0$ identity since $\boldsymbol{\nu}_{ij} \perp \boldsymbol{n}_i$. Thus we have:

$$\boldsymbol{\nu}_{ij} \cdot \boldsymbol{e}'_1 = \boldsymbol{\nu}_{ij}\left(-\sqrt{n_{i,3}^2 + n_{i,2}^2}\,\boldsymbol{e}_1 + \frac{n_{i,1}n_{i,2}}{\sqrt{n_{i,3}^2 + n_{i,2}^2}}\boldsymbol{e}_2 + \frac{n_{i,1}n_{i,3}}{\sqrt{n_{i,3}^2 + n_{i,2}^2}}\boldsymbol{e}_3\right) =$$

$$= -\sqrt{n_{i,3}^2 + n_{i,2}^2}\,\nu_{1ij} + \frac{n_{i,1}n_{i,2}}{\sqrt{n_{i,3}^2 + n_{i,2}^2}}\nu_{2ij} + \frac{n_{i,1}n_{i,3}}{\sqrt{n_{i,3}^2 + n_{i,2}^2}}\nu_{3ij} = \frac{-n_{i,3}^2\nu_{1ij} - n_{i,2}^2\nu_{1ij} + n_{i,1}n_{i,2}\nu_{2ij} + n_{i,1}n_{i,3}\nu_{3ij}}{\sqrt{n_{i,3}^2 + n_{i,2}^2}} =$$

$$= \frac{-n_{i,3}^2\nu_{1ij} - n_{i,2}^2\nu_{1ij} + n_{i,1}n_{i,2}\nu_{2ij} - n_{i,1}^2\nu_{1ij} - n_{i,1}n_{i,2}\nu_{2ij}}{\sqrt{n_{i,3}^2 + n_{i,2}^2}} = -\frac{\nu_{1ij}}{\sqrt{n_{i,3}^2 + n_{i,2}^2}} = -\frac{\cos(\boldsymbol{\nu}_{ij}, \boldsymbol{e}_1)}{\sin(\boldsymbol{n}_i, \boldsymbol{e}_1)} \ .$$

Using relations (99) and (103), (148) can be expressed in terms of the parameters introduced as follows:

$$\iint_{S_i} \frac{\partial}{\partial \xi_1}\left(\frac{1}{r_{MP}}\right) d\sigma_P = \iint_{S_i} \frac{\xi - x}{r_{MP}^3} d\sigma_P = \sum_{j=1}^{l(i)} \left(\cos\left(\boldsymbol{v}_{ij}, \boldsymbol{e}_1\right) C_{ij} - \cos\left(\boldsymbol{n}_i, \boldsymbol{e}_1\right) \Omega_{ij}\right). \tag{149}$$

In virtue of (149) we can give another expression of first derivatives of potential which will differ from (138) and (139):

$$U_1(M) = -G\rho_0 \sum_{i=1}^{n} h_i \iint_{S_i} \frac{\xi - x}{r_{MP}^3} d\sigma_P = -G\rho_0 \left(\sum_{i=1}^{n} h_i \sum_{j=1}^{l(i)} \cos\left(\boldsymbol{v}_{ij}, \boldsymbol{e}_1\right) C_{ij} - \cos\left(\boldsymbol{n}_i, \boldsymbol{e}_1\right) \sum_{i=1}^{n} h_i \sum_{j=1}^{l(i)} \Omega_{ij} \right) =$$

$$= -G\rho_0 \sum_{i=1}^{n} h_i \left(\sum_{j=1}^{l(i)} \left(\cos\left(\boldsymbol{v}_{ij}, \boldsymbol{e}_1\right) C_{ij} - \cos\left(\boldsymbol{n}_i, \boldsymbol{e}_1\right) \Omega_{ij}\right) \right) = -G\rho_0 \sum_{i=1}^{n} h_i \left(\sum_{j=1}^{l(i)} \left(C_{ij} \boldsymbol{v}_{ij} \cdot \boldsymbol{e}_1 - \Omega_{ij} \boldsymbol{n}_i \cdot \boldsymbol{e}_1\right) \right).$$

The same expression holds for the partial derivative with respect to *y* and *z*. The analytical formula of the first derivatives of potential generally can be written:

$$U_k(M) = -G\rho_0 \sum_{i=1}^{n} h_i \left(\sum_{j=1}^{l(i)} \left(C_{ij} \boldsymbol{v}_{ij} \cdot \boldsymbol{e}_k - \Omega_{ij} \boldsymbol{n}_i \cdot \boldsymbol{e}_k\right) \right), k = \overline{1,3} \tag{150}$$

$$\nabla_{\boldsymbol{r}_M} U(M) = -G\rho_0 \sum_{i=1}^{n} h_i \left(\sum_{j=1}^{l(i)} \left(C_{ij} \boldsymbol{v}_{ij} - \Omega_{ij} \boldsymbol{n}_i\right) \right). \tag{151}$$

Using the introduced vector quantities the expression (151) can be given as follows:

$$\nabla_{\boldsymbol{r}_M} U(M) = -G\rho_0 \sum_{i=1}^{n} \left(\boldsymbol{n}_i \cdot \boldsymbol{r}_i\right) \sum_{j=1}^{l(i)} \boldsymbol{b}_{ij} = -G\rho_0 \sum_{i=1}^{n} \left(\boldsymbol{n}_i \cdot \boldsymbol{r}_i\right) \sum_{j=1}^{l(i)} \left(C_{ij} \boldsymbol{v}_{ij} - \Omega_{ij} \boldsymbol{n}_i\right). \tag{152}$$

Using the P_{ij}, Q_{ij}, R_{ij}, I_{ij} constants introduced by Guptasarma and Singh (1999) and Singh and Guptasarma (2001) the first derivatives of potential can be given as:

$$C_{ij} \boldsymbol{v}_{ij} = \int_{L_{ij}} \frac{\left(\boldsymbol{\mu}_{ij} \times \boldsymbol{n}_i\right) dl}{r_{MP}} = \int_{L_{ij}} \frac{\left(d\boldsymbol{l} \times \boldsymbol{n}_i\right)}{r_{MP}} =$$

$$= \left(n_{i,3} \int_{L_{ij}} \frac{d\eta}{r_{MP}} - n_{i,2} \int_{L_{ij}} \frac{d\varsigma}{r_{MP}} \right) \boldsymbol{e}_1 + \left(n_{i,1} \int_{L_{ij}} \frac{d\varsigma}{r_{MP}} - n_{i,3} \int_{L_{ij}} \frac{d\xi}{r_{MP}} \right) \boldsymbol{e}_2 + \left(n_{i,2} \int_{L_{ij}} \frac{d\xi}{r_{MP}} - n_{i,1} \int_{L_{ij}} \frac{d\eta}{r_{MP}} \right) \boldsymbol{e}_3 =$$

$$= \left(n_{i,3} Q_{ij} - n_{i,2} R_{ij}\right) \boldsymbol{e}_1 + \left(n_{i,1} R_{ij} - n_{i,3} P_{ij}\right) \boldsymbol{e}_2 + \left(n_{i,2} P_{ij} - n_{i,1} Q_{ij}\right) \boldsymbol{e}_3 = I_{ij} \left(\boldsymbol{l}_{ij} \times \boldsymbol{n}_i\right). \tag{153}$$

where $d\boldsymbol{l} = \left(d\xi, d\eta, d\zeta\right)$, $\boldsymbol{r}_M = \left(x, y, z\right)$, $\boldsymbol{r}_P = \left(\xi, \eta, \zeta\right)$, $\boldsymbol{n}_i = \left(n_{i,1}, n_{i,2}, n_{i,3}\right)$, $l_{ij} = |\boldsymbol{l}_{ij}|$,

$\boldsymbol{l}_{ij} = \boldsymbol{r}_{2ij} - \boldsymbol{r}_{1ij} = \left(x_{2ij} - x_{1ij}, y_{2ij} - y_{1ij}, z_{2ij} - z_{1ij}\right)$ and P_{ij}, Q_{ij}, R_{ij}, I_{ij} are given by (93)-(95) expressions.

The general formula of the first derivatives of potential generated by a polyhedron is:

$$\nabla_{\boldsymbol{r}_M} U(M) = -G\rho_0 \left(\sum_{i=1}^{n} h_i \left(\sum_{j=1}^{l(i)} I_{ij} \left(\boldsymbol{l}_{ij} \times \boldsymbol{n}_i\right) - \Omega_i \boldsymbol{n}_i \right) \right). \tag{154}$$

The first component (derivatives with respect to *x*) of $\nabla_{\boldsymbol{r}_M} U$ is:

$$U_1(M) = -G\rho_0\left(\sum_{i=1}^{n} h_i\left(\sum_{j=1}^{l(i)}\left(n_{i,3}Q_{ij} - n_{i,2}R_{ij}\right) - \Omega_i n_{i,1}\right)\right). \tag{155}$$

From (138) and (152) arise the next identity between the introduced vector parameters:

$$\sum_{i=1}^{n}\boldsymbol{n}_i \cdot \left(\sum_{j=1}^{l(i)}\boldsymbol{b}_{ij}\cdot\boldsymbol{r}_{1ij}\right) = \sum_{i=1}^{n}\left(\boldsymbol{n}_i\cdot\boldsymbol{r}_i\right)\cdot\sum_{j=1}^{l(i)}\boldsymbol{b}_{ij}\ . \tag{156}$$

(156) is identical with Equation 9 given by Holstein (2002b). In the following we will demonstrate (156) in a direct way. From the fact that all the edges of a polyhedron belong to two faces, it follows that the number of edges E fulfils the following relation: $2E = \sum_{i=1}^{n} l(i)$. We use i, j and i^*, j^* notation to indices of faces and edges for two secant faces. Let $(\boldsymbol{n}_i, \boldsymbol{v}_{ij}, \boldsymbol{\mu}_{ij})$ and $(\boldsymbol{n}_{i^*}, \boldsymbol{v}_{i^*j^*}, \boldsymbol{\mu}_{i^*j^*})$ be the coordinate systems belonging to the common edges ij and i^*j^* (Fig. 8). Based on relation (106) we have:

$$\boldsymbol{n}_i\cdot\left(\boldsymbol{b}_{ij}\cdot\boldsymbol{r}_{1ij}\right) = \boldsymbol{n}_i\left(C_{ij}h_{ij} - \Omega_{ij}h_i\right) = C_{ij}h_{ij}\boldsymbol{n}_i - \Omega_{ij}h_i\boldsymbol{n}_i\ , \tag{157}$$

$$\left(\boldsymbol{n}_i\cdot\boldsymbol{r}_{1ij}\right)\cdot\boldsymbol{b}_{ij} = h_i C_{ij}\boldsymbol{v}_{ij} - h_i\Omega_{ij}\boldsymbol{n}\ . \tag{158}$$

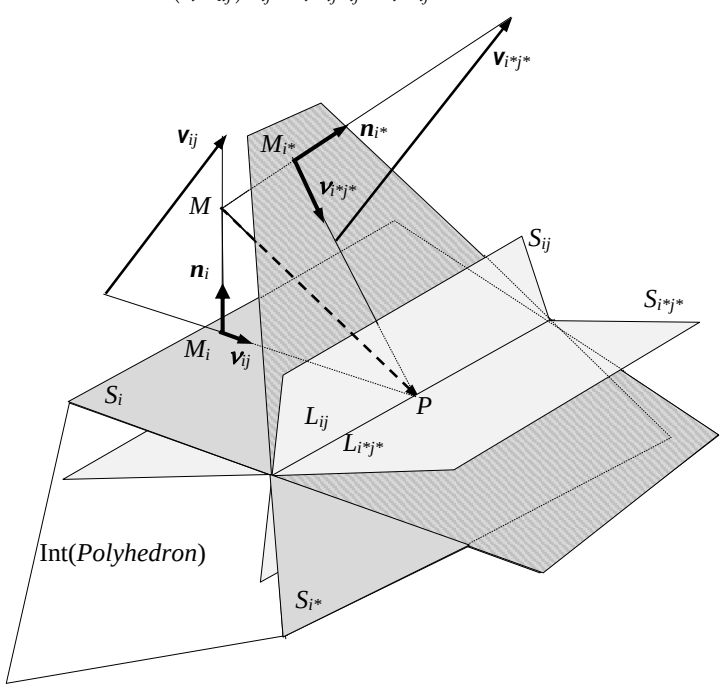

Fig. 8 The position of $\boldsymbol{n}_i$, $\boldsymbol{v}_{ij}$, $\boldsymbol{v}_{ij}$ and $\boldsymbol{n}_{i^*}$, $\boldsymbol{v}_{i^*j^*}$, $\boldsymbol{v}_{i^*j^*}$ vectors belonging to the polyhedron faces S_i, and S_{i^*} and the observation point M. S_{ij}, $S_{i^*j^*}$ are faces belonging to the common edges $L_{ij} = L_{i^*j^*}$ and perpendicular successively to the faces S_i-re and S_{i^*} . The dashed part represents extension of S_i and S_{i^*} polyhedron faces in Ext(*Polyhedron*) $\subset R^3$

The same relations are available for the i^*j^* edge too. In case of positive orientation of these two polygon faces the common edges ij and i^*j^* will get opposite direction. In the following we will prove the relation:

$$\sum_{i=1}^{n}\boldsymbol{n}_i\sum_{j=1}^{l(i)}C_{ij}h_{ij}=\sum_{i=1}^{n}h_i\sum_{j=1}^{l(i)}C_{ij}\boldsymbol{v}_{ij}\,. \tag{159}$$

We start with demonstration of the following identity:

$$\boldsymbol{n}_iC_{ij}h_{ij}+\boldsymbol{n}_{i^*}C_{i^*j^*}h_{i^*j^*}=h_iC_{ij}\boldsymbol{v}_{ij}+h_{i^*}C_{i^*j^*}\boldsymbol{v}_{i^*j^*}\,. \tag{160}$$

Using the identity $C_{ij}=-C_{i^*j^*}$ (Eq. 127) and simplifying expression (160) with C_{ij} we get the following identity:

$$\boldsymbol{n}_ih_{ij}-\boldsymbol{n}_{i^*}h_{i^*j^*}-\boldsymbol{v}_{ij}h_i+\boldsymbol{v}_{i^*j^*}h_{i^*}=\left(\boldsymbol{n}_ih_{ij}-\boldsymbol{v}_{ij}h_i\right)-\left(\boldsymbol{n}_{i^*}h_{i^*j^*}-\boldsymbol{v}_{i^*j^*}h_{i^*}\right)=\boldsymbol{v}_{ij}-\boldsymbol{v}_{i^*j^*}=0\,.$$

The S_i, S_{i*} polyhedron faces divide the space into four disjoint parts. The S_{ij} and S_{i*j*} planes going through the common edge of S_i and S_{i*} and successively perpendicular to these planes divide the space into four disjoint parts. The sign of h_i, h_{i*}, h_{ij}, h_{i*j*} is changing depending on the position of computation point M. In the proper situation as shown in Fig. 7 the sign of these quantities as a function of M are: $h_i<0$, $h_{i*}>0$, $h_{ij}>0$, $h_{i*j*}>0$. It can be easily demonstrated that length and direction of $\boldsymbol{v}_{ij}=\boldsymbol{n}_ih_{ij}-\boldsymbol{v}_{ij}h_i$ and $\boldsymbol{v}_{i^*j^*}=\boldsymbol{n}_{i^*}h_{i^*j^*}-\boldsymbol{v}_{i^*j^*}h_{i^*}$ vectors are the same, so (160) is demonstrated for the concrete position of point M presented in Fig. 8 Similar consideration can be carried out for an arbitrary position of M. Each edge in the summation (159) appears twice. Using the identity (160) the (159) and on this basis (156) are evident. Using (156) and applying the ∇ operator to the (108) formula of gravitational potential, we get:

$$\begin{aligned}\nabla_{\boldsymbol{r}_M}U(M)&=\frac{G\rho_0}{2}\nabla_{\boldsymbol{r}_M}\left(\sum_{i=1}^{n}(\boldsymbol{n}_i\cdot\boldsymbol{r}_i)\sum_{j=1}^{l(i)}\boldsymbol{b}_{ij}\boldsymbol{r}_{1ij}\right)=-\frac{G\rho_0}{2}\left(\sum_{i=1}^{n}\boldsymbol{n}_i\sum_{j=1}^{l(i)}\boldsymbol{b}_{ij}\boldsymbol{r}_{1ij}+\sum_{i=1}^{n}(\boldsymbol{n}_i\cdot\boldsymbol{r}_i)\sum_{j=1}^{l(i)}\left((\nabla_{\boldsymbol{r}_M}\boldsymbol{b}_{ij})\boldsymbol{r}_{1ij}-\boldsymbol{b}_{ij}\right)\right)=\\&=-\frac{G\rho_0}{2}\left(\sum_{i=1}^{n}\boldsymbol{n}_i\sum_{j=1}^{l(i)}\boldsymbol{b}_{ij}\boldsymbol{r}_{1ij}+\sum_{i=1}^{n}(\boldsymbol{n}_i\cdot\boldsymbol{r}_i)\sum_{j=1}^{l(i)}\boldsymbol{b}_{ij}\right)+\frac{G\rho_0}{2}\left(\sum_{i=1}^{n}(\boldsymbol{n}_i\cdot\boldsymbol{r}_i)\sum_{j=1}^{l(i)}(\nabla_{\boldsymbol{r}_M}\cdot\boldsymbol{b}_{ij})\boldsymbol{r}_{1ij}\right)=\\&=-G\rho_0\left(\sum_{i=1}^{n}\boldsymbol{n}_i\sum_{j=1}^{l(i)}\boldsymbol{b}_{ij}\cdot\boldsymbol{r}_{1ij}\right)+\frac{G\rho_0}{2}\left(\sum_{i=1}^{n}(\boldsymbol{n}_i\cdot\boldsymbol{r}_i)\sum_{j=1}^{l(i)}(\nabla_{\boldsymbol{r}_M}\cdot\boldsymbol{b}_{ij})\boldsymbol{r}_{1ij}\right).\end{aligned} \tag{161}$$

From (138) and (161) is apparent that the derivatives of $\boldsymbol{b}_{ij}$ vector fulfil the relation (10) given by Holstein 2002:

$$\sum_{i=1}^{n}(\boldsymbol{n}_i\cdot\boldsymbol{r}_i)\sum_{j=1}^{l(i)}(\nabla_{\boldsymbol{r}_M}\cdot\boldsymbol{b}_{ij})\boldsymbol{r}_{1ij}=0\,. \tag{162}$$

In the following, we derive (156) and (159) using the dyad and its properties. For symmetric dyads ϕ we have:

$$\boldsymbol{a}^T\phi=\phi\,\boldsymbol{a}, \tag{163}$$

where $\boldsymbol{a}$ is an arbitrary vector. Using relation (163), we have:

$$\begin{aligned}\nabla_{\boldsymbol{r}_M}U(M)&=-G\rho_0\sum_{i=1}^{n}\boldsymbol{n}_i\boldsymbol{r}_i\sum_{j=1}^{l(i)}\left(C_{ij}\boldsymbol{v}_{ij}-\Omega_{ij}\boldsymbol{n}_i\right)=-G\rho_0\left(\sum_{edge}C_{ij}\left((\boldsymbol{n}_i\boldsymbol{r}_{edge})\boldsymbol{v}_{ij}-(\boldsymbol{n}_{i^*}\boldsymbol{r}_{edge})\boldsymbol{v}_{i^*j^*}\right)+\sum_{face}\Omega_i(\boldsymbol{n}_i\boldsymbol{r}_i)\boldsymbol{n}_i\right)\\&=-G\rho_0\sum_{edge}C_{edge}\left(\boldsymbol{r}_{edge}^T\phi_{edge}\right)+G\rho_0\sum_{face}\Omega_i\left(\boldsymbol{r}_i^T\phi_i\right)=-G\rho_0\sum_{edge}C_{edge}\left(\phi_{edge}\boldsymbol{r}_{edge}\right)+G\rho_0\sum_{face}\Omega_i\left(\phi_i\boldsymbol{r}_i\right).\end{aligned} \tag{164}$$

(164) is equivalent with (141), thus the analytical expressions (138) and (152) of the first derivatives of gravitational potential are equivalent too.

1.2.8 The analytical formulas of second derivatives of gravitational potential generated by homogeneous polyhedron volume element

The second derivatives of potential are the derivatives of the gradient tensor $\nabla_{r_M} U$. The second derivatives form a tensor, namely the gravity gradient tensor or Eötvös-tensor is:

$$\mathbf{E} = \begin{bmatrix} \frac{\partial^2 U}{\partial x^2} & \frac{\partial^2 U}{\partial x \partial y} & \frac{\partial^2 U}{\partial x \partial z} \\ \frac{\partial^2 U}{\partial y \partial x} & \frac{\partial^2 U}{\partial y^2} & \frac{\partial^2 U}{\partial y \partial z} \\ \frac{\partial^2 U}{\partial z \partial x} & \frac{\partial^2 U}{\partial z \partial y} & \frac{\partial^2 U}{\partial z^2} \end{bmatrix} = \left[U_{kl}\right],\ k,l = \overline{1,3}, \tag{165}$$

where $U_{11} = \frac{\partial^2 U}{\partial x^2}, U_{12} = \frac{\partial^2 U}{\partial x \partial y}$ and similarly for the other indices.

For the variable we use the notation: $x_1=x$, $x_2=y$, $x_3=z$, $\xi_1=\xi$, $\xi_2=\eta$, $\xi_3=\zeta$ where x, y, z are the coordinates of computation point M and ξ, η, ζ are the coordinates of polyhedron point P. Based on (136) the elements of gravity gradient tensor can be given with the following surface integral:

$$U_{kl}(M) = \frac{\partial}{\partial x_l}\left(\frac{\partial}{\partial x_k}(U(M))\right) = -G\rho_0 \frac{\partial}{\partial x_l}\left(\sum_{i=1}^{n} \boldsymbol{n}_i \cdot \boldsymbol{e}_k \iint_{S_i} \frac{1}{r_{MP}} d\sigma_P\right) = G\rho_0 \sum_{i=1}^{n} \boldsymbol{n}_i \cdot \boldsymbol{e}_k \left(\iint_{S_i} \frac{\partial}{\partial \xi_l}\left(\frac{1}{r_{MP}}\right) d\sigma_P\right).$$

Using (149) the surface integral can be expressed in terms of constants C_{ij} and Ω_{ij}:

$$U_{kl}(M) = G\rho_0 \sum_{i=1}^{n} \boldsymbol{n}_i \cdot \boldsymbol{e}_k \sum_{j=1}^{l(i)} \left(\cos(\boldsymbol{v}_{ij}, \boldsymbol{e}_l) C_{ij} - \cos(\boldsymbol{n}_i, \boldsymbol{e}_l)\Omega_{ij}\right) = G\rho_0 \sum_{i=1}^{n} \boldsymbol{n}_i \cdot \boldsymbol{e}_k \sum_{j=1}^{l(i)} \left(\boldsymbol{v}_{ij} \cdot \boldsymbol{e}_l C_{ij} - \boldsymbol{n}_i \cdot \boldsymbol{e}_l \Omega_{ij}\right) =$$

$$= G\rho_0 \sum_{i=1}^{n} n_{i,k} \sum_{j=1}^{l(i)} \left(v_{ij,l} C_{ij} - n_{i,l}\Omega_{ij}\right) = G\rho_0 \sum_{i=1}^{n} n_{i,k} \sum_{j=1}^{l(i)} b_{ij,l} = G\rho_0 \sum_{i=1}^{n} \boldsymbol{n}_i \circ \sum_{j=1}^{l(i)} \boldsymbol{b}_{ij},\ k,l = \overline{1,3} \tag{166}$$

where $\boldsymbol{n}_i = (n_{i,1}, n_{i,2}, n_{i,3})$, $\boldsymbol{v}_i = (v_{i,1}, v_{i,2}, v_{i,3})$, $\boldsymbol{b}_i = (b_{i,1}, b_{i,2}, b_{i,3})$ and $\circ$ denotes the dyadic product defined on Section 1.2.6. The expression of Eötvös tensor elements in terms of P_{ij}, Q_{ij}, R_{ij}, I_{ij} is:

$$U_{kl}(M) = G\rho_0 \sum_{i=1}^{n} \boldsymbol{n}_i \cdot \boldsymbol{e}_k \sum_{j=1}^{l(i)} \left(\boldsymbol{v}_{ij} \cdot \boldsymbol{e}_l C_{ij} - \boldsymbol{n}_i \cdot \boldsymbol{e}_l \Omega_{ij}\right) = G\rho_0 \sum_{i=1}^{n} n_{i,k} \left(\sum_{j=1}^{l(i)} \left(n_{i,3} Q_{ij} - n_{i,2} R_{ij}\right) - n_{i,l}\Omega_i\right),\ k,l = \overline{1,3}. \tag{167}$$

The expression elements of the gravity gradient tensor as a function of dyads (Werner and Scheeres 1997, Eq. 16):

$$U_{kl}(M) = G\rho_0 \sum_{edge} C_{edge} \boldsymbol{e}_k^T \boldsymbol{\phi}_{edge} \boldsymbol{e}_l - G\rho_0 \sum_{i=1}^{n} \Omega_i \boldsymbol{e}_k^T \boldsymbol{\phi}_i \boldsymbol{e}_l, \tag{168}$$

and in matrix form:

$$\left[U_{kl}(M)\right]_{k,l=\overline{1,3}} = G\rho_0 \sum_{edge} C_{edge} \boldsymbol{\phi}_{edge} - G\rho_0 \sum_{i=1}^{n} \Omega_i \boldsymbol{\phi}_i \tag{169}$$

$\Delta U(M)$, the sum of the homogeneous tensor elements, or Lapacian, can be expressed as:

$$\Delta U(M) = \nabla(\nabla(U(M))) = U_{11}(M) + U_{22}(M) + U_{33}(M) = G\rho_0 \sum_{k=1}^{3} \sum_{i=1}^{n} n_{i,k} \sum_{j=1}^{l(i)} b_{ij,k} =$$

$$= G\rho_0 \sum_{i=1}^{n} \sum_{j=1}^{l(i)} \sum_{k=1}^{3} n_{i,k} b_{ij,k} = G\rho_0 \sum_{i=1}^{n} \sum_{j=1}^{l(i)} \boldsymbol{n}_i \cdot \boldsymbol{b}_{ij} = G\rho_0 \sum_{i=1}^{n} \boldsymbol{n}_i \cdot \sum_{j=1}^{l(i)} \boldsymbol{b}_{ij} \ . \tag{170}$$

(170) is identical with Eq 17 given by Werner and Scheeres (1997). Applying relations (40) and (41) presented in observation 2 and 3 of Theorem 12 regarding to the double layer potential we get the well known Laplace equation:

$$\Delta U(M) = G\rho_0 \sum_{i=1}^{n} \sum_{j=1}^{l(i)} \boldsymbol{n}_i \boldsymbol{b}_{ij} = G\rho_0 \sum_{i=1}^{n} \sum_{j=1}^{l(i)} \Omega_{ij} = G\rho_0 \sum_{i=1}^{n} \Omega_i = G\rho_0 \sum_{i=1}^{n} \int_{S_i} \frac{\cos(\boldsymbol{r}_{MP}, \boldsymbol{n}_i)}{r_{MP}^2} d\sigma_P =$$

$$= \begin{cases} 0 & \text{if } M \in \mathrm{Ext}\,\Sigma \\ -4\pi G\rho_0 & \text{if } M \in \mathrm{Int}\,\Sigma \end{cases} \tag{171}$$

This equation serves to decide the position of point M referring to the $\Sigma \subset R^3$ domain defined by the polyhedron. Applying the ∇ operator to (152) we get:

$$\nabla_{\boldsymbol{r}_M} \left(\nabla_{\boldsymbol{r}_M} U(M) \right) = \Delta U(M) = -G\rho_0 \nabla_{\boldsymbol{r}_M} \cdot \left(\sum_{i=1}^{n} \boldsymbol{n}_i \sum_{j=1}^{l(i)} \boldsymbol{r}_{1ij} \boldsymbol{b}_{ij} \right) = G\rho_0 \left(\sum_{i=1}^{n} \boldsymbol{n}_i \cdot \sum_{j=1}^{l(i)} \boldsymbol{b}_{ij} - \sum_{i=1}^{n} \boldsymbol{n}_i \cdot \sum_{j=1}^{l(i)} \left(\nabla_{\boldsymbol{r}_M} \boldsymbol{b}_{ij} \right) \boldsymbol{r}_{1ij} \right). \tag{172}$$

Comparing the equations (172) and (170) we have:

$$\sum_{i=1}^{n} \boldsymbol{n}_i \cdot \sum_{j=1}^{l(i)} \left(\nabla_{\boldsymbol{r}_M} \boldsymbol{b}_{ij} \right) \boldsymbol{r}_{1ij} = 0 \, . \tag{173}$$

From equations (173) and (162) arise the property of $\boldsymbol{b}_{ij}$ vectors regarding to the ∇ operator given by Holstein (2002b):

$$\sum_{j=1}^{l(i)} \left(\nabla_{\boldsymbol{r}_M} \boldsymbol{b}_{ij} \right) \boldsymbol{r}_{1ij} = 0 \, . \tag{174}$$

On this basis we get:

$$\nabla_{\boldsymbol{r}_M} \sum_{j=1}^{l(i)} \left(\boldsymbol{b}_{ij} \cdot \boldsymbol{r}_{1ij} \right) = \sum_{j=1}^{l(i)} \left(\nabla_{\boldsymbol{r}_M} \cdot \boldsymbol{b}_{ij} \right) \boldsymbol{r}_{1ij} + \sum_{j=1}^{l(i)} \left(\nabla_{\boldsymbol{r}_M} \cdot \boldsymbol{r}_{1ij} \right) \boldsymbol{b}_{ij} = \sum_{j=1}^{l(i)} \boldsymbol{b}_{ij} \ . \tag{175}$$

Based on (175) we can show that $\boldsymbol{b}_{ij}$ appears invariant (acts as a constant) to the gradient operation. Because of this property the $\boldsymbol{b}_{ij}$ quantities are called the gravimetric invariants of the polyhedron (Holstein 2002a, 2002b)

1.2.9 Summary of analytical formulas

Hereunder we list the analytical formulas of gravitational potential and its first and second derivatives generated by a polyhedron.

Analytical formulas in terms of constants C_{ij}, Ω_{ij}, Ω_i, Q_{ij}, R_{ij}, P_{ij}:

$$U(M)=\frac{G\rho_0}{2}\sum_{i=1}^{n}h_i\sum_{j=1}^{l(i)}c_{ij}=\frac{G\rho_0}{2}\sum_{i=1}^{n}h_i\left(\sum_{j=1}^{l(i)}h_{ij}C_{ij}-h_i\Omega_i\right)=\frac{G\rho_0}{2}\sum_{i=1}^{n}h_i\left(\sum_{j=1}^{l(i)}\left(h_{ij}C_{ij}-h_i\Omega_{ij}\right)\right), \tag{176}$$

$$U(M)=\frac{G\rho_0}{2}\sum_{i=1}^{n}h_i\sum_{j=1}^{l(i)}\left(\left(x_{1ij}-x\right)\left(n_{i,3}Q_{ij}-n_{i,2}R_{ij}\right)+\left(y_{1ij}-y\right)\left(n_{i,1}R_{ij}-n_{i,3}P_{ij}\right)+\left(z_{1ij}-z\right)\left(n_{i,2}P_{ij}-n_{i,1}Q_{ij}\right)\right)-$$
$$-\frac{G\rho_0}{2}\sum_{i=1}^{n}h_i^2\Omega_i\ . \tag{177}$$

$$\nabla_{\boldsymbol{r}_M}U(M)=-G\rho_0\sum_{i=1}^{n}h_i\left(\sum_{j=1}^{l(i)}\left(C_{ij}\boldsymbol{v}_{ij}-\Omega_{ij}\boldsymbol{n}_i\right)\right)=-G\rho_0\sum_{i=1}^{n}\boldsymbol{n}_i\left(\sum_{j=1}^{l(i)}\left(h_{ij}C_{ij}-h_i\Omega_{ij}\right)\right)=-G\rho_0\sum_{i=1}^{n}\boldsymbol{n}_i\sum_{j=1}^{l(i)}c_{ij}\ , \tag{178}$$

$$U_1(M)=-G\rho_0\left(\sum_{i=1}^{n}h_i\left(\sum_{j=1}^{l(i)}\left(n_{i,3}Q_{ij}-n_{i,1}R_{ij}\right)-\Omega_i n_{i,1}\right)\right),$$

$$U_2(M)=-G\rho_0\left(\sum_{i=1}^{n}h_i\left(\sum_{j=1}^{l(i)}\left(n_{i,1}R_{ij}-n_{i,3}P_{ij}\right)-\Omega_i n_{i,2}\right)\right),$$

$$U_3(M)=-G\rho_0\left(\sum_{i=1}^{n}h_i\left(\sum_{j=1}^{l(i)}\left(n_{i,2}P_{ij}-n_{i,1}Q_{ij}\right)-\Omega_i n_{i,3}\right)\right). \tag{179}$$

$$U_{kl}(M)=G\rho_0\sum_{i=1}^{n}n_{i,k}\sum_{j=1}^{l(i)}\left(v_{ij,l}C_{ij}-n_{i,l}\Omega_{ij}\right)=G\rho_0\sum_{i=1}^{n}n_{i,k}\sum_{j=1}^{l(i)}b_{ij,l}\ . \tag{180}$$

$$U_{k1}(M)=G\rho_0\sum_{i=1}^{n}n_{i,k}\left(\sum_{j=1}^{l(i)}\left(n_{i,3}Q_{ij}-n_{i,2}R_{ij}\right)-n_{i,1}\Omega_i\right),$$

$$U_{k2}(M)=G\rho_0\sum_{i=1}^{n}n_{i,k}\left(\sum_{j=1}^{l(i)}\left(n_{i,1}R_{ij}-n_{i,3}P_{ij}\right)-n_{i,2}\Omega_i\right),$$

$$U_{k3}(M)=G\rho_0\sum_{i=1}^{n}n_{i,k}\left(\sum_{j=1}^{l(i)}\left(n_{i,2}P_{ij}-n_{i,1}Q_{ij}\right)-n_{i,3}\Omega_i\right). \tag{181}$$

Analytical formulas in terms of vector invariants

$$U(M)=\frac{G\rho_0}{2}\sum_{i=1}^{n}\left(\boldsymbol{n}_i\cdot\boldsymbol{r}_i\right)\sum_{j=1}^{l(i)}\boldsymbol{b}_{ij}\cdot\boldsymbol{r}_{1ij}\ , \tag{182}$$

$$U(M)=\frac{G\rho_0}{2}\left(\sum_{i=1}^{n}h_i\sum_{j=1}^{l(i)}I_{ij}\boldsymbol{r}_{1ij}\cdot\left(\boldsymbol{l}_{ij}\times\boldsymbol{n}_i\right)-\sum_{i=1}^{l(i)}h_i^2\Omega_i\right), \tag{183}$$

$$\nabla_{\boldsymbol{r}_M}U(M)=-G\rho_0\sum_{i=1}^{n}\left(\boldsymbol{n}_i\cdot\boldsymbol{r}_{1ij}\right)\sum_{j=1}^{l(i)}\boldsymbol{b}_{ij}=-G\rho_0\sum_{i=1}^{n}\boldsymbol{n}_i\cdot\sum_{j=1}^{l(i)}\boldsymbol{b}_{ij}\cdot\boldsymbol{r}_{1ij}\ , \tag{184}$$

$$\nabla_{\boldsymbol{r}_M} U(M) = -G\rho_0 \left(\sum_{i=1}^{n} h_i \left(\sum_{j=1}^{l(i)} I_{ij} \left(\boldsymbol{l}_{ij} \times \boldsymbol{n}_i \right) - \Omega_i \boldsymbol{n}_i \right) \right), \tag{185}$$

$$U_{kl}(M) = G\rho_0 \sum_{i=1}^{n} \boldsymbol{n}_i \cdot \boldsymbol{e}_k \sum_{j=1}^{l(i)} \left(\boldsymbol{v}_{ij} \cdot \boldsymbol{e}_l C_{ij} - \boldsymbol{n}_i \cdot \boldsymbol{e}_l \Omega_{ij} \right). \tag{186}$$

Analytical formulas in terms of dyads:

$$U(M) = \frac{G\rho_0}{2} \sum_{edge} C_{edge} \left(\boldsymbol{r}_{edge} \boldsymbol{\phi}_{edge} \boldsymbol{r}_{edge} \right) - \frac{G\rho_0}{2} \sum_{face} \Omega_i \boldsymbol{r}_i \boldsymbol{\phi}_i \boldsymbol{r}_i \ , \tag{187}$$

$$\nabla_{\boldsymbol{r}_M} U(M) = -G\rho_0 \sum_{edge} C_{edge} \boldsymbol{\phi}_{edge} \boldsymbol{r}_{edge} + G\rho_0 \sum_{face} \Omega_i \boldsymbol{\phi}_i \boldsymbol{r}_i \ , \tag{188}$$

$$U_{kl}(M) = G\rho_0 \sum_{edge} C_{edge} \boldsymbol{e}_k^T \boldsymbol{\phi}_{edge} \boldsymbol{e}_l - G\rho_0 \sum_{i=1}^{n} \Omega_i \boldsymbol{e}_k^T \boldsymbol{\phi}_i \boldsymbol{e}_l \ ,$$

$$\left[U_{kl}(M) \right]_{k,l=\overline{1,3}} = G\rho_0 \sum_{edge} C_{edge} \boldsymbol{\phi}_{edge} - G\rho_0 \sum_{i=1}^{n} \Omega_i \boldsymbol{\phi}_i \ . \tag{189}$$

Relations between the constants and vector invariants:

$$h_{ij} = \boldsymbol{v}_{ij} \cdot \boldsymbol{r}_{1ij} \ , \ c_{ij} = \boldsymbol{b}_{ij} \cdot \boldsymbol{r}_{1ij} \ , \ h_i = \boldsymbol{n}_i \cdot \boldsymbol{r}_{MP} \ \text{ if } P \in S_i, \ c_{ij} = h_{ij} C_{ij} - h_i \Omega_{ij} \ ,$$

$$\boldsymbol{b}_{ij} = \boldsymbol{v}_{ij} C_{ij} - \boldsymbol{n}_i \Omega_{ij} \ , \ \boldsymbol{l}_{ij} = \boldsymbol{r}_{2ij} - \boldsymbol{r}_{1ij} = (x_{2ij} - x_{1ij}, y_{2ij} - y_{1ij}, z_{2ij} - z_{1ij}),$$

$$\boldsymbol{n}_i = \left(n_{i,1}, n_{i,2}, n_{i,3} \right), \ \boldsymbol{v}_{ij} = \left(v_{ij,1}, v_{ij,2}, v_{ij,3} \right), \ \boldsymbol{b}_{ij} = \left(b_{ij,1}, b_{ij,2}, b_{ij,3} \right). \tag{190}$$

The different analytical expressions of C_{ij} and Ω_i constants founded in the literature are summarized in Table 4.

1.2.10. Domain of definition of analytical formulas and its numerical properties

From the potential theory (Theorem 10) and based on relations (46)-(51) we can conclude that the gravitational potential and its derivatives generated by a homogeneous polyhedron has the following properties:

1. U and ∇U are continuous functions on the whole space, i.e.: $U \in C^1\left(R^3\right)$.

2. U is an infinitely differentiable function on the exterior of $\Sigma \subset R^3$ domain defined by the polyhedron, i.e.: $U \in C^\infty\left(R^3 \setminus \overline{\Sigma}\right)$.

3. In case of a homogeneous polyhedron the density function satisfies the condition $\rho \in C(\Sigma) \cap C^1(\mathrm{Int}(\Sigma))$, which is a sufficient condition to ensure the existence of second derivatives of U in the interior of the polyhedron, i.e.: $U \in C^2(\mathrm{Int}(\Sigma))$.

4. In exterior domain of the polyhedron the Laplace equation is valid, in the interior domain of the polyhedron the Poisson equation is valid, i.e.:

$$\Delta U(M) = \begin{cases} 0 & \text{if } M \in \mathrm{Int}(\Sigma) \\ -4\pi\rho_0 G & \text{if } M \in \mathrm{Ext}(\Sigma) \\ \textit{does not exist} & \text{if } M \in \partial\Sigma \end{cases}.$$

Domain of definition of the introduced constants and vectorial quantities deduced from integral form of its definition

The analytical formulas (177) – (189) determine the domain of definition of these quantities.

Considering Equation 92 the c_{ij} constants satisfy $\sum_{j=1}^{l(i)} c_{ij} = \int_{S_i} \frac{1}{r_{MP}} d\sigma_P$, where $c_{ij} = \int_{\Delta_{12ij}} \frac{1}{r_{MP}} d\sigma_P$. Based on Theorem 8 of potential theory these integrals exist for every point M of 3D space. Thus c_{ij} and $\sum_{j=1}^{l(i)} c_{ij}$ are defined in all 3D space, $\mathcal{D}(c_{ij}) = R^3$ and $\mathcal{D}\left(\sum_{j=1}^{l(i)} c_{ij}\right) = R^3$, where $\mathcal{D}$ denotes the largest possible domain of definition.

Using the relation (190) between the constants and vector quantities we have $\sum_{j=1}^{l(i)} c_{ij} = \sum_{j=1}^{l(i)} \boldsymbol{b}_{ij} \boldsymbol{r}_{1ij}$, from which results that the domain of definition of expression $\sum_{j=1}^{l(i)} \boldsymbol{b}_{ij} \boldsymbol{r}_{1ij}$ is R^3.

By right of (176) and (178) the domain of definition of $U(M)$ and $\nabla_{\boldsymbol{r}_M} U(M)$ are identical to that of $\sum_{j=1}^{l(i)} c_{ij}$. Similarly from (182) and (184) the domain of definition of $U(M)$ and $\nabla_{\boldsymbol{r}_M} U(M)$ are identical to that of $\sum_{j=1}^{l(i)} \boldsymbol{b}_{ij} \boldsymbol{r}_{1ij}$. Thus the domain of definition of gravitational potential and its first derivatives is the all 3D space R^3. The same conclusion can be drawn applying the Theorem 10, which states that the gravitational potential and its first derivatives generated by a homogeneous polyhedron are continuous in the whole space:

$$U \in C^1(R^3).$$

The domain of definition of c_{ij} and $\sum_{j=1}^{l(i)} c_{ij}$ is the intersection of the domains assigned to $h_{ij}C_{ij}$ and $h_i\Omega_{ij}$ because of the relation $c_{ij} = h_{ij}C_{ij} - h_i\Omega_{ij}$.

Relation (186) shows that the domain of definition of second derivatives of gravitational potential is intersection of domains of definitions of constants C_{ij} and Ω_i, which is equal to the domain of definition of vector quantities $\boldsymbol{b}_{ij} = \boldsymbol{v}_{ij}C_{ij} - \boldsymbol{n}_i\Omega_{ij}$.

In the following we investigate the domain of definition of C_{ij}, Ω_i and $h_{ij}C_{ij}$, $h_i\Omega_i$ quantities by right of its definition in integral form and respectively its analytical formulas. The numerical instability of these analytical formulas are investigated also. The integral form of the quantities C_{ij}, Ω_{ij}, Ω_i are:

$$C_{ij} = \int_{L_{ij}} \frac{1}{r_{MP}} dl \,, \tag{191}$$

$$\Omega_{ij} = \int_{\Delta_{12ij}} \frac{h_i}{r_{MP}^3} d\sigma_P = \int_{\Delta_{12ij}} \frac{1}{r_{MP}^2} \frac{\boldsymbol{r}_{MP}\boldsymbol{n}_i}{r_{MP}} d\sigma_P = \int_{\Delta_{i2ij}} \frac{\cos(\boldsymbol{r}_{MP}, \boldsymbol{n}_i)}{r_{MP}^2} d\sigma_P \,, \tag{192}$$

$$\Omega_i = \int_{S_i} \frac{h_i}{r_{MP}^3} d\sigma_P = \int_{S_i} \frac{1}{r_{MP}^2} \frac{\boldsymbol{r}_{MP}\boldsymbol{n}_i}{r_{MP}} d\sigma_P = \int_{S_i} \frac{\cos(\boldsymbol{r}_{MP}, \boldsymbol{n}_i)}{r_{MP}^2} d\sigma_P \,. \tag{193}$$

Based on the Observation 2 and 4 of Theorem 8 C_{ij} is defined and infinitely differentiable on the whole space except the L_{ij} segment, i.e. $\mathcal{D}\left(C_{ij}\right)=R^3 \setminus L_{ij}$ (Table 2).

Based on Theorem 12 regarding the double layer potential we can conclude that Ω_{ij}, Ω_i are defined and infinitely differentiable on whole space except the interfaces Δ_{12ij} and S_i, i.e. $\mathcal{D}\left(\Omega_{ij}\right)=R^3 \setminus \Delta_{12ij}$, $\mathcal{D}\left(\Omega_i\right)=R^3 \mid S_i$. On these interfaces Ω_{ij} and Ω_i are discontinuous of second kind, namely when approaching the surfaces from different directions the limit of integral formulas varies in function of directions (Table 3). From Theorem 12 we get the following limits for these quantities: $\Omega_{ij}(\infty)=0$, $\Omega_i(\infty)=0$.

Domain of definition of the introduced constants and vectorial quantities deduced from their analytical expressions. Investigation of numerical instability of these formulas

The analytical formulas of the constants C_{ij}, Ω_{ij}, Ω_i and the domain of definition of these analytical expressions are summarized in Table 4. It is shown that domain of definition of analytical formulas differs from domain of definition assigned by the integral form (henceforth will refer to it as theoretical domains of definition) of these constants. Based on Table 4 we can state that the theoretical domains of definition of C_{ij} coincide with the analytical domains only in the $C_{ij}^{Holstein}$ and C_{ij}^{HWSch} cases. In other cases the domains of analytical formulas are subsets of theoretical domains. The programming of gravity field parameters make use of analytical formulas of C_{ij}, Ω_{ij}, Ω_i constants, which requires the domain of definition of these constants because gravity related quantities can be evaluated only that specific domain. Out of domain of the analytical formulas the computed gravity parameters values will be "NaN". This can be avoided by introducing an ε threshold following the Pohànka (1988) idea. In this case we substitute the exact values $U(M)$, $U_k(M)$, $U_{kl}(M)$ with approximate numerical values $U(M, \varepsilon)$, $U_k(M, \varepsilon)$, $U_{kl}(M, \varepsilon)$. In Section 1.2.11 we will give a detailed analysis of the error introduced by the ε quantity. Making use of an adequate ε threshold we can extend the domain of definition of analytical expressions to the larger domain (theoretical domain). Thus the computation can be performed in this larger domain assigned by the integral form of these quantities without additional investigation regarding to the position of observation point compared to the polyhedron. Additionally it is important to know the behaviour of formulas from a numerical point of view and specify the domain of stability of these analytical expressions. Numerical stability means that the computed value is not dominated by rounding error. In Section 1.2.11 we will precisely determine the stability domains of C_{ij}, Ω_{ij}, Ω_i constants.

1. Analysis of the analytical formulas for the C_{ij} constant

Using notation introduced by Holstein and Ketteridge (1996), we denote with α the typical dimension of the target body (polyhedron) and with δ the typical distance of polyhedron from an observation point P. Their ratio $\gamma=\dfrac{\alpha}{\delta}$ is a dimensionless quantity.

The theoretical domain of definition of the C_{ij} constant derived from its integral form (191) is $D\left(C_{ij}\right)=R^3 \setminus L_{ij}=R^3 \setminus AB$. Without constraining the generality, the numerical investigation of the C_{ij} constants may be limited to an L_{ij} segment, where α denotes the length of the segment, and δ denotes the distance of the observation point from the segment. The value of C_{ij} depends on the relative position of the observation point and the L_{ij} segment. This means that varying the α length of the L_{ij} segment arbitrarily and the position δ of the observation point in accordance with the γ =, the C_{ij} value evaluated for these two different geometrical configuration will be the same. So these geometrical configurations which satisfy the γ =*const* relation can be considered equivalent. Let be L_{ij} = AB where A(0,-1,0), B(0,1,0). We perform the investigation of numerical stability of analytical formulas of C_{ij} (Table 4) by setting 4640 points around the boundary of domain of definition (L_{ij} edge)

and distant points from it. We fixed five points, from which three points (0,0.5,0),(0,1,0),(0,-1,0) were situated on the L_{ij} segment (boundary of domain of definition of C_{ij}) and two points (0,1.5,0),(0,-1.5,0) were situated on the exterior of the L_{ij} segment. We take lines (in total 29 lines), which have different gradients (***d***) and pass through the fixed limit point P_0. $P_0 + \boldsymbol{d} \cdot a$ is then the coordinates of points situated on these lines with ***d*** chosen as ((0,0,1), (-1,0,0), (-1,0,1), (0,±1,0), (-1,±1,0), (±1,±1,1)), and $a=2k\cdot 10^n$, where n varies between 8 and 25 and $k\in\{5,4,3,2,1\}$. In case of larger n the point $P_0+\boldsymbol{d}\cdot a$ moves away from P_0, in the contrary case $P_0+\boldsymbol{d}\cdot a$ approaches P_0. For the numerical investigation all computations were effectuated in double and quad precision. Stability problems arise both in distant points from L_{ij}, (γ<<1) and points near to L_{ij} (γ>>1). Due to the configuration of these 4640 points, in our investigation the lower limit of γ was $\gamma_{\min} = 2\cdot 10^{-9}$, the upper limit of γ was $\gamma_{\max} = 10^{25}$. In our earlier works (Benedek 2004, Benedek and Papp 2009) and a recent work (Benedek et al. 2018) in case of the applied local and regional model computations the limits of γ are situated between: $\gamma_{\max}^{modell} \approx 2000$ and $\gamma_{\min}^{modell} \approx 1.5\cdot 10^{-4}$, which do not exceed the $\gamma_{\min} = 2\cdot 10^{-9}$ and $\gamma_{\min} = 10^{25}$ limits.

In case of quad precision computation the first 24 decimals are identical for $C_{ij}^{Pohanka^3}$ and $C_{ij}^{Holstein}$ (Table 4) in the 4640 observation points which cover the investigated $\gamma \in (2\cdot 10^{-9}, 10^{25})$ range. So $C_{ij}^{Pohanka^3}$ and $C_{ij}^{Holstein}$ values coincide up to 24 decimal places on their common domain of definition. Accordingly in the course of numerical investigation we have considered as reference values the quad precision computed $C_{ij}^{Pohanka^3}$ and $C_{ij}^{Holstein}$ (notated by $_{r16}$ indices) compared to double precision values (notated by $_{r8}$ indices). The statement that $\left(C_{ij}^{Pohanka^3}\right)_{r16}$ and $\left(C_{ij}^{Holstein}\right)_{r16}$ can be considered as reference values is supported by the fact that in case of far computation points characterized with $\gamma \in (2\cdot 10^{-9}, 5)$ the limit of these values are equal up to 24 decimal digits with quad precision Taylor series approximation $\left(\widetilde{C}_{ij,n_0=30}\right)_{r16}$ (Table 4). When performing the same calculation in double precision we produce an approximation which is correct up to 16 decimal digits of accuracy. The values of $C_{ij}^{Pohanka^3}$ and $C_{ij}^{Holstein}$ near to the polyhedron and characterized by γ >>1 are numerically stable, because in these formulas in the numerator of logarithmic terms we can find the sum of the same order of magnitude quantities (r_{2ij} and $|l_{2ij}|$ and respectively r_{1ij} and $|l_{1ij}|$), whereas in case of *Pohànka*[1], *Pohànka*[2], *HPGL* analytical formulas (Table 4) appear the difference of these quantities. Based on quad computation *Pohànka*[1], *Pohànka*[2], *HPGL* formulas numerically are stable on $\gamma \in (2\cdot 10^{-9}, 10^{16})$. In double precision evaluation the numerical instability occurs for $\gamma > 10^7$. In *HWS* formula (Table 4) the $\Lambda_{ij} = \dfrac{l_{ij}}{r_{2ij} + r_{1ij}}$ quantity will converge to the value 1 if the computation point approaches the [*AB*] segment, therefore the denominator of *HWS* (logarithmic term of Λ_{ij}) will become numerically unstable in the near area of [*AB*]. In case of computation of quad precision the numerical instability arises for points close to the segment *AB* characterized with $\gamma > 10^{16}$. In case of computation of double precision the corresponding domain will be $\gamma > 10^7$. Out of points of AB segment ($R^3 \setminus [AB]$) *HWS* formula is stable on the feasible maximum domain $\gamma \in (\gamma_{\min} = 2\cdot 10^{-9}, \gamma_{\max} = 10^{25})$.

From the numerical value of quad precision computed C_{ij} we can conclude:

Comparing in domain $\gamma \in (2\cdot 10^{-9}, 10^5)$ each computes $(C_{ij})_{r16}$ with the chosen reference values $\left(C_{ij}^{Pohanka^3}\right)_{r16}$ and $\left(C_{ij}^{Holstein}\right)_{r16}$ we can conclude that they are practically identical (to 24 digits after the decimal point). In the $\gamma \in (10^5, 10^9)$ domain the absolute value of difference of these quantities is less than 10^{-16}, in case of the $\gamma \in (10^9, 10^{13})$ domain the difference between the computed and reference value is less than 10^{-8}, while on $\gamma \in (10^{13}, 10^{16})$ the difference is less than 10^{-2}.

Similarly from the double precision computation we can state:

The difference between the identical two reference values $\left(C_{ij}^{Pohanka^3}\right)_{r16}$ and $\left(C_{ij}^{Holstein}\right)_{r16}$ and $\left(C_{ij}^{Pohanka^3}\right)_{r8}$ and $\left(C_{ij}^{Holstein}\right)_{r8}$ values are less than 10^{-16} on the $\gamma \in (10^3, 10^{25})$ domain, on the $\gamma \in (10^{-4}, 10^3)$ domain the difference is less than 10^{-12}, and furthermore on the $\gamma \in (2\cdot 10^{-9}, 10^{-4})$ domain

the difference is less than 10^{-8}. Near to the segment *AB* characterized by the inequality $\gamma \in (10^3, 10^5)$ the rest of formulas (C_{ij})$_{r8}$ (*Pohànka*[1], *Pohànka*[2], *HPGL*, *HWS*) will approach the exact value less than 10^{-8}, in case of observation points more closely approaching ($\gamma \in (10^5, 10^7)$) the segment *AB* the difference will be less than 10^{-4}.

If the computation point converges to the source model the numerical error begins to dominate the C_{ij} and these formulas will become numerically unstable and the relative error will be growing. For example if the observation point satisfies the $\gamma \approx 10^{16}$ condition, the relative error of $\left(C_{ij}^{Pohanka^3}\right)_{r8}$, $\left(C_{ij}^{Holstein}\right)_{r8}$ formulas will attain 1%. The 1% limit of relative error in case of the $\left(C_{ij}^{HWSch}\right)_{r8}$ formula will appear when the observation point satisfies the $\gamma \approx 10^{15}$ condition. In case of the $\left(C_{ij}^{Pohanka^1}\right)_{r8}$, $\left(C_{ij}^{Pohanka^2}\right)_{r8}$ and $\left(C_{ij}^{HPGH}\right)_{r8}$ formulas this limit will be at $\gamma \approx 5 \cdot 10^6$.

If the observation point moves away from [*AB*] the C_{ij} value will converge to 0 ($\lim_{\gamma \to 0} C_{ij} = 0$), otherwise if the observation point approaches [*AB*] the C_{ij} will converge to infinity $\lim_{\gamma \to \infty} C_{ij} = \infty$ (Fig. 9, Table 2). In other points of space ($R^3 \setminus [AB]$) the limit of C_{ij} exists and is finite, i.e. $\lim_{M \to M_0, M_0 \in R^3 \setminus [AB]} C_{ij} \in R$ (Fig. 9, Table 2). In order to justify this we consider the following relation:

$$C_{ij}^{HWS} = \ln\left(\frac{r_{2ij} + r_{1ij} + l_{ij}}{r_{2ij} + r_{1ij} - l_{ij}}\right) = \ln\left(\frac{1+\Lambda_{ij}}{1-\Lambda_{ij}}\right), \text{ where } \Lambda_{ij} = \frac{l_{ij}}{r_{2ij} + r_{1ij}} = \frac{AB}{MA + MB} < 1 .$$

If the observation point *M* moves away from the [*AB*] segment, then $\Lambda_{ij} \to 0$, which implies $\lim_{\gamma \to 0} C_{ij} = \lim_{\Lambda_{ij} \to 0} \ln\left(\frac{1+\Lambda_{ij}}{1-\Lambda_{ij}}\right) = 0$, otherwise if the point *M* approaches the [*AB*] segment, then $\Lambda_{ij} \to 1$ and accordingly $\lim_{\gamma \to \infty} C_{ij} = \lim_{\Lambda_{ij} \to 1} \ln\left(\frac{1+\Lambda_{ij}}{1-\Lambda_{ij}}\right) = \infty$. If the *M* point approaches the $M_0 \in R^3 \setminus [AB]$ point, then $\lim_{M \to M_0} \Lambda_{ij} \in (0,1)$, thus $\lim_{M \to M_0, M_0 \in R^3 \setminus [AB]} C_{ij} \in R$ (Table 2).

The $h_{ij}C_{ij}$ term appears in the analytical formulas of gravitational potential and its first derivatives. If the observation point is approaching the [*AB*] segment, then the value of $h_{ij}C_{ij}$ scalar product will converge to 0 (Fig. 9, Table 2). This can be seen based on the following inequalities:

$$0 \le \lim_{\Lambda_{ij} \to 1} \left| h_{ij} C_{ij} \right| = \lim_{\Lambda_{ij} \to 1} \left| h_{ij} \ln\left(\frac{1+\Lambda_{ij}}{1-\Lambda_{ij}}\right) \right| \le \lim_{\Lambda_{ij} \to 1} r_{0ij} \ln\left(\frac{1+\Lambda_{ij}}{1-\Lambda_{ij}}\right) \le \lim_{\Lambda_{ij} \to 1} l_{ij} \frac{\sqrt{1-\left(\Lambda_{ij}\right)^2}}{2\Lambda_{ij}} \ln\left(\frac{1+\Lambda_{ij}}{1-\Lambda_{ij}}\right) = 0. \quad (194)$$

At this point we make use of inequality (31) given by Holstein (2003):

$$\left| h_{ij} \right| < r_{0ij} < l_{ij} \frac{\sqrt{1-\left(\Lambda_{ij}\right)^2}}{2\Lambda_{ij}} \text{ and} \quad (195)$$

$$\lim_{y \to 0} y^r \ln y = 0, r \in R_+ , \quad (196)$$

from which we can deduce the limit: $\lim_{\Lambda_{ij} \to 1} l_{ij} \sqrt{1-\left(\Lambda_{ij}\right)} \ln\left(1-\Lambda_{ij}\right) = 0$. (195) follows from relations: $r_{0ij}^2 = r_{2ij}^2 - l_{2ij}^2 = r_{1ij}^2 - l_{1ij}^2$ and $l_{ij} = \left| l_{2ij} - l_{1ij} \right|$.

The following inequality shows that if the observation point *M* moves away from [*AB*] segment, then $\left| h_{ij}C_{ij} \right|$ will be less than the length of segment (Fig. 10, Table 2):

$$0 \le \lim_{\Lambda_{ij}\to 0}\left|h_{ij}C_{ij}\right| \le \lim_{\Lambda_{ij}\to 0}\left|h_{ij}\ln\left(\frac{1+\Lambda_{ij}}{1-\Lambda_{ij}}\right)\right| \le \lim_{\Lambda_{ij}\to 0} r_{0ij}\ln\left(\frac{1+\Lambda_{ij}}{1-\Lambda_{ij}}\right) \le \lim_{\Lambda_{ij}\to 0} l_{ij}\frac{\sqrt{1-\left(\Lambda_{ij}\right)^2}}{2\Lambda_{ij}}\ln\left(\frac{1+\Lambda_{ij}}{1-\Lambda_{ij}}\right) =$$

$$= l_{ij}\lim_{y\to 1}\frac{\ln y}{y-1}\sqrt{y} = l_{ij}\,. \tag{197}$$

In order to demonstrate this one, we use the fact that the observation point *M* moves away from [*AB*] then $y = \frac{1+\Lambda_{ij}}{1-\Lambda_{ij}} \to 1$. The limit $\lim_{y\to 1}\frac{\ln y}{y-1} = 1$ can be demonstrated using the l'Hospital theorem. If the observation point *M* approaches a point situated on the line *AB* but outside the [*AB*] segment then $\lim_{M\to M_0\in AB\setminus[AB]} h_{ij}C_{ij} = 0$ (Fig. 10, Table 2). For $M_0 \in R^3\setminus AB$ we have: $\lim_{M\to M_0\in R^3\setminus AB} h_{ij}C_{ij} \in R\setminus\{0\}$. The behaviour of the C_{ij}, $h_{ij}C_{ij}$ functions and their limits in the limit points of the domain of definition are summarized in Table 2.

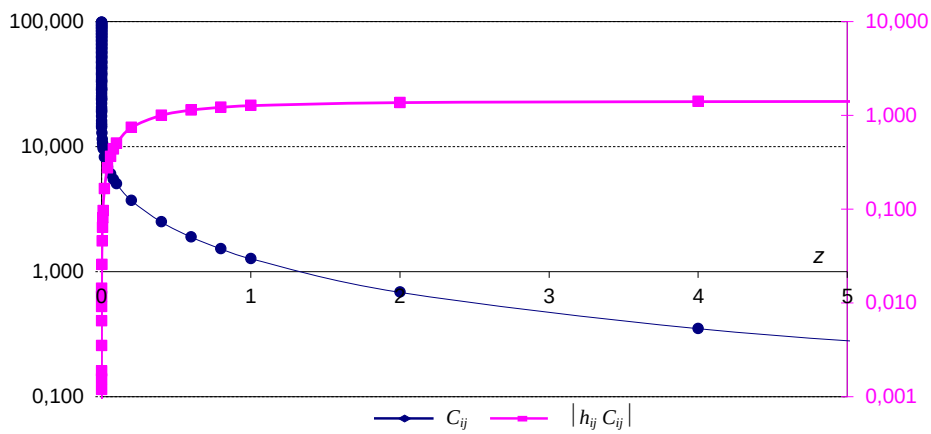

Fig. 9 The variation of C_{ij} and $|h_{ij}C_{ij}|$ along the *M*(-z, 0.5, z) points which are situated on the line (*d*: 0.5 = *y*, *x* + *z* = 0 ⇔ *M*(-*z*, 0.5, z)) perpendicular to L_{ij}=[*AB*] segment (*A*=(0,1,0), *B*=(0,-1,0)). The values of the functions are in the logarithmic scale. The value of γ accordingly with its definition is $\gamma = \sqrt{2}z^{-1}$. If the observation point *M*(-*z*, 0.5, z) approaches the M_0(0, 0.5, 0) point situated on the segment [*AB*], then *z*→0 and $\lim_{z\to 0} C_{ij} = \lim_{\gamma\to\infty} C_{ij} = \infty$, $\lim_{z\to 0} h_{ij}C_{ij} = \lim_{\gamma\to\infty} h_{ij}C_{ij} = 0$ (where h_{ij} is the projection of *M* point to the *z* = 0). $\Lambda_{ij} = \frac{l_{ij}}{r_{2ij}+r_{1ij}} = \frac{AB}{MA+MB} < 1$. If the observation point *M* moves away from the [*AB*] segment then |z|→∞ and $\lim_{|z|\to\infty} C_{ij} = \lim_{\gamma\to 0} C_{ij} = 0$, $\lim_{|z|\to\infty}\left|h_{ij}C_{ij}\right| = \lim_{\gamma\to 0}\left|h_{ij}C_{ij}\right| = l < 2 = l_{ij}$

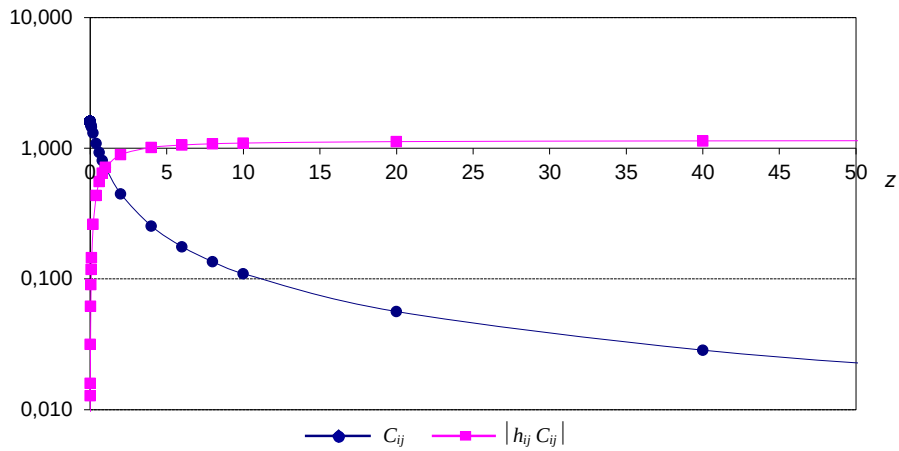

Fig. 10 The variation of C_{ij} and $|h_{ij}C_{ij}|$ along the $M(-z, z+1.5, z)$ points which are situated on a line (d: $-x = y-1.5 = z \Leftrightarrow M(-z, z+1.5, z)$). The values of the functions are in the logarithmic scale. The value of γ accordingly with its definition is $\gamma = \sqrt{2}z^{-1}$. If the observation point $M(-z, z+1.5, z)$ approaches the $M_0(0, 1.5, 0)$ the common point of segment $[AB]$ and the plane $z = 0$, then $z \to 0$ and $\lim_{z\to 0} C_{ij} = \lim_{\gamma\to\infty} C_{ij} = \infty$, $\lim_{z\to 0} h_{ij}C_{ij} = \lim_{\gamma\to\infty} h_{ij}C_{ij} = 0$ (where h_{ij} is the projection of M point to the $z = 0$). If the observation point M moves away from the $[AB]$ segment then $|z| \to \infty$ and $\lim_{|z|\to\infty} C_{ij} = \lim_{\gamma\to 0} C_{ij} = 0$, $\lim_{|z|\to\infty} |h_{ij}\, C_{ij}| = \lim_{\gamma\to 0} |h_{ij}\, C_{ij}| = l < 2 = l_{ij}$

Table 2. The limits of the C_{ij},and $h_{ij}C_{ij}$ functions

constant	investigated domain	limit	explanation
C_{ij}	$[AB]=[A_{ij}A_{ij+1}]$	∞	$M_0 \in [AB]$, $\lim_{M\to M_0} C_{ij} = \infty$
	$AB\backslash[AB]$	$\ln\lvert l_2/l_1\rvert$	$M_0 \in AB\backslash[AB]$,
	$R^3\backslash AB$	$\in$R	$M_0 \in AB$, $\lim_{M\to M_0,} C_{ij} \in R$
	$\gamma\to 0$	0	$dist(M,[AB]) \to \infty$, $\lim_{\gamma\to 0} C_{ij} = 0$
$h_{ij}C_{ij}$	$[AB]=[A_{ij}A_{ij+1}]$	0	$M_0 \in [AB]$, $\lim_{M\to M_0} h_{ij}C_{ij} = 0$
	$AB\backslash[AB]$	0	$M_0 \in AB\backslash[AB]$, $\lim_{M\to M_0} h_{ij}C_{ij} = 0$
	$R^3\backslash AB$	$\in R\backslash\{0\}$	$M_0 \in AB$, $\lim_{M\to M_0} h_{ij}C_{ij} \in R\backslash\{0\}$
	$\gamma\to 0$	$\in R$	$dist(M,[AB]) \to \infty$, $\lim_{\gamma\to 0}\lvert h_{ij}C_{ij}\rvert \in [0, l_{ij}]$
			$\lim_{\gamma\to 0}\lvert h_{ij}C_{ij}\rvert \in [0, l_{ij}]$

2. Numerical investigation of analytical functions of Ω_{ij}, Ω_i

We have constrained the numerical investigation of Ω_i to a single S_i triangular face, similarly we constrained the investigation of Ω_{ij} to a single edge of S_i namely to the Δ_{12ij} (Fig. 3). Without constraining the generality let be $S_i = [A_{i1}A_{i2}A_{i3}] = [ABC]$, where $A(0,-1,0)$, $B(0,1,0)$, $C(1,0,0)$. Accordingly $\Delta_{1212} = [M_iAB]$, $\Delta_{1223} = [M_iBC]$, $\Delta_{1231} = [M_iCA]$, where M_i is the projection of M to S_i plane. We assign the value $\alpha = 2$ to $S_i = [ABC]$ and we denote with δ the distance of observation point and the centroid of S_i. The analytical formulas of Ω_{ij}, Ω_i were evaluated near to the limit points of

their domains of definition and in points away from the triangular face S_i, in total 8510 points (Table 4). Similar to numerical investigations performed for C_{ij} the Ω_{ij}, Ω_i formulas where evaluated on lines with different directions (30 lines) around the (0,0.5,0), (0,1,0), (0,1.5,0), (0.5, 0,0) (-1,0.5,0) limit points. The computations were effectuated in double and quad precision. The numerical instability problems arise when the observation point is away from the S_i face ($\gamma << 1$) and near to the S_i face ($\gamma >> 1$). From computation of quad precision we state $\gamma_{\max} = 10^{25}$, and $\gamma_{\min} = 1.5 \cdot 10^{-9}$.

Moving away with the observation point from the S_i face the limits of Ω_{ij}, Ω_i and $h_i\Omega_i$ are 0 (Fig. 11, Fig. 12, Fig. 14, Fig. 15, Fig. 17, Fig. 18, Fig. 20, Fig. 21), whereas the limit of $h_i\Omega_{ij}$ depends on the direction of approaching the line (Fig. 13, 16, 19).

On the [AB], [BC], [AC] edges of S_i = [ABC] face Ω_{ij} and Ω_i are not defined (Table 4). The inner points of this face are points of discontinuity of the second kind or essential discontinuity of Ω_i since the limit in these points are functions of the direction of the approaching line (Fig. 20, Table 3).

Ω_i is continuous in the $R^3 \setminus S_i$ domain. The limit at points adherent to set $s \setminus S_i$ i.e. belonging to the s plane defined by the ABC face without the points of the S_i face is 0 (Fig. 15, Fig. 18 and Table 3).

The points of plane s are discontinuous of the second kind for Ω_{ij} (Fig. 12, Fig. 15, Fig. 18), whereas on $R^3 \setminus s$ points Ω_{ij} is continuous (Table 3).

The $h_i\Omega_{ij}$, $h_i\Omega_i$ are continuous in all space. In the special case when the observation point belongs to s, the limit of $h_i\Omega_{ij}$ and $h_i\Omega_i$ is 0 (Fig. 11, Fig. 13, Fig. 14, Fg. 16, Fig. 17, Fig. 19, Fig. 21, Table 3), i.e., $h_i\Omega_{ij}$, $h_i\Omega_i \to 0$ if $h_i \to 0$.

We will justify our statements below. Moving away with the observation point from the S_i face is evident from geometrical interpretation of Ω_{ij}, Ω_i that the limit of these expressions will be 0. This affirmation can be demonstrated directly starting with identity (73):

$$\Omega_{ij}^{Pohanka^3} = 2\,\mathrm{sign}(h_i)\,\mathrm{atan}\frac{2h_{ij}l_{ij}}{(r_{2ij}+r_{1ij})^2 - l_{ij}^2 + 2(r_{2ij}+r_{1ij})|h_i|}, \text{ where } l_{ij} = l_{2ij} - l_{1ij}.$$

Using the $\Lambda_{ij} = \dfrac{l_{ij}}{r_{2ij}+r_{1ij}} = \dfrac{AB}{MA+MB}$ notation and the inequality $|h_{ij}| < r_{0ij} < l_{ij}\dfrac{\sqrt{1-(\Lambda_{ij})^2}}{2\Lambda_{ij}}$:

$$0 \le \left|\frac{2h_{ij}l_{ij}}{(r_{2ij}+r_{1ij})^2 - l_{ij}^2 + 2(r_{2ij}+r_{1ij})|h_i|}\right| \le \frac{2|h_{ij}|l_{ij}}{(r_{2ij}+r_{1ij})^2 - l_{ij}^2} \le \frac{2\dfrac{\sqrt{1-(\Lambda_{ij})^2}}{2\Lambda_{ij}}\Lambda_{ij}^2}{1-\Lambda_{ij}^2} = \frac{\Lambda_{ij}}{\sqrt{1-(\Lambda_{ij})^2}} \to 0.$$

(198)

For distant points from S_i it holds $\Lambda_{ij} \to 0$, and for this reason $\Omega_{ij} \to 0$. Since Ω_i is the sum of Ω_{ij} we can conclude that $\Omega_i \to 0$ if $\Lambda_{ij} \to 0$ (Table 3).

Approaching the plane s, then $h_i \to 0$. Since Ω_{ij} is a bounded function ($|\Omega_{ij}| < 2\pi$) then $h_i\Omega_{ij}$ and $h_i\Omega_i \to 0$, if $h_i \to 0$ (Table 3).

Moving away with the observation point from the S_i face along a d line, then $h_i \to \infty$ or $h_{ij} \to \infty$. We examined the following cases:

1. d is perpendicular to the plane s ($d \perp s$) $\Leftrightarrow \angle(d, s) = \pi/2$. Then $|h_i| \to \infty$ and h_{ij} will be a bounded quantities. Using (197):

$$h_i\Omega_{ij}^{Pohanka^3} = 2|h_i|\,\mathrm{atan}\frac{2h_{ij}l_{ij}}{(r_{2ij}+r_{1ij})^2 - l_{ij}^2 + 2(r_{2ij}+r_{1ij})|h_i|} \tag{199}$$

the argument of the atan function will converge to 0. Based on the well-known limit $\lim\limits_{x\to 0}\dfrac{\mathrm{atan}\,x}{x} = 1$ and the following inequality:

$$0 \le \lim_{|h_i|\to\infty} \left|h_i \Omega_{ij}\right| = \lim_{|h_i|\to\infty} \frac{4|h_i||h_{ij}|l_{ij}}{\left(r_{2ij}+r_{1ij}\right)^2 - l_{ij}^2 + 2\left(r_{2ij}+r_{1ij}\right)|h_i|} \le \lim_{|h_i|\to\infty} \frac{|h_{ij}|l_{ij}}{r_{2ij}+r_{1ij}} = 0 \tag{200}$$

we can conclude:

$$\lim_{|h_i|\to\infty} h_i \Omega_{ij} = 0 . \tag{201}$$

In (200) we use the inequality $\left(r_{2ij}+r_{1ij}\right)/h_i \le 2$ and the limit $\lim_{|h_i|\to\infty} \frac{l_{ij}}{|h_i|} = 0$. Whereas Ω_i is the sum of the Ω_{ij} belonging to the face i, from (201) we get the following limit: $\lim_{|h_i|\to\infty} h_i \Omega_i = 0$.

2. If $\angle(d,s)=0$, i.e. $d \,||\, s$ then follows that $|h_{ij}|\to\infty$ and h_i is bonded, which assures the convergence to 0 of argument of the atan function: $\lim_{|h_{ij}|\to\infty} h_i \Omega_{ij} = 0$ and $\lim_{|h_{ij}|\to\infty} h_i \Omega_i = 0$.

3. If $\angle(d,s)\in(0,\pi/2)$, then it holds $|h_{ij}|\to\infty$ and $|h_i|\to\infty$. We introduce the parameter $m=\tan(d,s)$ and the notations $d'=\mathrm{proj}_s d$ and $M_0 = d\cap s$. In the s plane we take the (M_0, x', y') local coordinate system, where the x' axis coincides with the d' line and its direction is identical with the moving point direction. Let φ be the rotation angle between the (O, x, y) and (M_0, x', y') coordinate systems. The equation defining this transformation, which rotates the xy axes counter clockwise through an angle φ into the $x'y'$ axes is: $\begin{bmatrix} x' \\ y' \end{bmatrix} = \begin{bmatrix} \cos\varphi & \sin\varphi \\ -\sin\varphi & \cos\varphi \end{bmatrix} \begin{bmatrix} x \\ y \end{bmatrix} + \begin{bmatrix} x_0 \\ y_0 \end{bmatrix}$. $(h_i/m, 0, h_i)$ is the coordinate of the observation point. The $h_i\Omega_{ij}$ limit is independent from the coordinate system, so without limiting the generality the calculations are effectuated in the (x', y', z) coordinate system. For $|h_i|\to\infty$ the argument of the atan function in expression of Ω_{ij} will converge to 0 and the $0 \cdot \infty$ indeterminate form will arise for $h_i\Omega_{ij}$. According to $\lim_{y\to 0} \frac{\operatorname{atan} y}{y} = 1$, we can write the following identity:

$$\lim_{|h_i|\to\infty} \left|h_i \Omega_{ij}\right| = \frac{\left|\sin\varphi\left(x_{2ij}-x_{1ij}\right) - \cos\varphi\left(y_{2ij}-y_{1ij}\right)\right|}{|m|\left(1+m^{-2}+\sqrt{1+m^{-2}}\right)} = \frac{\left|y'_{2ij}-y'_{1ij}\right|}{|m|\left(1+m^{-2}+\sqrt{1+m^{-2}}\right)} . \tag{202}$$

(202) shows that $h_i\Omega_{ij}$ has a limit which depends on the direction of d denoted by m (Fig. 13, Fig. 16, Fig. 19). Using (202) we can deduce the limit of $h_i\Omega_i$ as follows:

$$\lim_{|h_i|\to\infty} h_i \Omega_i = \lim_{|h_i|\to\infty} \sum_{j=1}^{3} h_i \Omega_{ij} = \operatorname{sign}(h_i) \lim_{|h_i|\to\infty} \sum_{j=1}^{3} \operatorname{sign}(\Omega_{ij}) \left|h_i \Omega_{ij}\right| =$$

$$= \operatorname{sign}(h_i) \sum_{j=1}^{3} \operatorname{sign}(\Omega_{ij}) \frac{\left|y'_{2ij}-y'_{1ij}\right|}{|m|\left(1+m^{-2}+\sqrt{1+m^{-2}}\right)} .$$

If S_i is positive oriented then $\operatorname{sign}(\Omega_{ij}) = -\operatorname{sign}\left(y'_{2ij}-y'_{1ij}\right)$. Thus:

$$\lim_{|h_i|\to\infty} h_i \Omega_i = \frac{\operatorname{sign}(h_i)}{|m|\left(1+m^{-2}+\sqrt{1+m^{-2}}\right)} \sum_{j=1}^{3} \left(y'_{2ij} - y'_{1ij}\right) = 0 .$$

Furthermore we investigated the limit of Ω_i in points of plane s. We consider the (125) expression of Ω_i:

$$\Omega_i^{WS} = 2\operatorname{atan} 2\left(\boldsymbol{r}_1\left(\boldsymbol{r}_2 \times \boldsymbol{r}_3\right), r_1 r_2 r_3 + r_1 \boldsymbol{r}_2 \boldsymbol{r}_3 + r_2 \boldsymbol{r}_1 \boldsymbol{r}_3 + r_3 \boldsymbol{r}_1 \boldsymbol{r}_2\right) .$$

We can distinguish three cases: (1) $M_0 \in s \backslash S_i$, (2) $M_0 \in S_i$ and (3) $M_0 \in \partial S_i$. If the observation point M converges to (1) $M_0 \in s \backslash S_i$, then

$$r_1 r_2 r_3 + r_1 \boldsymbol{r}_2 \boldsymbol{r}_3 + r_2 \boldsymbol{r}_1 \boldsymbol{r}_3 + r_3 \boldsymbol{r}_1 \boldsymbol{r}_2 \to r_1^0 r_2^0 r_3^0 + r_1^0 \boldsymbol{r}_2^0 \boldsymbol{r}_3^0 + r_2^0 \boldsymbol{r}_1^0 \boldsymbol{r}_3^0 + r_3^0 \boldsymbol{r}_1^0 \boldsymbol{r}_2^0 = 4 r_1^0 r_2^0 r_3^0 \cos\frac{\alpha}{2} \cos\frac{\beta}{2} \cos\frac{\gamma}{2}, \quad (203)$$

where $\boldsymbol{r}_1^0 = \overrightarrow{M_0 A}$, $\boldsymbol{r}_2^0 = \overrightarrow{M_0 B}$, $\boldsymbol{r}_3^0 = \overrightarrow{M_0 C}$, α, β, γ are the angles between the vectors $\boldsymbol{r}_1^0$ and $\boldsymbol{r}_2^0$, $\boldsymbol{r}_3^0$ and $\boldsymbol{r}_2^0$, $\boldsymbol{r}_1^0$ and $\boldsymbol{r}_3^0$ successively, i.e. $\alpha = \angle(\boldsymbol{r}_1^0, \boldsymbol{r}_2^0) < \pi$, $\beta = \angle(\boldsymbol{r}_3^0, \boldsymbol{r}_2^0) < \pi$, $\gamma = \angle(\boldsymbol{r}_1^0, \boldsymbol{r}_3^0) < \pi$. Since $M_0 \in s \backslash S_i$, the maximum of α, β and γ angles will equal the sum of the other two, thus:

$$4 r_1^0 r_2^0 r_3^0 \cos\frac{\alpha}{2} \cos\frac{\beta}{2} \cos\frac{\gamma}{2} > 0 . \quad (204)$$

If we approach the point $M_0 \in s \setminus S_i$ along points situated outside of the plane s ($M \in R^3 \setminus s$), then

$$\lim_{M \to M_0 \in s / S_i} \boldsymbol{r}_1 (\boldsymbol{r}_2 \times \boldsymbol{r}_3) = \boldsymbol{r}_1^0 (\boldsymbol{r}_2^0 \times \boldsymbol{r}_3^0) = 0 .$$

If we approach the point $M_0 \in s$ along points in s then $\boldsymbol{r}_1 (\boldsymbol{r}_2 \times \boldsymbol{r}_3) = 0$ and holds:

$$\lim_{M \to M_0 \in s / S_i} \Omega_i = 2 \lim_{M \to M_0 \in s / S_i} \operatorname{atan} 2\left(\boldsymbol{r}_1 (\boldsymbol{r}_2 \times \boldsymbol{r}_3), r_1 r_2 r_3 + r_1 \boldsymbol{r}_2 \boldsymbol{r}_{31} + r_2 \boldsymbol{r}_1 \boldsymbol{r}_3 + r_3 \boldsymbol{r}_1 \boldsymbol{r}_2\right) = 0 . \quad (205)$$

If M_0 is situated inside of S_i, i.e. $M_0 \in \mathrm{Int}(S_i)$, then for the angles α, β, γ it holds that $\alpha + \beta + \gamma = 2\pi$, thus:

$$4 r_1^0 r_2^0 r_3^0 \cos\frac{\alpha}{2} \cos\frac{\beta}{2} \cos\frac{\gamma}{2} < 0 . \quad (206)$$

If M_0 is situated on boundary of S_i, i.e. $M_0 \in \partial S_i$ then one of the angles α, β, γ takes the value π, thus:

$$4 r_1^0 r_2^0 r_3^0 \cos\frac{\alpha}{2} \cos\frac{\beta}{2} \cos\frac{\gamma}{2} = 0 . \quad (207)$$

Based on (203), (206) and (207):

$$\lim_{M \to M_0 \in S_i} \left(r_1 r_2 r_3 + r_1 \boldsymbol{r}_2 \boldsymbol{r}_3 + r_2 \boldsymbol{r}_1 \boldsymbol{r}_3 + r_3 \boldsymbol{r}_1 \boldsymbol{r}_2\right) = \begin{cases} 0 \text{ if } & M_0 \in \partial S_i \\ <0 \text{ if } & M_0 \in \mathrm{Int}(S_i) \end{cases} . \quad (208)$$

The limit of the scalar triple product is:

$$\lim_{M \to M_0 \in S_i} \boldsymbol{r}_1 (\boldsymbol{r}_2 \times \boldsymbol{r}_3) = \begin{cases} 0 & \text{if } M \in s \\ \operatorname{sign}(\boldsymbol{r}_1 (\boldsymbol{r}_2 \times \boldsymbol{r}_3)) \cdot 0 & \text{if } M \notin s \end{cases} . \quad (209)$$

By right of the (208), (209) relations we have:

$$\lim_{M \to M_0 \in S_i} \Omega_i = \begin{cases} 2 \operatorname{atan}(f(m)) & \text{if } M_0 \in \partial S_i, (d,s) \in \left[0, \frac{\pi}{2}\right) \\ \operatorname{sign}(\boldsymbol{r}_1 (\boldsymbol{r}_2 \times \boldsymbol{r}_3)) \cdot \pi & \text{if } M_0 \in \partial S_i, (d,s) \in \left[0, \frac{\pi}{2}\right) \\ \operatorname{sign}(\boldsymbol{r}_1 (\boldsymbol{r}_2 \times \boldsymbol{r}_3)) \cdot \pi & \text{if } M_0 \in \mathrm{Int}(S_i) \end{cases}, \quad (210)$$

where m is the tangent of the angle between the line d and plane s, i.e. $m = \tan(d,s)$. $f(m)$ is the expression of indeterminate form 0/0 changing as a function of m, that is the directional derivatives (Fig. 19). In order to evaluate the expression of $f(m)$ we define a local coordinate system in the s plane

with the origin in (M_0, x', y'), where x' is identical with $d' = \mathrm{proj}_s\, d$ and is assumed to coincide with the direction of the moving observation point. Let $\left(x'_{1ij}, y'_{1ij}\right)$ and $\left(x'_{2ij}, y'_{2ij}\right)$ be the coordinates in this local system of vertices of the jth ($j = \overline{1,3}$) edge of ∂S_i. $f(m)$ is independent of the chosen local frame. The following formula can be demonstrated simply:

$$f(m) = \frac{\mathrm{sign}\left(\boldsymbol{r}_1\left(\boldsymbol{r}_2 \times \boldsymbol{r}_3\right)\right) \cdot m \begin{vmatrix} x'_{2ij} - x'_{1ij} & y'_{2ij} - y'_{1ij} \\ x'_{3ij} - x'_{1ij} & y'_{3ij} - y'_{1ij} \end{vmatrix}}{\sum_{j=1}^{3} \frac{x'_{1ij}\left(x'^2_{1ij+1} + x'^2_{1ij+1}\right)\left(x'^2_{1ij+2} + x'^2_{1ij+2}\right)}{\sqrt{\left(x'^2_{1ij} + y'^2_{1ij}\right)\left(x'^2_{1ij+1} + y'^2_{1ij+1}\right)\left(x'^2_{1ij+2} + y'^2_{1ij+2}\right)}} + \sum_{k=1}^{3} \frac{x'_{1ij}\left(x'_{1i+1j}x'_{1ij+2} + y_{1ij+1}y'_{1ij+2}\right)}{\sqrt{\left(x'^2_{1ij} + y'^2_{1ij}\right)}} + \sum_{k=1}^{3} \sqrt{x'^2_{1ij} + y'^2_{1ij}}\left(x'_{1ij+1} + x'_{1ij+2}\right)} \tag{211}$$

The numerical stability of Ω_i was analyzed in 8510 points fulfilling the relation $\gamma \in (\gamma_{min}, \gamma_{max}) = (1.5 \cdot 10^{-9}, 10^{25})$. The values of Ω_i obtained from quad precision computation were considered as reference.

In the distant domain characterized with $\gamma > 1.5 \cdot 10^{-8}$ and $R^3 \setminus s$ the Ω_i values will be erroneous due to the numerical error. Moving away from S_i the limit of Ω_i is 0, between the $\gamma < 1.5 \cdot 10^{-8}$ and $\gamma_{\min} = 1.5 \cdot 10^{-9}$ region the absolute error of Ω_i is characterized as $\left|\left(\Delta\Omega_i\right)_{r16}\right| < 10^{-16}$. The limit of errorless values of Ω_i computed with double precision is $\gamma < 3.5 \cdot 10^{-6}$, if $\gamma \in (\gamma_{\min}, 3.5 \cdot 10^{-6})$ then the absolute error of Ω_i is $\left|\left(\Delta\Omega_i\right)_{r8}\right| < 10^{-11}$. In case of distant points situated in plane s the absolute error of Ω_i computed with double and quad precision is $\left|\left(\Delta\Omega_i\right)_{r16}\right| < 10^{-32}$ and $\left|\left(\Delta\Omega_i\right)_{r8}\right| < 10^{-15}$ successively.

When the computation point is situated outside the plane s and approaches a point in this plane then Ω_i computed with quad precision satisfies $\left|\left(\Delta\Omega_i\right)_{r16}\right| < 10^{-16}$ in computation points characterized with $\gamma \in (1.5 \cdot 10^{-8}, 5 \cdot 10^{-5})$. In the $\gamma \in (5 \cdot 10^{-5}, 1.5 \cdot 10^{8})$ domain we have $\left|\left(\Delta\Omega_i\right)_{r16}\right| < 10^{-16}$, in the $\gamma \in (1.5 \cdot 10^{8}, 1.5 \cdot 10^{18})$ domain stands the $\left|\left(\Delta\Omega_i\right)_{r16}\right| < 10^{-16}$ relation, in the $\gamma \in (1.5 \cdot 10^{18}, 4 \cdot 10^{20})$ domain the $\left|\left(\Delta\Omega_i\right)_{r16}\right| < 10^{-12}$ and in the $\gamma \in (4 \cdot 10^{8}, \gamma_{\max})$ domain the $\left|\left(\Delta\Omega_i\right)_{r16}\right| < 10^{-9}$ inequalities are holding. The same computation in double precision gives the fpllowing results: $\left|\left(\Delta\Omega_i\right)_{r16}\right| < 10^{-4}$ in the $\gamma \in (3.5 \cdot 10^{-6}, 5 \cdot 10^{-4})$ domain, $\left|\left(\Delta\Omega_i\right)_{r16}\right| < 10^{-8}$ in the $\gamma \in (5 \cdot 10^{-4}, 3 \cdot 10^{-2})$ domain, $\left|\left(\Delta\Omega_i\right)_{r16}\right| < 10^{-12}$ in the $\gamma \in (3 \cdot 10^{-2}, 1.5 \cdot 10^{4})$ domain, $\left|\left(\Delta\Omega_i\right)_{r16}\right| < 10^{-8}$ in the $\gamma \in (1.5 \cdot 10^{4}, 1.5 \cdot 10^{8})$ and $\left|\left(\Delta\Omega_i\right)_{r16}\right| < 10^{-4}$ in the $\gamma \in (1.5 \cdot 10^{8}, 1.5 \cdot 10^{11})$ domain. In observation points characterized by $\gamma \in (1.5 \cdot 10^{11}, \gamma_{\max})$ the numerical errors will dominate the true value of Ω_i.

The magnitude of relative error in case of Ω_i computed with double precision both in near and far field regions from the polyhedron can reach the value 100%. In far field points from the polyhedron defined successively by relations (1) $\gamma \approx 10^{-6}$ the relative error is around 1%, (2) $\gamma \approx 10^{-7}$ the relative error can reach the value 100%. In near field points from the polyhedron satisfying the $\gamma \approx 1.5 \cdot 10^{13}$ relation the relative error can reach 1%.

If the observation point is situated in the $s \setminus S_i$ domain and near to lines which define the boundary triangle face S_i then the value of Ω_i computed with double precision in these points can be compared with its theoretical value $\Omega_i = 0$ in the limit point. From this comparison we can conclude that the absolute error in observation points characterized by $\gamma \in (\gamma_{\min}, 10^{15})$ fulfils $\left|\left(\Delta\Omega_i\right)_{r16}\right| < 10^{-18}$, whereas in the $\gamma \in (\gamma_{\min}, \gamma_{\max})$ domain it holds that $\left|\left(\Delta\Omega_i\right)_{r16}\right| < 10^{-8}$. In the domain $\gamma < 1.5 \cdot 10^{8}$ for Ω_i computed with double precision it holds that $\left|\left(\Delta\Omega_i\right)_{r8}\right| < 10^{-7}$. However in the $\gamma > 1.5 \cdot 10^{8}$ domain Ω_i

is dominated by numerical error. In the $\gamma \in (1.5\cdot 10^{16}, \gamma_{\max})$ domain the *Holstein*[1], *Holstein*[2], *Holstein*[3] (Table 4) are identically zero, so they coincide with the theoretical value, as against the expression of Werner and Scheeres becomes indefinite.

Finally if the observation point is situated in plane s and converges to a point in $s\backslash S_i$, the absolute error can be characterized by inequalities $\left|\left(\Delta\Omega_i\right)_{r16}\right| < 10^{-32}$ and respectively $\left|\left(\Delta\Omega_i\right)_{r16}\right| < 10^{-15}$ in case of quad and double precision. The results concerning the limit of Ω_{ij}, Ω_i, $h_i\Omega_{ij}$ and $h_i\Omega_j$ we have summarized in Table 3.

Based on the investigated limit of the C_{ij}, $h_{ij}C_{ij}$, Ω_{ij}, Ω_i, $h_i\Omega_{ij}$ and $h_i\Omega_i$ functions we can derive the limits of gravitational potential and its first and second derivatives in the limit points of the domain of definition. Based on formulas (176) and (178) the analytical expressions of potential and its first derivatives consists only of the $h_{ij}C_{ij}$ and $h_i\Omega_i$ terms, which have finite limits in every point of space. In the concrete case when $M_0 \in S_{i_0}$ and the observation point M approaches M_0:

$$\lim_{M\to M_0} U(M) = \lim_{M\to M_0} \frac{G\rho_0}{2}\sum_{i=1}^{n} h_i\left(\sum_{j=1}^{l(i)} h_{ij}C_{ij} - h_i\Omega_i\right) =$$

$$= \frac{G\rho_0}{2}\sum_{i=1,i\neq i_0}^{n} h_i\left(\sum_{j=1}^{l(i)} h_{ij}C_{ij} - h_i\Omega_i\right) + \frac{G\rho_0}{2}\lim_{M\to M_0} h_{i_0}\left(\sum_{j=1}^{l(i_0)} h_{i_0 j}C_{i_0 j} - h_{i_0}\Omega_{i_0}\right) = \frac{G\rho_0}{2}\sum_{i=1,i\neq i_0}^{n} h_i\left(\sum_{j=1}^{l(i)} h_{ij}C_{ij} - h_i\Omega_i\right),$$

$$\lim_{M\to M_0} \nabla_{\boldsymbol{r}_M} U(M) = -G\rho_0 \lim_{M\to M_0}\sum_{i=1}^{n} \boldsymbol{n}_i\left(\sum_{j=1}^{l(i)} h_{ij}C_{ij} - h_i\Omega_i\right) =$$

$$= -G\rho_0 \sum_{i=1,i\neq i_0}^{n} \boldsymbol{n}_i\left(\sum_{j=1}^{l(i)} h_{ij}C_{ij} - h_i\Omega_i\right) + G\rho_0\boldsymbol{n}_{i_0}\lim_{M\to M_0}\left(\sum_{j=1}^{l(i_0)} h_{i_0 j}C_{i_0 j} - h_{i_0}\Omega_{i_0}\right) =$$

$$= -G\rho_0 \sum_{i=1,i\neq i_0}^{n} \boldsymbol{n}_i\left(\sum_{j=1}^{l(i)} h_{ij}C_{ij} - h_i\Omega_i\right) + G\rho_0\boldsymbol{n}_{i_0}\left(\sum_{j=1}^{l(i_0)} b_{i_0 j}\right),$$

$$\lim_{M\to M_0} U_{kl}(M) = G\rho_0 \lim_{M\to M_0}\sum_{i=1}^{n} n_i^k\left(\sum_{j=1}^{l(i)} v_{ij}^l C_{ij} - n_i^l\Omega_i\right) =$$

$$= G\rho_0 \sum_{i=1,i\neq i_0}^{n} n_i^k\left(\sum_{j=1}^{l(i)} v_{ij}^l C_{ij} - n_i^l\Omega_i\right) + G\rho_0 \lim_{M\to M_0} n_{i_0}^k\left(\sum_{j=1}^{l(i_0)} v_{i_0 j}^l C_{i_0 j} - n_{i_0}^l\Omega_{i_0}\right) =$$

$$= G\rho_0 \sum_{i=1,i\neq i_0}^{n} n_i^k\left(\sum_{j=1}^{l(i)} v_{ij}^l C_{ij} - n_i^l\Omega_i\right) + G\rho_0 n_{i_0}^k \sum_{j=1}^{l(i_0)} v_{i_0 j}^l C_{i_0 j} - G\rho_0 n_{i_0}^k n_i^l \lim_{M\to M_0}\Omega_{i_0}\ .$$

We made use of the following relations valid for $M_0 \in S_{i_0}$:

$$\lim_{M\to M_0} h_{i_0 j}C_{i_0 j} = b_{i_0 j} \in R\ ,\ j = \overline{1, l(i_0)},\ \lim_{M\to M_0} h_{i_0}\Omega_{i_0} = 0\ ,\ \lim_{M\to M_0} h_{i_0} = 0\ .$$

On this basis the gravitational potential and its first derivatives have a finite limit in any M_0 point situated on the S_{i_0} face of the polyhedron. Due to the fact that Ω_i has a jump discontinuity at any point of S_{i_0} (Table 3) the second derivatives of potential likewise will have a jump discontinuity in these points.

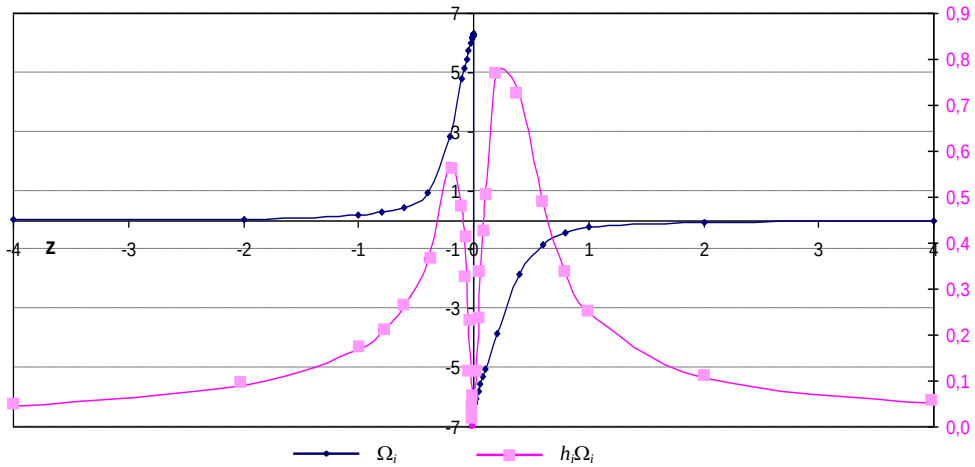

Fig. 11 Let $S_i = [ABC]$ (A = (0,1,0), B = (0,-1,0), C = (1,0,0)) be the face of the polyhedron and let M_0 (0.5,0,0) $\in S_i$ be a point of S_i. The values Ω_i and $h_i\Omega_i$ are computed on the points M(0.5-z, z, z) situated along the line d: 0.5-x = y = z ⇔ M(0.5-z, z, z) and converging to the point M_0 (0.5,0,0) $\in S_i$ ($M \to M_0$). Then we have $z \to 0$ and $\lim_{z\to 0,\, z>0} \Omega_i = -2\pi$, $\lim_{z\to 0,\, z<0} \Omega_i = 2\pi$, $\lim_{z\to 0} h_i\Omega_i = 0$. If the observation point M moves away from M_0 then it holds that |z|→∞ and $\lim_{|z|\to\infty} \Omega_i = \lim_{|z|\to\infty} h_i\Omega_i = 0$

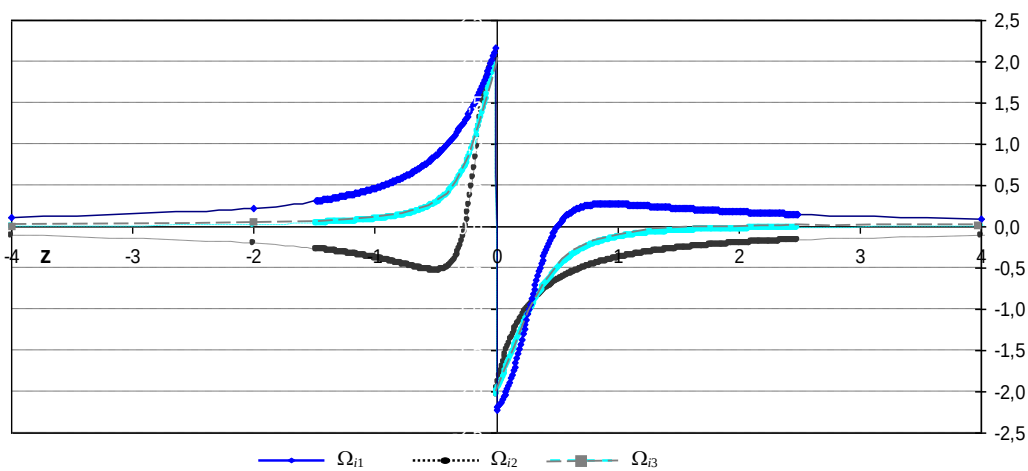

Fig. 12 Let $S_i = [ABC]$ (A = (0,1,0), B = (0,-1,0), C = (1,0,0)) be the face of the polyhedron and let M_0 (0.5,0,0) $\in S_i$ be a point of S_i. The values Ω_{ij}, j=1,3 are computed on points M(0.5-z, z, z) situated along the line d: 0.5-x = y = z ⇔ M(0.5-z, z, z) and converging to the point M_0(0.5,0,0)$\in S_i$ ($M \to M_0$). Then we have $z \to 0$ and $\lim_{z\to 0, z>0} \Omega_{i1} = -a$, $\lim_{z\to 0, z<0} \Omega_{i1} = a$, $\lim_{z\to 0, z>0} \Omega_{i2} = -b$, $\lim_{z\to 0, z<0} \Omega_{i2} = b$, $\lim_{z\to 0, z>0} \Omega_{i3} = -c$, $\lim_{z\to 0, z<0} \Omega_{i3} = c$, where $a = \tan(AP_0B)$, $b = c = \tan(BP_0C)$, a+ b +c=2π. If the observation point M moves away from M_0 then it holds that |z|→∞ and $\lim_{|z|\to\infty} \Omega_{ij} = 0, j = \overline{1,3}$

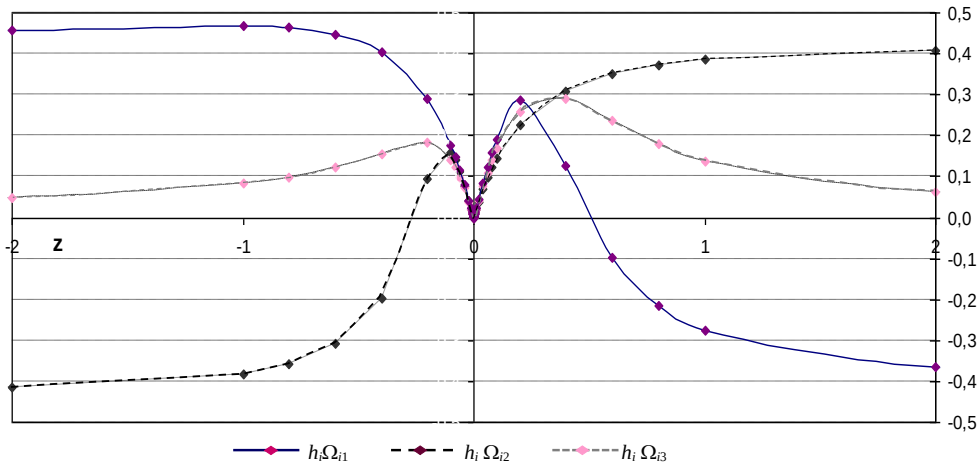

Fig. 13 Let S_i = [*ABC*] (*A* = (0,1,0), *B* = (0,-1,0), *C* = (1,0,0)) be the face of the polyhedron and let M_0 (0.5,0,0) $\in S_i$ be a point of S_i. The value $h_i\Omega_{ij}$, j=1,3 are computed in points *M*(0.5-*z*, *z*, z) situated along the line *d*: 0.5-*x* = *y* = *z* ⇔ *M*(0.5-*z*, *z*, z) and converging to the point M_0(0.5,0,0)$\in S_i$ ($M \to M_0$). Then we have $z \to 0$ and $\lim_{z\to 0}\Omega_{ij} = 0,\ j=\overline{1,3}$. If the observation point *M* moves away from M_0 then it holds that |z|→∞ and based on (201) it holds that $\lim_{z\to\infty}\left|h_i\,\Omega_{i1}\right| = l_1$, $\lim_{z\to\infty}\left|h_i\,\Omega_{i2}\right| = l_2$, $\lim_{z\to\infty}\left|h_i\,\Omega_{i3}\right| = l_3$, $l_1 = l_2 = \left(3-\sqrt{3}\right)/3$, $l_3 = 0$, ($m = \sqrt{2}/2, y_1' = -\sqrt{2}/4, y_2' = 3\sqrt{2}/4, y_3' = -\sqrt{2}/4$)

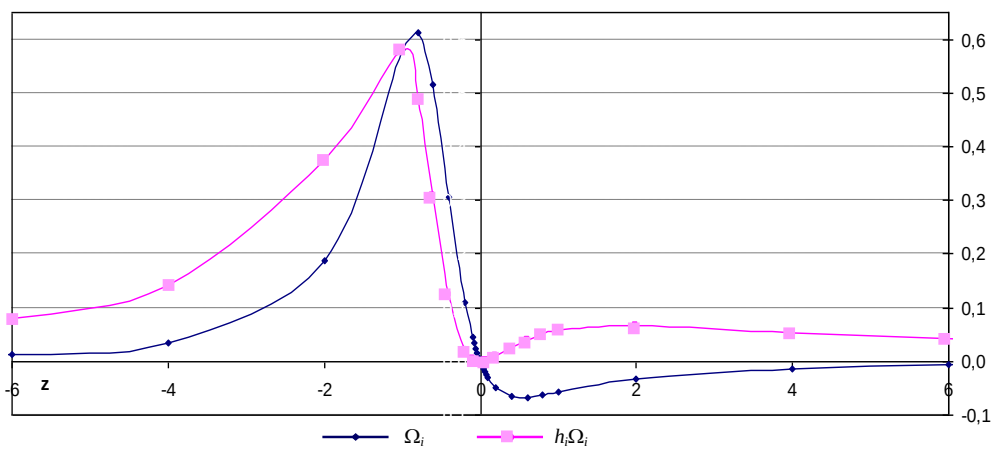

Fig. 14 Let S_i = [*ABC*] (*A* = (0,1,0), *B* = (0,-1,0), *C* = (1,0,0)) be the face of the polyhedron and let M_0 (-1,0.5,0) $\in$ Ext(S_i) be a point in exterior domain of S_i. The values Ω_i and $h_i\Omega_i$ are computed on the points *M*(-1 - *z*, 0.5, z) situated along the line *d*: *y* = 0.5, *x* + *z* +*1* = 0 ⇔ *M*(-1 - *z*, 0.5, z) and converging to the point M_0(-1,0.5,0)$\in$ Ext(S_i) ($M \to M_0$). Then we have $z \to 0$ and $\lim_{z\to 0}\Omega_i = 0$, $\lim_{z\to 0} h_i\Omega_i = 0$. If the observation point *M* moves away from M_0 then it holds that |z|→∞ and $\lim_{|z|\to\infty}\Omega_i = \lim_{|z|\to\infty} h_i\Omega_i = 0$

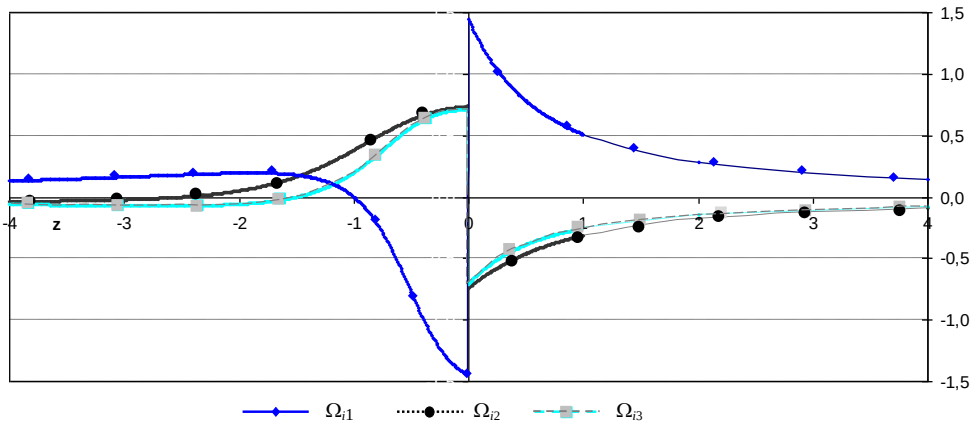

Fig. 15 Let $S_i = [ABC]$ (A = (0,1,0), B = (0,-1,0), C = (1,0,0)) be the face of the polyhedron and let M_0 (-1,0.5,0) $\in$ Ext(S_i) be a point in exterior domain of S_i. The values Ω_{ij}, j=1,3 are computed on the points M(-1 - z, 0.5, z) situated along the line d: y = 0.5, $x + z + 1 = 0 \Leftrightarrow M(-1 - z, 0.5, z)$ ($M \to M_0$). Then we have $\lim\limits_{z\to 0, z>0} \Omega_{i1} = a$, $\lim\limits_{z\to 0, z<0} \Omega_{i1} = -a$, $\lim\limits_{z\to 0, z>0} \Omega_{i2} = -b$, $\lim\limits_{z\to 0, z<0} \Omega_{i2} = b$, $\lim\limits_{z\to 0, z>0} \Omega_{i3} = -c$, $\lim\limits_{z\to 0, z<0} \Omega_{i3} = c$, $a=\angle AP_0B$, $b=\angle BP_0C$, $c=\angle CP_0A$, $b + c = a$. If the observation point M moves away from M_0 then it holds that $|z|\to\infty$ and $\lim\limits_{|z|\to\infty} \Omega_{ij} = 0, j = \overline{1,3}$

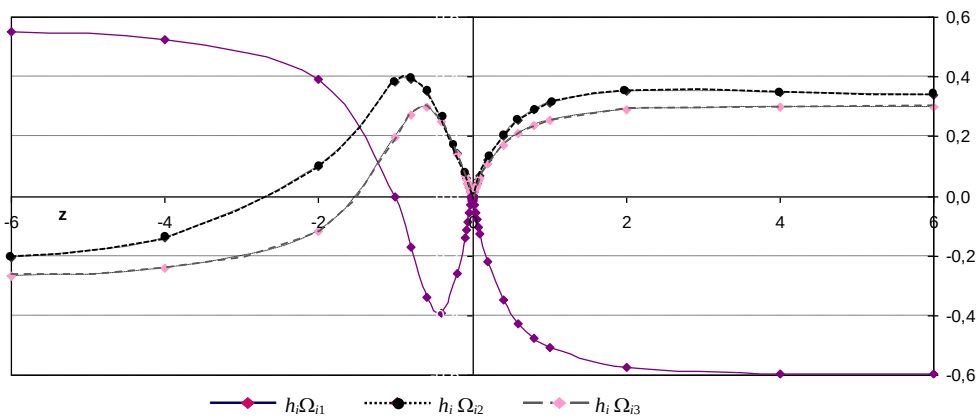

Fig. 16 Let $S_i = [ABC]$ (A = (0,1,0), B = (0,-1,0), C = (1,0,0)) be the face of the polyhedron and let M_0 (-1,0.5,0) $\in$ Ext(S_i) be a point in exterior domain of S_i. The values $h_i\Omega_{ij}$, j=1,3 are computed on the points M(-1 - z, 0.5, z) situated along the line d: y = 0.5, $x + z + 1 = 0 \Leftrightarrow M(-1 - z, 0.5, z)$ ($M \to M_0$). Then we have $z \to 0$ and $\lim\limits_{z\to 0} h_i\Omega_{ij} = 0, j = \overline{1,3}$. If the observation point M moves away from M_0 then it holds that $|z|\to\infty$ and based on (201) we have $\lim\limits_{z\to\infty} |h_i\Omega_{i1}| = l_1$, $\lim\limits_{z\to\infty} |h_i\Omega_{i2}| = l_2$, $\lim\limits_{z\to\infty} |h_i\Omega_{i3}| = l_3$, $l_1 = 2-\sqrt{2}, l_2 = l_3 = \left(2-\sqrt{2}\right)/2$ ($m = 1, y_1' = -0.5, y_2' = 1.5, y_3' = 0.5$)

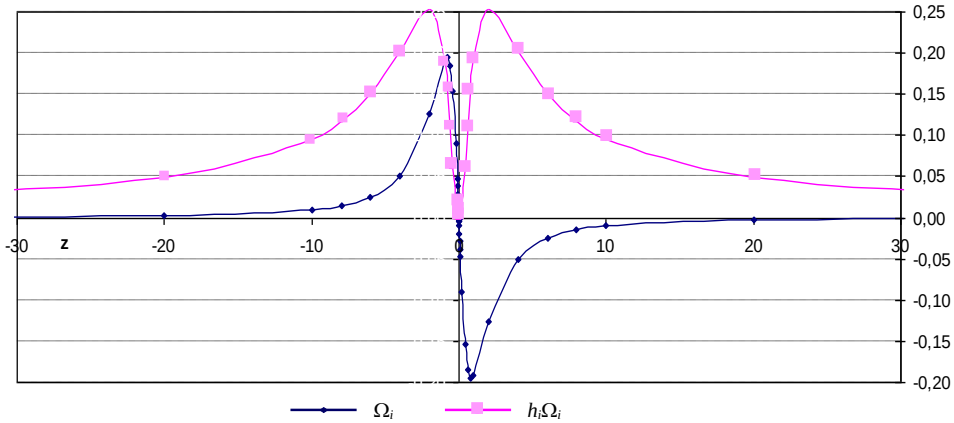

Fig. 17 Let $S_i = [ABC]$ ($A = (0,1,0)$, $B = (0,-1,0)$, $C = (1,0,0)$) be the face of the polyhedron and let $M_0\,(0,1.5,0) \in \mathrm{Ext}(S_i)$ be a point in exterior domain of S_i. The values Ω_i and $h_i\Omega_i$ are computed ont the points $M(0, 1.5, z)$ situated along the line d: $x = 0$, $y = 1.5 \Leftrightarrow M(0, 1.5, z)$ and converging to $M_0(0,1.5,0) \in \mathrm{Ext}(S_i)$ point ($M \to M_0$). Then we have $z \to 0$ and $\lim\limits_{z\to 0}\Omega_i = 0$, $\lim\limits_{z\to 0} h_i\Omega_i = 0$. If the observation point M moves away from M_0 then it holds that $|z|\to\infty$ and $\lim\limits_{|z|\to\infty}\Omega_i = \lim\limits_{|z|\to\infty} h_i\Omega_i = 0$

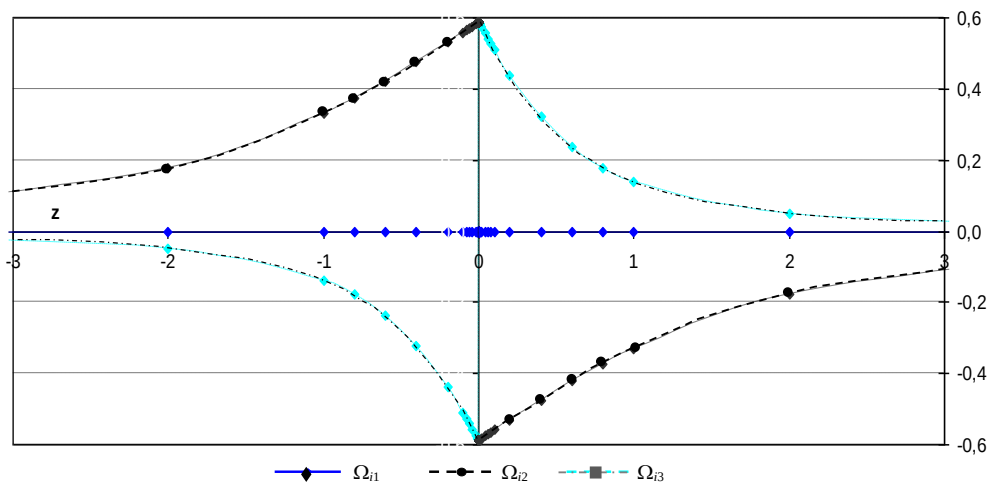

Fig. 18 Let $S_i = [ABC]$ ($A = (0,1,0)$, $B = (0,-1,0)$, $C = (1,0,0)$) be the face of the polyhedron and let $M_0\,(0,1.5,0) \in \mathrm{Ext}(S_i)$ be a point in exterior of S_i. The values Ω_{ij}, $j=1,3$ are computed on the points $M(0, 1.5, z)$ situated along the line d: $x = 0$, $y = 1.5 \Leftrightarrow M(0, 1.5, z)$ and converging to the point $M_0(0,1.5,0) \in \mathrm{Ext}(S_i)$ ($M \to M_0$). Then we have $z \to 0$ and $\lim\limits_{z\to 0}\Omega_{i1} = 0$, $\lim\limits_{z\to 0, z>0}\Omega_{i2} = -a$, $\lim\limits_{z\to 0, z<0}\Omega_{i2} = a$, $\lim\limits_{z\to 0, z>0}\Omega_{i3} = -a$, $\lim\limits_{z\to 0, z<0}\Omega_{i3} = -a$. If the observation point M moves away from M_0 then it holds that $|z|\to\infty$ and $\lim\limits_{|z|\to\infty}\Omega_{ij} = 0, j = \overline{1,3}$

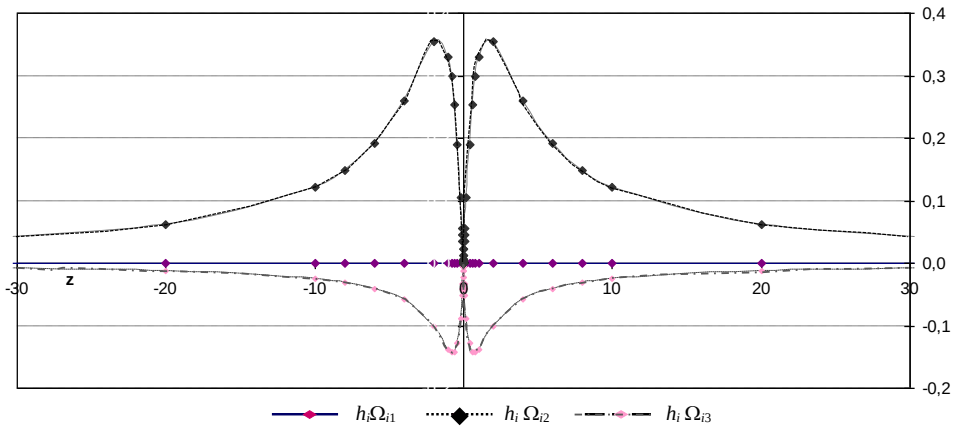

Fig. 19 Let $S_i = [ABC]$ (A = (0,1,0), B = (0,-1,0), C = (1,0,0)) be the face of the polyhedron and let M_0 (0,1.5,0) ∈ Ext(S_i) be a point in exterior domain of S_i. The value $h_i\Omega_{ij}$, j=1,3 are computed on the points M(0, 1.5, z) situated along the line d: x = 0, y = 1.5 ⇔ M(0, 1.5, z) and converging to the point M_0(0,1.5,0)∈ Ext(S_i) ($M \to M_0$). Then we have $z \to 0$ and $\lim_{z\to 0} h_i\Omega_{ij} = 0, j = \overline{1,3}$. If the observation point M moves away from M_0 then it stands |z|→∞ and considering (201) then it holds that $\lim_{z\to\infty} h_i\Omega_{ij} = 0, j = \overline{1,3}$

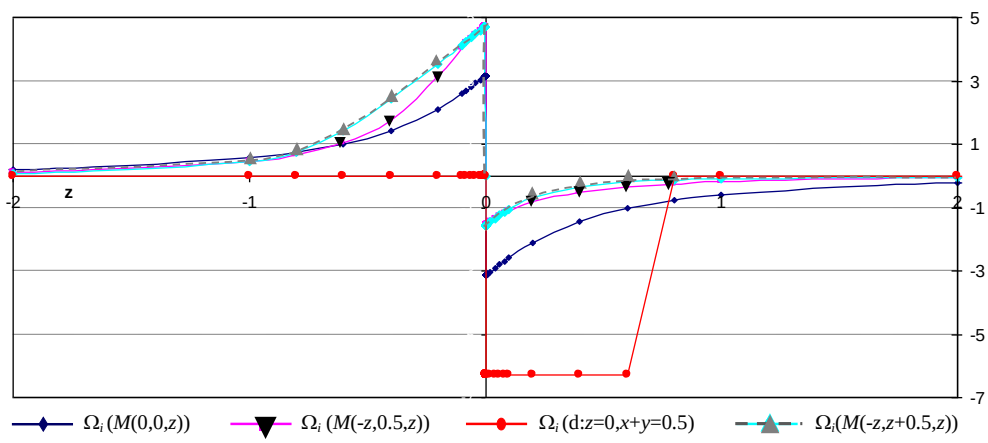

Fig. 20 Let $S_i = [ABC]$ (A = (0,1,0), B = (0,-1,0), C = (1,0,0)) be the face of the polyhedron and let M_0 (0,0.5,0) ∈ (AB) be a point of S_i. The value Ω_i are computed on the points M situated along the lines (1) d_1: x = 0, y = 0.5 ⇔ M(0, 0.5, z), (2) d_2: y = 0.5, $x + z$ = 0 ⇔ M(-z, 0.5, z), (3) d_3: z = 0, $x + y$ = 0.5, (4) d_4: -x = y - 0.5 = z ⇔ M(-z, 0.5 + z, z). We denote with $\boldsymbol{d}_k$, $k = \overline{1,4}$ the unit vectors belonging to d_1, d_2, d_3, d_4. These vectors are successively (0,0,1) ($d_1 \perp S_i$), (-1,0,1), (-1,1,0), (-1,1,1). Converging to M_0(0,1.5,0) with the observation point M ($M \to M_0$) we have $z \to 0$ and considering (209) the limit of Ω_i depends on the direction of the line so we get successively (1) $\boldsymbol{d}_1$: $\lim_{z\to 0, z>0} \Omega_i = -\pi$, $\lim_{z\to 0, z<0} \Omega_i = \pi$, (2) $\boldsymbol{d}_2$: $\lim_{z\to 0, z>0} \Omega_i = -\pi/2$, $\lim_{z\to 0, z>0} \Omega_i = -\pi/2$, (3) $\boldsymbol{d}_3$: $\lim_{x\to 0, z>0} \Omega_i = -2\pi$, $\lim_{x\to 0, x<0} \Omega_i = 0$ and (4) $\boldsymbol{d}_4$: $\lim_{x\to 0, x<0} \Omega_i = 0$, $\lim_{z\to 0, z<0} \Omega_i = 3\pi/2$. If the observation point M moves away from M_0 then it holds that |z|→∞ and $\lim_{|z|\to\infty} \Omega_i = 0$

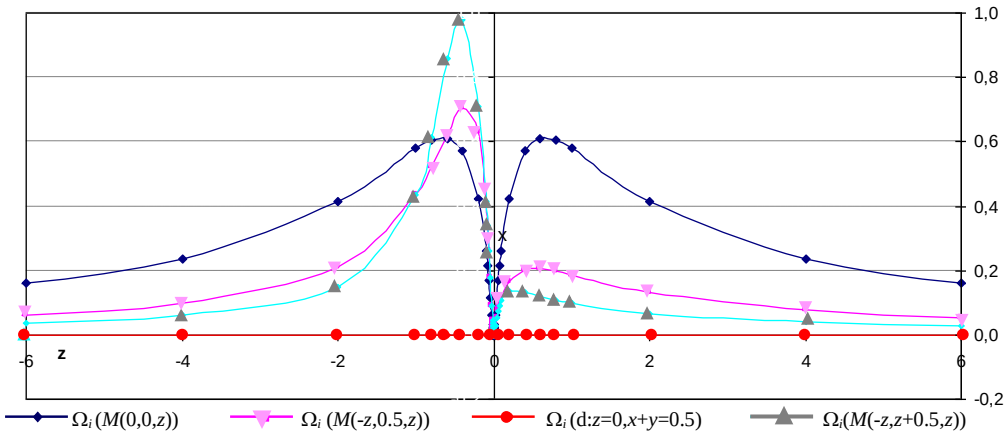

Fig. 21 Let $S_i = [ABC]$ ($A = (0,1,0)$, $B = (0,-1,0)$, $C = (1,0,0)$) be the face of the polyhedron and let $M_0\,(0,0.5,0) \in (AB)$. The value $h_i\Omega_i$ are computed on the points M situated along the lines (1) d_1: $x = 0$, $y = 0.5 \Leftrightarrow M(0, 0.5, z)$, (2) d_2: $y = 0.5$, $x + z = 0 \Leftrightarrow M(-z, 0.5, z)$, (3) d_3: $z = 0$, $x + y = 0.5$, (4) d_4: $-x = y - 0.5 = z \Leftrightarrow M(-z, 0.5 + z, z)$. Converging to the point $M_0(0,0.5,0)$ ($M \to M_0$) we have $z \to 0$ and $\lim_{z\to 0} h_i\Omega_i = 0$. If the observation point M moves away from M_0 then it holds that $|z|\to\infty$ and $\lim_{|z|\to\infty} h_i\Omega_i = 0$

Table 3 Classification of limits of Ω_{ij}, Ω_i, $h_i\Omega_{ij}$ and $h_{ij}\Omega_{ij}$ functions

function	domain	limit	explanation
Ω_{ij}	$S_i = [ABC]$	does not exist	$M_0 \in S_i$, $\nexists \lim\limits_{M \to M_0} \Omega_{ij}$.
	$s \setminus S_i$	does not exist	$M_0 \in s \setminus S_i$, $\nexists \lim\limits_{M \to M_0} \Omega_{ij}$.
	$R^3 \setminus s$	$\in R$	$M_0 \in R^3 \setminus s$, $\lim\limits_{M \to M_0,} \Omega_{ij} \in R$.
	$\gamma \to 0$	0	$\mathrm{dist}(M, S_i) \to \infty$, $\lim\limits_{\gamma \to 0} \Omega_{ij} = 0$.
Ω_i	$S_i = [ABC]$	does not exist	$M_0 \in S_i$, do $\nexists \lim\limits_{M \to M_0} \Omega_i$, $\lim\limits_{M \to M_0} \Omega_i = \begin{cases} 2\,\mathrm{atan}(f(m)) & if \;\; M_0 \in \partial S_i, (d,s) \in \left[0, \frac{\pi}{2}\right[\\ \mathrm{sign}(h_i) \cdot \pi & if \;\; M_0 \in \partial S_i, (d,s) = \frac{\pi}{2} \\ \mathrm{sign}(h_i) \cdot 2\pi & if \;\; M_0 \in \mathrm{Int}(S_i) \end{cases}$. sign(h_i)>0, if M and the normal vector of S_i plane are in the same subspace $f(m)$ is defined by formula (210)
	$s \setminus S_i$	0	$M_0 \in s \setminus S_i$, $\lim\limits_{M \to M_0} \Omega_i = 0$.
	$R^3 \setminus s$	$\in R$	$M_0 \in R^3 \setminus s$, $\lim\limits_{M \to M_0,} \Omega_i \in R$.
	$\gamma \to 0$	0	$\mathrm{dist}(M, S_i) \to \infty$, $\lim\limits_{\gamma \to 0} \Omega_i = 0$.
$h_i\Omega_{ij}$	$S_i = [ABC]$	0	$M_0 \in S_i$, $\lim\limits_{M \to M_0} h_i\Omega_{ij} = 0$.
	$s \setminus S_i$	0	$M_0 \in s \setminus S_i$, $\lim\limits_{M \to M_0} h_i\Omega_{ij} = 0$.
	$R^3 \setminus s$	$\in R$	$M_0 \in R^3 \setminus s$, $\lim\limits_{M \to M_0,} h_i\Omega_{ij} \in R$.
	$\gamma \to 0$	does not exist	$\mathrm{dist}(M, S_i) \to \infty$, not $\exists \lim\limits_{\gamma \to 0} h_i\Omega_{ij}$.
$h_i\,\Omega_i$	$S_i = [ABC]$	0	$M_0 \in S_i$, $\lim\limits_{M \to M_0} h_i\Omega_i = 0$.
	$s \setminus S_i$	0	$M_0 \in s \setminus S_i$, $\lim\limits_{M \to M_0} h_i\Omega_i = 0$.
	$R^3 \setminus s$	$\in R$	$M_0 \in R^3 \setminus s$, $\lim\limits_{M \to M_0,} h_i\Omega_i \in R$.
	$\gamma \to 0$	0	$\mathrm{dist}(M, S_i) \to \infty$, $\lim\limits_{\gamma \to 0} h_i\Omega_i = 0$.

Table 4 The analytical formulas of C_{ij}, Ω_{ij} P_{ij}, Q_{ij}, R_{ij} given by different authors

Function	Analytical formula	Author	Domain of definition in the maximal domain ($\gamma_{\min}$, $\gamma_{\max}$) assigned to the computations performed in double precision ($\gamma_{\min}=2\cdot10^{-9}$, $\gamma_{\max}=10^{25}$) for C_{ij} ($\gamma_{\min}=1.5\cdot10^{-9}$, $\gamma_{\max}=10^{25}$) for Ω_{ij}
$C_{ij}^{Pohanka^1}$	$-\left[\ln\left(r_{MP}-l\right)\right]_{l_{1ij}}^{l_{2ij}}$	Pohànka	$M\in R^3\setminus A_{ij}A_{ij+1}\Big]_{\substack{i=\overline{1,n}\\ j=\overline{1,J(i)}}}$ Expression becomes indefinite on $\operatorname{dist}\left(M, A_{ij}A_{ij+1}\ {}_{\substack{i=\overline{1,n}\\ j=\overline{1,J(i)}}}\right)<10^{-8}$ domain. Out of this domain expression is stable on: $\gamma_{\min}<\gamma<10^7$.
$C_{ij}^{Pohanka^2}$	$\left[\ln\left(r_{MP}+l\right)\right]_{l_{1ij}}^{l_{2ij}}$	Pohànka	$M\in R^3\setminus A_{ij}A_{ij+1}\ {}_{\substack{i=\overline{1,n}\\ j=\overline{1,J(i)}}}$ Expression becomes indefinite on $\operatorname{dist}\left(M, A_{ij+1}A_{ij}\ {}_{\substack{i=\overline{1,n}\\ j=\overline{1,J(i)}}}\right)<10^{-8}$. Out of this domain expression is stable on: $\gamma_{\min}<\gamma<10^7$.
$C_{ij}^{Pohanka^3}$	$\operatorname{sign}\left(l_{2ij}\right)\ln\dfrac{r_{2ij}+\left\|l_{2ij}\right\|}{r_{0ij}}-\operatorname{sign}\left(l_{1ij}\right)\ln\dfrac{r_{1ij}+\left\|l_{1ij}\right\|}{r_{0ij}}$	Pohànka	$M\in R^3\setminus A_{ij}A_{ij+1}\ {}_{\substack{i=\overline{1,n}\\ j=\overline{1,J(i)}}}$ Expression becomes indefinite on $10^{-25}<\operatorname{dist}\left(M, A_{ij}A_{ij+1}\ {}_{\substack{i=\overline{1,n}\\ j=\overline{1,J(i)}}}\right)<10^{9}$.
C_{ij}^{HPGL}	$\left[\ln\left(\dfrac{r_{MP}+l}{r_{0ij}}\right)\right]_{l_{1ij}}^{l_{2ij}}$	Holstein, Petrovič, Götze and Lahmeyer	$M\in R^3\setminus A_{ij}A_{ij+1}\ {}_{\substack{i=\overline{1,n}\\ j=\overline{1,J(i)}}}$ Expression becomes indefinite on $\operatorname{dist}\left(M, A_{ij+1}A_{ij}\ {}_{\substack{i=\overline{1,n}\\ j=\overline{1,J(i)}}}\right)<10^{-8}$. Out of this domain expression is stable on: $\gamma_{\min}<\gamma<10^7$.
C_{ij}^{HWSch}	$\left[\ln\left(\dfrac{r_{2ij}+r_{1ij}+l_{ij}}{r_{2ij}+r_{1ij}-l_{ij}}\right)\right]=\ln\left(\dfrac{1+\Lambda_{ij}}{1-\Lambda_{ij}}\right)=2\operatorname{atanh}\Lambda_{ij}$, where $\Lambda_{ij}=\dfrac{l_{ij}}{r_{2ij}+r_{1ij}}<1$.	Holstein, Werner and Scheeres	$M\in R^3\setminus\left[A_{ij}A_{ij+1}\right]_{\substack{i=\overline{1,n}\\ j=\overline{1,J(i)}}}$ Expression becomes indefinite on $\operatorname{dist}\left(M,\left[A_{ij+1}A_{ij}\right]_{\substack{i=\overline{1,n}\\ j=\overline{1,J(i)}}}\right)<10^{-8}$. In the surroundings of the segment [AB] the expression is defined on $\gamma_{\min}<\gamma<10^7$. Out of this domain expression is stable on: $\gamma_{\min}<\gamma<\gamma_{\max}$.
$C_{ij}^{Holstein}$	$\begin{cases}\operatorname{sign}\left(l_{2ij}\right)\left[\ln\left(\dfrac{r_{2ij}+\left\|l_{2ij}\right\|}{r_{1ij}+\left\|l_{1ij}\right\|}\right)\right] & \text{if } \operatorname{sign}\left(l_{2ij}\right)=\operatorname{sign}\left(l_{1ij}\right)\\ \operatorname{sign}\left(l_{2ij}\right)\left[\ln\left(\dfrac{\left(r_{2ij}+\left\|l_{2ij}\right\|\right)\left(r_{1ij}+\left\|l_{1ij}\right\|\right)}{r_{0ij}^2}\right)\right] & \text{if } \operatorname{sign}\left(l_{2ij}\right)\neq\operatorname{sign}\left(l_{1ij}\right)\end{cases}$	Holstein	$M\in R^3\setminus\left[A_{ij}A_{ij+1}\right]_{\substack{i=\overline{1,n}\\ j=\overline{1,J(i)}}}$ Expression is defined on $10^{-25}<\operatorname{dist}\left(M, A_{ij}A_{ij+1}\ {}_{\substack{i=\overline{1,n}\\ j=\overline{1,J(i)}}}\right)<10^{9}$ thus on $\gamma_{\min}<\gamma<\gamma_{\max}$ domain.

$\tilde{C}_{ij,n_0}$	$2\left(\sum_{k=1}^{n_0}\frac{(\Lambda_{ij})^k}{k}\right)$, where $\Lambda_{ij}=\frac{l_{ij}}{r_{2ij}+r_{1ij}}$	Taylor series	
$\boldsymbol{\Omega_{ij}^{Pohanka^1}}$	$\left[2\,\mathrm{sign}(h_i)\,\mathrm{atan}\frac{r_{MP}-l+\lvert h_i\rvert}{h_{ij}}\right]_{l_{1ij}}^{l_{2ij}}$	Pohànka	$M\in R^3\setminus\left[A_{ij}A_{ij+1}\right]_{\substack{i=\overline{1,n}\\ j=\overline{1,l(i)}}}$ Expression is defined on $\gamma_{\min}<\gamma<\gamma_{\max}$ domain.
$\boldsymbol{\Omega_{ij}^{Pohanka^2}}$	$-\left[2\,\mathrm{sign}(h_i)\,\mathrm{atan}\frac{r_{MP}+l+\lvert h_i\rvert}{h_{ij}}\right]_{l_{1ij}}^{l_{2ij}}$	Pohànka	$M\in R^3\setminus A_{ij}A_{ij+1}\Big]_{\substack{i=\overline{1,n}\\ j=\overline{1,l(i)}}}$ Expression is defined on $\gamma_{\min}<\gamma<\gamma_{\max}$.
$\boldsymbol{\Omega_{ij}^{Pohanka^3}}$	$2\,\mathrm{sign}(h_i)\,\mathrm{atan}\frac{2h_{ij}(l_{2ij}-l_{1ij})}{(r_{2ij}+r_{1ij})^2-(l_{2ij}-l_{1ij})^2+2(r_{2ij}+r_{1ij})\lvert h_i\rvert}$	Pohànka	$M\in R^3\setminus\left[A_{ij}A_{ij+1}\right]_{\substack{i=\overline{1,n}\\ j=\overline{1,l(i)}}}$ Expression is defined on $\gamma_{\min}<\gamma<\gamma$.
$\boldsymbol{\Omega_{ij}^{Holstein^1}}$	$\mathrm{sign}(h_i)\cdot\left[\mathrm{atan}\left(\frac{l}{h_{ij}}\right)\right]_{l_{1ij}}^{l_{2ij}}-\left[\mathrm{atan}\left(\frac{h_i l}{r_{MP}h_{ij}}\right)\right]_{l_{1ij}}^{l_{2ij}}$	Holstein	$M\in R^3\setminus A_{ij}A_{ij+1}\,{}_{\substack{i=\overline{1,n}\\ j=\overline{1,l(i)}}}$ Expression is defined on $\gamma_{\min}<\gamma<1.5\cdot10^{16}$.
$\boldsymbol{\Omega_{ij}^{Holstein^2}}$	$\mathrm{sign}(h_i)\cdot\left[\mathrm{atan}\left(\frac{h_{ij}l}{r_{0ij}^2+r_{MP}\lvert h_i\rvert}\right)\right]_{l_{1ij}}^{l_{2ij}}$	Holstein	$M\in R^3\setminus A_{ij}A_{ij+1}\,{}_{\substack{i=\overline{1,n}\\ j=\overline{1,l(i)}}}$ Expression is defined on $\gamma_{\min}<\gamma<1.5\cdot10^{16}$.
$\boldsymbol{\Omega_{ij}^{Holstein^3}}$	$\begin{cases}2\,\mathrm{sign}(h_i)\,\mathrm{atan}\frac{2h_{ij}(l_{2ij}-l_{1ij})}{(r_{2ij}+r_{1ij}+d_{ij})(r_{2ij}+r_{1ij}-d_{ij})+2(r_{2ij}+r_{1ij})\lvert h_i\rvert} & if\ \mathrm{sign}(l_{2ij})=\mathrm{sign}(l_{1ij})\\ 2\,\mathrm{sign}(h_i)\,\mathrm{atan}\frac{2h_{ij}(l_{2ij}-l_{1ij})}{(r_{2ij}+r_{1ij}+d_{ij})^2/a_{ij}+2(r_{2ij}+r_{1ij})\lvert h_i\rvert} & if\ \mathrm{sign}(l_{2ij})\neq\mathrm{sign}(l_{1ij})\end{cases}$	Holstein	$M\in R^3\setminus\left[A_{ij}A_{ij+1}\right]_{\substack{i=\overline{1,n}\\ j=\overline{1,l(i)}}}$ Expression is defined on $\gamma_{\min}<\gamma<1.5\cdot10^{16}$.
$\boldsymbol{\Omega_{i}^{Petrovic}}$	$\sum_{j=1}^{l(i)}\Omega_{ij}=-\sum_{j=1}^{l(i)}\left[\mathrm{atan}\left(\frac{h_i l}{r_{MP}h_{ij}}\right)\right]_{l_{1ij}}^{l_{2ij}}+\mathrm{sign}(h_i)\theta_i$	Petrovič	$M\in R^3\setminus A_{ij}A_{ij+1}\,{}_{\substack{i=\overline{1,n}\\ j=\overline{1,l(i)}}}$
$\boldsymbol{\Omega_{i}^{G-L}}$	$-\sum_{j=1}^{l(i)}\left[\mathrm{atan}\left(\frac{l^2+h_i^2+lr_{MP}}{h_i h_{ij}}\right)\right]_{l_{1ij}}^{l_{2ij}}+\mathrm{sign}(h_i)\theta_i$	Götze and Lahmeyer	$M\in R^3\setminus A_{ij}A_{ij+1}\,{}_{\substack{i=\overline{1,n}\\ j=\overline{1,l(i)}}}$
$\boldsymbol{\Omega_{i}^{WSch}}$	$2\sum_{k=2}^{l(i)-1}\mathrm{atan}\,2\left(\boldsymbol{r}_1(\boldsymbol{r}_k\times\boldsymbol{r}_{k+1}),r_1r_kr_{k+1}+r_1\boldsymbol{r}_k\boldsymbol{r}_{k+1}+r_k\boldsymbol{r}_1\boldsymbol{r}_{k+1}+r_{k+1}\boldsymbol{r}_1\boldsymbol{r}_k\right)$	Werner and Scheeres	$M\in R^3\setminus S_i, i=\overline{1,n}$ Expression is defined on $\gamma_{\min}<\gamma<1.5\cdot10^{16}$.
P_{ij} Q_{ij} R_{ij} I_{ij}	$(x_{2ij}-x_{1ij})I_{ij}$, $(y_{2ij}-y_{1ij})I_{ij}$, $(z_{2ij}-z_{1ij})I_{ij}$ $I_{ij}=\begin{cases}\frac{1}{l_{ij}}\ln\frac{\sqrt{\boldsymbol{l}_{ij}^2+2\boldsymbol{r}_{1ij}\boldsymbol{l}_{ij}+\boldsymbol{r}_{1ij}^2}+l_{ij}+\boldsymbol{r}_{1ij}\boldsymbol{\mu}_{ij}}{r_{1ij}+\boldsymbol{r}_{1ij}\boldsymbol{\mu}_{ij}} & if\ r_{1ij}+\boldsymbol{r}_{1ij}\boldsymbol{\mu}_{ij}\neq0\\ \frac{1}{l_{ij}}\ln\frac{\lvert l_{ij}-r_{1ij}\rvert}{r_{1ij}} & if\ r_{1ij}+\boldsymbol{r}_{1ij}\boldsymbol{\mu}_{ij}=0\end{cases}$	Guptasarma and Singh	$M\in R^3\setminus A_{ij}A_{ij+1}\,{}_{\substack{i=\overline{1,n}\\ j=\overline{1,l(i)}}}$ The formula becomes indefinite in domain: $\mathrm{ist}\left(M,A_{ij}A_{ij+1}\,{}_{\substack{i=\overline{1,n}\\ j=\overline{1,l(i)}}}\right)<10^{-7}$

3. The analysis from numerical point of view of analytical formulas of gravitational potential and its derivatives

Holstein and Ketteridge (1996) and Holstein et al. (1999) investigate the numerical stability of analytical formulas of gravitational potential and its first derivatives in the far domain (distant points from polyhedron). Numerical errors of analytical formulas for the gravity potential and its first and second derivatives generated by a uniform polyhedral body increase with distance of observation point while the magnitude of these quantities decreases to 0. Similarly in case of observation point situated fairly near to polyhedron instead of convergence of analytical formulas to a real number provided by the potential theory the formulas can return a NaN value. Therefore, a limited range (a minimum for the observation points situated near to the target body and a maximum for the observation points situated far from the target body) of target distances can be specified in which domain the formulas are operational, beyond which the calculations are dominated by rounding error or become indefinite. Let α be the target body dimension which is a number characterizing the extension of a polyhedron body (e.g. the average of edges or the radius of inscribed or circumscribed sphere or the average of these radii) and δ the distance from the observation point. Their ratio $\gamma = \alpha/\delta$ is a dimensionless quantity geometrically representing the inverse distance normalized with the dimension of the body, which defines the angular extent of the polyhedron.

Following formula (Holstein et al. 1999, Eq. 71) gives the relation between γ and the numerical error of the first derivatives of the gravitational potential:

$$\gamma \geq (\varepsilon 100/p)^{1/\nu} \Leftrightarrow \delta \leq \frac{\alpha}{(\varepsilon 100/p)^{1/\nu}}\,, \tag{212}$$

where p is percent of the rounding error, ε is the floating-point precision and for ν the authors estimate $\nu = 4$ based on model computation using a concave elementary body with 8 faces, 10 vertices and with dimension $\alpha = 24$. In case of applied double precision computation the value of ε is $2^{-52} \approx 10^{-16}$. For a required rounding error of p percent (212) gives the upper limit of target distance $\delta_{\max} = \frac{\alpha}{(\varepsilon 100/p)^{1/\nu}}$ below of which the percent of rounding error becomes less than p and above of which the percent of rounding error becomes larger than p. In case of p = 100% and $\varepsilon=2^{-52}$ for γ we get as limit $\gamma = \gamma(\nu) = (\varepsilon 100/100)^{1/\nu} = 2^{-52/\nu}$.

We repeat the investigation presented by Holstein et al. (1999) in double and quad precision and complete with the same formulas concerning the gravitational potential and its second derivatives (Table 5, 6, 7) using the same model. In these computations we considered ν as unknown parameter, the coordinates of observation points were chosen $(x,y,z)=(d,d,0)$ where $d = d(\nu) = \delta(\nu)/\sqrt{2}$ [km], $\delta(\nu) = \alpha/\gamma(\nu)$ and $\gamma = \gamma(\nu) = 2^{-52/\nu}$. The values of the parameter ν are given in the first column of Tables 5, 6, 7, the coordinates of observation points are given in the following three columns of the tables. The computations were done in double and quad precision and these observation results are given in the 6th and 10th columns.

The realistic density models applied both in the local and regional modelling (Benedek and Papp 2009, Benedek 2004) are built by different dimensions of volume elements (prisms or polyhedrons). In case of applied regional models the minimum and maximum values for the α parameter were found $(\alpha_{model})_{\min}$ = 250 m, $(\alpha_{model})_{\max}$ = 750 km. The most frequent dimensions of the elements were: 500 m, 1 km, 5 km, 10 km, 100 km and 500 km. The statistics in case of applied local models are: $(\alpha_{model})_{\min}$ = 10 m and the most frequent dimensions of elements were 25 m and 50 m. All model computations given by Holstein et al. (1999) we have repeated for different $\alpha \in \{2400, 240, 2.4, 0.24, 0.024\}$ [km] model dimensions to verify the dimensional independence of relation (212) both with double precision denoted by r8 indices and quadruple precision denoted by r16 indices. The different

dimensional models were generated from the Holstein model, multiplied the model vertices with a constant C, $C \in \{100, 10, 0.1, 0.01, 0.001\}$ and accordingly with this the coordinate of observation points were ($C \cdot d$, $C \cdot d$, 0). For the volume element with $\alpha \approx 24$ [km] dimension corresponds the $C = 1$ scale factor. For every C and the corresponding model computation have to fulfil the following relations:

$$U(d,d,0) = U(Cd,Cd,0)/C^2 \,,\; U_z(d,d,0) = U_z(Cd,Cd,0)/C \;,$$
$$U_{zz}(d,d,0) = U_{zz}(Cd,Cd,0)\,, \tag{213}$$

where in the left side of the equations are the results obtained for the initial model ($\alpha = 24$) and in the right side of the equations are the results for the model with $\alpha = 24 \cdot C$ dimensions. This means that for each $\alpha = 24 \cdot C$ values the model computations are effectuated in (Cd, Cd, 0) points, where $d = d(\nu) = \delta(\nu)/\sqrt{2}$ [km], $\delta(\nu) = C\alpha/\gamma(\nu)$ [km] and $\gamma = \gamma(\nu) = 2^{-52/\nu}$ with different ν values. The observation results for gravitational potential and its first and second derivatives are presented successively in Tables 6, 5 and 7. The $(U_z(Cd,Cd,0))_{r16}/C$ values computed with different values of the C parameter and fulfilling the condition $\nu \geq 2.4$ are the same up to ten decimal places, so these values can be considered as reference or exact values notated by U_z and listed in the 6th column of Table 5. The same expressions $\widetilde{U}_z$ computed with double precision we have considered as approximations of exact values U_z. The columns with labels "abs. error in r16", "abs. error in r8" and "$p = \left|\left(\widetilde{U}_z / U_z - 1\right)\right| \cdot 100[\%]$" give information about the magnitude of numerical errors obtained with the different C values. By right of our computation the numerical error reaches 100% for $\nu = 4.0$ which is in accordance with the ν value given by Holstein et al. (1999). The $(U_z(Cd,Cd,0))_{r16}/C$ values computed with different values for the C parameter and $\nu \geq 2.0$ are the same up to ten decimal places, so these values can be considered as reference or exact values denoted by U and listed in the 6th column of Table 6. The same expressions $\widetilde{U}$ computed with double precision we have considered as approximation of exact values. The $\left(U_{zz}(Cd,Cd,0)\right)_{r16}/C$ values computed with different values of the C parameter in domain defined by $\nu \geq 1.4$ are the same up to ten decimal places, so these values can be considered as reference or exact values denoted by U_{zz} and listed in the 6th column of Table 7. The same expressions $\widetilde{U}_{zz}$ computed with double precision we have considered as approximation of exact values. In case of gravitational potential and its second derivatives based on same model computation we get successively $\nu = 3.0$ and $\nu = 2.2$ in case that errors attain 100 %.

The following part describes local and regional model computations (Benedek 2004, Benedek and Papp 2009). As we mentioned previously the applied density models are composed from elementary volume elements (prisms or polyhedrons) denoted by Σ_i with different dimensions. The error analysis of these models is done by reconducting the Holstein model error analysis. For each Σ_i model element we assigned a scale factor C so that the element dimension will be approximately equal to C times the dimension of the Holstein elementary model. Furthermore for each Σ_i model element we assigned a domain of the observation point defined by the minimal $\left(h^i_{\min}\right)$ and maximal distance $\left(h^i_{\max}\right)$ of the observation point from the centre of mass of Σ_i where the error of gravity potential and its derivatives is less than 1%. For each Σ_i volume element the coordinates of computation points were $M(x = d, y = d, 0)$. In this way for each Σ_i we can determine the dimensionless quantities $(\alpha/h)^i_{\min} = \alpha_i / h^i_{\max}$ and $(\alpha/h)^i_{\max} = \alpha_i / h^i_{\min}$ and for the complete model the $(\alpha/h)_{\min} = \min_{i=1,n}\left\{(\alpha/h)^i_{\min}\right\}$ and $(\alpha/h)_{\max} = \min_{i=1,n}\left\{(\alpha/h)^i_{\max}\right\}$ values where n is the number of model elements. In this investigation we have chosen the values of C so that they characterize the minimal, the maximal and the most frequent volume elements dimensions applied in local and regional models. From this analysis we obtain the following values: $\alpha \in \{600$ km, 120 km, 24 km, 12 km, 4.8 km, 1.2 km, 480 m, 48 m, 24 m, 12 m$\}$

and correspondingly we obtain $C \in \{25, 5, 1, 0.5, 0.2, 0.05, 0.02, 0.002, 0.001, 0.0005\}$ values for the scaling factor. For each volume element characterized by the C scale factor the coordinate of observation points were ($C \cdot d$, $C \cdot d$, 0). The values of $x = y = d$ given in Tables 8, 9, 10 are the observation distances corresponding to $C = 1$, and the relation $d = 10 + 24 / \left(\sqrt{2} \cdot (\alpha/h)\right)$ is fulfilled for d. In Tables 8, 9, 10 are presented successively the observation results of first derivatives of potential, the geoid undulation values (N) computed from the gravitational potential using formula $N = U/9.780312$ (Bruns formula). The computations were performed both in double and quad precision. The quad precision computation results (gravitational potential and its first and second derivatives) were independent from the C scale factor so we have considered them as reference or exact values. The values computed with double precision we have considered as approximations of reference values. The local model computations presented by Benedek and Papp (2009) can be characterized by $3400 > \alpha/h > 10^{-3}$ arising from the volume elements dimension and the position of computation points. From this numerical analysis (Table 8) we can conclude that in double precision computation the numerical error of first derivatives of gravitational potential generated by each volume element is less than 1%, i.e. $\left|\tilde{U}_z^i - U_z^i\right| < \frac{U_z^i}{100}$, where i denotes the ith volume element of the density model, U_z^i, $\tilde{U}_z^i$ are the exact (computed with quad precision) and the approximate value (computed with double precision) of first derivatives of gravitational potential in the domain of computation. Using the

$$\left|\tilde{U}_z - U_z\right| = \left|\sum_{i=1}^{n} \tilde{U}_z^i - \sum_{i=1}^{n} U_z^i\right| < \sum_{i=}^{n} \left|\tilde{U}_z^i - U_z^i\right| < \frac{\sum_{i=1}^{n} U_z^i}{100} = \frac{U_z}{100} \quad , \tag{214}$$

inequality, where n is the number of volume elements in the applied density model we can deduce that the numerical error of gravitational potential generated by the whole density model is less than 1% as well. Similarly we investigated the numerical error of gravitational potential and its second derivatives generated by the regional density model used by Benedek and Papp (2009). The model element and the domain of observation points can be characterized by the $17 > \alpha/h > 1.5 \cdot 10^{-4}$ inequality. Thus using the numerical error information given in Tables 9 and 10 we can conclude that the numerical errors of gravitational potential and its second derivatives generated by this regional model is far below 1%.

Table 5. The first derivatives of the gravitational potential generated by a polyhedron model given in the paper by Holstein et al. (1999) Appendix A, computed in the points ($x = d$, $y = d$, 0), where $\gamma = \alpha/\left(d\sqrt{2}\right) \Leftrightarrow d = \alpha/\left(\gamma\sqrt{2}\right)$ [km], α = 24 [km] and $\gamma = 2^{-52/\nu}$. All computations were performed in quad precision (r16) and double precision (r8). The models involved in these investigations (Benedek 2004, Benedek and Papp 2009) consist of volume elements of different dimension α_{model} with the help of which we can define the scale factor $C = \alpha_{model}/(\alpha = 24)$. The chosen scale factors were: $C = 100 \Leftrightarrow \alpha_{model} = 2400$ [km], $C = 10 \Leftrightarrow \alpha_{model} = 240$ [km], $C = 1 \Leftrightarrow \alpha_{model} = 24$ [km], $C = 0.1 \Leftrightarrow \alpha_{model} = 2.4$ [km], $C = 0.01 \Leftrightarrow \alpha_{model} = 240$ [m] and $C = 0.001 \Leftrightarrow \alpha_{model} = 24$ [m]. The first derivatives of the gravitational potential computed with quad precision (U_z) were considered as reference values, which are listed in the C =1 (r16) column. The double prevision computed values for different C scale factors provide the approximated values ($\widetilde{U}_z$). The ratio of these two values gets the relative error $p = \left|\widetilde{U}_z/U_z - 1\right| \cdot 100[\%]$. The table shows that the error of derivatives computed with double precision achieve 100% in case of ν = 4.0. Absolute error column shows the number of significant decimal places of the mantissa in the normal form of $\widetilde{U}_z$ (if U_z = □.□□□□□□□×10^n, where n is the exponent of U_z.)

ν	x[km]	y[km]	z [km]	γ	U_z [mGal] C=1 (r16)	Abs. error in r16	$\widetilde{U}_z$ [mGal] C=100 (r8)	C=10 (r8)	C=1 (r8)	C=0.1 (r8)	C=0.01 (r8)	C=0.001 (r8)	Abs. error	Relativ error
8.2	1376.2	1376.2	0	1.2331878E-02	2.33006368E-04		2.33006000E-02	2.33006363E-03	2.33006370E-04	2.33006370E-05	2.33006374E-06	2.33006372E-07	8 decim	
8.0	1536.0	1536.0	0	1.1048543E-02	1.67522767E-04		1.67523000E-02	1.67522759E-03	1.67522768E-04	1.67522762E-05	1.67522761E-06	1.67522766E-07		
6.0	6896.4	6896.4	0	2.4607832E-03	1.84750445E-06		1.84745000E-04	1.84753809E-05	1.84752590E-06	1.84748300E-07	1.84755109E-08	1.84753438E-09	5 decim	
5.8	8483.7	8483.7	0	2.0003702E-03	9.92327047E-07		9.92415000E-05	9.92283057E-06	9.92328168E-07	9.92268196E-08	9.92364454E-09	9.92384090E-10	4 decim	
5.6	10591.9	10591.9	0	1.6022175E-03	5.09861358E-07		5.09847000E-05	5.09764402E-06	5.09918274E-07	5.09839512E-08	5.09900197E-09	5.09893661E-10		<1%
5.4	13443.2	13443.2	0	1.2623874E-03	2.49364670E-07		2.49447000E-05	2.49341790E-06	2.49401570E-07	2.49386457E-08	2.49384359E-09	2.49448422E-10	3 decim	
5.2	17377.9	17377.9	0	9.7656251E-04	1.15433374E-07		1.15468000E-05	1.15393792E-06	1.15401426E-07	1.15261315E-08	1.15418940E-09	1.15314174E-10		
5.0	22930.2	22930.2	0	7.4009597E-04	5.02428319E-08		5.03326000E-06	5.02730824E-07	5.02407255E-08	5.01738942E-09	5.03263253E-10	5.03531122E-11		
4.8	30963.8	30963.8	0	5.4807717E-04	2.04041190E-08		2.05838000E-06	2.03326864E-07	2.05232272E-08	2.02748932E-09	2.03652634E-10	2.05304132E-11	2 decim	
4.6	42918.4	42918.4	0	3.9541417E-04	7.66188548E-09	10 decim	7.38989000E-07	7.69803656E-08	7.64373198E-09	7.63939881E-10	7.32584387E-11	8.02113167E-12	1 decim	~1% (1-5%)
4.4	61280.7	61280.7	0	2.7693177E-04	2.63200483E-09		2.94927000E-07	2.47035025E-08	2.60839916E-09	2.58946433E-10	2.60552701E-11	2.32712868E-12		~10% l (<12%)
4.2	90517.9	90517.9	0	1.8748303E-04	8.16669228E-10		6.69653000E-08	1.02221130E-08	1.29619587E-09	6.63789659E-11	1.32825127E-11	-5.97686590E-14		
4.0	139022.9	139022.9	0	1.2207031E-04	2.25415936E-10		1.50449000E-08	3.57587002E-10	6.29311794E-11	8.58868671E-11	1.05773859E-12	4.46727345E-14		~100%
3.8	223385.0	223385.0	0	7.5970007E-05	5.43346414E-11		-1.33302000E-07	8.80269005E-09	-1.19296880E-10	-1.06800425E-10	-2.81322589E-12	1.00935756E-12		
3.6	378361.8	378361.8	0	4.4852737E-05	1.11818683E-11		-4.08218000E-07	-4.69877884E-09	-6.20270379E-10	1.85704392E-12	-2.48865423E-11	1.76623968E-12		
3.4	681843.0	681843.0	0	2.4889251E-05	1.91065037E-12		3.08193000E-08	3.87762423E-08	1.50063305E-09	2.55022131E-10	2.19542462E-11	1.10034058E-12		
3.2	1322615.7	1322615.7	0	1.2831061E-05	2.61777526E-13		1.56670000E-07	5.52229677E-08	2.23885569E-09	1.53604237E-10	2.70058110E-11	7.97777070E-12		
3.0	2802525.0	2802525.0	0	6.0554545E-06	2.75159344E-14		-5.38590000E-07	1.24449329E-07	-1.82679660E-08	-1.32687343E-09	-8.51183009E-11	-1.00197465E-12		>>100%
2.8	6610789.2	6610789.2	0	2.5671009E-06	2.09639223E-15		-1.76883000E-07	-1.64372968E-07	-6.17825645E-08	3.00344182E-09	2.82256560E-11	-2.90845536E-11	noisy in r8	
2.6	17794924.8	17794924.8	0	9.5367432E-07	1.07484006E-16		7.07336000E-06	-1.15579453E-06	-1.37862664E-08	-1.14370368E-08	-6.35401926E-10	-1.29118267E-10		
2.4	56495364.7	56495364.7	0	3.0038859E-07	3.35887465E-18	9 decim	2.45649000E-05	4.63092491E-06	1.43836760E-07	-2.32415904E-08	1.37807513E-09	1.23640626E-11		
2.2	221284343.2	221284343.2	0	7.6691204E-08	5.58944889E-20	4 decim	1.15019000E-04	-1.07851996E-05	-8.74076349E-07	-5.89919397E-09	-7.83865570E-09	8.22200422E-10		
2.0	1138875187.5	1138875187.5	0	1.4901161E-08	4.16575530E-22	2 decim	-1.08854000E-04	-9.03104347E-06	-8.18672962E-07	-6.99829114E-08	1.84917681E-08	2.46398612E-09		
1.8	8435645892.4	8435645892.4	0	2.0117680E-09	-4.44614761E-23		6.16550000E-04	-1.00627185E-03	6.39252929E-06	-2.89848746E-06	-1.28740652E-07	2.42652800E-08		
1.6	103079215104	103079215104	0	1.6463613E-10	-1.37441100E-22	noisy in r16	3.63016000E-02	6.50548212E-04	-4.86472198E-04	3.34667484E-05	-1.12734072E-06	4.06848920E-07		>>100%
1.4	2575196471075	2575196471075	0	6.5900070E-12	-3.80719835E-22		8.91947000E-01	-8.23030011E-02	8.44832952E-03	1.68807674E-03	-1.52403090E-04	1.75588850E-05		
1.2	188074271955079	188074271955079	0	9.0233303E-14	-1.81854380E-18		-1.04912000E+02	5.37853531E+00	4.57271546E-01	3.82479820E-02	3.40485315E-03	6.32037693E-04		

Table 6. The geoid undulation (N=U/9.780312 [cm]) generated by a polyhedron model given in the paper by Holstein et al. (1999) Appendix A computed in the points ($x = d$, $y = d$, 0), where $\gamma = \alpha/\left(d\sqrt{2}\right) \Leftrightarrow d = \alpha/\left(\gamma\sqrt{2}\right)$ [km], α = 24 [km] and γ=$2^{-52/\nu}$. All computations were performed in quad precision (r16) and double precision (r8). The models involved in these investigations (Benedek 2004, Benedek and Papp 2009) consist of volume elements of different dimension α_{model} with the help of which we can define the scale factor $C = \alpha_{model}/(\alpha = 24)$. The chosen scale factors were: $C = 100 \Leftrightarrow \alpha_{model} = 2400$ [km], $C = 10 \Leftrightarrow \alpha_{model} = 240$ [km], $C = 1 \Leftrightarrow \alpha_{model} = 24$ [km], $C = 0.1 \Leftrightarrow \alpha_{model} = 2.4$ [km], $C = 0.01 \Leftrightarrow \alpha_{model} = 240$ [m] and $C = 0.001 \Leftrightarrow \alpha_{model} = 24$ [m]. The geoid undulation computed with quad precision (U) were considered as reference values, which are listed in the C =1 (r16) column. The double prevision computed values for different C scale factors provide the approximated values ($\widetilde{N}$). The ratio of these two values gets the relative error $p = \left|\widetilde{N}/N - 1\right| \cdot 100[\%] = \left|\widetilde{N}/N - 1\right| \cdot 100[\%]$. The table shows that the error of derivatives computed with double precision achieve 100% in case of ν = 3.0. Absolute error column shows the number of significant decimal places of the mantissa in the normal form of $\widetilde{N}$ (if N = □.□□□□□□×10^n, where n is the exponent of N.)

ν	x[km]	y[km]	z [km]	γ	N [cm] C=1 (r16)	Abs. error in r16	$\widetilde{N}$ [cm] C=100 (r8)	C=10 (r8)	C=1 (r8)	C=0.1 (r8)	C=0.01 (r8)	C=0.001 (r8)	Abs. error	Relativ error (%)
8.2	1376.2	1376.2	0	1.2331878E-02	5.14558934E+00		5.14559000E+04	5.14558934E+02	5.14558934E+00	5.14558934E-02	5.14558934E-04	5.14558934E-06	9 decim	
8.0	1536.0	1536.0	0	1.1048543E-02	4.60954659E+00		4.60955000E+04	4.60954659E+02	4.60954659E+00	4.60954659E-02	4.60954659E-04	4.60954659E-06		
6.0	6896.4	6896.4	0	2.4607832E-03	1.02581759E+00		1.02582000E+04	1.02581758E+02	1.02581758E+00	1.02581759E-02	1.02581761E-04	1.02581759E-06	8 d.	
5.8	8483.7	8483.7	0	2.0003702E-03	8.33849822E-01		8.33850000E+03	8.33849802E+01	8.33849807E-01	8.33849831E-03	8.33849825E-05	8.33849838E-07		
5.6	10591.9	10591.9	0	1.6022175E-03	6.67855041E-01		6.67855000E+03	6.67855055E+01	6.67855052E-01	6.67855039E-03	6.67855035E-05	6.67855067E-07	7 decim	
5.4	13443.2	13443.2	0	1.2623874E-03	5.26185761E-01		5.26186000E+03	5.26185797E+01	5.26185794E-01	5.26185766E-03	5.26185749E-05	5.26185734E-07		
5.2	17377.9	17377.9	0	9.7656251E-04	4.07037553E-01		4.07038000E+03	4.07037523E+01	4.07037494E-01	4.07037525E-03	4.07037520E-05	4.07037668E-07		<1%
5.0	22930.2	22930.2	0	7.4009597E-04	3.08469714E-01		3.08470000E+03	3.08469823E+01	3.08469754E-01	3.08469880E-03	3.08469660E-05	3.08469580E-07		
4.8	30963.8	30963.8	0	5.4807717E-04	2.28432617E-01		2.28432000E+03	2.28432700E+01	2.28432265E-01	2.28432812E-03	2.28432718E-05	2.28432725E-07	6 decim	
4.6	42918.4	42918.4	0	3.9541417E-04	1.64801892E-01		1.64802000E+03	1.64802058E+01	1.64801931E-01	1.64802070E-03	1.64801893E-05	1.64801560E-07		
4.4	61280.7	61280.7	0	2.7693177E-04	1.15419120E-01		1.15419000E+03	1.15419146E+01	1.15419110E-01	1.15418939E-03	1.15418942E-05	1.15419152E-07		
4.2	90517.9	90517.9	0	1.8748303E-04	7.81381576E-02	10 decim	7.81377000E+02	7.81380766E+00	7.81373406E-02	7.81382305E-04	7.81402917E-06	7.81357655E-08	4 decim	
4.0	139022.9	139022.9	0	1.2207031E-04	5.08754786E-02		5.08735000E+02	5.08724201E+00	5.08702963E-02	5.08803938E-04	5.08751293E-06	5.08750325E-08		
3.8	223385.0	223385.0	0	7.5970007E-05	3.16620239E-02		3.16524000E+02	3.16664190E+00	3.16504816E-02	3.16850609E-04	3.16634894E-06	3.16602043E-08	3 decim	
3.6	378361.8	378361.8	0	4.4852737E-05	1.86932213E-02		1.86616000E+02	1.86882176E+00	1.86317320E-02	1.87293597E-04	1.87258181E-06	1.86343224E-08		<1%
3.4	681843.0	681843.0	0	2.4889251E-05	1.03730432E-02		1.03595000E+02	1.04291053E+00	1.03297340E-02	1.05041635E-04	1.02034628E-06	1.03614041E-08	2 decim	~1%
3.2	1322615.7	1322615.7	0	1.2831061E-05	5.34756924E-03		5.63698000E+01	5.63228886E-01	5.07697948E-03	5.89381856E-05	5.44377843E-07	5.91603158E-09	1 decim	~10 % (5-18%)
3.0	2802525.0	2802525.0	0	6.0554545E-06	2.52371496E-03		4.15821000E+01	-8.58851495E-02	4.03235811E-03	2.10753310E-05	3.26574148E-07	2.18922906E-09		~100% (20-135%)
2.8	6610789.2	6610789.2	0	2.5671009E-06	1.06988316E-03		-1.49162000E+02	1.02835453E+00	-2.12797701E-03	-3.23949907E-05	1.00936572E-06	-1.08014912E-08		
2.6	17794924.8	17794924.8	0	9.5367432E-07	3.97460003E-04		3.57322000E+02	-4.75641776E+00	-6.47168074E-02	-1.13655931E-04	-8.84403601E-06	6.62960615E-08		
2.4	56495364.7	56495364.7	0	3.0038859E-07	1.25192048E-04		1.37306000E+04	-8.72837762E+00	4.77626796E-01	1.25808811E-03	-4.07738515E-05	-8.92382823E-08		
2.2	221284343.2	221284343.2	0	7.6691204E-08	3.19623619E-05		9.52308000E+04	5.37646565E+02	9.50349066E+00	5.66717720E-02	-6.80472057E-04	5.47392589E-06	Noisy in r8	>>100%
2.0	1138875187.5	1138875187.5	0	1.4901161E-08	6.21031198E-06		2.31969000E+06	-2.34671764E+04	1.82665429E+02	-4.72501206E-01	2.04136270E-03	5.16204300E-04		
1.8	8435645892.4	8435645892.4	0	2.0117680E-09	8.38438486E-07	7 decim	-1.55795000E+07	-5.32600610E+05	-1.44497407E+04	-1.03528518E+02	-1.42960126E-01	7.69074072E-03		
1.6	103079215104	103079215104	0	1.6463613E-10	6.86140811E-08	4 decim	-4.99720000E+09	-1.16832594E+08	1.59875395E+06	3.23022575E+04	-7.49687169E+01	-1.75339634E+00		
1.4	2575196471075	2575196471075	0	6.5900070E-12	1.42902520E-09	Noisy in r16	6.19766000E+12	-1.50744939E+10	6.56589740E+08	1.52275171E+07	1.13187864E+05	1.96890909E+03		>>100%
1.2	188074271955079	188074271955079	0	9.0233303E-14	-2.53516928E-06		-1.00631000E+16	2.65565078E+14	-2.55736982E+11	1.52088666E+11	3.68609215E+08	-1.00856532E+07		

Table 7. The second derivatives of the gravitational potential generated by a polyhedron model given in in the paper by Holstein et al. (1999) Appendix A computed in the points ($x = d$, $y = d$, 0), where $\gamma = \alpha/\left(d\sqrt{2}\right) \Leftrightarrow d = \alpha/\left(\gamma\sqrt{2}\right)$ [km], $\alpha = 24$ [km] and $\gamma = 2^{-52/\nu}$. All computations were performed in quad precision (r16) and double precision (r8). The models involved in these investigations (Benedek 2014, Benedek and Papp 2009) consist of volume elements of different dimension α_{model} with the help of which we can define the scale factor $C = \alpha_{model}/(\alpha = 24)$. The chosen scale factors were: $C = 100 \Leftrightarrow \alpha_{model} = 2400$ [km], $C = 10 \Leftrightarrow \alpha_{model} = 240$ [km], $C = 1 \Leftrightarrow \alpha_{model} = 24$ [km], $C = 0.1 \Leftrightarrow \alpha_{model} = 2.4$ [km], $C = 0.01 \Leftrightarrow \alpha_{model} = 240$ [m] and $C = 0.001 \Leftrightarrow \alpha_{model} = 24$ [m]. The second derivatives of the gravitational potential computed with quad precision (U_{zz}) were considered as reference values, which are listed in the C =1 (r16) column. The double prevision computed values for different C scale factors provide the approximated values ($\widetilde{U}_{zz}$). The ratio of these two values gets the relative error $p = \left|\widetilde{U}_{zz}/U_{zz} - 1\right| \cdot 100[\%]$. The table shows that the error of derivatives computed with double precision achieve 100% in case of ν = 2.2. Absolute error column shows the number of significant decimal places of the mantissa in the normal form of $\widetilde{U}_{zz}$ (if U_{zz} = □.□□□□□□□×10^n, where n is the exponent of U_{zz}.)

					U_{zz} [s^{-2}]	Abs. error in r16	$\widetilde{U}_{zz}$ [s^{-2}]						Abs. error	Relativ error(%)
ν	x[km]	y[km]	z[km]	γ	C=1 (r16)		C=100 (r8)	C=10 (r8)	C=1 (r8)	C=0.1 (r8)	C=0.01 (r8)	C=0.001 (r8)		
8.2	1376.2	1376.2	0	1.2331878E-02	1.06063652E-04		1.06063650E-04	1.06063652E-04	1.06063652E-04	1.06063652E-04	1.06063652E-04	1.06063652E-04		
8.0	1536.0	1536.0	0	1.1048543E-02	8.46226499E-05		8.46226500E-05	8.46226499E-05	8.46226499E-05	8.46226499E-05	8.46226499E-05	8.46226499E-05	10 decim	
6.0	6896.4	6896.4	0	2.4607832E-03	4.01992920E-06		4.01992920E-06	4.01992921E-06	4.01992921E-06	4.01992920E-06	4.01992920E-06	4.01992920E-06		
5.8	8483.7	8483.7	0	2.0003702E-03	2.64985904E-06		2.64985900E-06	2.64985904E-06	2.64985904E-06	2.64985904E-06	2.64985904E-06	2.64985904E-06		
5.6	10591.9	10591.9	0	1.6022175E-03	1.69634693E-06		1.69634690E-06	1.69634693E-06	1.69634694E-06	1.69634694E-06	1.69634693E-06	1.69634693E-06		
5.4	13443.2	13443.2	0	1.2623874E-03	1.05113652E-06		1.05113650E-06	1.05113652E-06	1.05113653E-06	1.05113652E-06	1.05113652E-06	1.05113653E-06	9 decim	
5.2	17377.9	17377.9	0	9.7656251E-04	6.28058476E-07		6.28058480E-07	6.28058477E-07	6.28058476E-07	6.28058477E-07	6.28058473E-07	6.28058475E-07		
5.0	22930.2	22930.2	0	7.4009597E-04	3.60260514E-07		3.60260510E-07	3.60260514E-07	3.60260513E-07	3.60260515E-07	3.60260519E-07	3.60260515E-07		
4.8	30963.8	30963.8	0	5.4807717E-04	1.97364230E-07		1.97364230E-07	1.97364226E-07	1.97364235E-07	1.97364227E-07	1.97364230E-07	1.97364228E-07		
4.6	42918.4	42918.4	0	3.9541417E-04	1.02642317E-07		1.02642320E-07	1.02642313E-07	1.02642319E-07	1.02642316E-07	1.02642317E-07	1.02642316E-07	8 decim	<1%
4.4	61280.7	61280.7	0	2.7693177E-04	5.03135912E-08		5.03135950E-08	5.03135899E-08	5.03135898E-08	5.03135883E-08	5.03135896E-08	5.03135897E-08		
4.2	90517.9	90517.9	0	1.8748303E-04	2.30489053E-08		2.30489050E-08	2.30489070E-08	2.30489063E-08	2.30489028E-08	2.30489057E-08	2.30489062E-08		
4.0	139022.9	139022.9	0	1.2207031E-04	9.76765479E-09	10 decim	9.76765640E-09	9.76765601E-09	9.76765522E-09	9.76765464E-09	9.76765316E-09	9.76765310E-09	7 decim	
3.8	223385.0	223385.0	0	7.5970007E-05	3.78219883E-09		3.78219960E-09	3.78219861E-09	3.78220015E-09	3.78219371E-09	3.78219992E-09	3.78219915E-09		
3.6	378361.8	378361.8	0	4.4852737E-05	1.31814605E-09		1.31814820E-09	1.31814531E-09	1.31815254E-09	1.31814464E-09	1.31814170E-09	1.31815280E-09	6 decim	
3.4	681843.0	681843.0	0	2.4889251E-05	4.05846258E-10		4.05848630E-10	4.05843711E-10	4.05846931E-10	4.05842690E-10	4.05851388E-10	4.05847881E-10		
3.2	1322615.7	1322615.7	0	1.2831061E-05	1.07853484E-10		1.07852960E-10	1.07853277E-10	1.07853298E-10	1.07850270E-10	1.07855477E-10	1.07852198E-10	5 decim	
3.0	2802525.0	2802525.0	0	6.0554545E-06	2.40207361E-11		2.40200070E-11	2.40239163E-11	2.40229768E-11	2.40190774E-11	2.40232173E-11	2.40229378E-11	4 decim	
2.8	6610789.2	6610789.2	0	2.5671009E-06	4.31688379E-12		4.32226480E-12	4.31453850E-12	4.31727424E-12	4.31751880E-12	4.31227607E-12	4.31856792E-12	2 decim	
2.6	17794924.8	17794924.8	0	9.5367432E-07	5.95772969E-13		5.90097000E-13	5.99953633E-13	5.96169632E-13	5.97395273E-13	5.99060911E-13	5.89410352E-13		
2.4	56495364.7	56495364.7	0	3.0038859E-07	5.91079521E-14		5.62453580E-14	6.07294517E-14	6.06282676E-14	5.77353224E-14	6.22907555E-14	5.63651410E-14	1 decim	~2-6%
2.2	221284343.2	221284343.2	0	7.6691204E-08	3.85273943E-15		3.51123710E-15	1.39560379E-15	4.98346502E-15	2.08373072E-15	1.13349152E-15	8.07115183E-16		<100%(30-80%)
2.0	1138875187	1138875187	0	1.4901161E-08	1.45451633E-16		1.87008350E-15	9.05478266E-16	-3.76978168E-15	-4.63434899E-15	4.58263764E-16	-7.54078662E-15		
1.8	8435645892	8435645892	0	2.0117680E-09	2.65114909E-18		-4.29414300E-15	-1.53279017E-17	3.50340901E-15	-1.59990747E-15	9.21022126E-17	-5.10342493E-15		
1.6	103079215104	103079215104	0	1.6463613E-10	1.77553248E-20		-5.77351840E-16	1.36447188E-15	3.11364923E-16	-7.12725896E-15	1.63278660E-16	3.60180307E-18	Noisy r8-ban	>>100%
1.4	2575196471075	2575196471075	0	6.5900070E-12	2.84478920E-23		-5.53380030E-17	5.45224198E-16	8.37845035E-16	-3.08523505E-15	-2.23192417E-15	-2.16707841E-15		
1.2	188074271955079	188074271955079	0	9.0233303E-14	5.33349881E-27	6 decim	-1.03378590E-15	-2.86043712E-15	-1.46461571E-15	-6.01631504E-15	-1.70132999E-15	-4.01313339E-15		

Table 8. The first derivatives of the gravitational potential generated by a polyhedron model given in in the paper by Holstein et al. (1999) Appendix A computed in the points ($x = d$, $y = d$, 0), where $\alpha = 24$ [km], h=dist(M,modell), $d = 10 + 24/\left(\sqrt{2}\cdot(\alpha/h)\right)$.. All computations were performed in quad precision (r16) and double precision (r8). The models involved in these investigations (Benedek 2004, Benedek and Papp 2009) consist of volume elements of different dimension α_{model} with the help of which we can define the scale factor $C = \alpha_{model}/(\alpha = 24)$. The chosen scale factors were: $C = 100 \Leftrightarrow \alpha_{model} = 2400$ [km], $C = 10 \Leftrightarrow \alpha_{model} = 240$ [km], $C = 1 \Leftrightarrow \alpha_{model} = 24$ [km], $C = 0.1 \Leftrightarrow \alpha_{model} = 2.4$ [km], $C = 0.01 \Leftrightarrow \alpha_{model} = 240$ [m] and $C = 0.001 \Leftrightarrow \alpha_{model} = 24$ [m]. The first derivatives of the gravitational potential computed with quad precision (U_z) were considered as reference values, which are listed in the C =25 (r16) column. The double prevision computed values for different C scale factors provide the approximated values ($\tilde{U}_z$). The ratio of these two values gets the relative error $p = \left|\tilde{U}_z/U_z - 1\right|\cdot 100[\%]$. Absolute error column shows the number of significant decimal places of the mantissa in the normal form of $\tilde{U}_z$ (if U_z = □.□□□□□□×10^n, where n is the exponent of U_z.)

				U_z [mGal]	$\tilde{U}_z$ [mGal]											
α/h	$x=d$ [km]	$y=d$ [km]	z [km]	C25_r16 (α=600 km)	C25_r8 (α=600 km)	C5_r8 (α=120 km)	C1_r8 (α=24 km)	C0.5_r8 (α=12 km)	C0.2_r8 (α=4.8 km)	C0.05_r8 (α=1.2 km)	C0.02_r8 (α=480 m)	C0.002_r8 (α=48 m)	C0.001_r8 (α=25 m)	C0.0005_r8 (α=12 m)	Abs. error	Rel. error
0	0.00	0.00	0	3.71469421E+03	3.71469421E+03	7.42938842E+02	1.48587768E+02	7.42938842E+01	2.97175537E+01	7.42938842E+00	2.97175537E+00	2.97175537E-01	1.48587768E-01	7.42938842E-02		
3400	10.005	10.005	0	3.17114765E+03	3.17114765E+03	6.34229529E+02	1.26845906E+02	6.34229529E+01	2.53691812E+01	6.34229529E+00	2.53691812E+00	2.53691812E-01	1.26845906E-01	6.34229529E-02		
340	10.05	10.05	0	3.16591294E+03	3.16591294E+03	6.33182588E+02	1.26636518E+02	6.33182588E+01	2.53273035E+01	6.33182588E+00	2.53273035E+00	2.53273035E-01	1.26636518E-01	6.33182588E-02		
34	10.5	10.5	0	3.11275964E+03	3.11275964E+03	6.22551928E+02	1.24510386E+02	6.22551928E+01	2.49020771E+01	6.22551928E+00	2.49020771E+00	2.49020771E-01	1.24510386E-01	6.22551928E-02		
17	110	11.0	0	3.05210782E+03	3.05210782E+03	6.10421565E+02	1.22084313E+02	6.10421565E+01	2.44168626E+01	6.10421565E+00	2.44168626E+00	2.44168626E-01	1.22084313E-01	6.10421565E-02		
3.4	15.0	15.0	0	2.52773361E+03	2.52773361E+03	5.05546723E+02	1.01109345E+02	5.05546723E+01	2.02218689E+01	5.05546723E+00	2.02218689E+00	2.02218689E-01	1.01109345E-01	5.05546723E-02		
2	18.5	18.5	0	2.04938586E+03	2.04938586E+03	4.09877171E+02	8.19754343E+01	4.09877171E+01	1.63950869E+01	4.09877171E+00	1.63950869E+00	1.63950869E-01	8.19754343E-02	4.09877171E-02	10 d.	
0.8	31.0	31.0	0	6.74356368E+02	6.74356368E+02	1.34871274E+02	2.69742547E+01	1.34871274E+01	5.39485095E+00	1.34871274E+00	5.39485095E-01	5.39485095E-02	2.69742547E-02	1.34871274E-02		
0.5	42.0	42.0	0	2.46674876E+02	2.46674876E+02	4.93349751E+01	9.86699502E+00	4.93349751E+00	1.97339900E+00	4.93349751E-01	1.97339900E-01	1.97339900E-02	9.86699502E-03	4.93349751E-03		
0.3	70.0	70.0	0	4.79808817E+01	4.79808817E+01	9.59617634E+00	1.91923527E+00	9.59617634E-01	3.83847054E-01	9.59617634E-02	3.83847054E-02	3.83847054E-03	1.91923527E-03	9.59617634E-04		<1%
0.08	220	200	0	1.66045721E+00	1.66045721E+00	3.32091442E-01	6.64182883E-02	3.32091442E-02	1.32836577E-02	3.32091442E-03	1.32836577E-03	1.32836577E-04	6.64182883E-05	3.32091442E-05		
0.05	320	320	0	4.67802440E-01	4.67802440E-01	9.35604880E-02	1.87120976E-02	9.35604879E-03	3.74241952E-03	9.35604879E-04	3.74241952E-04	3.74241952E-05	1.87120976E-05	9.35604879E-06		
0.03	585	585	0	7.61162488E-02	7.61162488E-02	1.52232498E-02	3.04464995E-03	1.52232497E-03	6.08929991E-04	1.52232498E-04	6.08929991E-05	6.08929990E-06	3.04464995E-06	1.52232498E-06	9 d.	
0.02	1000	1000	0	1.51967985E-02	1.51967985E-02	3.03935969E-03	6.07871941E-04	3.03935970E-04	1.21574388E-04	3.03935971E-05	1.21574389E-05	1.21574388E-06	6.07871941E-07	3.03935970E-07	8 d.	
0.008	2100	2100	0	1.63776695E-03	1.63776713E-03	3.27553416E-04	6.55106972E-05	3.27553486E-05	1.31021347E-05	3.27553368E-06	1.31021373E-06	1.31021364E-07	6.55106818E-08	3.27553409E-08	6 d.	
0.005	3200	3200	0	4.62597724E-04	4.62597805E-04	9.25195314E-05	1.85038938E-05	9.25194689E-06	3.70078002E-06	9.25195004E-07	3.70077956E-07	3.70077916E-08	1.85038958E-08	9.25194790E-09		
0.003	5680	5680	0	8.26793284E-05	8.26795247E-05	1.65356681E-05	3.30718286E-06	1.65359143E-06	6.61434383E-07	1.65358596E-07	6.61443115E-08	6.61434216E-09	3.30717108E-09	1.65358554E-09	4 d.	
0.0016	10600	10600	0	1.27174115E-05	1.27175216E-05	2.54303075E-06	5.08605673E-07	2.54302836E-07	1.01735171E-07	2.54337927E-08	1.01747026E-08	1.01734004E-09	5.08670021E-10	2.54335010E-10		
0.0010	17000	17000	0	3.08258594E-06	3.08207098E-06	6.16609868E-07	1.23213731E-07	6.16068656E-08	2.46608532E-08	6.16521331E-09	2.46692015E-09	2.46584880E-10	1.23292440E-10	6.16462199E-11	3 d.	
0.0005	34000	34000	0	3.85283399E-07	3.75093210E-07	7.72676867E-08	1.52379455E-08	7.61897276E-09	3.09164423E-09	7.72911057E-10	3.06474679E-10	3.05693338E-11	1.52846669E-11	7.64233346E-12	2d.	~1%
0.0003	56600	56000	0	8.48507151E-08	8.65397292E-08	1.54405301E-08	3.51652209E-09	1.75826105E-09	6.26844892E-10	1.56711223E-10	7.89945995E-11	5.69989593E-12	2.84994797E-12	1.42497398E-12	1 d.	~ 10%
0.0002	75000	75000	0	3.589291652E-08	4.413632787E-08	7.528588294E-09	1.298760922E-09	6.493804609E-10	2.263992049E-10	5.659980123E-11	2.401095696E-11	2.689165154E-12	6.72291289E-13	1.16678851E-12		
0.00017	100000	100000	0	1.514214713E-08	1.106517761E-08	7.644171941E-09	5.297137833E-10	2.648568916E-10	2.450820024E-10	6.127050061E-11	1.498032785E-11	1.600368804E-12	4.00092201E-13	2.53124786E-13		~100%
0.00015	110000	110000	0	1.137648299E-08	1.193375954E-08	2.068936300E-09	-2.753002340E-10	-1.376501170E-10	1.783007028E-10	4.457517569E-11	5.129042102E-12	-1.714481252E-12	-4.28620313E-13	2.66994109E-13	noisy	>>100%

Table 9. The geoid undulation (N=U/9.780312 [cm]) generated by a polyhedron model given in in the paper by Holstein et al. (1999) Appendix A computed in the points ($x = d$, $y = d$, 0), where α = 24 [km], h=dist(M,modell), $d = 10 + 24/\left(\sqrt{2}\cdot(\alpha/h)\right)$.. All computations were performed in quad precision (r16) and double precision (r8). The models involved in these investigations (Benedek 2004, Benedek and Papp 2009) consist of volume elements of different dimension α_{model} with the help of we can define the scale factor $C = \alpha_{model}/(\alpha = 24)$. The chosen scale factors were: $C = 100 \Leftrightarrow \alpha_{model} = 2400$ [km], $C = 10 \Leftrightarrow \alpha_{model} = 240$ [km], $C = 1 \Leftrightarrow \alpha_{model} = 24$ [km], $C = 0.1 \Leftrightarrow \alpha_{model} = 2.4$ [km], $C = 0.01 \Leftrightarrow \alpha_{model} = 240$ [m] and $C = 0.001 \Leftrightarrow \alpha_{model} = 24$ [m]. The geoid undulation computed with quad precision (N) were considered as reference values, which are listed in the C =25 (r16) column. The double prevision computed values for different C scale factors provide the approximated values ($\widetilde{N}$). The ratio of these two values gets the relative error $p = \left|\widetilde{U}/U - 1\right|\cdot 100[\%] = \left|\widetilde{N}/N - 1\right|\cdot 100[\%]$. Absolute error column shows the number of significant decimal places of the mantissa in the normal form of $\widetilde{N}$ (if N = □.□□□□□□×10^n, where n is the exponent of N.)

				N [cm]	$\widetilde{N}$ [cm]											
α/h	x[km]	y[km]	z[km]	C25_r16 (α=600 km)	C25_r8 (α=600 km)	C5_r8 (α=120 km)	C1_r8 (α=24 km)	C0.5_r8 (α=12 km)	C0.2_r8 (α=4.8 km)	C0.05_r8 (α=1.2 km)	C0.02_r8 (α=480 m)	C0.002_r8 (α=48 m)	C0.001_r8 (α=24 m)	C0.0005_r8 (α=12 m)	Abs. error	Rel. error
0	0.00	0.00	0	2.67852140E+05	2.67852140E+05	1.07140856E+04	4.28563423E+02	1.07140856E+02	1.71425369E+01	3.85707081E-01	1.71425369E-01	1.71425369E-01	4.28563423E-04	1.07140856E-04		
3400	10.005	10.005	0	2.51184141E+05	2.51184141E+05	1.00473656E+04	4.01894625E+02	1.00473656E+02	1.60757850E+01	3.61705162E-01	1.60757850E-01	1.60757850E-01	4.01894625E-04	1.00473656E-04		
340	10.05	10.05	0	2.51004777E+05	2.51004777E+05	1.00401911E+04	4.01607642E+02	1.00401911E+02	1.60643057E+01	3.61446878E-01	1.60643057E-01	1.60643057E-01	4.01607642E-04	1.00401911E-04		
34	10.5	10.5	0	2.49172882E+05	2.49172882E+05	9.96691528E+03	3.98676611E+02	9.96691528E+01	1.59470645E+01	3.58808950E-01	1.59470645E-01	1.59470645E-01	3.98676611E-04	9.96691528E-05		
17	110	11.0	0	2.47059031E+05	2.47059031E+05	9.88236123E+03	3.95294449E+02	9.88236123E+01	1.58117780E+01	3.55765004E-01	1.58117780E-01	1.58117780E-01	3.95294449E-04	9.88236123E-05		
3.4	15.0	15.0	0	2.27765096E+05	2.27765096E+05	9.11060383E+03	3.64424153E+02	9.11060383E+01	1.45769661E+01	3.27981738E-01	1.45769661E-01	1.45769661E-01	3.64424153E-04	9.11060383E-05		
2	18.5	18.5	0	2.08707595E+05	2.08707595E+05	8.34830378E+03	3.33932151E+02	8.34830378E+01	1.33572861E+01	3.00538936E-01	1.33572861E-01	1.33572861E-01	3.33932151E-04	8.34830378E-05	10 tizedes	
0.8	31.0	31.0	0	1.43983552E+05	1.43983552E+05	5.75934208E+03	2.30373683E+02	5.75934208E+01	9.21494733E+00	2.07336315E-01	9.21494733E-02	9.21494733E-02	2.30373683E-04	5.75934208E-05		
0.5	42.0	42.0	0	1.07371931E+05	1.07371931E+05	4.29487722E+03	1.71795089E+02	4.29487722E+01	6.87180355E+00	1.54615580E-01	6.87180355E-02	6.87180355E-02	1.71795089E-04	4.29487722E-05		
0.3	70.0	70.0	0	6.42367526E+04	6.42367526E+04	2.56947010E+03	1.02778804E+02	2.56947010E+01	4.11115216E+00	9.25009237E-02	4.11115216E-02	4.11115216E-02	1.02778804E-04	2.56947010E-05		
0.08	220	200	0	2.11682573E+04	2.11682573E+04	8.46730292E+02	3.38692117E+01	8.46730292E+00	1.35476847E+00	3.04822905E-02	1.35476847E-02	1.35476847E-02	3.38692117E-05	8.46730292E-06		
0.05	320	320	0	1.38809436E+04	1.38809436E+04	5.55237742E+02	2.22095097E+01	5.55237742E+00	8.88380388E-01	1.99885587E-02	8.88380388E-03	8.88380388E-03	2.22095097E-05	5.55237742E-06		<<1%
0.03	585	585	0	7.57697297E+03	7.57697297E+03	3.03078919E+02	1.21231568E+01	3.03078919E+00	4.84926270E-01	1.09108411E-02	4.84926270E-03	4.84926270E-03	1.21231568E-05	3.03078919E-06		
0.02	1000	1000	0	4.42762686E+03	4.42762686E+03	1.77105074E+02	7.08420297E+00	1.77105074E+00	2.83368119E-01	6.37578268E-03	2.83368119E-03	2.83368119E-03	7.08420297E-06	1.77105074E-06		
0.008	2100	2100	0	2.10662782E+03	2.10662782E+03	8.42651128E+01	3.37060451E+00	8.42651127E-01	1.34824180E-01	3.03354406E-03	1.34824180E-03	1.34824180E-03	3.37060451E-06	8.42651127E-07	9 tizedes	
0.005	3200	3200	0	1.38210751E+03	1.38210751E+03	5.52843002E+01	2.21137201E+00	5.52843002E-01	8.84548803E-02	1.99023481E-03	8.84548803E-04	8.84548803E-04	2.21137201E-06	5.52843001E-07		
0.003	5680	5680	0	7.78478774E+02	7.78478768E+02	3.11391510E+01	1.24556604E+00	3.11391510E-01	4.98226414E-02	1.12100943E-03	4.98226410E-04	4.98226410E-04	1.24556605E-06	3.11391512E-07	8 tizedes	
0.0016	10600	10600	0	4.17091254E+02	4.17091261E+02	1.66836499E+01	6.67345991E-01	1.66836498E-01	2.66938414E-02	6.00611395E-04	2.66938403E-04	2.66938403E-04	6.67346023E-07	1.66836506E-07	7 tizedes	
0.0010	17000	17000	0	2.60053492E+02	2.60053464E+02	1.04021379E+01	4.16085639E-01	1.04021410E-01	1.66434218E-02	3.74477032E-04	1.66434225E-04	1.66434225E-04	4.16085535E-07	1.04021384E-07		
0.0005	34000	34000	0	1.30020456E+02	1.30020298E+02	5.20080988E+00	2.08032720E-01	5.20081801E-02	8.32130389E-03	1.87228938E-04	8.32131016E-05	8.32131016E-05	2.08033118E-07	5.20082794E-08	6 tizedes	
0.0003	56600	56000	0	7.85177167E+01	7.85175686E+01	3.14071720E+00	1.25628155E-01	3.14070388E-02	5.02512317E-03	1.13065910E-04	5.02514097E-05	5.02514097E-05	1.25628145E-07	3.14070363E-08		
0.0002	75000	75000	0	5.89410463E+01	5.89417262E+01	2.35766507E+00	9.43057359E-02	2.35764340E-02	3.77225379E-03	8.48759732E-05	3.77227193E-05	3.77227193E-05	9.43054943E-08	2.35763736E-08		
0.00017	100000	100000	0	4.42055421E+01	4.42057898E+01	1.76815679E+00	7.07304211E-02	1.76826053E-02	2.82904274E-03	6.36535682E-05	2.82908989E-05	2.82908989E-05	7.07289796E-08	1.76822449E-08	4 tizedes	
0.00015	110000	110000	0	4.01867963E+01	4.01885477E+01	1.60744320E+00	6.42987612E-02	1.60746903E-02	2.57180124E-03	5.78700111E-05	2.57193246E-05	2.57193246E-05	6.43001446E-08	1.60750361E-08		

Table 10. The second derivatives of the gravitational potential generated by a polyhedron model given in Holstein et al. (1999) Appendix A computed in the points ($x = d$, $y = d$, 0), where α = 24 [km], h=dist(M,modell), $d = 10 + 24/\left(\sqrt{2}\cdot(\alpha/h)\right)$. All computations were performed in quad precision (r16) and double precision (r8). The models involved in these investigations (Benedek 2004, Benedek and Papp 2009) consist of volume elements of different dimension α_{model} with the help of which we can define the scale factor $C = \alpha_{model}/(\alpha = 24)$. The chosen scale factors were: $C = 100 \Leftrightarrow \alpha_{model} = 2400$ [km], $C = 10 \Leftrightarrow \alpha_{model} = 240$ [km], $C = 1 \Leftrightarrow \alpha_{model} = 24$ [km], $C = 0.1 \Leftrightarrow \alpha_{model} = 2.4$ [km], $C = 0.01 \Leftrightarrow \alpha_{model} = 240$ [m] and $C = 0.001 \Leftrightarrow \alpha_{model} = 24$ [m]. The first derivatives of the gravitational potential computed with quad precision (U_{zz}) were considered as reference values, which are listed in the C =25 (r16) column. The double prevision computed values for different C scale factors provide the approximated values ($\widetilde{U}_{zz}$). The ratio of these two values gets the relative error $p = \left|\widetilde{U}_{zz}/U_{zz} - 1\right|\cdot 100[\%]$. Absolute error column shows the number of significant decimal places of the mantissa in the normal form of $\widetilde{U}_{zz}$ (if U_{zz} = □.□□□□□□□×10^n, where n is the exponent of U_{zz}.)

				U_{zz} [s^{-2}]	$\widetilde{U}_{zz}$ [s^{-2}]											
α/h	x[km]	y[km]	z [km]	C25_r16 (α=600 km)	C25_r8 (α=600 km)	C5_r8 (α=120 km)	C1_r8 (α=24 km)	C0.5_r8 (α=12 km)	C0.2_r8 (α=4.8 km)	C0.05_r8 (α=1.2 km)	C0.02_r8 (α=480 m)	C0.002_r8 (α=48 m)	C0.001_r8 (α=24 m)	C0.0005_r8 (α=12 m)	Abs. error	Rel. error
0	0.00	0.00	0	6.89197306E+00	6.89197306E+00	6.89197306E+00	6.89197306E+00	6.89197306E+00	6.89197306E+00	6.89197306E+00	6.89197306E+00	6.89197306E+00	6.89197306E+00	6.89197306E+00		
3400	10.005	10.005	0	3.57518936E+00	3.57518936E+00	3.57518936E+00	3.57518936E+00	3.57518936E+00	3.57518936E+00	3.57518936E+00	3.57518936E+00	3.57518936E+00	3.57518936E+00	3.57518936E+00		
340	10.05	10.05	0	3.55579419E+00	3.55579419E+00	3.55579419E+00	3.55579419E+00	3.55579419E+00	3.55579419E+00	3.55579419E+00	3.55579419E+00	3.55579419E+00	3.55579419E+00	3.55579419E+00		
34	10.50	10.5	0	3.35843709E+00	3.35843709E+00	3.35843709E+00	3.35843709E+00	3.35843709E+00	3.35843709E+00	3.35843709E+00	3.35843709E+00	3.35843709E+00	3.35843709E+00	3.35843709E+00		
17	1100	11.0	0	3.13224451E+00	3.13224451E+00	3.13224451E+00	3.13224451E+00	3.13224451E+00	3.13224451E+00	3.13224451E+00	3.13224451E+00	3.13224451E+00	3.13224451E+00	3.13224451E+00		
3.4	15.00	15.0	0	1.17672299E+00	1.17672299E+00	1.17672299E+00	1.17672299E+00	1.17672299E+00	1.17672299E+00	1.17672299E+00	1.17672299E+00	1.17672299E+00	1.17672299E+00	1.17672299E+00		
2	18.50	18.5	0	-4.04481899E-01	-4.04481899E-01	-4.04481899E-01	-4.04481899E-01	-4.04481899E-01	-4.04481899E-01	-4.04481899E-01	-4.04481899E-01	-4.04481899E-01	-4.04481899E-01	-4.04481899E-01		
0.8	31.00	31.0	0	1.28302614E+00	1.28302614E+00	1.28302614E+00	-1.28302614E+00	-1.28302614E+00	-1.28302614E+00	-1.28302614E+00	-1.28302614E+00	-1.28302614E+00	-1.28302614E+00	-1.28302614E+00	10 decim	
0.5	42.00	42.0	0	-2.01113790E-01	-2.01113790E-01	-2.01113790E-01	-2.01113790E-01	-2.01113790E-01	-2.01113790E-01	-2.01113790E-01	-2.01113790E-01	-2.01113790E-01	-2.01113790E-01	-2.01113790E-01		
0.3	70.00	70.0	0	3.49076964E-02	3.49076964E-02	3.49076964E-02	3.49076964E-02	3.49076964E-02	3.49076964E-02	3.49076964E-02	3.49076964E-02	3.49076964E-02	3.49076964E-02	3.49076964E-02		
0.08	220	200	0	5.92322494E-03	5.92322494E-03	5.92322494E-03	5.92322494E-03	5.92322494E-03	5.92322494E-03	5.92322494E-03	5.92322494E-03	5.92322494E-03	5.92322494E-03	5.92322494E-03		
0.05	320	320	0	2.26961562E-03	2.26961562E-03	2.26961562E-03	2.26961562E-03	2.26961562E-03	2.26961562E-03	2.26961562E-03	2.26961562E-03	2.26961562E-03	2.26961562E-03	2.26961562E-03		<<1%
0.03	585	585	0	6.29476013E-04	6.29476013E-04	6.29476013E-04	6.29476013E-04	6.29476013E-04	6.29476013E-04	6.29476013E-04	6.29476013E-04	6.29476013E-04	6.29476013E-04	6.29476013E-04		
0.02	1000	1000	0	2.05138332E-04	2.05138332E-04	2.05138332E-04	2.05138332E-04	2.05138332E-04	2.05138332E-04	2.05138332E-04	2.05138332E-04	2.05138332E-04	2.05138332E-04	2.05138332E-04		
0.008	2100	2100	0	4.46244021E-05	4.46244021E-05	4.46244021E-05	4.46244021E-05	4.46244021E-05	4.46244021E-05	4.46244021E-05	4.46244021E-05	4.46244021E-05	4.46244021E-05	4.46244021E-05		
0.005	3200	3200	0	1.89507327E-05	1.89507327E-05	1.89507327E-05	1.89507327E-05	1.89507327E-05	1.89507327E-05	1.89507327E-05	1.89507327E-05	1.89507327E-05	1.89507327E-05	1.89507327E-05		
0.003	5680	5680	0	5.94270063E-06	5.94270063E-06	5.94270063E-06	5.94270063E-06	5.94270063E-06	5.94270063E-06	5.94270063E-06	5.94270063E-06	5.94270063E-06	5.94270063E-06	5.94270063E-06	9 decim	
0.0016	10600	10600	0	1.69375127E-06	1.69375128E-06	1.69375128E-06	1.69375127E-06	1.69375127E-06	1.69375127E-06	1.69375127E-06	1.69375127E-06	1.69375127E-06	1.69375127E-06	1.69375127E-06		
0.0010	17000	17000	0	6.56365741E-07	6.56365741E-07	6.56365743E-07	6.56365740E-07	6.56365740E-07	6.56365745E-07	6.56365745E-07	6.56365738E-07	6.56365746E-07	6.56365746E-07	6.56365746E-07	8 decim	
0.0005	34000	34000	0	1.63645237E-07	1.63645236E-07	1.63645239E-07	1.63645238E-07	1.63645238E-07	1.63645237E-07	1.63645237E-07	1.63645233E-07	1.63645233E-07	1.63645233E-07	1.63645233E-07		
0.0003	56600	56000	0	5.95641424E-08	5.95641457E-08	5.95641441E-08	5.95641415E-08	5.95641415E-08	5.95641438E-08	5.95641438E-08	5.95641418E-08	5.95641445E-08	5.95641445E-08	5.95641445E-08		
0.0002	75000	75000	0	3.35806356E-08	3.35806364E-08	3.35806361E-08	3.35806367E-08	3.35806367E-08	3.35806313E-08	3.35806313E-08	3.35806325E-08	3.35806361E-08	3.35806361E-08	3.35806361E-08	7 decim	
0.00017	100000	100000	0	1.88832367E-08	1.88832385E-08	1.88832394E-08	1.88832356E-08	1.88832356E-08	1.88832345E-08	1.88832345E-08	1.88832391E-08	1.88832354E-08	1.88832354E-08	1.88832354E-08		
0.00015	110000	110000	0	1.56046571E-08	1.56046523E-08	1.56046579E-08	1.56046568E-08	1.56046568E-08	1.56046562E-08	1.56046562E-08	1.56046593E-08	1.56046577E-08	1.56046577E-08	1.56046577E-08		

1.2.11. Investigation of run-time efficiency of certain analytical formulas

The sum in analytical formula (176) of gravitational potential contains the $h_i \sum_{j=1}^{l(i)} \Omega_{ij}$ term. From the observation point of view it is advantageous first to compute the sum and then the product i.e. $h_i \sum_{j=1}^{l(i)} \Omega_{ij}$. In order to choose the most efficient analytical expression it is advantageous if the domain of definition of the expression coincides with its theoretical domain of definition. From Table 6 we can conclude that for the C_{ij}, Ω_{ij}, Ω_i constants this assumption is realized for the C_i^{HWSch}, $\Omega_{ij}^{Pohanka^3}$, $\Omega_{ij}^{Holstein^3}$ and Ω_i^{HWSch} analytical formulas. The points where the analytical formulas of C_{ij}, Ω_{ij}, Ω_i are not defined we have to take in consideration in the course of programming or we can avoid singularities based on the fact that these points represent removable discontinuities. This means that the constants C_{ij}, Ω_{ij}, Ω_i have discontinuities for which the constants' limits exist and are finite. Thus instead of $U(M)$, $U_k(M)$, $U_{kl}(M)$ we get approximations of these values $U(M,\varepsilon)$, $U_k(M,\varepsilon)$, $U_{kl}(M,\varepsilon)$ as small as is required substituting $|h_i|+\varepsilon$ instead of $|h_i|$.
Using the $C_{ij}^{Pohanka^3}$ and $\Omega_{ij}^{Pohanka^3}$ formulas (Table 6) and substituting $|h_i|+\varepsilon$ instead of $|h_i|$ we get the following approximations:

$$C_{ij_\varepsilon} = \operatorname{sign}(l_{2ij}) \ln \frac{r_{2ij_\varepsilon} + |l_{2ij}|}{r_{0ij_\varepsilon}} - \operatorname{sign}(l_{1ij}) \ln \frac{r_{1ij_\varepsilon} + |l_{1ij}|}{r_{0ij_\varepsilon}}, \tag{215}$$

$$\Omega_{ij_\varepsilon} = -2 \operatorname{sign}(h_i) \arctan \frac{2h_{ij}(l_{2ij} - l_{1ij})}{(r_{2ij_\varepsilon} + r_{1ij_\varepsilon})^2 - (l_{2ij} - l_{1ij})^2 + 2(r_{2ij_\varepsilon} + r_{1ij_\varepsilon})(|h_i| + \varepsilon)}, \tag{216}$$

where

$$r_{0ij_\varepsilon} = \sqrt{R_{MP}^2 + (h_i + \varepsilon)^2}, \; r_{1ij_\varepsilon} = \sqrt{R_{MP}^2 + l_{1ij}^2 + (h_i + \varepsilon)^2}, \; r_{1ij_\varepsilon} = \sqrt{R_{MP}^2 + l_{1ij}^2 + (h_i + \varepsilon)^2}. \tag{217}$$

An estimation can be given of the errors $|\delta \nabla_{\boldsymbol{r}_M} U(M,\varepsilon)| = |\nabla_{\boldsymbol{r}_M} U(M) - \nabla_{\boldsymbol{r}_M} U(M,\varepsilon)|$, $|\delta U(M,\varepsilon)| = |U(M) - U(M,\varepsilon)|$ and $|\delta U_{kl}(M,\varepsilon)| = |U_{kl}(M) - U_{kl}(M,\varepsilon)|$ induced by this approach using the difference between the calculated approximation values $U(M,\varepsilon)$, $U_k(M,\varepsilon)$, $U_{kl}(M,\varepsilon)$ and the exact values $U(M)$, $U_k(M)$, $U_{kl}(M)$ making use of formulas (176), (178) and (180):

$$U(M) = \frac{G\rho_0}{2} \sum_{i=1}^{n} h_i \left(\sum_{j=1}^{l(i)} h_{ij} C_{ij} - h_i \Omega_i \right) = \frac{G\rho_0}{2} \sum_{i=1}^{n} h_i \left(\sum_{j=1}^{l(i)} (h_{ij} C_{ij} - h_i \Omega_{ij}) \right),$$

$$\nabla_{\boldsymbol{r}_M} U(M) = -G\rho_0 \sum_{i=1}^{n} \boldsymbol{n}_i \left(\sum_{j=1}^{l(i)} (h_{ij} C_{ij} - h_i \Omega_{ij}) \right), \; U_{kl}(M) = G\rho_0 \sum_{i=1}^{n} n_i^k \sum_{j=1}^{l(i)} (v_{ij}^l C_{ij} - n_i^l \Omega_{ij}).$$

Thus we have:

$$U(M,\varepsilon) = \frac{G\rho_0}{2} \sum_{i=1}^{n} h_i \left(\sum_{j=1}^{l(i)} h_{ij} C_{ij_\varepsilon} - h_i \Omega_{i_\varepsilon} \right) = \frac{G\rho_0}{2} \sum_{i=1}^{n} h_i \left(\sum_{j=1}^{l(i)} (h_{ij} C_{ij_\varepsilon} - h_i \Omega_{ij_\varepsilon}) \right), \tag{218}$$

$$\nabla_{\boldsymbol{r}_M} U(M,\varepsilon) = -G\rho_0 \sum_{i=1}^{n} \boldsymbol{n}_i \left(\sum_{j=1}^{l(i)} (h_{ij} C_{ij_\varepsilon} - h_i \Omega_{ij_\varepsilon}) \right), U_{kl}(M,\varepsilon) = G\rho_0 \sum_{i=1}^{n} n_i^k \sum_{j=1}^{l(i)} (v_{ij}^l C_{ij_\varepsilon} - n_i^l \Omega_{ij_\varepsilon}). \tag{219}$$

Based on Pohànka (1988) we get an estimation of error $\left|\delta\nabla_{\boldsymbol{r}_M} U(M,\varepsilon)\right| = \left|\nabla_{\boldsymbol{r}_M} U(M) - \nabla_{\boldsymbol{r}_M} U(M,\varepsilon)\right|$. Using the Eqs. (56), (61), (62) of this paper we have:

$$\left|h_{ij}\right|\left|C_{ij} - C_{ij_\varepsilon}\right| \le \varepsilon \text{ and } \left|h_i\right|\left|\Omega_{ij} - \Omega_{ij_\varepsilon}\right| \le 4\varepsilon . \tag{220}$$

Based on eq. (66) of this paper it holds:

$$\left|\delta\nabla_{\boldsymbol{r}_M} U(M,\varepsilon)\right| = \left|\nabla_{\boldsymbol{r}_M} U(M) - \nabla_{\boldsymbol{r}_M} U(M,\varepsilon)\right| \le G\left|\rho_0\right|\sum_{i=1}^{n}\sum_{j=1}^{l(i)}\left(\left|h_{ij}\right|\left|C_{ij} - C_{ij_\varepsilon}\right| + \left|h_i\right|\left|\Omega_{ij} - \Omega_{ij_\varepsilon}\right|\right) \le$$

$$\le G\left|\rho_0\right|\sum_{i=1}^{n}\sum_{j=1}^{l(i)} 5\varepsilon = 5G\left|\rho_0\right|\varepsilon\sum_{i=1}^{n} L(i) . \tag{221}$$

Similarly we can get same relations for the gravitational potential and its second derivatives:

$$\left|\delta U(M,\varepsilon)\right| = \left|U(M) - U(M,\varepsilon)\right| \le \frac{G\rho_0}{2}\sum_{i=1}^{n}\sum_{j=1}^{l(i)}\left(\left|h_i h_{ij}\right|\left|C_{ij} - C_{ij_\varepsilon}\right| + h_i^2\left|\Omega_{ij} - \Omega_{ij_\varepsilon}\right|\right), \tag{222}$$

$$\left|\delta U_{kl}(M,\varepsilon)\right| = \left|U_{kl}(M) - U_{kl}(M,\varepsilon)\right| \le G\rho_0\sum_{i=1}^{n}\sum_{j=1}^{l(i)}\left(\left|C_{ij} - C_{ij_\varepsilon}\right| + \left|\Omega_{ij} - \Omega_{ij_\varepsilon}\right|\right). \tag{223}$$

The problem can be interpreted as a stability one in the sense that inducing an infinitesimally small ε shift in the $\left|h_i\right|$ variable we are interested in the impact of its on gravity field parameters i.e. we have to clarify the relation between the ε and $\left|\delta\nabla_{\boldsymbol{r}_M} U(M,\varepsilon)\right|$, $\left|\delta U(M,\varepsilon)\right|$, $\left|\delta U(M,\varepsilon)\right|$ quantities. Using (220) we can give estimation of the $\left|h_{ij}\right|\left|C_{ij} - C_{ij_\varepsilon}\right|$ and $\left|h_i\right|\left|\Omega_{ij} - \Omega_{ij_\varepsilon}\right|$ expression as functions of ε. Based on (221), (222) and (223) the $\left|\delta\nabla_{\boldsymbol{r}_M} U(M,\varepsilon)\right|$, $\left|\delta U(M,\varepsilon)\right|$, $\left|\delta U_{kl}(M,\varepsilon)\right|$ quantities can be expressed in terms of $\left|h_{ij}\right|\left|C_{ij} - C_{ij_\varepsilon}\right|$, $\left|C_{ij} - C_{ij_\varepsilon}\right|$, $\left|h_i h_{ij}\right|\left|C_{ij} - C_{ij_\varepsilon}\right|$, $\left|h_i\right|\left|\Omega_{ij} - \Omega_{ij_\varepsilon}\right|$, $h_i^2\left|\Omega_{ij} - \Omega_{ij_\varepsilon}\right|$ and $\left|\Omega_{ij} - \Omega_{ij_\varepsilon}\right|$. We investigated numerically the variation of these terms as a function of ε by setting the following values: $\varepsilon = 10^{-8}$, $\varepsilon = 10^{-15}$, $\varepsilon = 10^{-25}$ and $\varepsilon = 10^{-35}$ in points fulfilling the $\gamma \in (\gamma_{min} = 2\cdot10^{-9}$, $\gamma_{max} = 10^{25})$ condition. The results are presented in Tables 11 and 12. In the near domain of the body ($\gamma >> 1$) the term $\left|C_{ij} - C_{ij_\varepsilon}\right|$ becomes instable. In the model computations presented in the papers by Benedek (2004) and Benedek and Papp (2009) the upper bound of γ_{model} is 10^4 ($\gamma < 10^4$), where C_{ij} is stable as Table 11 shows. The estimated magnitude of the upper bound of the quantity $\left|h_{ij}\right|\left|C_{ij} - C_{ij_\varepsilon}\right|$ (first row in Table 11) from a particular ε differs (are consistently larger) from the upper bound deduced theoretically. The quantity $\left|h_{ij}\right|\left|C_{ij} - C_{ij_\varepsilon}\right|$ is stable for each of the four selected ε values in the $\gamma \in (\gamma_{min}, \gamma_{max})$ domain. $\left|\Omega_{ij} - \Omega_{ij_\varepsilon}\right|$ becomes unstable near the surface of the polyhedron ($\gamma >> 1$). In case of model computation restricted by $\gamma_{model} < 10^4$ the condition $\left|\Omega_{ij} - \Omega_{ij_\varepsilon}\right|$ becomes stable for $\varepsilon = 10^{-25}$, $\varepsilon = 10^{-35}$ (Table 12). The upper bound of $\left|h_i\right|\left|\Omega_{ij} - \Omega_{ij_\varepsilon}\right|$ determined numerically (first row of Table 12) is consistently smaller than $4\cdot\varepsilon$ which is theoretically derived. The expression $h_i^2\left|\Omega_{ij} - \Omega_{ij_\varepsilon}\right|$ is stable for each of the gravitational four selected ε values on the domain $\gamma \in (\gamma_{min}, \gamma_{max})$. By right of these numerical investigations we can conclude that the first and second derivatives of the gravitational potential are stable on the domain $\gamma \in (\gamma_{min} = 2\cdot10^{-9}, \gamma_{max} = 10^{25})$ for each ε values. The gravitational

potential is stable on the domain $\gamma < 10^4$ in case of $\varepsilon = 10^{-25}$, $\varepsilon = 10^{-35}$. For the other two values $\varepsilon = 10^{-8}$, $\varepsilon = 10^{-15}$ choosing an adequate lower bound for γ we can assure the stability of the gravitational potential.

Table 11 Numerical estimation of the upper bound of the $|h_{ij}||C_{ij}-C_{ij_\varepsilon}|$, $|C_{ij}-C_{ij_\varepsilon}|$, $|h_{ij}h_i||C_{ij}-C_{ij_\varepsilon}|$ expressions as a function of ε where ε is an infinitesimally small quantity which is introduced to modify the $|h_i|$ value

expression	$\varepsilon=10^{-8}$		$\varepsilon=10^{-15}$		$\varepsilon=10^{-25}$		$\varepsilon=10^{-35}$	
	Upper bound	computation domain	Upper bound	computation domain	Upper bound	computation domain	Upper bound	computation domain
$\lvert h_{ij}\rvert\lvert C_{ij}-C_{ij_\varepsilon}\rvert$	$2.3\cdot\varepsilon$	$\gamma\in(2\cdot10^{-9}, 10^{25})$	$2.3\cdot\varepsilon$	$\gamma\in(2\cdot10^{-9}, 10^{25})$	$4.2\cdot\varepsilon$	$\gamma\in(2\cdot10^{-9}, 10^{25})$	$2.5\cdot\varepsilon$	$\gamma\in(2\cdot10^{-9}, 10^{25})$
					$K\cdot\varepsilon$, $K<10^{-14}$	$\gamma\in(2\cdot10^{-9}, 10^{9})$	$K\cdot\varepsilon$, $K<10^{-14}$	$\gamma\in(2\cdot10^{-9}, 10^{20})$
$\lvert C_{ij}-C_{ij_\varepsilon}\rvert$	$7.8\cdot10^{9}\cdot\varepsilon$	$\gamma\in(2\cdot10^{-9}, 10^{25})$	$7.2\cdot10^{16}\cdot\varepsilon$	$\gamma\in(2\cdot10^{-9}, 10^{25})$	$7.2\cdot10^{25}\cdot\varepsilon$	$\gamma\in(2\cdot10^{-9}, 10^{25})$	$7.2\cdot10^{20}\cdot\varepsilon$	$\gamma\in(2\cdot10^{-9}, 10^{25})$
	$2.5\cdot\varepsilon$	$\gamma\in(2\cdot10^{-9}, 10^{5})$	$2.5\cdot\varepsilon$	$\gamma\in(2\cdot10^{-9}, 10^{5})$	$K\cdot\varepsilon$, $K<10^{-14}$	$\gamma\in(2\cdot10^{-9}, 10^{10})$	$K\cdot\varepsilon$, $K<10^{-14}$	$\gamma\in(2\cdot10^{-9}, 10^{20})$
$\lvert h_{ij}h_i\rvert\lvert C_{ij}-C_{ij_\varepsilon}\rvert$	$2.3\cdot\varepsilon$	$\gamma\in(2\cdot10^{-9}, 10^{25})$	$2.4\cdot\varepsilon$	$\gamma\in(2\cdot10^{-9}. 10^{25})$	$K\cdot\varepsilon$, $K<10^{-9}$	$\gamma\in(2\cdot10^{-9}, 10^{25})$	$K\cdot\varepsilon$, $K<10^{-20}$	$\gamma\in(2\cdot10^{-9}, 10^{25})$

Table 12. Numerical estimation of the upper bound of the $|h_i||\Omega_{ij}-\Omega_{ij_\varepsilon}|$, $|\Omega_{ij}-\Omega_{ij_\varepsilon}|$, $h_i^2|\Omega_{ij}-\Omega_{ij_\varepsilon}|$ expressions as a function of ε where ε is an infinitesimally small quantity which is introduced to modify the $|h_i|$ value

expression	$\varepsilon=10^{-8}$		$\varepsilon=10^{-15}$		$\varepsilon=10^{-25}$		$\varepsilon=10^{-35}$	
	Upper bound	computation domain	Upper bound	computation domain	Upper bound	computation domain	Upper bound	computation domain
$\lvert h_i\rvert\lvert\Omega_{ij}-\Omega_{ij_\varepsilon}\rvert$	$1.0\cdot\varepsilon$	$\gamma\in(1.5\cdot10^{-9}, 10^{25})$	$1.5\cdot\varepsilon$	$\gamma\in(1.5\cdot10^{-9}, 10^{25})$	$2.1\cdot\varepsilon$	$\gamma\in(1.5\cdot10^{-9}, 10^{25})$	$1.3\cdot\varepsilon$	$\gamma\in(1.5\cdot10^{-9}, 10^{25})$
					$K\cdot\varepsilon$, $K<10^{-14}$	$\gamma\in(1.5\cdot10^{-9}, 10^{9})$	$K\cdot\varepsilon$, $K<10^{-14}$	$\gamma\in(1.5\cdot10^{-9}, 10^{18})$
$\lvert\Omega_{ij}-\Omega_{ij_\varepsilon}\rvert$	$3.2\cdot10^{8}\cdot\varepsilon$	$\gamma\in(1.5\cdot10^{-9}, 10^{25})$	$6.3\cdot10^{15}\cdot\varepsilon$	$\gamma\in(1.5\cdot10^{-9}, 10^{25})$	$1.6\cdot10^{25}\cdot\varepsilon$	$\gamma\in(1.5\cdot10^{-9}, 10^{25})$	$2\cdot10^{26}$	$\gamma\in(1.5\cdot10^{-9}, 10^{25})$
	$3.4\cdot10^{5}\cdot\varepsilon$	$\gamma\in(1.5\cdot10^{-9}, 10^{5})$	$3.4\cdot10^{5}\cdot\varepsilon$	$\gamma\in(1.5\cdot10^{-9}, 10^{5})$	$K\cdot\varepsilon$, $K<10^{-14}$	$\gamma\in(1.5\cdot10^{-9}, 10^{9})$	$K\cdot\varepsilon$, $K<10^{-14}$	$\gamma\in(1.5\cdot10^{-9}, 10^{19})$
	$100\cdot\varepsilon$	$\gamma\in(1.5\cdot10^{-9}, 10^{2})$	$100\cdot\varepsilon$	$\gamma\in(1.5\cdot10^{-9}, 10^{2})$				
$h_i^2\lvert\Omega_{ij}-\Omega_{ij_\varepsilon}\rvert$	$2.3\cdot\varepsilon$	$\gamma\in(1.5\cdot10^{-9}, 10^{25})$	$2.7\cdot\varepsilon$	$\gamma\in(1.5\cdot10^{-9}, 10^{25})$	$K\cdot\varepsilon$, $K<10^{-8}$	$\gamma\in(1.5\cdot10^{-9}. 10^{25})$	$K\cdot\varepsilon$, $K<10^{-19}$	$\gamma\in(1.5\cdot10^{-9}, 10^{25})$

In certain points of the domain of definition of the analytical formulas of C_{ij}, Ω_{ij}, Ω_i these expressions can become indeterminate. For example somewhere around the edge *AB* the C_{ij} can turn into NaN, similarly around the plane *s* the Ω_{ij} can turn into NaN. These are is not real singularities but numerical instabilities of the analytical formulas can appear. We found the following stability domain for the particular analytical formulas of the C_{ij} and Ω_i constants:

The $C_{ij}^{Holstein}$, $C_{ij}^{Pohanka^3}$ analytical expressions of the constant C_{ij} have stability problems around the edge *AB*. The stability of these formulas is provided by inequality constraints $10^{-8} = \gamma_{\min} < \gamma < \gamma_{\max} = 10^{25}$. C_{ij}^{HWSch} is unstable near to *AB*, this can be avoided by restricting the observation domain around *AB*/[*AB*] and [*AB*] to points fulfilling the inequalities $10^{-8} = \gamma_{\min} < \gamma < \gamma_{\max} = 10^{25}$ and $10^{-8} = \gamma_{\min} < \gamma < 10^{7}$ successively. The other analytical expressions of C_{ij} ($C_{ij}^{Pohanka^1}$, $C_{ij}^{Pohanka^2}$, C_{ij}^{HPGL}) are unstable in points around the edge *AB* which violate the $10^{-8} = \gamma_{\min} < \gamma < 10^{7}$ condition.

The instability of analytical formulas of Ω_i appears around the S_i face. All analytical expressions of Ω_i except Ω_i^{WSch} become unstable in points situated near to the vertices of S_i. The value of Ω_i as the observation point approaches these vertices across points situated in the *s* plane defined by the face S_i becomes unstable when the $\gamma > 10^8$ condition is violated. Otherwise when the computation point is outside the *s* plane the instability of Ω_i takes place when $\gamma > 10^{11}$. In case of points situated near to the S_i edges the formulas $\Omega_{ij}^{Pohanka^1}$, $\Omega_{ij}^{Pohanka^2}$, $\Omega_{ij}^{Pohanka^3}$, $\Omega_{ij}^{Holstein^1}$, $\Omega_{ij}^{Holstein^2}$, $\Omega_{ij}^{Holstein^3}$, Ω_{ij}^{WSch} becomes unstable. In addition if these points are situated on the plane *s* the instability of $\Omega_i^{Pohanka^1}$, $\Omega_i^{Pohanka^2}$, $\Omega_i^{Pohanka^3}$ and $\Omega_i^{Holstein^2}$, $\Omega_i^{Holstein^3}$, Ω_i^{WSch} occurs for $\gamma > 10^8$

and $\gamma > 10^{14}$ successively. In addition when the computation points are near to the edges of S_i and are situated outside the s plane the instability of Ω_i takes place when $\gamma > 10^{13}$ for all Ω_i analytical formulas. In the inner points of S_i and $s \backslash S_i$ the condition $\gamma < 10^{14}$ ensures the stability of Ω_i.

Time consumption is an important consideration in selecting the optimal observation formula. This was tested by a simple model with double precision computation. In the first test, the computation was repeated in a single observation point ($5 \cdot 10^8$ repetition for C_{ij} and $5 \cdot 10^7$ repetition for Ω_{ij}) in the second test the computation was performed for a set of observation points and than this repeated. The obtained results are presented in Tables 13 and 14. We can conclude that formula denoted by *HWSch* has the best performance. Furthermore the time consumption of C_{ij} is approximately 20% of Ω_{ij} computational time.

Table 13. The time consumption (t) of constants using the repetition (nr) of one observation point. The computational time of C_{ij} constants are compared with computational time of *Pohànka*^{3} formula. The *Holstein*^{3} formulas were chosen as reference formula for the Ω_{ij} constants. The $\sum_{j=1}^{l(i)} \Omega_{ij}$ sum in the *Pohànka*^{3} formula (in our model computation $l(i) = 3$) consists of $l(i)$ terms of arctangent function. Using relation (221) the $l(i)$ terms of the arctangent function can be transformed to only one term of the arctangent function. The deduced formula is denoted by (*Pohànka*^{3})*

constants	nr	t %
$C_{ij}^{Pohanka^3}$	$5 \cdot 10^8$	100% (8.6 min)
$C_{ij}^{Holstein}$	$5 \cdot 10^8$	70% (6.0 min)
C_{ij}^{HWSch}	$5 \cdot 10^8$	60% (5.3 min)
$\Omega_i^{Pohanka^3}$	$5 \cdot 10^7$	90% (3.9 min)
$(\Omega_i^{Pohanka^3})^*$	$5 \cdot 10^7$	77% (3.3 min)
$\Omega_i^{Holstein^3}$	$5 \cdot 10^7$	100% (4.3 min)
Ω_i^{WSch}	$5 \cdot 10^7$	13% (0.6 min)

Table 14. The time consumtion (t_A, t_B) of constants using the repetition (nr_A, nr_B) in case of observation points given in A and B sets. The computational time of C_{ij} constants are compared with computational time of *Pohànka*^{3} formula. The *Holstein*^{3} formulas were chosen as reference formula for the Ω_{ij} constants. The *Pohànka*^{3} formula $\sum_{j=1}^{l(i)} \Omega_{ij}$ (in our model computation $l(i) = 3$) consist of $l(i)$ terms of arctangent function. Using relation (221) the $l(i)$ terms of the arctangent function can be transformed to only one term of the arctangent function. The deduced formula is denoted by (*Pohànka*^{3})*. The A and B sets consist of 4930 and 8510 computation points

constants	nr_A	t_A %	nr_B	t_B %
$C_{ij}^{Pohanka^3}$	$5 \cdot 10^5$	100% (10.6 min)	$5 \cdot 10^5$	100% (16.1 min)
$C_{ij}^{Holstein}$	$5 \cdot 10^5$	61% (6.5 min)	$5 \cdot 10^5$	71% (11.4 min)
C_{ij}^{HWSch}	$5 \cdot 10^5$	45% (4.6 min)	$5 \cdot 10^5$	60% (8.4 min)
$\Omega_i^{Pohanka^3}$	$5 \cdot 10^4$	86% (4.6 min)	$5 \cdot 10^4$	88% (7.0 min)
$(\Omega_i^{Pohanka^3})^*$	$5 \cdot 10^4$	98% (5.2 min)	$5 \cdot 10^4$	86% (6.9 min)
$\Omega_i^{Holstein^3}$	$5 \cdot 10^4$	100% (5.3 min)	$5 \cdot 10^4$	100% (8.0 min)
Ω_i^{WSch}	$5 \cdot 10^4$	14% (0.7 min)	$5 \cdot 10^4$	13% (1.0 min)

As we mentioned we can transform the $l(i)$ terms of the sum $\sum_{j=1}^{l(i)} \Omega_{ij}$ into one term using the following relation:

$$\sum_j \operatorname{atan} x_j = \arg\left(\prod_j (1 + i x_k) \right). \tag{224}$$

Taking into account the limits of Ω_i, i.e. $\Omega_i \in (-2\pi, -2\pi)$ and the expression of Ω_{ij} as $\Omega_{ij} = 2 \operatorname{atan} x_j$, it follows that $\sum_j \operatorname{atan} x_j \in (-\pi, \pi)$, thus expression $\arg\left(\prod_j (1 + i x_k) \right)$ can be determined uniquely.

Reducing the sum of $l(i)$ number arctangent functions to one arctangent term we generate the $\left(\Omega_i^{Pohanka^3}\right)^*$ formula (Tables 5, 6). The numerical behaviour of the $\left(\Omega_i^{Pohanka^3}\right)^*$ formula is the same as $\Omega_i^{Pohanka^3}$, except if we are approaching the limit points of S_i across the s/S_i points. Then the instability of $\left(\Omega_i^{Pohanka^3}\right)^*$ appears when the condition $\gamma < 10^8$ is violated.

1.2.12 Description of the computational algorithm for gravitational potential and its derivatives applied in gravity field modelling

In the following we present the computational algorithm developed by us. The analytical formulas involved in the algorithm:

$$U(M,\varepsilon)=\frac{G\rho_0}{2}\sum_{i=1}^{n}h_{i\varepsilon}\left(\sum_{j=1}^{l(i)}\left(h_{ij}C_{ij\varepsilon}^{Pohanka^3}-z_{i\varepsilon}\theta_{ij\varepsilon}^{Pohanka^3}\right)\right) \tag{225}$$

$$\nabla_{r_M}U(M,\varepsilon)=-G\rho_0\sum_{i=1}^{n}\boldsymbol{n}_i\left(\sum_{j=1}^{l(i)}\left(h_{ij}C_{ij\varepsilon}^{Pohanka^3}-z_{i\varepsilon}\theta_{ij\varepsilon}^{Pohanka^3}\right)\right) \tag{226}$$

$$U_{ij}(M,\varepsilon)=G\rho_0\sum_{i=1}^{n}\boldsymbol{n}_i\boldsymbol{e}_k\sum_{j=1}^{l(i)}\left(\boldsymbol{v}_{ij}\boldsymbol{e}_l C_{ij\varepsilon}^{Pohanka^3}-\boldsymbol{n}_i\boldsymbol{e}_l\,\mathrm{sign}(h_i)\theta_{ij\varepsilon}^{Pohanka^3}\right). \tag{227}$$

The definitions of the constants $C_{ij\varepsilon}^{Pohanka^3}$, $\theta_{ij\varepsilon}^{Pohanka^3}$ are:

$$C_{ij\varepsilon}^{Pohanka^3}=C_{ij\varepsilon}^{Pohanka^3}\left(l_{1ij},l_{2ij},h_{ij},h_i,\varepsilon\right)=\mathrm{sign}\left(l_{2ij}\right)\cdot\ln\left(\frac{V_{ij\varepsilon}+\left|l_{2ij}\right|}{W_{ij\varepsilon}}\right)-\mathrm{sign}\left(l_{1ij}\right)\cdot\ln\left(\frac{Q_{ij\varepsilon}+\left|l_{1ij}\right|}{W_{ij\varepsilon}}\right) \tag{228}$$

$$\theta_{ij\varepsilon}^{Pohanka^3}=\theta_{ij\varepsilon}^{Pohanka^3}\left(l_{1ij},l_{2ij},h_{ij},z_i,\varepsilon\right)=\mathrm{sign}\left(h_i\right)\Omega_{ij\varepsilon}^{Pohanka^3}=2\,\mathrm{atan}\frac{2h_{ij}l_{ij}}{\left(T_{ij\varepsilon}+l_{ij}\right)\cdot\left|T_{ij\varepsilon}-l_{ij}\right|+2T_{ij\varepsilon}z_{i_\varepsilon}}, \tag{229}$$

where

$$z_{i\varepsilon}=z_i+\varepsilon,\ W_{ij\varepsilon}=\sqrt{h_{ij}^2+z_\varepsilon^2},\ Q_{ij\varepsilon}=\sqrt{l_{1ij}^2+W_{ij\varepsilon}^2},\ V_{ij\varepsilon}=\sqrt{l_{2ij}^2+W_{ij\varepsilon}^2},\ T_{ij\varepsilon}=Q_{ij\varepsilon}+V_{ij\varepsilon} \tag{230}$$

$$\boldsymbol{l}_{ij}=\boldsymbol{a}_{ij+1}-\boldsymbol{a}_{ij},\ l_{ij}=\left|\boldsymbol{a}_{ij+1}-\boldsymbol{a}_{ij}\right|,\ \boldsymbol{\mu}_{ij}=\frac{\boldsymbol{a}_{ij+1}-\boldsymbol{a}_{ij}}{\left|\boldsymbol{a}_{ij+1}-\boldsymbol{a}_{ij}\right|},\ \boldsymbol{n}_i=\frac{\boldsymbol{l}_{i1}\times\boldsymbol{l}_{i2}}{\left|\boldsymbol{l}_{i1}\times\boldsymbol{l}_{i2}\right|},\ \boldsymbol{v}_{ij}=\boldsymbol{\mu}_{ij}\times\boldsymbol{n}_i, \tag{231}$$

$$\boldsymbol{r}_{1ij}=\boldsymbol{a}_{ij}-\boldsymbol{r}_M,\ \boldsymbol{r}_{2ij}=\boldsymbol{a}_{ij+1}-\boldsymbol{r}_M, \tag{232}$$

$$l_{1ij}=\boldsymbol{r}_{1ij}\cdot\boldsymbol{\mu}_{ij},\ h_{ij}=\boldsymbol{r}_{1ij}\cdot\boldsymbol{v}_{ij},\ z_i=\left|h_i\right|=\left|\boldsymbol{r}_{1ij}\cdot\boldsymbol{n}_i\right|,\ l_{2ij}=l_{1ij}+l_{ij}. \tag{233}$$

n is the number of polyhedron faces, $l(i)$ is the number of vertices of the ith face.

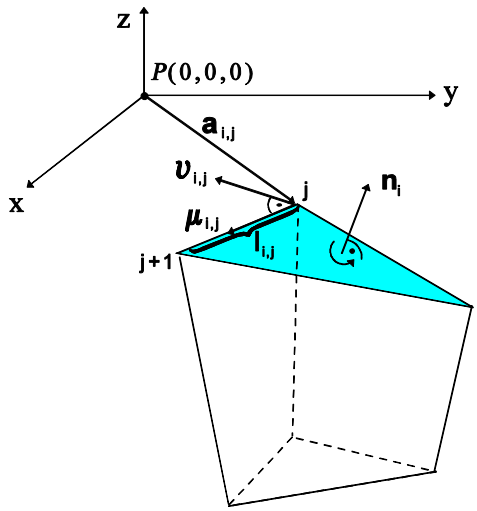

Fig. 21 Geometrical explanation of quantities occurring in expression (230)

The normal vectors of the local coordinate system belonging to the i face and j vertex indices are successively $\boldsymbol{n}_i$ the normal vector of the ith face, $\boldsymbol{\mu}_{ij}$ the normal vector of the edge connecting the j and $j+1$ vertices belonging of the ith face (succession j, $j+1$, $j+2$... of vertices is considered positively oriented), $\boldsymbol{v}_{i,j}$ is a unit vector situated in the plane S_i and perpendicular to $\boldsymbol{\mu}_{ij}$ so that ($\boldsymbol{\mu}_{ij}$, $\boldsymbol{n}_i$, $\mathbf{v}_{ij}$) form a right-handed system belonging to the (i, j) index pair. In practical implementation in the first step for each plane S_i the positive orientation of vertices is assigned as described in Section 1.2.3. Based on this we start with an arbitrary orientation of vertices belonging to the face S_i. We denote with $\boldsymbol{a}_{i1}^0, \boldsymbol{a}_{i2}^0, \ldots, \boldsymbol{a}_{ij}^0, \ldots, \boldsymbol{a}_{il(i)}^0$ the position vectors in order of initial considered orientation. If $f\left(\boldsymbol{a}_{i1}^0 + \boldsymbol{l}_{i1}^0 \times \boldsymbol{l}_{i2}^0\right) \cdot f\left(x_G, y_G, z_G\right) < 0$, then it means that the initial orientation is adequate, namely $\boldsymbol{a}_{ij} = \boldsymbol{a}_{ij}^0, \boldsymbol{l}_{ij} = \boldsymbol{l}_{ij}^0, j = \overline{1, l(i)}$, where $\boldsymbol{a}_{i1}, \boldsymbol{a}_{i2}, \ldots, \boldsymbol{a}_{ij}, \ldots, \boldsymbol{a}_{il(i)}$ denotes the desired positive oriented vertices. If $f\left(\boldsymbol{a}_{i1}^0 + \boldsymbol{l}_{i1}^0 \times \boldsymbol{l}_{i2}^0\right) \cdot f\left(x_G, y_G, z_G\right) > 0$, then we will choose the opposite of initial orientation of vertices, thus $\boldsymbol{a}_{ij} = \boldsymbol{a}_{il(i)+2-j}^0, \boldsymbol{l}_{ij} = \boldsymbol{l}_{il(i)+2-j}^0, j = \overline{2, l(i)}$. We denote with ($x_G$, y_G, z_G) the coordinates of mass centre of polyhedron, let $f(x, y, z)$ be the analytical equation of the S_i plane, i.e.:

$$f(x, y, z) = \begin{vmatrix} x & y & z & 1 \\ x_{i1} & y_{i1} & z_{i1} & 1 \\ x_{i2} & y_{i2} & z_{i2} & 1 \\ x_{i3} & y_{i3} & z_{i3} & 1 \end{vmatrix},$$

where $\boldsymbol{a}_{i1}^0 = (x_{i1}, y_{i1}, z_{i1}), \boldsymbol{a}_{i2}^0 = (x_{i2}, y_{i2}, z_{i2}), \boldsymbol{a}_{i3}^0 = (x_{i3}, y_{i3}, z_{i3})$.

The scalar quantities l_{1ij}, l_{2ij}, h_{ij}, h_i, z_i belonging to the jth vertex are computed using (231) relations. The l_{1ij}, h_i, h_{ij} scalars geometrically represents the signed projection of $\boldsymbol{r}_{1ij}$ on $\boldsymbol{\mu}_{ij}$, $\boldsymbol{n}_i$, $\boldsymbol{v}_{ij}$. The $C_{ij\varepsilon}$, $\theta_{ij\varepsilon}$ scalars are computed with formulas (228)-(229) in each vertex of each plane using the l_{1ij}, l_{2ij}, h_{ij}, h_i, z_i and $W_{ij\varepsilon}$, $Q_{ij\varepsilon}$, V_{ij} quantities. l_{1ij}, l_{2ij}, h_{ij}, h_i, z_i are computed based on (232), substituting them in (229) we obtain $W_{ij\varepsilon}$, $Q_{ij\varepsilon}$, $V_{ij\varepsilon}$, where the first quantity represents the distance of computation point P to the edge belonging to the jth vertex, the second and third ones are the distances of computation point from the j and $j+1$vertices. The value of sign(h_i) is -1, if $\boldsymbol{n}_i$ points in the direction of half space determined by the computation point and the S_i plane, 0 if the computation point is located on S_i plane and +1 otherwise. ε is an arbitrary small positive quantity introduced to avoid the singularities (Pohànka 1988) which can appear on polyhedron vertices, edges or faces. Thus all analytical expressions of

gravitational filed related quantities presented previously will be valid in all space. Both in regional and local modelling the value of ε was chosen as 10^{-25}.

The developed Fortran program in its present form works for a particular polyhedron with 5 faces, namely truncated triangular prisms (two triangles and three quadrilaterals, see Fig. 21) which we found to be the most suitable elementary volume element to describe the 3-D volume element model of the crustal structure and density distribution of the regional model of Pannonian-Basin (Benedek 2004, Benedek and Papp 2009). The program can handle the degenerated volume elements which occurs when one (triangular pyramid or tetrahedron) or two (quadrilateral pyramid) vertices of the two triangle faces coincide. The input data of the program is a set of elementary volume elements of truncated triangular prisms or their degenerated forms, i.e, triangular or quadrilateral pyramids given by the coordinates of vertices. We get as output the gravitational potential and its derivatives generated by the integrated model as a sum of gravitational effects generated by the input elementary volume elements (principle of superposition). The input file consists of the geometrical (coordinates) and physical parameters (density) of n truncated triangular prisms given in n rows and in each row are listed the coordinates of six vertices of the truncated triangular prisms as x, y and z coordinates and the density of particular volume elements comes last. The ranking of vertices is obtained from the positive orientation as described previously of the one of the triangular face (assigned as top of polyhedron) and this is followed by the adherent vertices of the other triangular face (assigned as bottom of polyhedron), a total of 6 points i.e. 18 coordinates. The list of input data file of n volume elements is:

$$x_1^1, x_2^1, x_3^1, x_4^1, x_5^1, x_6^1, y_1^1, y_2^1, y_3^1, y_4^1, y_5^1, y_6^1, z_1^1, z_2^1, z_3^1, z_4^1, z_5^1, z_6^1, \rho^1 ,$$
$$\vdots$$
$$x_1^n, x_2^n, x_3^n, x_4^n, x_5^n, x_6^n, y_1^n, y_2^n, y_3^n, y_4^n, y_5^n, y_6^n, z_1^n, z_2^n, z_3^n, z_4^n, z_5^n, z_6^n, \rho^n ,$$

where the lower index indicates the rank of vertex, the upper index denotes the rank of volume elements in the input file, ρ^i is the density value of the ith homogeneous polyhedron volume element. In case of degenerate truncated triangular prisms one (triangular pyramid or tetrahedron) or two (quadrilateral pyramid) vertices of top and bottom triangular faces are identical. The second input data is the list of the observation points which can be randomly-spaced given by (x_P, y_P, z_P) coordinates or gridded data points generally given at the same height with respect to a reference surface (geoid or ellipsoid) or to the terrain. The grid can be defined by its origin and cell sizes (Δx, Δy), the horizontal coordinates of grid points can be specified by Δx, Δy, and by n_x, n_y grid points number in the x and y direction. After we have finished data reading we shift the origin of the initial coordinate system in the actual observation point (x_P, y_P, z_P) (Fig. 21). The new coordinates of the kth volume element will be:

$$x_1^k - x_P, x_2^k - x_P, x_3^k - x_P, x_4^k - x_P, x_5^k - x_P, x_6^k - x_P, y_1^k - y_P, y_2^k - y_P, y_3^k - y_P, y_4^k - y_P, y_5^k - y_P,$$
$$y_6^k - y_P, z_1^k - z_P, z_2^k - z_P, z_3^k - z_P, z_4^k - z_P, z_5^k - z_P, z_6^k - z_P, \rho^k .$$

The program starts to compute the gravitational effect generated by each volume element in this new coordinate system with respect to the origin $O(0,0,0)$. In case of each volume element we pass through the faces. For the ith face is chosen the adequate order of vertices of this face which assign the positive orientation to this polygonal face. Using (231)-(233) formulas we compute the l_{1ij}, l_{2ij}, h_{ij}, h_i, z_i and $W_{ij\varepsilon}$, $Q_{ij\varepsilon}$, $V_{ij\varepsilon}$ constants belonging to the ith face, furthermore applying the (228)-(229) relations for these constants we get $\theta_{ij\varepsilon}^{Pohanka^3}$, $C_{ij\varepsilon}^{Pohanka^3}$. Passing through each face of the kth polyhedron we generate the mentioned constants and inserting these values into equations (225)-(227) we get the gravitational potential and its derivatives generated by the kth volume element. Based on the superposition principle the sum of the quantities belonging to the particular volume elements gives the integrated gravitational effect.

Compared to the rectangular prism the analytical formulas of the gravitational potential and its higher order derivatives are more complicated so their calculation is more time consuming. The necessary

runtime is approximately twice (2.3 times) of what is required by rectangular prism computations. If the model extension and/or resolution are increasing, the computational time will grow linearly. The actual polyhedron model of the lithosphere that contains more than one million volume elements needs approximately one month of computation time on a computer dedicated to general IT tasks if the number of computation points is around 10^5. The parallel programming of HP rx2800 i4 4-core platform can reduce the computational time by more than 30 times, so the mentioned model computations will take some days only.

2 Theses

In the following the thesis formulated on basis of this work (first three theses) and on basis of two publications (Benedek 2004, Benedek and Papp 2009) are presented:

1. I defined the general solution $\boldsymbol{f}_i(\boldsymbol{r}_P) = \frac{\phi^*\left(\frac{y'}{x'}\right) + r_{MP}}{s_{MP}^2}\boldsymbol{s}_{MP}$ of that quasi-linear partial differential equation $\nabla_{r_P}\boldsymbol{f}_i(\boldsymbol{r}_P) = \frac{1}{r_{MP}}$ to which the analytical formula for the gravitational potential of a polyhedron can be reduced. In the general solution by choosing a suitable function ϕ^* we can get the individual solutions of other authors back. I completed the existing analytical formulas for the first order derivatives of the potential given by other authors with formulas for the potential and the second order derivatives of the potential in case when these were not determined by them.
   I determined numerical stability ranges for constants involved in the analytical formulas of gravitational potential and its first and second order derivatives. I also determined limiting values of constants in critical points and I set up a classification for the formulas determining the constants based on the needed computation time.

2. I gave an estimation and defined functions for the numerical errors of analytical formulas of potential and its derivatives. The errors are for the polyhedron function of normalised distance (normalisation was effectuated by linear dimension of polyhedron) of the computation point. I handled the exponent appearing in these functions as a parameter. It was 2.2 and 3.0 in case of the potential and the second order derivatives of the potential applying the conditions of double precision computation and 100% error level. I showed that the numerical error is less than 1% either for far (at e.g. GOCE orbital altitude) or near surface (<1 m) points if the polyhedron model of the crustal structure of ALPACA (Alpine–Pannonian–Carpathian) region is used for forward computations.

3. I found a correlation between the time of the computation and the computational parameters (number of volume elements and observation points) of the polyhedron and rectangular prism model. The time needed for calculating gravity potential and its first order derivative with the algorithm developed by me is ~2 times more using polyhedrons than the one optimised by Nagy (1988) for the rectangular prisms, applying double precision arithmetic.

4. Modelling the vertical gradient of gravity (VG) in near-surface points based on DTM having 10m × 10m resolution the rectangular prism approach does not provide enough accuracy. The change of the second order derivatives by *z* of disturbing potential can be too high even between adjacent points (25 m). In near surface points the second order derivative by *z* reacts sensitively to the stepped structure of the modelled surface due to the geometry of the rectangular prism. Therefore the observed correlation between the surface and the gradients, the existence of which follows from the theory is very weak. The application of polyhedrons, however, may improve significantly the correlation even if the resolution of the basic DTM is not increased as it is proven by the computations on the Sóskút test area of TUB. I also showed that using a polyhedron model, the changes of the computed VG (vertical gradient) values between the 6 networks points correlate well with the changes of the VG values derived from in situ gravity observations.

5. By the application of forward modelling, I demonstrated that the individual contributions of the topography and of the upper mantle to the second derivatives of the disturbing potential T certainly reaches one Eötvös unit in the planned altitude (~250 km) of the GOCE (Gravity and Steady-State Ocean Circulation Experiment) satellite. The contribution is only several hundredths Eötvös in case of the Neogene-Quaternary sedimentary complex. Additionally, I found that in the ALPACA region the effect of the Earth's curvature is an average of 10% of the absolute value of local contributions i.e. several hundredth Eötvös unit in the studied altitude range (300 km – 400 km). Considering the topography the effect of the Earth's curvature on the second order derivatives of the potential highly exceeds the sensitivity of the satellite gradiometer. In case of the sediments this effect is estimated to be within the expected noise range of the measurements.
   I found also that when one eliminates the effect of topography and of the sediments from the measurements of GOCE, the gradient observations can be transformed into density contrast values by means of inversion of the residual effect. It gives a real chance to increase the precision of the density contrast values at the Moho surface.

3 Outlook

Currently available high-resolution digital elevation models permit computations of terrain-related gravitational parameters with an unprecedented accuracy. It is ±0.1 mGal (1mGal=10^{-5} m/s^2) and ±10 E unit (1Eötvös=10^{-9} s^{-2}) in terms of the first and second derivatives of the gravitational potential, respectively. These grid models, however, mean a huge number of elementary polyhedron volume elements (even ~100 million polyhedrons in case of a country as small as Hungary) the computation of the gravitational effect of which is a real challenge when fully analytical solution is preferred. If the characteristic number i.e. the number of volume elements times the number of observation points is around 10^{12} the runtime may take a few months on a single processor (core) designed for general IT purposes. A static generalization technique presented in Journal of Geodesy (Benedek et al 2018), however, may reduce the number of volume elements efficiently to 5 – 10 % if the known/estimated accuracy of the terrain data is interpreted as a threshold parameter. The methods are based on the statistical equivalence of a theoretically infinite number of models describing the reality represented by erroneous data. This statistical rule makes the description of a surface with a triangular mesh composed by a minimum number of triangles having variable dimensions possible. The measure of optimization depends on the accuracy and the variability of the input data. In the range of the threshold all the possible realizations of the real topography may give statistically equivalent results in gravitational forward modelling. Obviously, the decrease of the number of volume elements has a favourable influence on the computation time. Based on experience sometimes it can be decreased at least to 10% of the processing time of the initial input model whereas the error of modelled data remains consistent with the errors of input surface data.

The efficiency of the methods can be evaluated by the GGMplus model (Hirt et al. 2013) providing data of Earth's gravity at 200 m grid resolution with near-global coverage. By the application of the proposed generalization technique the agreement between gravity data synthetically computed from the local model HU-DTM30 and GGMplus gravity can be analysed up to the ultra-high frequency components provided by the SRTM3 global elevation model for GGMplus. If the discrepancy is not significant the use of the SRTM3 surface model instead of HU-DTM30 in the geodetic computations can also be feasible but at the same time it reduces the computational time by a factor of 10 due to the resolution differences. In this case even a global model can be applied for local/regional modelling of the gravitational effect of the topographical masses in the ALCAPA region. Otherwise the merging of the local terrain model (HU-DTM30) and the regional surface model (SRTM3) will be necessary to generate a suitable topographical model which can describe the local gravity field with sufficient accuracy.

The model optimization methods developed by us can be applied for the optimal discretization of the ocean surface starting from source data (e.g. RECON_SEA_LEVEL_OST_L4_V) is an important step in the modelling of the ocean loading effect in tidal analysis too. The triangular mesh describing the water surface deforming in time according to the instantaneous tidal forces can be used to form a volumetric model by polyhedron volume elements. Its time variant gravitational effect can be calculated analytically in a global coordinate system. One of the main questions of the research is if the ocean loading effect can be modelled consistently with the observations with sub-microgal precision. Observations performed in the previous NKFIH-OTKA project (K101603) show that the variation of M2 tidal amplitude strongly influenced by ocean loading effect may reach several tenths of 1microGal in the Pannonian Basin. Based on synthetic loading data obtained from the FES2014 model the increase of the ratio should be much higher so an independent validation of the results is necessary. An adequate ocean loading model quantitatively consistent with our tidal gravity measurements will provide a tidal model even with sub-microGal accuracy for the Pannonian basin. Elimination using an accurate tidal model will help the correct interpretation of tendencies of long periodic and secular changes in the gravity field on a shorter time base. An improved tidal model will help the quick indication of the gravity effect of these processes reducing the cost of monitoring.

As a continuation of the work of Dezső Nagy (e.g. Nagy 1966) the forward modelling program systems written by the applicants in Fortran language (on HP Unix platforms) are available from the early '90s and from 2000 for the calculation of the gravitational effect of prism and polyhedron volume elements, respectively, and are continuously developed. Although very complex modeller systems equipped by graphical user interface, like IGMAS (Götze and Lahmeyer 1988) also exist and are available for the research community, basic research usually needs high flexibility in program coding to defer to the continuously varying requirements and aims. As a result of it the PI of this proposal could e.g. speed up the calculation of the gravitational effect of the polyhedron volume element so now it is only twice of what is needed when prisms (the computation of which has been already optimized by Dezső Nagy) are applied.

For the task of regional gravity inversion a reliable regional model of the 3D density distribution based on geological and seismological information, composed by rectangular volume elements (prisms) of different dimensions is available for the Pannonian basin and its orogenic surroundings for the uppermost 50 km of the lithosphere (Papp and Kalmár 1995, 1996, Papp and Benedek 2000, Benedek and Papp 2009, http://www.ggki.hu/fileadmin/user_upload/ggki/Munkatarsak/papp/e-cikkek/geoid1.html). The model contains four submodels of the main structural units of the lithosphere: the models of the surface topography, the Neogene –Quaternary sedimentary complex, the lower crust and the upper mantle. The limited spatial extent of this model and its relatively simple density distribution restrict the accuracy of the computations. This model, however, is being updated from time to time as more and more geological and geophysical data about the crustal structure of the Pannonian basin become available. In addition, because of the rigorous functional relations between the gravity field parameters computed from the density model by forward modelling, it is possible to validate numerical methods (for example a specific solution of the Stokes integral) in a closed-loop test way. The reliability of the model can be checked by different quantities of the observed gravity field (e.g. measured gravity anomalies, geoid undulations computed from measured, potential related data, etc.). This technique has been used to study the compaction of the Neogene-Quaternary sedimentary filling of the Pannonian Basin, and its relation to the observed anomalous gravity field (Papp and Kalmár 1995). In addition it has been proved that the local part of geoid undulation ($\lambda < 300$ km) can be successfully interpreted by the model (Papp 1996a, Papp and Kalmár 1996) at the level of ±10 cm in terms of standard deviations of the residual undulations. The 3D lithosphere model of the Alpine-Carpathian-Pannonian region makes possible – by certain conditions – to determine different parameters of the gravity field (gravity acceleration, geoid undulation, gravity potential, gravity anomaly) analytically (Papp 1996a, Papp 1996b, Papp and Benedek 2000, Benedek 2001, Papp et al 2004, Papp et al 2009). Beyond rectangular prisms polyhedrons can also be used to discretize the density distribution inside 3D models of geological structures (Benedek and Papp 2009, Benedek 2009). This way the geometrical description of the density interfaces considered can be significantly improved and modelling can be extended to global coordinate systems easily. In between the interfaces, where data are available, further refinement of the discretization is possible.

For instance, the borehole measurements sampling vertically the sedimentary complex in the Pannonian basin show significant compaction of the sedimentary rocks, providing typical non-linear density-to-depth functions. Their weighted average density contrast is -460 kg/m^3 so the presence of the sediments represents a significant lack of mass relative to the 2750 kg/m^3 average density of the crust (the average crust is represented by one block with ρ = 2750 kg/m^3). Taking this information into account the model of Neogene-Quaternary sediments consists of ~31000 polyhedron volume elements. A density contrast value averaged along the depth from the density-to-depth function is assigned to each element. In this way (using the density contrast function) the Pre-Neogene crystalline basement (Kilényi and Rumpler 1984, Brezsánszky 1989 and Kilenyi et al. 1991) is involved in our lithosphere model with a constant density (ro = 2750 kg/m^3) value.

In the case of surface topography geological maps from the area of Czech Republic, Slovakia (Pavel Novak pers. comm.) and Hungary (Rónai 1985) were used to improve its density distribution which significantly deviates from the 2670 kg/m^3 value uniformly used in forward modelling (Völgyesi et al. 2005).

Based on the unprecedented progress in satellite, but also airborne and terrestrial measurements global/regional digital terrain models (e.g. SRTM3) and data sets describing the Earth's inner structure with high resolution give new possibilities for refined studies on a synthetic terrestrial gravity field. This ensures both the spatial extension of the existing model of the lithosphere and the improvement of its geometrical and physical parameters (Kalmár et al. 1996). In continental-scale gravity field modelling the high resolution (3-arc-sec by 3-arc-sec), SRTM3 elevation model (Farr et al. 2007) providing nearly global coverage and derived from the analysis of the Shuttle Radar Topography Mission has a great importance (GGMPlus, Hirt et al. 2013) since the most dominant near surface density interface is the topography itself (transition from 1000 kg/m^3 – 2700 kg/m^3 to ~ 0 kg/m^3). Useful geometrical and physical data about the inner structure of the Earth is supplied by PREM, the CRUST2.0 (Mooney et al. 1998) and CRUST1.0 (Laskei et al. 2013) in global scale.

Regionally the freely available new Moho map (Grad et al. 2009, http://www.igf.fuw.edu.pl/mohomap2007a) covering the European continent gives the possibility to extend our present lithospheric model horizontally.

The application of prism volume elements, however, is limited by the extension of the model, due to the curvature of the Globe. The application of polyhedron volume elements in a global Cartesian coordinate system overrides this problem and improves the geometrical description of the bounding surfaces. Choosing a proper density value for every polyhedron volume element according to the geological/geophysical constraints it is possible to generate a density model with discrete density distribution both in local map projection (planar) and global (e.g. WGS84) systems. Analytical expressions for the gravity field of a polyhedral body with constant, linearly and polynomially varying density are also available (Garcia-Abdealem J, 1992, 2005, Pohánka 1998, Hansen R O 1999, Holstein H 2003, Zhou X 2009) thus can be conveniently implemented in the current program system used in this stady. This enables modelling of the continuous density variation inside a single volume element where the geological data justifies its existence.

Regional investigation of synthetic gradiometric data calculated from both prism- and polyhedron-based density models shows that the effect of the difference between the two volume elements could not be negligible at the Gravity Field and Steady-State Ocean Circulation Explorer (GOCE) orbit altitude (Benedek 2009, Benedek and Papp 2009). The differences are mainly related to the effect of the curvature and their magnitude depends on which structural part of the lithosphere is considered. For the sediments it is in the range of noise of the gradiometric measurements whereas for the other parts (e.g. topography) it is not negligible. Furthermore the model computation shows that the anomalous individual contributions of the topography and the upper mantle to the second derivatives of the disturbing potential can reach 1 E unit. In case of the Neogene - Quaternary sediments this contribution is several hundredths of E unit only, but this is still higher than the measurement accuracy at satellite altitude. At the GOCE altitude the dominance of regional variation can be observed, ensuring the spectral consistency of the initial model and the residual effect which is a necessary condition for the gravity inversion process.

The application of gravity gradients observed at GOCE satellite altitude is a current research topic in global and regional geophysical interpretation (Bouman et al. 2016, Holzrichter 2013). For forward model computations the tesseroid and polyhedron volume elements are both used. The lithospheric structure of the Western Carpathian-Pannonian Basin region using 3D modelling was investigated by Tasarova et al. (2009) and a gravity model of the region consistent with petrological data collected from various geophysical datasets was determined. Later on the 3D lithosphere model LitMod 3D of Central Europe was also compiled (Tasarova et al. 2016). It combines a large number of geophysical, geological, and petrological data having different resolution. The results of these efforts can be inferred and used as reference in the further investigations.

Our model optimization methods can be applied for the optimal discretization of the ocean surface in order to model the ocean loading effects starting even from source data e.g. https://podaac.jpl.nasa.gov/dataset/RECON_SEA_LEVEL_OST_L4_V1. This model computation will provide the gravity effect generated by the ocean loading effect in given location and epoch. One of the main questions of the research is if the ocean loading effect can be modeled consistently with the observations with sub-microGal precision.

The two most well-known global environmental datasets are the Global Shuttle Radar Topographic Mission (SRTM) Digital Elevation Model (Jarvis et al 2008) and the Advanced Spaceborne Thermal Emission and Reflection Radiometer Global Digital Elevation Model (ASTER GDEM). The heights of both models are referenced to the EGM96 geoid, the horizontal datum is WGS84. SRTM3 is post-processed from SRTM data (Reuter et al. 2007) and has 3 arc second (approx. 90m) horizontal resolution, ASTER GDEM has a resolution of 1 arc-sec. It is important to note that these models are surface models and should be distinguished clearly from terrain models due to acquisition method. The estimated vertical accuracies derived from comparison with geodetic network points are ±16 m at 90% confidence level, and ±20 m at 95% confidence level (Papp and Szűcs 2011). Both models are publicly available.

A high resolution (30 m x 30 m) digital terrain model of Hungary became recently available which allows the computation of terrain effects in gravitational modelling with a resolution higher than ever before. This resolution, however, generates an unprecedented number of elementary polyhedron volume elements (~100 millions) for the topography model. This is an increase by one order of magnitude related to the recent model used for calculations which can only be handled applying the model optimization methods previously described.

Since the GGMplus model (Global Gravity Model plus, Hirt et al. 2013) is available from 2013, providing data of Earth's gravity at 200 m resolution with near-global coverage, it can be efficiently used to check the results of forward calculations of terrain effects from the available national digital topographic model mentioned above. In this way the discrepancy between the elevation (i.e. surface) and terrain models can be investigated according to the theoretical concepts (e.g. regularization of boundary values for geoid determination) of physical geodesy. If the discrepancy is not significant the use of the SRTM3 elevation model in the geodetic computations can be also reasonable which reduces more than 10 times the computational time due to the lower resolution of the SRTM3 model. Otherwise the combination of the local terrain model and the regional elevation model will be necessary to generate a suitable topographical model which can describe the local effect of topographical masses with sufficient accuracy (Papp et al. 2009).

It is also known that since 2015 the SRTM data are in the public domain at 1 arc-sec resolution (30 m postings). The combination of this new elevation data set with the national DTM allows generating an unprecedented-resolution (1 arc-sec) model of the topographic gravity field over the entire ALCAPA.

Acknowledgements The author gratefully thanks the financial support of National Scientific Research Found NKFIH-OTKA K101603 Project and expresses her sincere gratitude to Dr. Gábor Papp for his encouragement to write the English version of her PhD Dissertation written in Hungarian and defended in 2009 at West Hungarian University. She is also deeply thankful to reviewers Prof. Martin Vermeer Aalto University and Dr. Ernő Prácser MTA CSFK GGI for the valuable comments and suggestions which improved the content of this work.

REFERENCES

Barnett CT (1976): Theoretical modeling of the magnetic and gravitational fields of an arbitrarily shaped three-dimensional body. Geophysics, 41(6), 1353-1364

Benedek J (2000): A gravimetriai adatok sűrűségének hatása a Stokes-FFT módszerrel számított geoidundulációk pontosságára. Geomatika Közlemények III. 157 - 164

Benedek J (2001): The effect of the Point Density of Gravity Data on the Accuracy of Geoid Undulations Investigated by 3D Forward Modeling. Österreichische Beiträge zu Meteorologie und Geophysik, Proceedings of the 8th International Meeting on Alpine Gravimetry, Leoben 2000, edited by Bruno Meurers, Department of Meteorology and Geophysics, University of Vienna, 159-166

Benedek J (2002): Polyhedron térfogatelem alkalmazása a nehézségi erőtér paramétereinek kiszámításában. Geomatika Közlemények V., 175-190

Benedek J (2004): The application of polyhedron volume element in the calculation of gravity related quantities. In Meurers B. and Pail R. (eds): Proc. 1st Workshop on Int. Gravity Field Research, Österreichische Beiträge zu Meteorologie und Geophysik, 28, 99-106

Benedek J, Papp G (2006): Az Eötvös tenzor elemeinek szimulációja a GOCE műhold pályamagasságában. Geomatika Közlemények X., 187-200

Benedek J, Papp G (2009): Geophysical inversion of on board satellite gradiometer data: A feasibility study in the ALPACA Region, Central Europe, Acta Geod. Geoph. Hung., 44(2), 179-190

Benedek J, Papp G, Kalmár J (2018): Generalization techniques to reduce the number of volume elements for terrain effect calculations in fully analytical gravitational modelling, Journal of Geodesy, 92(4), 361-381

Bouman J, Ebbing J, Fuchs M, Sebera J, Lieb V, Szwillus W, Haagmans R, Novak P (2016): Satellite gravity gradient grids for geophysics. Nature Scientific Reports, 6, 21050,10.1038/srep21050

Brezsnyánszky K (1989): Magyarország és környékének hegységszerkezete, 1:2000000,Kartográfiai Vállalat, Budapest, 630318

Cady JW (1980): Calculation of gravity and magnetic anomalies of finite-length right polygonal prism. Geophysics, 45, 1507-1512

Csapó G, Papp G (2000): A nehézségi erő vertikális gradiensének mérése és modellezése - hazai példák alapján. Geomatika Közlemények III., 109-123

Ebbing J, Götze HJ (2001): Preliminary 3D density modeling along the TRANSALP-profile. In: Meurers, B. (ed.), Proceedings of the 8th International Meeting on Alpine Gravimetry, Leoben 2000, Special Issue of Österreichische Beiträge zu Meteorologie und Geophysik, 26, 125-136

Farr TG, Rosen PA, Caro E, Crippen R, Duren R, Hensley S, Kobrick M, Paller M, Rodriguez E, Roth L, Seal D, Shaffe S, Shimada J, Umland J, Werner M, Oskin M, Burbank D, Alsdorf D (2007): The Shuttle Radar Topography Mission. Rev. Geophys., 45, RG2004, doi:10.1029/2005RG000183

Furnes P (1994): A physical approach to computing magnetic fields. Geophysical Prospecting, 42, 405-416

Furnes P (2000): Computing three-dimensional gravitational fields with equivalent sources. Geophysical Prospecting, 48, 603-615

Garcia-Abdealem J (1992) Gravitational attraction of a rectangular prism with depth-dependent density, Geophysics, 57(3), 470-473.

García-Abdeslem J, Martin-Atienza B (2001): A method to compute terrain corrections for gravimeter stations using a digital elevation model. Geophysics, 66(4), 1110-1115

Garcia-Abdealem J (2005) The gravitational attraction of a right rectangular prism with density varying with depth following a cubic polynomial, Geophysics, 70(6), 339-342

Götze HJ, Lahmeyer B (1988): Application of three-dimensional interactive modeling in gravity and magnetics. Geophysics, 53(8), 1096-1108

Grad M,Tiira T,ESC Moho Working Group (2009): The Moho depth of the European plate Geophys. J. Int.176, 279-292

Guptasarma D, Singh B (1999): New scheme for computing the magnetic field resulting from a uniformly magnetized arbitrary polyhedron. Geophysics, 64(1), 70-74

Hansen RO (1999): An analytical expression for the gravity field of a polyhedral body with linearly varying density. Geophysics, 64(1), 75-77

Hikida H, Wieczorek MA (2007): Crustal thickness of the Moon: New constraints from gravity inversions using polyhedral shape models. Icarus, 192(1), 150-166

Hirt C, Fecher T, Claessens SJ, Kuhn M, Pail R, Rexer M (2013): New ultra-high resolution picture of Earth's gravity field, Geophysical Research Letters,Vol 40

Holstein H, Ketteridge B (1996): Gravimetric analysis of uniform polyhedra. Geophysics, 61(2), 357-364

Holstein H, Schürholz P, Starr A J, Chakraborty M (1999): Comparison of gravimetric formulas for uniform polyhedra.

Geophysics, 64(5), 1434-1446
Holstein H (2002a): Gravimagnetic similarity in anomaly formulas for uniform polyhedra. Geophysics, 67(4), 1126-1133
Holstein H (2002b): Invariance in gravimagnetic anomaly formulas for uniform polyhedra. Geophysics, 67(4), 1134-1137
Holstein H (2003): Gravimagnetic anomaly formulas for polyhedra of spatially linear media. Geophysics, 68(1), 157-167
Holzrichter N (2013): Processing and interpretation of satellite and ground based gravity data at different lithospheric scales, Dissertation, Kiel, pp127. (http://macau.unikiel.de/servlets/MCRFileNodeServlet/dissertation_derivate_00005115/Dissertation_NHolzrichter.pdf)
Ivan M (1996): Polyhedral approximations in physical geodesy. Journal of Geodesy 70, 755-767
Jarvis A, Reuter HI, Nelson A, Guevara E (2008): Hole-filled SRTM for the globe Version 4, available from the CGIAR-CSI SRTM 90m Database (http://srtm.csi.cgiar.org).
Kalmár J, Papp G, Szabó T (1995): DTM-based surface and volume approximation. Geophysical applications. Comp. and Geosci., 21, 245-257
Kilényi É, Rumpler J (1984): Pre-Tertiary basement relief map of Hungary. Geophysical Transactions 30, p. 425-428
Kilényi É, Kröll A, Oberhauser D, Šefara J, Steinhauser P, Szabó Z, Wessely G (1991): Pre-Tertiary basement contour map of the Carpathian Basin beneath Austria, Chechoslovakia and Hungary. Geophysical Transactations 36, 15-36
Kuder J (2002): 3D Schwerefeldmodellierung zur Erfassung des tiefen Untergrundes im Nordost-Deutschen Becken. Dissertation, FB Geowissenschaften, FU Berlin. http://www.diss.fu-berlin.de/2002/139/
Kwok Y-K (1991a): Gravity gradient tensor due to a polyhedron with polygonal facets. Geophysical Prospecting 39, 435-443
Kwok Y-K (1991b): Singularities in gravity computation for vertical cylinders and prisms, Geophys. J. Int. 104, 1-10
Laske G, Masters G, MZ, Pasyanos M (2013): Update on CRUST1.0 - A 1-degree Global Model of Earth's Crust, Geophys. Res. Abstracts, 15, Abstract EGU2013-2658
MacMillan WD (1958): The Theory of the Potential, p 196. Dover Publications, New York.
Mahatsente R, Jentzsch G, Jahr T (1999): Crustal structure of the Main Ethiopian Rift from gravity data: 3-dimensional modelling. Tectonophysics, 313(4), 30
Mooney WD, Laske G, Masters G (1998): CRUST 5.1: A global crustal model at 5°x5°. Journal of Geophysical Research, 103, 727-747.
Nagy D (1966): The gravitational attraction of a right rectangular prism. Geophysics, 31, 362-371
Nagy D (1988): A short program for three-dimensional gravity modeling. Acta Geod. Geoph. Mont. Hung. 23, (2-4), 449-459
Nagy D, Papp G, Benedek J (2000): The gravitational potential and its derivatives for the prism. Journal of Geodesy, 74 (7-8). 552-560
Okabe M (1979): Analytical expressions for gravity anomalies due to homogeneous polyhedral bodies and translation into magnetic anomalies. Geophysics, 44(4) 730-741
Papp G (1996a): A Pannon-medence nehézségi erőterének modellezése, Kandidátusi értekezés, MTA Geodéziai és Geofizikai Kutatóintézet Sopron
Papp G (1996b): On the application of physical filtering in 3-D forward gravity field modelling. In: Meurers, B. (ed.), Proceedings of the 7th International Meeting on Alpine Gravimetry, Special Issue of Österreichische Beiträge zu Meteorologie und Geophysik, Heft 14, 145-154
Papp G, Kalmár J (1995): Investigation of sediment compaction in the Pannonian basin using 3-D gravity modeling. Phys. Earth Planet Int., 88: 89-100
Papp G, Kalmár J (1996): Toward the physical interpretation of the geoid in the Pannonian Basin using 3-D model of the litosphere, IGeS Bulletin,DIIAR, Polihecnico di Milano, 5, 63-87
Papp G, Wang ZT (1996): Truncation effects in using spherical harmonic expansions for forward local gravity field modelling. Acta Geod. Geoph. Hung., 31, 47-66.
Papp G, Benedek J (2000): Numerical modeling of gravitational field lines - the effect of mass attraction on horizontal coordinates. Journal of Geodesy, 73(12), 648 – 659
Papp G, Benedek J, Nagy D (2004): On the information equivalence of gravity field related parameters – a comparison of gravity anomalies and deflection of vertical data. In: Meurers, B. (ed.), Proceedings of the 1st Workshop on International Gravity Field Research, Graz 2003, Special Issue of Österreichische Beiträge zu Meteorologie und Geophysik, Heft 31., pp. 71-78.
Papp G, Szűcs E (2011): Effect of the difference between surface and terrain models on gravity field related quantities,Acta Geod. Geoph. Hung., 46(4), 441-456 DOI: 10.1556/AGeod.46.2011.4.6
Papp G, Szeghy E, Benedek J (2009): The determination of potential difference by the joint application of measured and synthetical gravity data: a case study in Hungary. Journal of Geodesy, 83(6), 509-522.DOI: 10.1007/s00190-008-0257-2
Paul M K (1974): The gravity effect of a homogeneous polyhedron for three-dimensional Interpretation. Pure and Applied Geophysics 112, 553-561.
Petrovič S (1996): Determination of the potential of homogeneous polyhedral bodies using line integrals. Journal of Geodesy, 71, 44-52.
Pohànka V (1988a): Optimum expression for computation of the gravity field of homogeneous polyhedral body. Geophysical Prospecting 36, 733-751
Pohánka V (1998b): Optimum expression for computation of the gravity field of a polyhedral body with linearly increasing density. Geophysical Prospecting 46, 391-404
Polyanin AD, Zaitsev VF, Moussiaux A (2002): Handbook of First Order Partial Differential Equations, Taylor & Francis, London

Reuter HI, Nelson A, Jarvis A (2007): An evaluation of void filling interpolation methods for SRTM data, International Journal of Geographic Information Science, 21:9, 983-1008.

Rónai A (1985): The Quaternary of the Great Hungarian Plain. Geol. Hung. Ser. Geol. Vol. 21, 446 p

Singh B, Guptasarma D (2001): New method for fast computation of gravity and magnetic anomalies from arbitrary polyhedra. Geophysics, 66(2), 521-526

Tsoulis D, Petrovič S (2001): On the singularities of the gravity field of homogeneous polyhedral body. Geophysics, 66(2), 535-539

Tašárová A, Afonso JC, Bielik M, Götze H-J,Hók J (2009): The lithospheric structure of the Western Carpathian–Pannonian Basin region based on the CELEBRATION 2000 seismic experiment and gravity modelling, Tectonophysics, 475, 3–4, 454–469.

Tašárová A, Fullea J, Bielik M, Środa P (2016): Lithospheric structure of Central Europe: Puzzle pieces from Pannonian Basin to Trans-European Suture Zone resolved by geophysical-petrological modelling, Tectonics, DOI:10.1002/2015TC003935.

Vlagyimirov VSz (1979): Bevezetés a parciális differenciálegyenletek elméletébe, Műszaki Könyvkiadó, Budapest

Völgyesi L, Szabó Z, Csapó G (2005): Relation between time variation of gravity and Pannonian sediment thickness in the Carpathian basin. Reports on Geodesy, Warsaw University of Technology, Vol. 73, Nr. 2. pp. 255-262

Werner RA, Scheeres DJ (1997): Exterior gravitation of polyhedron derived and compared with harmonic and mascon gravitation representations of asteroid 4769 Castalia. Celestial Mechanics and Dynamical Astronomy 65, 313-344

Zach FX. (1811): Zach's Monatliche Correspondenz zur Beförderung der Erd- und Himmelskunde, Bd., XXVII, 522

Zhou X (2009): Three-dimensional (3D) vector gravity potential and line integrals for the gravity anomaly of a rectangular prism with 3D variable density contrast.Geophysics,74(6): I43-I53